

DISS. ETH NO. 30021

Temporal Dynamics of Freshwater Microbial Membrane Lipids: Impact of Environmental Variables on brGDGTs across Short and Long Time-scales

Fatemeh Ajallooeian



DISS. ETH NO. 30021

Temporal Dynamics of Freshwater Microbial Membrane Lipids: Impact of Environmental Variables on brGDGTs across Short and Long Time-scales

A thesis submitted to attain the degree of
DOCTOR OF SCIENCES
(Dr. sc. ETH Zürich)

presented by

Fatemeh Ajallooeian

*Master of Science in Atmospheric Science,
University of Helsinki
born on 22.09.1993*

Accepted on the recommendation of:

Prof. Dr. C. De Jonge, examiner

Prof. Dr. T. I. Eglinton, co-examiner

Prof. Dr. M. A. Lever, co-examiner

Dr. P. Martínez-Sosa, co-examiner

Dr. S. Naeher, co-examiner

Prof. Dr. J. McFarlin, co-examiner

2024

TABLE OF CONTENTS

Summary	6
Chapter 1: Introduction	8
1.1. BrGDGTs as paleoclimate proxies	9
1.2. Core Lipid (CL) and Intact Polar (IPL) GDGTs	11
1.3. In-situ production of brGDGTs in freshwater systems and calibrations	12
1.4. Seasonality.....	14
1.5. Bacterial source organisms of brGDGTs	14
1.6. Direct vs indirect environmental impacts on brGDGTs.....	15
1.7. Lake Rot (Rotsee) and Sihl River as unique settings	16
Chapter 2: Seasonal Temperature Dependency of Branched Glycerol Dialkyl Glycerol Tetraethers (brGDGTs): A Mesocosm Approach	24
1. Introduction	26
2. Materials and Methods	28
2.1. Sampling sites and Seasons	28
2.2. Experimental Design	29
2.3. Sampling and Characterization of brGDGT Lipids, Water Chemistry and Bacterial DNA	30
2.3.1. Sampling.....	30
2.3.2. Lipid Extraction.....	31
2.3.3. Water Chemistry Measurement	32
2.3.4. DNA Extraction, Quantitative qPCR, and 16S rRNA Gene Sequencing.....	32
2.4. Statistical Analysis	33
3. Results	34
3.1. Water Chemistry Parameters	34
3.2. DNA Quantification and Sequencing Data	35
3.3. BrGDGT Concentrations and Distributions	36
3.3.1. Environmental Distribution (T0).....	36
3.3.2. Mesocosm Distribution Changes.....	37
4. Discussion	45
4.1. Performance of Mesocosms for brGDGT Production	45

4.2. In-situ Seasonal brGDGT Signatures	49
4.3. Impact of Temperature on brGDGT Distribution.....	49
4.4. Impact of Water Chemistry on brGDGT Variability.....	52
4.5. Bacterial Community Composition as a source of brGDGT Variability	54
5. Conclusions	56
Chapter 3: Controls on brGDGTs Distributions in Particulate Matter of the Seasonally Anoxic Water Column of Lake Rot (Rotsee)	83
1. Introduction	84
2. Materials and Methods	86
2.1. Study site	86
2.2. Water column and surface sediment sampling.....	87
2.3. Lipid extraction.....	88
2.4. Quantifying and sequencing of the 16S Gene.....	91
2.5. Statistical methods.....	92
3. Results	92
3.1. Mixing regime and water chemistry of Lake Rot.....	92
3.2. Patterns of brGDGTs in Lake Rot suspended Particulate Matter (SPM).....	94
3.2.1. GDGTs concentration variability.....	94
3.2.2. GDGTs distributions variability.....	97
3.3. Lake Rot 16S rRNA gene-based bacterial community.....	100
4. Discussion	100
4.1. Abiotic and biotic drivers of brGDGTs production in lake water column.....	100
4.2. Environmental drivers on brGDGTs concentration and distribution.....	104
4.2.1. Proposed temperature-sensitive brGDGT Ia, IIa, and IIIa and ratios.....	104
4.2.2. Chemistry-sensitive 6-methyl and cyclopentane-containing brGDGTs, IR, CBT' and DC'.....	106
4.3. Implications for Paleoclimate Proxies.....	107
5. Conclusions	108
Chapter 4: Provenance and Drivers of brGDGTs in Lake Rot Sediments	130
1. Introduction	131
2. Materials and Methods	133
2.1. Known paleoclimatic variability of Lake Rot system.....	133

2.2. Core sedimentology and Age-Depth Model.....	134
2.3. XRF elemental composition and bulk organic measurements.....	134
2.4. Lipid extraction and brGDGT indices calculation.....	135
2.5. Statistical analysis.....	136
3. Results.....	137
3.1. Chemistry and Age-depth Model.....	137
3.2. Variability in brGDGT concentration and distribution.....	139
4. Discussion.....	144
4.1. Provenance and environmental driver of sedimentary GDGTs.....	144
4.2. Implications for GDGT-based paleoclimate reconstructions.....	148
4.3. Quantitative climate reconstruction of Lake Rot sediments.....	148
5. Conclusions.....	150
 Chapter 5: Conclusions.....	 166
 Acknowledgments.....	 175

“Love of learning is the most necessary passion, in it lies our utmost happiness”

Émile du Châtelet

French philosopher and mathematician

ره آسمان درون است، پر عشق را بجنبان (مولانا)

Summary

In pursuit of a deeper understanding of Earth's climate history, and the forces influencing its changes, the importance of reliable paleoclimatic data becomes evident. Such records offer invaluable insights into past climatic variations, enriching our understanding of the diverse consequences of global warming. BrGDGTs, membrane-spanning lipids produced by bacteria are at the basis of the MBT'_{5ME} , a biomarker ratio that has been used as paleotemperature proxy. However, the response of the MBT'_{5ME} to temperature changes, particularly in freshwater systems, remains incompletely understood. In this study, a combination of experimental and empirical tests was carried out to gain a comprehensive mechanistic understanding of the environmental drivers influencing the brGDGTs distribution variability. In the first step, oxic mesocosms were used to assess the temperature sensitivity of brGDGTs and their producers, sampled from a lake (Lake Rot) and river (Sihl River) in three different seasons. Although an increase in MBT'_{5ME} in response to some warming incubations was observed, the temperature-sensitivity of MBT'_{5ME} , as expected from GDGT studies on a global scale, was not supported by this experiment. Additionally, no response was observed in cooling treatments, potentially indicating limited sensitivity to cold temperatures. With coeval changes in the composition of the bacterial community, the microbial GDGT producers were determined to constrain the MBT'_{5ME} response to temperature changes. Consequently, investigating the GDGT distribution of the natural freshwater column, the oxic epilimnion of Lake Rot exhibited temperature variations, with MBT'_{5ME} showing a muted increase in this layer during the stratified summer months, primarily associated with increases in brGDGT Ia concentrations and a cold signal mainly linked to upwelling of hypolimnion IIIa during mixing period. Contrary to MBT'_{5ME} , IR showed a more robust correlation with temperature in the epilimnion. In the hypolimnion, while MBT'_{5ME} correlated with water pH rather than temperature, IR correlated with the dissolved oxygen, highlighting the water chemistry's influence on the hypolimnion GDGTs. Although the surface sediment samples underlying the oxic water column revealed a lower MBT'_{5ME} value due to sedimentary production of brGDGT IIIa, coring at the oxic part of seasonally stratified lakes were suggested for paleoclimate reconstruction purposes to achieve more realistic lake surface temperature signals. This approach avoids the influence of water chemistry on hypolimnion GDGT signals. Lastly, the analysis of brGDGT variations within Lake Rot's sediment core revealed insights into the lake's environmental history and the interplay of brGDGTs, as seen in the paleotemperature proxy MBT'_{5ME} and IR. Recording a cold Glacial interstadial, the core further exhibited GDGT variations in the Holocene era based on the lake's mixing regimes. Notably, elevated brGDGT Ia levels during oligotrophic phases provided evidence of water column stratification, confirming its role along with the correlation between MBT'_{5ME} and IR, as epilimnion-specific climate markers. While the link between MBT'_{5ME} and temperature in the epilimnion was established during the oligotrophic phase, the eutrophic phase showcased instances of hypolimnion influence and potential complexities in MBT'_{5ME} and IR due to water chemistry. Coring at the lake's oxic zone proved effective for using MBT'_{5ME} as a paleothermometer. These findings have significant implications for paleoclimate research utilizing brGDGTs, emphasizing the importance of considering establishment of a seasonal stratification rather than focusing solely on temperature changes when interpreting paleoclimatic data.

Zusammenfassung

Paläoklimatische Daten sind entscheidend für das Verständnis der Erdklimageschichte. BrGDGTs, membranumspannende Lipide von Bakterien, dienen als Basis für MBT'5ME, einen Paläotemperaturproxy. Ihre Sensitivität gegenüber Temperaturschwankungen, besonders in Süßwassersystemen, ist noch nicht klar. Diese Studie kombiniert Experimente und Tests zur Analyse der Umweltauswirkungen auf brGDGTs. In oxischen Mesokosmen wurden Proben aus See (Rotsee) und Fluss (Sihl) in verschiedenen Jahreszeiten genommen. MBT'5ME reagierte auf einige wärmende Inkubationen, bestätigte jedoch nicht die erwartete globale Temperatursensitivität. Mikrobielle GDGT-Produzenten und GDGT-Verteilungsanalysen in der natürlichen Süßwassersäule wurden untersucht, wobei saisonale Schichtung und Wasserkemi beeinflussten. Die Analyse ergab, dass das oxische Epilimnion des Rotsees Temperaturschwankungen aufwies. MBT'5ME zeigte einen gedämpften Anstieg in den geschichteten Sommermonaten, hauptsächlich aufgrund erhöhter brGDGT Ia-Konzentrationen und eines Kältesignals im Zusammenhang mit dem Auftrieb des Hypolimnions IIIa. Im Gegensatz dazu zeigte die IR eine stärkere Korrelation mit der Temperatur im Epilimnion. MBT'5ME korrelierte eher mit dem pH-Wert im Hypolimnion als mit der Temperatur, während IR mit dem gelösten Sauerstoff korrelierte, was den Einfluss der Wasserchemie auf GDGTs im Hypolimnion verdeutlichte.

Oberflächensedimentproben unter der oxischen Wassersäule wiesen aufgrund der sedimentären Produktion von brGDGT IIIa niedrigere MBT'5ME-Werte auf. Für die Rekonstruktion des Paläoklimas wurde daher die Entnahme von Bohrkernen im oxischen Teil von saisonal geschichteten Seen vorgeschlagen. Dieser Ansatz vermeidet den Einfluss der Wasserchemie auf GDGT-Signale im Hypolimnion.

Die Analyse der brGDGT-Variationen im Rotseesedimentkern gewährte Einblicke in die Umweltgeschichte des Sees und das Zusammenspiel von brGDGTs. Der Kern, der ein kaltes Glazial-Interstadial aufzeichnete, zeigte auch GDGT-Variationen im Holozän, basierend auf den Durchmischungsregimen des Sees. Insbesondere die erhöhten brGDGT Ia-Werte während oligotropher Phasen lieferten Beweise für die Wassersäulenschichtung und bestätigten deren Rolle als Epilimnion-spezifische Klimamarker.

Während die Verbindung zwischen MBT'5ME und der Temperatur im Epilimnion während oligotropher Phasen etabliert wurde, zeigte die eutrophe Phase Einflüsse des Hypolimnions und potenzielle Komplexitäten in MBT'5ME und IR aufgrund der Wasserchemie. Die Entnahme von Bohrkernen in der oxischen Zone des Sees erwies sich als effektiv für die Verwendung von MBT'5ME als Paläothermometer.

Diese Ergebnisse haben erhebliche Auswirkungen auf die Paläoklimaforschung unter Verwendung von brGDGTs und unterstreichen die Notwendigkeit, saisonale Schichtung bei der Interpretation paläoklimatischer Daten zu berücksichtigen, anstatt sich nur auf Temperaturänderungen zu konzentrieren.

Chapter 1

1. Introduction

In the pursuit of a deeper understanding of Earth's climate system and the factors driving its changes, reliable paleoclimatic data emerges as a critical resource. Paleoclimate records offer invaluable insights into the planet's past climatic variability and enhance our understanding of diverse effects of global warming (Pancost, 2017; Tierney et al., 2020). On long timescales, paleoclimate reconstruction allows to illustrate the earth's climate system in hothouse or coolhouse conditions, grounding our understanding in the context of Earth's climatic history (Esper and Buntgen., 2021). Similarly, a temperature reconstruction of the last 12000 years, a period of relative climate stability called the Holocene, allows to construct a more accurate and comprehensive perspective on the sensitivity of our planet on the impact of anthropogenic climate change (e.g. Kaufman and Broadman, 2023).

The central role of reconstructing lake surface temperatures to allow an estimate of local temperature variability as part of the global climate system, cannot be overstated (Sachs et al., 2013; Smittenberg, 2023; Sinninghe Damsté et al., 2012; Russell et al., 2018).

Traditional plant and animal fossil remains, such as pollen, chironomids, and $\delta^{18}\text{O}$ of diatoms, have proven effective in reconstructing paleoclimate in various lacustrine systems (Ramos-Roman et al., 2018; Velle et al., 2005; Leng et al., 2005). Nevertheless, these methods have inherent limitations, including the need for taxonomic identification and large sample volumes. As such the development of molecular-proxy studies bring numerous benefits compared to previous methods. Using sensitive analytical platforms such as gas and liquid chromatography, allows us to work with smaller sample sizes, and the ongoing discovery of new proxies, facilitated by lipid biomarkers, strengthens our capabilities in this field (Eglinton and Eglinton, 2008; Inglis et al., 2022). Specifically, the significant progress made by the development of organic geochemical techniques, targeting a suite of lipid classes (e.g. archaeal or bacterial membrane lipids, plant waxes) for environmental and temperature reconstructions has generated more reliable paleotemperature reconstructions (Berke. 2018). As our understanding of the temperature response of these paleoclimate tools is fundamental, here, we outline the current understanding of a widely used group of bacterial membrane-spanning lipid biomarkers branched GDGTs used in this study.

1.1. BrGDGTs as paleoclimate proxies

For some time now bacterial membrane spanning lipids; branched glycerol dialkyl glycerol tetraethers (brGDGTs), have been used as paleoclimate indicators in geological archives such as paleosoils (Peterse et al., 2011; Zang et al., 2018), marine (Zell et al., 2014; Xiao et al., 2016) and lake sediments (Loomis et al., 2014; Dang et al., 2018). Originally retrieved from modern peat (Sinninghe Damsté et al., 2000) and mineral soils (Weijers et al., 2006), these compounds contain two glycerol backbones attached to two branched alkyl chains with four ether bonds (Fig. 1), (Sinninghe Damsté et al., 2000; Weijers et al., 2006). Because of the stereochemistry of the brGDGT glycerol group, these lipids were clearly assigned to a bacterial source (Weijers et al., 2006).

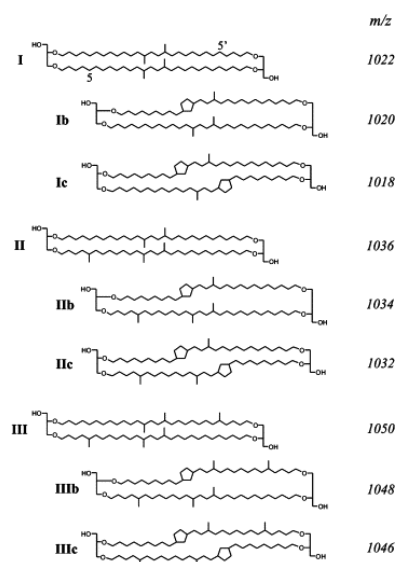


Fig. 1. Original structural diversity of brGDGT membrane lipids (Weijers et al., 2006)

These membrane-spanning lipids have been identified to possess varying numbers of methyl branches, with compounds containing 4 (tetramethylated), 5 (pentamethylated), and 6 (hexamethylated), denoted as brGDGTs Ia, IIa, and IIIa, respectively (Fig. 1). Subsequent internal cyclization of the methyl branches leads to the formation of brGDGT compounds with 1 or 2 cyclopentane moieties, labeled as brGDGT Ib, Ic, IIb, IIc, IIIb, and IIIc (Weijers et al., 2006). Following a first analysis of a dataset of 130 globally distributed soils, brGDGT distribution was linked to soil temperature and pH (Weijers et al., 2007). To summarize changes in brGDGTs distribution, two paleoclimate ratios (indices) were formulated; with the MBT index (Methylation of branched tetraethers) capturing changes methylation while the CBT index (cyclization of branched tetraethers) was proposed to summarize changes in the relative abundance of brGDGTs with cyclopentane moieties (Eqs. 1-2, respectively).

$$MBT = \frac{Ia+Ib+Ic}{Ia+Ib+Ic+IIa+IIb+IIc+IIIa+IIIb+IIIc} \quad [Eq. 1]$$

$$CBT = -\log \frac{Ib+IIb}{Ia+Ib+Ic+IIa+IIb+IIc} \quad [\text{Eq. 2}]$$

The MBT was shown to correlate strongly with Mean Annual Air Temperature (MAAT) in soils and less significantly with the soil pH (Weijers et al., 2007), producing the equation below:

$$MBT = 0.867 - 0.096 * pH + 0.021 * MAAT \quad [r^2=0.82, p<0.0001] \quad [\text{Eq. 3}]$$

The CBT, however, due to a nonlinear trend, has been correlated with pH on a negative log scale as described above, producing the equation:

$$CBT = 3.33 - 0.38 * pH \quad [r^2=0.70, p<0.0001] \quad [\text{Eq. 4}]$$

With the MBT correlating with both the soil pH and MAAT, a pH-correction (using the CBT) was needed when reconstructing temperature. Subsequently, the MBT and CBT ratios were modified after inclusion of a wider range of local-global soils in the calibration (Peterse et al., 2012). Nevertheless, the residual standard mean error (RSME) of the calibration remained high with 5.7 °C.

De Jonge et al. (2013) found that the pentamethylated brGDGTs (IIa, IIb, IIc, IIIa, IIIb, IIIc) were all composed of 2 previously coeluting isomers (Fig. 2). Instead of having a branch located only on α - and/or ω -5 methyl (so-called 5-methyl brGDGTs), an alternative structure exists where the branch is located on the α - and/or ω -6 methyl position (so-called 6-methyl brGDGTs). After analysis of the dataset of globally distributed soils, to allow quantification of all 15 brGDGT compounds, De Jonge et al. (2014a) showed that with the exclusion of 6-methyl methylated brGDGTs (II'-III'), the calibration between the MBT index (now: MBT'_{5ME}, equation 3) and measured MAAT became pH-independent. Furthermore, both the presence of cyclopentane-containing brGDGT Ic, and the relative increase of 6-methyl brGDGTs compared with their 5-methyl counterparts was now captured in the novel CBT' ratio.

$$MBT'_{5ME} = \frac{Ia+Ib+Ic}{Ia+Ib+Ic+IIa+IIb+IIc+IIIa} \quad [\text{Eq. 5}]$$

$$CBT' = 10_{\log} \frac{Ic+IIa'+IIb'+IIc'+IIIa'+IIIb'+IIIc'}{Ia+Ib+Ic+IIa+IIb+IIc+IIIa} \quad [\text{Eq. 6}]$$

The improved MBT'_{5ME} and CBT' yielded well-correlated MAAT and pH calibrations:

$$MAAT = -8.57 + 31.45 * MBT'_{5ME} \quad [r^2=0.66, RSME=4.8 \text{ °C}] \quad [\text{Eq. 7}]$$

$$pH = 7.15 + 1.59 * CBT' \quad [r^2=0.85, p\text{-value}<0.0001] \quad [\text{Eq. 8}]$$

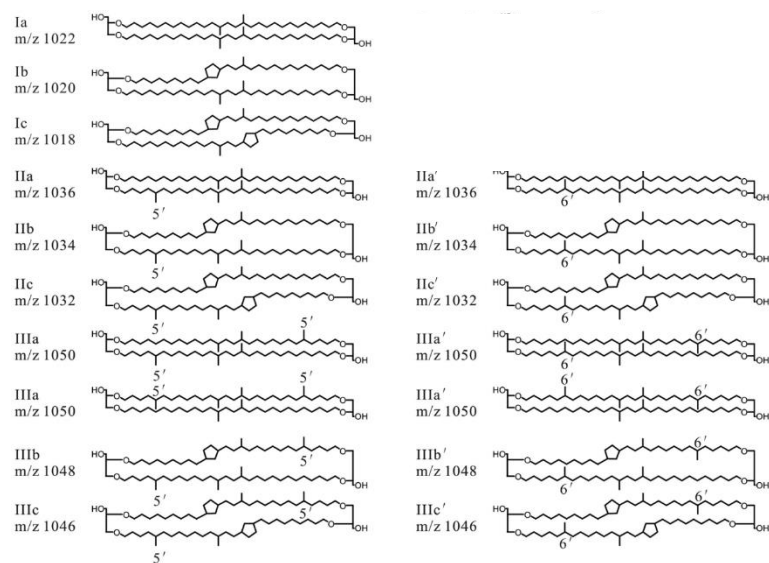


Fig. 2: Structural variability of brGDGTs after separation of 5 and 6-methyl isomers used in the MBT'_{5ME} and CBT' ratios (after: De Jonge et al., 2014a).

Similar to the observation done by Weijers et al., (2007), i brGDGTs distribution in temperate and cold environments were characterized by increased fractional abundances of 5-methyl pentamethylated (brGDGTs IIa, IIb, IIc) and 5-methyl hexamethylated brGDGTs (brGDGTs IIIa, IIIb, IIIc), resulting in a strong correlation between MBT'_{5ME} and MAT values ($r^2 = 0.66$; De Jonge et al., 2014a). Correspondingly, the fractional abundance of 6-methyl compounds increased with increasing soil pH ($r^2 = 0.85$, De Jonge et al., 2014a).

1.2. Core lipid (CL) and Intact Polar (IPL) GDGTs

In the environment, brGDGTs can be encountered either as core lipids (CL: Fig. 2), or as intact polar lipids attached to glyco- or phospho-lipid headgroups (Liu et al., 2010; Peterse et al., 2011). Their diversity in soils was described to include glucuronosyl and glucosyl (Liu et al., 2010; Raberg et al., 2022) and hexose-glycuronic acid, phospho-hexose, or hexose-phosphoglycerol head groups (Peterse et al., 2011). In lake surface sediments, a large variability in brGDGT headgroup composition was observed, with a larger contribution of phosphohexose headgroups compared to surrounding soils (Raberg et al., 2022). However, upon initiation of cell degradation (typically cell lysis), these polar headgroups are cleaved relatively quickly (Peterse et al., 2011; Tierney et al., 2012) and convert into the more rigid core lipid format (CL). Consequently, IPL brGDGTs have been proposed to serve as indicators of living or recently living microbes (Harvey et al., 1986; Pitcher et al., 2011; Liu et al., 2010; Peterse et al., 2011; Raberg et al., 2022) whereas the “broken” GDGT core lipid (CL) is interpreted as the aged or fossil lipid pool. Still, most extraction

methods used for paleoclimate reconstructions, where a dominance of CL brGDGT is assumed, convert all available IPL lipids to their core lipid counterpart by hydrolyzation of these headgroups (Weber et al., 2018). Only when performing modern distribution studies, IPL, and CL lipids are often considered separately (i.e. Zink and Mangelsdorf., 2004, Tierney et al., 2012; Raberg et al., 2022), since this distinction helps to understand the recent response of bacteria to environmental changes.

However, different headgroups potentially show different degradation rates, as was shown for archaeal isoprenoid GDGT lipids in marine sediments (Lengger et al., 2014) and for bacterial brGDGT lipids in lacustrine sediments (Raberg et al., 2022). Furthermore, it is currently not clear whether all brGDGTs are present as IPLs in bacterial membranes of cultured GDGT producers, as the extraction methods employed (acid hydrolysis) would transfer any IPLs into their CL counterpart (Halamka et al., 2022; Chen et al., 2022). This raises the possibility that not all IPL GDGTs represent living or recently living bacterial biomass and are instead aged, while CL GDGTs may be modern and contemporary with IPL brGDGTs.

1.3. In-situ production of brGDGTs in freshwater systems and calibrations

Initially, brGDGTs found in marine and lacustrine sediments, were assumed to be mainly soil-derived. However, it has since been confirmed that they are also produced within the water column of freshwater systems (lake and river; De Jonge et al., 2014b; Loomis et al., 2014; Russell et al. 2018; Martínez-Sosa et al., 2020), and the surface sediments (Pearson et al., 2011; Tierney et al., 2012; Buckles et al., 2014a; Stefanescu et al., 2021; Zhao et al., 2021; Raberg et al., 2022).

Generally, the study of brGDGT production in freshwater environments has been performed by comparing the brGDGT signal in lacustrine surface sediment, with that in surrounding watershed soils. For instance, the total concentration (normalized per TOC) of brGDGTs in sediments of Lower King Pond Lake are reported to be double as reported in the watershed soils (Loomis et al., 2014). Furthermore, the distribution has shifted, with the highest relative abundance of methylated compound Ia in soils and IIIa [IIIa+IIIa', as measured on single column method] in lake sediments, respectively. The overall methylation of brGDGTs is reported to be higher in sediments than in soils, which agrees well with the results from other temperate lakes (Tierney et al., 2012; Martínez-Sosa et al., 2020). Lately, brGDGT production in the water column has been targeted more specifically, by analyzing brGDGTs in suspended particulate matter and/or surface sediment traps (Zink et al., 2010; Loomis et al., 2014; Russell et al., 2018; Raberg et al., 2022). And only recently, experimental approaches have been applied (Martínez-Sosa et al., 2019; 2020) to investigate GDGT variability of water column.

Though the study of brGDGTs in freshwater is relatively novel, there is a growing consensus that the brGDGT in lacustrine sediments are dominantly lake-derived (Tierney et al., 2012; Buckles et al., 2014b; Russell et al., 2018; Martínez-Sosa et al., 2020; Zhao et al., 2021). While it's worth noting that many

lacustrine calibrations primarily reconstruct air temperatures rather than lake temperatures, it is, in fact, the latter that directly influence the in-situ production of brGDGTs within the water column (Loomis et al., 2012). Nonetheless, there has been a strong correlation observed between Mean Annual Air Temperature (MAAT) and real-time lake temperature on large spatial scales ($r^2 = 0.98$, $p\text{-value} < 0.0001$) (Loomis et al., 2017; Russell et al., 2018). This relationship suggests that calibrations based on MAAT or Mean Air temperatures during months above Freezing (MAF °C) can be deemed reliable for accurate lake temperature reconstructions.

As the temperature dependency between the brGDGTs and MAF °C is different compared to soil calibrations (Fig. 3A), several lacustrine calibrations have been developed to reconstruct MAAT and/or MAF. For instance, employing MBT_{5ME} linear transfer functions (Russell et al., 2018, MAAT, RMSE= 2.4 °C), Bayesian regression (Martínez-Sosa et al., 2021, MAF, RMSE= 2.7 °C, Fig. 3A), multiple linear regression of individual fractional abundances (Raberg et al., 2021, MAF, RMSE= 1.97 °C, Fig. 3B) and stepwise forward selection models (Bauersachs et al., 2024, RMSE= 1.47 °C). Although MBT_{5ME} correlates well with MAF over large spatial scales, the slope and intercept of these regressions can be different (Fig. 3).

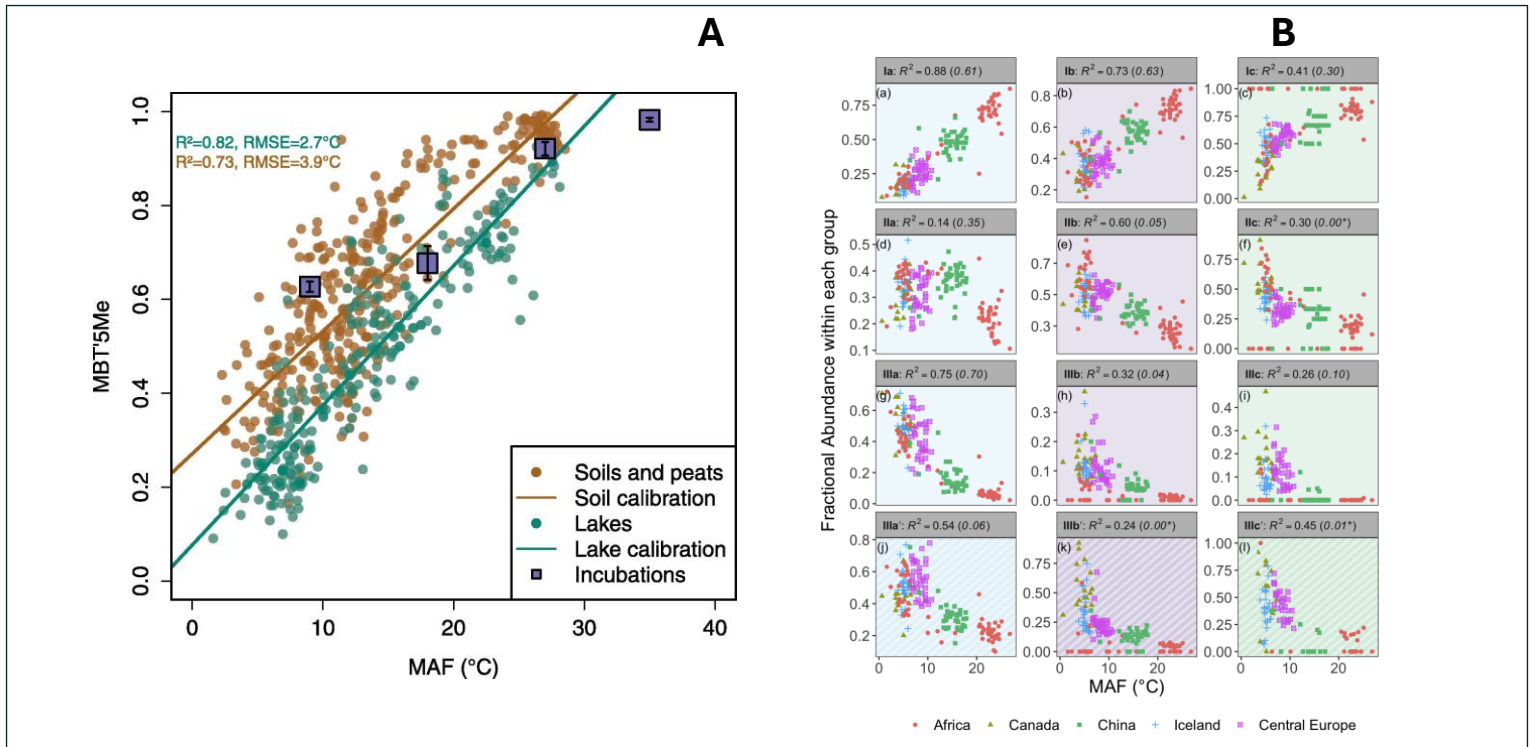


Fig. 3. (A) the MBT_{5ME} plotted against Mean Annual temperature above Freezing (MAF; Martínez-Sosa et al., (2021)) and (B) fractional abundance of brGDGTs within each group plotted against MAF (Raberg et al., (2021)). r^2

values reported for each graph in panel B depict the respective compounds correlation with MAF (°C) and r^2 values for the standard Full FAs given in parentheses for comparison.

1.4. Seasonality

While lacustrine calibrations on large spatial scales generally correlate brGDGT distribution against mean annual temperature, several authors have proposed that the brGDGT lipids produced rather reflect a given season (Loomis et al., 2014; Deng et al., 2016; Cao et al., 2018). Specifically, seasonal changes in brGDGT concentrations and distributions in lakes have been observed to vary with environmental parameters seasonally, with reported increases in brGDGT concentration during spring and fall isothermal mixing (Loomis et al., 2014; Miller et al., 2018). This can introduce a seasonal production bias (Loomis et al., 2014; Miller et al., 2018), and it remains unclear whether changes in water temperature, water chemistry (e.g., dissolved oxygen), or bacterial community composition are the underlying drivers (Shade et al., 2007).

Considering such observations, seasonality has been vaguely defined in the existing literature, and often refers to one of the two parameters discussed below. Firstly, there is the ‘seasonal range’, which depicts the temperature difference between the coldest and warmest months and is a parameter discussed mainly in soil studies (Lei et al., 2016, Wang et al., 2018). Secondly, the so-called ‘seasonal variability’, defines the changes in brGDGTs production between seasons and is often used in lacustrine systems where these changes can be observed (Woltering et al., 2012, Loomis et al., 2014). Here, the latitudinal aspect of the study location will determine both the seasonal range and the presence and timing of seasonal variability. For instance, the seasonal cycle in a tropical location is smaller compared to a temperate location such as Switzerland, where the maxima (summer) and minima (winter) of a seasonal cycle are considerably more divergent (-2-26°C; source: meteoswiss.admin.ch).

Moreover, it is important to bear in mind that both ‘seasonal range’ and ‘seasonal variability’ can vary over large timescales (i.e. centuries, millennia and etc.), as seasonal range and variability of solar insolation changes. This becomes especially crucial to consider when reconstructing paleoclimate conditions as they are usually examined over geological timescales.

1.5. Bacterial source organisms of brGDGTs

Previous environmental research has consistently highlighted the potential role of Acidobacteria as significant contributors to GDGT production in terrestrial ecosystems, particularly in soil environments (Weijers et al., 2009; Peterse et al., 2010; De Jonge et al., 2019). This hypothesis gains substantial support from the presence of iso-diabolic acids, which are considered precursors of brGDGT lipids, within the cell

membranes of Acidobacteria subdivisions 1, 3, 4, and 6 (Sinninghe Damsté et al., 2011, 2014, 2018). Notably, certain Acidobacterial strains, including *A2-4c* and *E. aggregans Wbg-1* (both from Acidobacteria subgroup 1), have been observed to produce trace amounts of brGDGT Ia (Sinninghe Damsté et al., 2011). Furthermore, controlled experiments with pure cultures have unequivocally demonstrated the capability of *Solibacter usitatus*, a member of Acidobacteriaceae (Acidobacteria Subgroup 1), to synthesize brGDGTs Ia, IIa, IIIa, Ib, I Ib (Chen et al., 2022; Halamka et al., 2022). Nevertheless, not all 15 known brGDGT compounds identified in both soil and aquatic ecosystems, have yet been detected in pure culture experiments. Moreover, recent research has shed light on the existence of biosynthetic genes potentially linked to GDGT production across a wide spectrum of bacterial phyla (Sahonero-Canavesi et al., 2022; Zeng et al., 2022).

The phylogenetic diversity of potential brGDGT producers is expected to vary between soil and freshwater environments, primarily due to distinct differences in the distribution of brGDGTs between these two habitats (Weber et al., 2018). In addition, Acidobacteria are relatively scarce in freshwater (Parfenova et al., 2013; Dedysh and Sinninghe Damsté, 2018; Weber et al., 2018; Van Bree et al., 2020), accounting for only 0.1% of the prokaryotic population in environments such as African Lake Challa (Van Bree et al., 2020). While some freshwater studies have proposed specific bacterial candidates, including Acidobacteria, Actinobacteria, Chloroflexi, and Firmicutes, as potential producers of various brGDGT compounds (Weber et al., 2018, Van Bree et al., 2020), the full extent of possible brGDGT producers in freshwater ecosystems remains an ongoing area of investigation. The potential diversity in brGDGT producers (Parfenova et al., 2013; Dedysh and Sinninghe Damsté, 2018; Weber et al., 2018; Van Bree et al., 2020) can be particularly significant in the context of the water column.

1.6. Direct versus indirect environmental impacts on brGDGTs

The potential wide range of bacterial producers of brGDGTs raises a fundamental question regarding the mechanism that causes the observed changes in GDGT compositions. It is well-established that many bacteria have the capacity to modify the chemical compositions of their membrane lipids in response to temperature variations (e.g., De Rosa, 1980), a phenomenon commonly referred to as "homeoviscous adaptation" (Sinenski, 1974). Indeed, there is substantial evidence to suggest that this mechanism, physiological adaptations to temperature of the membrane, plays a significant role in determining the GDGT composition. Modeling studies have demonstrated the potential impact of altered GDGT composition on membrane fluidity, supporting the idea that microorganisms adjust their membrane lipid structures in response to changing temperature conditions (Naafs et al., 2021). On the other hand, environmental soil studies have shown that shifts in the composition of microbial communities are coeval

with changes in brGDGT lipid concentration and distribution (De Jonge et al., 2019, 2021). The impact of changing abundance of Acidobacterial subgroups on brGDGTs on the GDGT distribution in soils is supported by the presence of distinct precursors for 5-methyl and 6-methyl brGDGTs in pure cultures that are derived from different subgroups (Sinninghe Damsté et al., 2018). In freshwater systems similarly, changes in brGDGTs that are coeval with bacterial community changes have been reported across the redox gradient in the water column of a Swiss lake (Weber et al., 2018). However, it remains unverified whether changes in the bacterial community directly drive the variations in brGDGT distribution.

1.7. Lake Rot (Rotsee) and Sihl River as unique settings

Lake Rot (Rotsee, 47°21'05.8" N; 8°31'12.7" E) is a small prealpine lake with a surface area of 0.48 km² and maximum depth of 16 m. This eutrophic lake follows a monomictic regime, featuring seasonal water column isothermal stratification that results in hypolimnion anoxia typically occurring during August and September. Sihl River with a 68 km length, is a subalpine river flowing from Drusberg (at 1872 m altitude) to the catchment mouth (402 m altitude) in canton of Zurich (Schwab et al., 2022). Climatic data from the 1961–1990 period reveals average July and annual air temperatures of 15.8°C and 9°C, respectively, for the region (source: www.MeteoSchweiz.ch, last access: 15 Dec 2023). These freshwater systems are both targeted to determine the unique effect of temperature on the brGDGT distribution. In addition, considering the seasonality of temperature and oxygenation of the Lake Rot water column, investigating the GDGT variability throughout the year is possible. Extending this analysis to encompass longer timescales, such as the Holocene, can prove promising for gaining fresh insights into how GDGTs respond to environmental changes across various temporal scales.

Bibliography, Chapter 1

Bauersachs, T., Schubert, C. J., Mayr, C., Gilli, A., and Schwark, L. (2024). Branched GDGT-based temperature calibrations from Central European lakes. *Science of The Total Environment*, 906, 167724.

Berke, M. A. (2018). Reconstructing terrestrial paleoenvironments using sedimentary organic biomarkers. *Methods in paleoecology: Reconstructing Cenozoic terrestrial environments and ecological communities*, 121-149.

Brown, J. L., Hill, D. J., Dolan, A. M., Carnaval, A. C., and Haywood, A. M. (2018). PaleoClim, high spatial resolution paleoclimate surfaces for global land areas. *Scientific data*, 5(1), 1-9.

Buckles, L. K., Weijers, J. W., Verschuren, D., and Sinninghe Damsté, J. S. (2014a). Sources of core and intact branched tetraether membrane lipids in the lacustrine environment: Anatomy of Lake Challa and its catchment, equatorial East Africa. *Geochimica et Cosmochimica Acta*, 140, 106-126.

Buckles, L. K., Weijers, J. W. H., Tran, X. M., Waldron, S., and Sinninghe Damsté, J. S. (2014b). Provenance of tetraether membrane lipids in a large temperate lake (Loch Lomond, UK): implications for glycerol dialkyl glycerol tetraether (GDGT)-based palaeothermometry. *Biogeosciences*, 11(19), 5539-5563.

Cao, M., Rueda, G., Rivas-Ruiz, P., Trapote, M. C., Henriksen, M., Vegas-Vilarrúbia, T., and Rosell-Melé, A. (2018). Branched GDGT variability in sediments and soils from catchments with marked temperature seasonality. *Organic Geochemistry*, 122, 98-114.

Chen, Y., Zheng, F., Yang, H., Yang, W., Wu, R., Liu, X., Liang, H., Chen, H., Pei, H., Zhang, C., Pancost, R.D., Zeng, Z. (2022). The production of diverse brGDGTs by an Acidobacterium providing a physiological basis for paleoclimate proxies. *Geochimica et Cosmochimica Acta*, 337, 155-165.

Sinninghe Damsté, J. S., Hopmans, E. C., Pancost, R. D., Schouten, S., and Geenevasen, J. A. (2000). Newly discovered non-isoprenoid glycerol dialkyl glycerol tetraether lipids in sediments. *Chemical Communications*, (17), 1683-1684.

Dang, X., Ding, W., Yang, H., Pancost, R. D., Naafs, B. D. A., Xue, J., Xiao, L., Jiyai, L., and Xie, S. (2018). Different temperature dependence of the bacterial brGDGT isomers in 35 Chinese lake sediments compared to that in soils. *Organic Geochemistry*, 119, 72-79.

De Jonge, C., Hopmans, E. C., Stadnitskaia, A., Rijpstra, W. I. C., Hofland, R., Tegelaar, E., and Sinninghe Damsté, J. S. (2013). Identification of novel penta- and hexamethylated branched glycerol dialkyl glycerol tetraethers in peat using HPLC-MS2, GC-MS and GC-SMB-MS. *Organic geochemistry*, 54, 78-82.

- De Jonge, C., Hopmans, E. C., Zell, C. I., Kim, J. H., Schouten, S., and Sinninghe Damsté, J. S. (2014a). Occurrence and abundance of 6-methyl branched glycerol dialkyl glycerol tetraethers in soils: Implications for palaeoclimate reconstruction. *Geochimica et Cosmochimica Acta*, *141*, 97-112.
- De Jonge, C., Stadnitskaia, A., Hopmans, E. C., Cherkashov, G., Fedotov, A., and Sinninghe Damsté, J. S. (2014b). In situ produced branched glycerol dialkyl glycerol tetraethers in suspended particulate matter from the Yenisei River, Eastern Siberia. *Geochimica et Cosmochimica Acta*, *125*, 476-491.
- De Jonge, C., Radujković, D., Sigurdsson, B. D., Weedon, J. T., Janssens, I., and Peterse, F. (2019). Lipid biomarker temperature proxy responds to abrupt shift in the bacterial community composition in geothermally heated soils. *Organic Geochemistry*, *137*, 103897.
- De Jonge, C., Kuramae, E. E., Radujković, D., Weedon, J. T., Janssens, I. A., and Peterse, F. (2021). The influence of soil chemistry on branched tetraether lipids in mid-and high latitude soils: Implications for brGDGT-based paleothermometry. *Geochimica et Cosmochimica Acta*, *310*, 95-112.
- De Rosa, M., Esposito, E., Gambacorta, A., Nicolaus, B., and Bu'Lock, J. D. (1980). Effects of temperature on ether lipid composition of *Caldariella acidophila*. *Phytochemistry*, *19*(5), 827-831.
- Dedysh, S. N., and Sinninghe Damsté, J. S. (2018). Acidobacteria. *eLS*, 1-10.
- Eglinton, T. I., and Eglinton, G. (2008). Molecular proxies for paleoclimatology. *Earth and Planetary Science Letters*, *275*(1-2), 1-16.
- Esper, J., and Büntgen, U. (2021). The future of paleoclimate. *Climate Research*, *83*, 57-59.
- Halamka, T. A., Raberg, J. H., McFarlin, J. M., Younkin, A. D., Mulligan, C., Liu, X. L., and Kopf, S. H. (2022). Production of diverse brGDGTs by *Acidobacterium Solibacter usitatus* in response to temperature, pH, and O₂ provides a culturing perspective on brGDGT proxies and biosynthesis. *Geobiology*, *21*(1), 102-118.
- Harvey, H. R., Fallon, R. D., and Patton, J. S. (1986). The effect of organic matter and oxygen on the degradation of bacterial membrane lipids in marine sediments. *Geochimica et Cosmochimica Acta*, *50*(5), 795-804.
- Inglis, G. N., Bhattacharya, T., Hemingway, J. D., Hollingsworth, E. H., Feakins, S. J., and Tierney, J. E. (2022). Biomarker approaches for reconstructing terrestrial environmental change. *Annual Review of Earth and Planetary Sciences*, *50*, 369-394.

- Kaufman, D. S., & Broadman, E. (2023). Revisiting the Holocene global temperature conundrum. *Nature*, 614(7948), 425-435.
- Lei, Y., Yang, H., Dang, X., Zhao, S., and Xie, S. (2016). Absence of a significant bias towards summer temperature in branched tetraether-based paleothermometer at two soil sites with contrasting temperature seasonality. *Organic Geochemistry*, 94, 83-94.
- Leng, M. J., Metcalfe, S. E., & Davies, S. J. (2005). Investigating Late Holocene climate variability in central Mexico using carbon isotope ratios in organic materials and oxygen isotope ratios from diatom silica within lacustrine sediments. *Journal of Paleolimnology*, 34, 413-431.
- Lengger, S. K., Hopmans, E. C., Sinninghe Damsté, J. S., and Schouten, S. (2014). Fossilization and degradation of archaeal intact polar tetraether lipids in deeply buried marine sediments (Peru Margin). *Geobiology*, 12(3), 212-220.
- Liu, X. L., Leider, A., Gillespie, A., Gröger, J., Versteegh, G. J., and Hinrichs, K. U. (2010). Identification of polar lipid precursors of the ubiquitous branched GDGT orphan lipids in a peat bog in Northern Germany. *Organic Geochemistry*, 41(7), 653-660.
- Loomis, S. E., Russell, J. M., Ladd, B., Street-Perrott, F. A., and Sinninghe Damsté, J. S. (2012). Calibration and application of the branched GDGT temperature proxy on East African lake sediments. *Earth and Planetary Science Letters*, 357, 277-288.
- Loomis, S. E., Russell, J. M., Heurix, A. M., D'Andrea, W. J., and Sinninghe Damsté, J. S. (2014). Seasonal variability of branched glycerol dialkyl glycerol tetraethers (brGDGTs) in a temperate lake system. *Geochimica et Cosmochimica Acta*, 144, 173-187.
- Loomis, S. E., Russell, J. M., Verschuren, D., Morrill, C., De Cort, G., Sinninghe Damsté, J. S., Olago, D., Eggermont, H., Street-Perrott, F., and Kelly, M. A. (2017). The tropical lapse rate steepened during the Last Glacial Maximum. *Science advances*, 3(1), e1600815.
- Martínez-Sosa, P., and Tierney, J. E. (2019). Lacustrine brGDGT response to microcosm and mesocosm incubations. *Organic Geochemistry*, 127, 12-22.
- Martínez-Sosa, P., Tierney, J. E., and Meredith, L. K. (2020). Controlled lacustrine microcosms show a brGDGT response to environmental perturbations. *Organic Geochemistry*, 145, 104041.
- Martínez-Sosa, P., Tierney, J. E., Stefanescu, I. C., Crampton-Flood, E. D., Shuman, B. N., and Routson, C. (2021). A global Bayesian temperature calibration for lacustrine brGDGTs. *Geochimica et Cosmochimica Acta*, 305, 87-105.

- Miller, D. R., Habicht, M. H., Keisling, B. A., Castañeda, I. S., and Bradley, R. S. (2018). A 900-year New England temperature reconstruction from in situ seasonally produced branched glycerol dialkyl glycerol tetraethers (brGDGTs). *Climate of the Past*, 14(11), 1653-1667.
- Naafs, B. D. A., Oliveira, A. S. F., and Mulholland, A. J. (2021). Molecular dynamics simulations support the hypothesis that the brGDGT paleothermometer is based on homeoviscous adaptation. *Geochimica et Cosmochimica Acta*, 312, 44-56.
- Naeher, S., Peterse, F., Smittenberg, R. H., Niemann, H., Zigah, P. K., and Schubert, C. J. (2014). Sources of glycerol dialkyl glycerol tetraethers (GDGTs) in catchment soils, water column and sediments of Lake Rotsee (Switzerland)—Implications for the application of GDGT-based proxies for lakes. *Organic Geochemistry*, 66, 164-173.
- Pancost, R. D. (2017). Climate change narratives. *Nature Geoscience*, 10(7), 466-468.
- Parfenova, V. V., Gladkikh, A. S., and Belykh, O. I. (2013). Comparative analysis of biodiversity in the planktonic and biofilm bacterial communities in Lake Baikal. *Microbiology*, 82, 91-101.
- Pearson, E. J., Juggins, S., Talbot, H. M., Weckström, J., Rosén, P., Ryves, D. B., Roberts, S. J., and Schmidt, R. (2011). A lacustrine GDGT-temperature calibration from the Scandinavian Arctic to Antarctic: Renewed potential for the application of GDGT-paleothermometry in lakes. *Geochimica et Cosmochimica Acta*, 75(20), 6225-6238.
- Peterse, F., Nicol, G. W., Schouten, S., and Sinninghe Damsté, J. S. (2010). Influence of soil pH on the abundance and distribution of core and intact polar lipid-derived branched GDGTs in soil. *Organic Geochemistry*, 41(10), 1171-1175.
- Peterse, F., Hopmans, E. C., Schouten, S., Mets, A., Rijpstra, W. I. C., and Sinninghe Damsté, J. S. (2011). Identification and distribution of intact polar branched tetraether lipids in peat and soil. *Organic Geochemistry*, 42(9), 1007-1015.
- Peterse, F., van der Meer, J., Schouten, S., Weijers, J. W., Fierer, N., Jackson, R. B., Jung-Hyun, K., and Sinninghe Damsté, J. S. (2012). Revised calibration of the MBT–CBT paleotemperature proxy based on branched tetraether membrane lipids in surface soils. *Geochimica et Cosmochimica Acta*, 96, 215-229.
- Raberg, J. H., Harning, D. J., Crump, S. E., de Wet, G., Blumm, A., Kopf, S., Geirsdóttir, A., Miller, G. H., and Sepúlveda, J. (2021). Revised fractional abundances and warm-season temperatures substantially improve brGDGT calibrations in lake sediments. *Biogeosciences*, 18(12), 3579-3603.

Raberg, J. H., Flores, E., Crump, S. E., de Wet, G., Dildar, N., Miller, G. H., Geirsdóttir, A., and Sepúlveda, J. (2022). Intact polar brGDGTs in Arctic lake catchments: Implications for lipid sources and paleoclimate applications. *Journal of Geophysical Research: Biogeosciences*, 127(10), e2022JG006969.

Ramos-Román, M. J., Jiménez-Moreno, G., Camuera, J., García-Alix, A., Anderson, R. S., Jiménez-Espejo, F. J., and Carrión, J. S. (2018). Holocene climate aridification trend and human impact interrupted by millennial-and centennial-scale climate fluctuations from a new sedimentary record from Padul (Sierra Nevada, southern Iberian Peninsula). *Climate of the Past*, 14(1), 117-137.

Russell, J. M., Hopmans, E. C., Loomis, S. E., Liang, J., and Sinninghe Damsté, J. S. (2018). Distributions of 5-and 6-methyl branched glycerol dialkyl glycerol tetraethers (brGDGTs) in East African lake sediment: Effects of temperature, pH, and new lacustrine paleotemperature calibrations. *Organic Geochemistry*, 117, 56-69.

Sachs, J. P., Pahnke, K., Smittenberg, R., and Zhang, Z. (2013). Biomarker indicators of past climate. *Encyclopedia of Quaternary science*, 775-779.

Sahonero-Canavesi, D. X., Siliakus, M. F., Abdala Asbun, A., Koenen, M., von Meijenfeldt, F. B., Boeren, S., Bale, N. J., Engelman, J. C., Fiege, C., Strack van Schijndel, L., Sinninghe Damsté, J. S., Villanueva, L. (2022). Disentangling the lipid divide: Identification of key enzymes for the biosynthesis of membrane-spanning and ether lipids in Bacteria. *Science advances*, 8(50), eabq8652.

Schubert, C.J., Lucas, F.S., Durisch-Kaiser, E., Stierli, R., Diem, T., Scheidegger, O., Vazquez, F. and Müller, B., 2010. Oxidation and emission of methane in a monomictic lake (Rotsee, Switzerland). *Aquatic sciences*, 72, pp.455-466.

Schwab, M. S., Gies, H., Freymond, C. V., Lupker, M., Haghypour, N., and Eglinton, T. I. (2022). Environmental and hydrologic controls on sediment and organic carbon export from a subalpine catchment: insights from a time series. *Biogeosciences*, 19(23), 5591-5616.

Sinensky, M. (1974). Homeoviscous adaptation—a homeostatic process that regulates the viscosity of membrane lipids in *Escherichia coli*. *Proceedings of the National Academy of Sciences*, 71(2), 522-525.

Smittenberg, R. H. (2023). Biomarker indicators of past climate.

Stefanescu, I. C., Shuman, B. N., and Tierney, J. E. (2021). Temperature and water depth effects on brGDGT distributions in sub-alpine lakes of mid-latitude North America. *Organic Geochemistry*, 152, 104174.

Tierney, J. E., Schouten, S., Pitcher, A., Hopmans, E. C., and Sinninghe Damsté, J. S. (2012). Core and intact polar glycerol dialkyl glycerol tetraethers (GDGTs) in Sand Pond, Warwick, Rhode Island (USA): Insights into the origin of lacustrine GDGTs. *Geochimica et Cosmochimica Acta*, 77, 561-581.

Tierney, J.E., Poulsen, C.J., Montañez, I.P., Bhattacharya, T., Feng, R., Ford, H.L., Hönlisch, B., Inglis, G.N., Petersen, S.V., Sagoo, N. and Tabor, C.R., 2020. Past climates inform our future. *Science*, 370(6517), p.eaay3701.

Van Bree, L. G., Peterse, F., Baxter, A. J., De Crop, W., Van Grinsven, S., Villanueva, L., Verschren, D., Sinninghe Damsté, J. S. (2020). Seasonal variability and sources of in situ brGDGT production in a permanently stratified African crater lake. *Biogeosciences*, 17(21), 5443-5463.

Velle, G., Brooks, S. J., Birks, H. J. B., & Willassen, E. (2005). Chironomids as a tool for inferring Holocene climate: an assessment based on six sites in southern Scandinavia. *Quaternary Science Reviews*, 24(12-13), 1429-1462.

Wang, M., Zong, Y., Zheng, Z., Man, M., Hu, J., and Tian, L. (2018). Utility of brGDGTs as temperature and precipitation proxies in subtropical China. *scientific Reports*, 8(1), 194.

Weber, Y., Sinninghe Damsté, J. S., Zopfi, J., De Jonge, C., Gilli, A., Schubert, C. J., Lepori, L., Lehmann, M. F., Niemann, H. (2018). Redox-dependent niche differentiation provides evidence for multiple bacterial sources of glycerol tetraether lipids in lakes. *Proceedings of the National Academy of Sciences*, 115(43), 10926-10931.

Weijers, J.W., Schouten, S., Spaargaren, O.C. and Sinninghe Damsté, J.S., 2006. Occurrence and distribution of tetraether membrane lipids in soils: Implications for the use of the TEX86 proxy and the BIT index. *Organic Geochemistry*, 37(12), pp.1680-1693.

Weijers, J. W., Schouten, S., van den Donker, J. C., Hopmans, E. C., and Sinninghe Damsté, J. S. (2007). Environmental controls on bacterial tetraether membrane lipid distribution in soils. *Geochimica et Cosmochimica Acta*, 71(3), 703-713.

Weijers, J. W., Panoto, E., van Bleijswijk, J., Schouten, S., Rijpstra, W. I. C., Balk, M., Stams, A. J. M., Sinninghe Damsté, J. S. (2009). Constraints on the biological source (s) of the orphan branched tetraether membrane lipids. *Geomicrobiology Journal*, 26(6), 402-414.

Woltering, M., Werne, J. P., Kish, J. L., Hicks, R., Sinninghe Damsté, J. S., and Schouten, S. (2012). Vertical and temporal variability in concentration and distribution of thaumarchaeotal tetraether lipids in Lake

Superior and the implications for the application of the TEX86 temperature proxy. *Geochimica et Cosmochimica Acta*, 87, 136-153.

Xiao, W., Wang, Y., Zhou, S., Hu, L., Yang, H., and Xu, Y. (2016). Ubiquitous production of branched glycerol dialkyl glycerol tetraethers (brGDGTs) in global marine environments: a new source indicator for brGDGTs. *Biogeosciences*, 13(20), 5883-5894.

Zang, J., Lei, Y., and Yang, H. (2018). Distribution of glycerol ethers in Turpan soils: implications for use of GDGT-based proxies in hot and dry regions. *Frontiers of Earth Science*, 12, 862-876.

Zell, C., Kim, J. H., Hollander, D., Lorenzoni, L., Baker, P., Silva, C. G., Nittouer, C., Sinninghe Damsté, J. S. (2014). Sources and distributions of branched and isoprenoid tetraether lipids on the Amazon shelf and fan: Implications for the use of GDGT-based proxies in marine sediments. *Geochimica et Cosmochimica Acta*, 139, 293-312.

Zeng, Z., Chen, H., Yang, H., Chen, Y., Yang, W., Feng, X., Pei., H., and Welander, P. V. (2022). Identification of a protein responsible for the synthesis of archaeal membrane-spanning GDGT lipids. *Nature communications*, 13(1), 1545.

Zhao, B., Castañeda, I. S., Bradley, R. S., Salacup, J. M., de Wet, G. A., Daniels, W. C., and Schneider, T. (2021). Development of an in situ branched GDGT calibration in Lake 578, southern Greenland. *Organic Geochemistry*, 152, 104168.

Zink, K. G., and Mangelsdorf, K. (2004). Efficient and rapid method for extraction of intact phospholipids from sediments combined with molecular structure elucidation using LC–ESI–MS–MS analysis. *Analytical and Bioanalytical Chemistry*, 380, 798-812.

Zink, K. G., Vandergoes, M. J., Mangelsdorf, K., Dieffenbacher-Krall, A. C., and Schwark, L. (2010). Application of bacterial glycerol dialkyl glycerol tetraethers (GDGTs) to develop modern and past temperature estimates from New Zealand lakes. *Organic Geochemistry*, 41(9), 1060-1066.

Chapter 2

Seasonal Temperature Dependency of Aquatic Branched Glycerol Dialkyl Glycerol Tetraethers: A Mesocosm Approach (published in *Organic Geochemistry*, Volume 189, March 2024, 104742)

Ajalloeian Fatemeh ^{a*}, Deng Longhui ^b, Lever Mark A. ^{b, c}, De Jonge Cindy ^a

*Corresponding author: F. Ajalloeian– Fatemeh.ajalloeian@erdw.ethz.ch

a Geological Institute, Earth Science Department, ETH Zurich. Sonnegstrasse 5, 8092 Zurich, Switzerland.

b Institute of Biogeochemistry and Pollutant Dynamics, ETH Zurich, Universtitatstrasse 16, 8092 Zürich, Switzerland.

c Marine Science Institute, University of Texas at Austin, TX, Port Aransas, USA

Abstract

BrGDGTs, membrane-spanning lipids produced by bacteria are at the basis of the MBT'_{5ME}, a biomarker ratio that has been used as paleotemperature proxy. However, the response of the MBT'_{5ME} to temperature changes, particularly in freshwater systems, remains incompletely understood. In this study, oxic mesocosms are used to assess the temperature sensitivity of brGDGTs and their producers, sampled from a lake (Lake Rot) and river (Sihl River) in three different seasons. Three temperature treatments are employed (10-17.5-25°C), representing control (in-situ temperatures), cooling, and/or warming treatments, with GDGTs and the bacterial community measured at several timepoints (24h, 1, 2, 3 and 5 weeks). The control experiments showed that this experimental approach could not replicate natural conditions exactly, with small changes in chemistry (pH, conductivity, alkalinity) and bacterial community composition. Still, our mesocosm setup yielded valuable insights into the temperature-dependent production of lacustrine brGDGTs and MBT'_{5ME} values, especially in warming treatments, while no response was observed in cooling treatments, potentially indicating limited sensitivity to cold temperatures. In the river mesocosms not the MBT'_{5ME} but the IR ratio showed a temperature dependency, potentially driven by small changes in the water pH. Coeval changes in the composition of the bacterial community and the MBT'_{5ME} and IR are determined to constrain potential GDGT producers. Although an increase in MBT'_{5ME} in response to some warming incubations is observed, the temperature-sensitivity of MBT'_{5ME}, as expected from GDGT studies on a global scale, is not supported by this experiment.

1. Introduction

Quantitative continental temperature proxies, based on geological and biological indicators measured in ice cores, tree rings, sediment cores, or other environmental records are used to reconstruct past climatic conditions. These paleoclimate reconstructions are used to improve climate model predictions (Harning et al., 2020; Tierney et al., 2020). Providing more accurate values that allow for quantitative analyses of past temperature variations, aids in understanding the mechanism, magnitude, and frequency of past climate change (Marcott and Shakun., 2015).

A group of bacterial membrane spanning lipids, so-called branched glycerol dialkyl glycerol tetraethers (brGDGTs), have been used as paleotemperature (mean annual temperature: MAT) indicators (Weijers et al., 2007; Peterse et al., 2009; Tierney and Russell., 2009) in geological archives such as paleosoils, marine and lake sediments (Zang et al., 2018; Xiao et al., 2016; Russell et al., 2018). These lipid molecules contain two glycerol backbones that are attached to two branched alkyl chains with four ether bonds (Sinninghe Damsté et al., 2000, Weijers et al., 2006). Their structural variability (Supp. Fig. 1) is caused by a change in the degree of methylation (containing 4 to 6 branches, so-called tetra, penta and hexamethylated brGDGTs) and by the presence of 1 or 2 cyclopentyl moieties formed by internal cyclization (Schouten et al., 2013). Compounds with the outer branch(es) located on the C- α and/or ω 5 are denoted as 5-methyl, brGDGTs, whereas compounds with the outer methyl branch(es) on C- α and/or ω 6 are referred to as 6-methyl brGDGTs (De Jonge et al., 2013).

As brGDGT compounds are generally abundant in soils (Schouten et al., 2000), their presence in marine and lacustrine sediments was initially assumed to indicate the presence of a soil organic matter. However, it has since been confirmed that brGDGTs measured in the lacustrine water column and sediments are dominantly produced within the water column of lakes and rivers (De Jonge et al., 2014a; Loomis et al., 2014; Martínez-Sosa and Tierney, 2019; Martínez-Sosa et al., 2020) or within surface sediments (Buckles et al., 2014). On a global scale, the degree of methylation of 5-methyl brGDGTs (calculated as the MBT'_{5ME} ratio) correlates with temperature (Martínez-Sosa et al., 2021) in lacustrine settings. Similarly, the cyclization index of tetraethers (CBT' ratio), which expresses the relative abundance of cyclopentane-containing tetramethylated brGDGT Ic and 6-methyl penta- and hexamethylated brGDGTs compared to their 5-methyl counterparts without cyclopentane group, correlates with lake pH (Raberg et al., 2021). The isomer ratio (IR, De Jonge et al. 2014b; Halffman et al., 2022), which expresses the relative abundance of 6-methyl penta- and hexamethylated brGDGTs compared to their 5-methyl counterparts, reflect variation in similar pH-sensitive compounds as the CBT' ratio. As such, IR values have also been linked to both pH and conductivity (Russell et al., 2018; Martínez-Sosa et al., 2020; Raberg et al., 2021), but also with temperature (Martínez-Sosa et al., 2020). To translate variation in MBT'_{5ME} values and mean annual

temperature (MAT), or temperature above freezing, several lacustrine calibrations have been developed (e.g., Russell et al., 2018; Martínez-Sosa et al., 2021; Raberg et al., 2021). These calibration between the MBT'_{5ME} ratio and MAT have been based on empirical dependencies, either among global or local temperature gradients (e.g., Russell et al., 2018, Stefanescu et al., 2021).

More recently, these empirical calibrations have been underpinned by mechanistic understanding of the temperature-dependency of the MBT'_{5ME} ratio. Using computer simulations, Naafs et al. (2021) corroborate the notion that bacterial membrane lipids change directly with temperature, a process referred to as homeoviscous adaptation. This is supported by temperature-dependent adjustments in the composition of GDGT lipids of specific bacterial cultures (*S. usitatus*) (Chen et al., 2022; Halamka et al., 2022). These studies support the idea that the empirical calibration of MBT'_{5ME} relies on the homeoviscous adaptation of a potentially limited diversity of bacteria.

However, previous studies have employed simultaneous analysis of GDGT lipids and 16S rDNA-based community composition to propose that brGDGT distributions change as the communities of bacterial brGDGT producers change in the environment (e.g. Weber et al., 2018; De Jonge et al., 2019; 2021; Guo et al., 2021). As the phylogenetically diverse phylum Acidobacteria is a potentially important source for brGDGTs in soils (Weijers et al., 2009), acidobacterial cultures from different subgroups have been the subject of lipid profiling. Here, Sinninghe Damsté et al. (2011, 2014, 2018) report the presence of distinct ether and ester-bound iso-diabolic acids and branched fatty acids that are possible precursors of brGDGT lipids, in subgroups 1, 3, 4 and 6. In soil environments, shifts between Acidobacterial subgroups are observed when 6-methyl GDGTs or brGDGT Ia are produced in non-arid soils (De Jonge et al., 2019; 2021), while Verrucomicrobiae (Spartobacteria) are potential producers in arid soils (Guo et al., 2021). The substantial production of brGDGTs contrasts with the low abundances of Acidobacteria in lake water columns (Dedysh and Sinninghe Damsté, 2018; Weber et al., 2018; van Bree et al., 2020), and raises the question whether additional groups are involved in brGDGT synthesis in aquatic settings. Moreover, genomic analyses show the widespread potential among bacterial phyla to produce membrane-spanning lipids that contain ether bonds (Sahonero-Canavesi et al. 2022; Zeng et al. 2022).

Although changes in bacterial community composition across freshwater redox gradients (e.g., the oxic, suboxic water columns) are coeval with changes in brGDGT signature and MBT'_{5ME} values and bacterial community composition (Weber et al., 2018), the impact of temperature on lacustrine brGDGT producers is still poorly constrained. Characterizing the temperature response of brGDGT lipids, together with potential bacterial brGDGT producers allows to study whether homeoviscous adaptation or changes in the bacterial community drive temperature-dependent brGDGT variation in freshwater systems.

Understanding these drivers behind brGDGT variations in freshwater systems is especially important as these settings experience seasonal changes. To determine the temperature response of brGDGTs, their

distributions have been tracked over different seasons within individual lakes (Loomis et al., 2014; Miller et al., 2018). However, because other variables, such as water chemistry and bacterial community also undergo seasonal changes (Shade et al., 2007), a laboratory approach is needed to study the unique impact of temperature on GDGTs as done by Martínez-Sosa et al., (2020) using mesocosms. We build both upon this experimental approach and the knowledge on confounding factors on empirical calibrations. A mesocosm approach will allow to experimentally change (specifically, temperature), while measuring proposed confounding variables such as water chemistry (pH, alkalinity, conductivity), and allow monitoring of both production of brGDGTs and their bacterial producers. Here we experimentally assess the following hypotheses: (H1) use of oxic mesocosms consistently allows to replicate natural freshwater systems and brGDGT production (H2) the same temperature dependency of MBT'_{5ME} is observed in local freshwater settings (both in situ and after incubation) as at the global scale, (H3) temperature changes have a stronger impact on brGDGT compositions than changes in water chemistry and (H4) changes in the MBT'_{5ME} and IR are coeval with changes in the bacterial community composition. Examining the temperature sensitivity of brGDGTs in freshwater systems using an experimental approach can enhance the proxy's reliability for past temperature calibrations.

2. *Materials and Methods*

2.1. *Sampling sites and seasons*

Two sites, a freshwater lake and a river, are each sampled in 3 different seasons. Water was collected from the oxic surface of Lake Rot (Rotsee, 47°04'10.1"N; 8°18'48.1"E) and Sihl River (47°21'05.8"N; 8°31'12.7"E), from the lake shore and riverbank, on a seasonal basis in April-May, July-August, and October-November 2021. With a surface area of 0.48 km² and depth of 16 m, eutrophic Lake Rot (Smith et al., 1999; Su et al., 2017) experiences seasonal stratification and the development of an anoxic bottom layer every summer because of the high aerobic mineralization rates of phytoplankton-derived organic matter (Schubert et al., 2010; Naeher et al., 2014). Brook Ron, a small artificial subsidiary of the Reuss River, is the single inlet flowing into Lake Rot. Sihl River has a total length of 73 kilometers with a headwater located at 1650 m altitude (Druesberg mountain), including the Sihlsee reservoir at 41 km upstream of the sampling point. As a subalpine river, the Sihl is mainly characterized by a steep morphology, high turbidity, and dynamic waterflow throughout the year (Schwab et al., 2022). For this experiment, water was collected from a downstream location with less turbidity.

2.2. Experimental design

For each starting condition (n=6, three seasons and two sites), 2 liters of freshwater are filtered on site to record brGDGT of in situ conditions (T₀). Afterwards, water canisters (360 L in total) were transported back to the Swiss Federal Institute of Technology (ETH Zurich), Geological Institute. Here, the water was divided into 2 L mesocosm bottles (n=30 for each starting condition, Fig. 1). The bottles were placed on stirring plates (v=100 rpm) to ensure water mixing and covered with perforated plastic caps to allow circulation of air. The bottles (“Mesocosms”) were set up in a temperature-controlled climate chamber, where the natural day/night cycles were mimicked (both light intensity and duration of the day-night cycle mimicked seasonal condition (e.g., spring mesocosms were set up with light intensity and daylight hours similar to spring in Switzerland). They were subjected to 3 different temperature treatments, that were selected based on 24-hour averages of sampling dates during the past 5 years to reflect realistic in situ temperatures at the 3 seasons under study (10 °C, 17.5 °C and 25 °C, for spring, autumn, and summer, respectively, Fig. 1). Mesocosm bottles were thus subjected either to constant temperatures comparable to temperatures at the time of sampling (‘control treatment’), increased temperatures (‘warming treatments’) or colder temperatures (‘cooling treatments’). Specifically, for spring, where T₀ water temperature was 10 °C and 11.1 °C in Lake Rot (LR) and Sihl River (SR), respectively, 10 mesocosm bottles received a control treatment (10 °C), while two sets of 10 bottles were subjected to two separate warming treatments (17.5 °C and 25 °C). For autumn waters (in situ water temperatures LR= 15.5 °C, SR= 18 °C), mesocosm bottles were subjected either to a control treatment (17.5 °C), a warming treatment (25 °C) or a cooling treatment (10 °C). In summer, the 25 °C represented the control treatment (T₀ water temperatures at LR:22.5 °C, SR:23 °C), while two sets of mesocosm bottles were subjected to cooling treatments (at 10 °C and 17.5 °C). The range of temperatures was thus realistic, although the rate of temperature change (sudden warming or cooling) did not mimic natural conditions. To capture the response of brGDGTs and their bacterial producers to these individual temperature

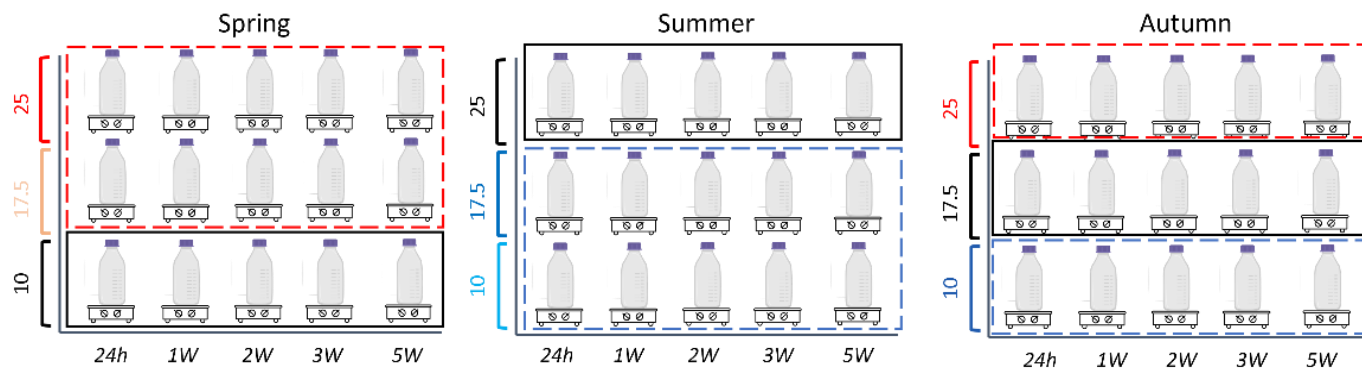


Fig. 1. A diagram illustrating the seasonal mesocosm setup. The control mesocosms for spring, summer, and autumn are maintained at in-situ temperatures of 10°C, 17.5°C, and 25°C, respectively marked by black boxes around the mesocosms. Spring mesocosms are subjected to two warming treatments (17.5°C and 25°C) marked by red dashed boxes, while summer mesocosms are subjected to two cooling treatments (10°C and 17.5°C) marked by blue dashed boxes. In the case of autumn incubations, both a cooling (10°C, blue series) and warming (25°C, red series) treatments are employed. [Color should be used for print version]

treatments with time, the two entire 2 L mesocosms were sacrificed and filtered at 5 timepoints (24 hrs, 1 week, 2 weeks, 3 weeks, and 5 weeks (T1 to T5, respectively)). The timepoints were selected using previous information on approximate growth/decay times of brGDGTs, with maximum brGDGT concentrations observed after 1-2 weeks, and a gradual decrease in concentration thereafter (Martínez-Sosa and Tierney, 2019). For each timepoint, the water chemistry and GDGT distribution of two independent, duplicate, mesocosms were analysed as duplicates, to determine variability. Due to an extraction preparation error, the Sihl River autumn mesocosms reports are based on 1 set of bottles (no duplicates).

2.3. Sampling and characterization of brGDGT lipids, water chemistry and bacterial DNA

2.3.1. Sampling

The mesocosms of each temperature treatment were filtered over 0.22 µm PVDF membrane filters (Durapore®, Germany) placed on a titanium tripod (cleaned using EtOH, MeOH, DCM between samples). PVDF filters allow collection of brGDGT lipids with high efficiency (Martínez-Sosa and Tierney, 2019) at their respective timepoints. Following filtration, a fixed area of the PVDF filter (16 mm²) for bacterial community analysis was preserved and stored at -20 °C for later analysis, the remaining filter was dissected and subjected to lipid biomarker extraction.

2.3.2. Lipid extraction

Lipid extraction was performed by acid hydrolysis of the filters, where the freeze-dried filters were placed in centrifuge tubes and 10 mL of 1.5N HCL (HCl/MeOH 1:7 (v:v)) was added. Tubes were capped and wrapped with Teflon tape and heated at 80°C for 2 hours. This process allows the conversion of all intact polar lipids (IPL) into core lipid (CL) brGDGTs to maximize the recovery of all brGDGT compounds (Weber et al., 2017). Afterwards, dichloromethane (DCM) was added to samples to obtain a MeOH/DCM 1:1 (v:v) solvent composition and allow phase separation. Subsequently, the samples were extracted with DCM three times. The total lipid extract (TLE) was subjected to column chromatography using a 3.4 cm column packed with aluminium oxide (alox), using 3 solvent mixtures, hexane/DCM 9:1 (v:v), hexane/DCM 1:1 and MeOH/DCM 1:1 for the fraction containing GDGTs. After the addition of a known amount of C46 GTGT standard (Huguet et al., 2006), the polar fractions were filtered over a 0.45 µm PTFE filter, dried under N₂ and re-dissolved in 50 µl of hexane/isopropanol (IPA) 99:1 (v:v) before analysis using a high-performance liquid chromatography–mass spectrometry (HPLC–MS, Agilent Technologies®-1200, USA) after Hopmans et al., (2016), with modified column temperature (40 °C) and an injection volume of 10 µl. This method allows detection of all 15 brGDGT compounds (Schouten et al., 2007; Hopmans et al., 2016). Ions with known mass over charge ratios (*m/z* 1050, 1048, 1046, 1036, 1034, 1032, 1022, 1020, 1018) for brGDGTs were detected and semi-quantified according to the internal standard's (*m/z* 744) peak area corresponding to the added concentration (10 µl= 49.6 ng). The instrumental error was determined to be approximately 15% of concentrations.

The MBT'_{5ME} (De Jonge et al., 2014b) and the Isomer Ratio (IR) were calculated after De Jonge et al. (2014a), including only compounds without cyclopentane moieties. While IR has been described to vary both with pH in soils (Naafs et al., 2017) and temperature in lakes (Russell et al., 2018; Martínez-Sosa et al., 2021), other indices including CBT' (De Jonge et al., 2014a) and DC' (Sinninghe Damsté et al., 2009) have been proposed to correlate with soil pH (De Jonge et al., 2014b, 2021) and lake water column pH (Russell et al., 2018). The reconstructed water temperature (*T*_{rec.}) was calculated based on both Russell et al. (2018) and Martínez-Sosa et al., (2021) calibrations, although both yielded comparable results. Expressions of Indices discussed above are described below:

$$MBT'_{5ME} = \frac{Ia+Ib+Ic}{Ia+Ib+Ic+IIa+IIb+IIc+IIIa}$$

$$IR = \frac{IIa'+IIIa'}{IIa'+IIIa'+IIa+IIIa}$$

$$DC' = \frac{Ib+IIb+IIb'}{Ib+IIb+IIb'+Ia+IIa+IIa'}$$

$$CBT' = \log_{10} \frac{(Ic+IIa'+IIb'+IIc'+IIIa'+IIIb'+IIIc')}{Ia+IIa+IIIa}$$

$$MATrec = -1.21 + 32.42 \times MBT'_{5ME} (R^2= 0.92, p\text{-value}<0.0001, RMSE= 2.44 \text{ } ^\circ\text{C})$$

2.3.3. Water chemistry measurements

To characterize changes in the water chemistry through time, at each time point (T0 –T5W) aliquots of each mesocosm were taken for anions (Nitrate - NO_3^- , Sulfate - SO_4^{2-} , Chloride - Cl^-), and cations (Calcium - Ca^{2+} , Sodium - Na^+) (measurements using ion chromatography (compact ion chromatograph pro, Model 88, Metrohm Inc, Switzerland) and alkalinity measurements using an 862 Compact Titrosampler (Metrohm Inc, Switzerland, international standard organization method EN ISO 9963-1:1995)). Furthermore, pH, temperature and conductivity of the samples were measured with a multimeter (MultiLine® IDS 3620, Xylem Inc. USA) at the time of filtration.

2.3.4. DNA extraction, quantitative PCR, and 16S rRNA gene sequencing

A known fraction (16 mm^2) of each filter was cut-up and stored in 2ml PCR-clean tubes. These samples underwent DNA extraction following the modular protocol of Lever et al. (2015). In short, dNTP solution (10 mM) was added to samples to reduce DNA sorption and allow maximum DNA recovery, followed by the addition of cell lysis solution and incubation of samples on a shaker for 1h at $50 \text{ } ^\circ\text{C}$. Subsequently the DNA containing supernatant was washed twice with a cold 24:1 (v:v) chloroform-isoamyl alcohol mixture. NaCl, Linear Polyacrylamide (LPA) and EtOH were added, and the extracted DNAs were precipitated in room temperature at dark for 2h. DNA pellets were washed three times with 70% EtOH to remove excess NaCl and were dried before dissolution in molecular grade water.

The abundance of bacterial 16S rRNA genes were determined by quantitative PCR (qPCR) assay using a LightCycler 480 II (Roche Life Science, Switzerland) (Deng et al. 2020, Han et al. 2020). The 16S bacterial primers BAC908F (5'-AACTCAAAGGAATTGACGGG-3') and BAC1075R (5'-CACGAGCTGACGACARCC-3') were mixed with a SYBR Green I-based master mix (0.5 μL of each primer, 5 μL of SYBR Green I (Roche Life Science, Switzerland), 1 μL of H_2O , 1 μL of BSA). The 16S Bacteria DNA quantification was performed by comparison with a dilution series of a known DNA concentration. During the qPCR runs, the negative control (molecular grade water) showed average C_p values of 28-30. To ensure accuracy, a C_p cut-off of 27 was selected. Samples exhibiting a higher C_p value (>27) were determined to have too low 16S rRNA contents and excluded from downstream analyses. Instead, bacterial OTUs (Operational Taxonomic Units) identified using samples with $C_p >27$ were used as examples of potential contaminant taxa. Sequence libraries were prepared according to a standard workflow

(Deng et al. 2020, Han et al. 2020). Briefly, amplicons of bacterial 16S rRNA gene were obtained through PCR reactions using the primer pairs S-D-Bact-0341-b-S-17 (5'-CCTACGGGNGGCWGCAG-3')/S-D-Bact-0785-a-A-21 (5'-GACTACHVGGGTATCTAATCC-3'). Amplicon sequencing was done via paired sequencing using the Illumina MiSeq platform at the genetic diversity center (GDC) of ETH Zurich. Positive (Plasmids of 16S rRNA genes from *Holophaga foetida* (Acidobacteria)) and negative controls (molecular grade water) were added to ensure the quality of the sequencing run.

Although data loss was not significant during the back-mapping efficiency of the raw sequencing data, the number of high-quality zOTUs (denoised sequencing data) remained high and about 30% of the sequences could not be mapped to clusters. An abundance threshold of 5 was adopted which resulted in increased mapped sequences with an increased number of zOTUs (n= 7893). Chimera reads were consequently removed, and 5348 non-chimeric OTUs were kept. The USEARCH algorithm with global alignments with the identity threshold of 97% was used to map all the sequencing reads, providing an OTU Table with 3817 taxa and a total of 4,517,711 OTU reads. The total reads were then rarefied to the depth of 5100 reads per sample, retaining 3037 taxa, and total of 117300 reads in 25 samples. The 16S rRNA genes of all T0 conditions were quantified and sequenced successfully.

2.4. Statistical analysis

A one-way ANOVA was computed to determine significant differences between seasonal brGDGT concentrations at both sites. To determine whether brGDGTs distribution showed variation after the start of the incubation, the MBT_{5ME} and IR were compared with values measured at T24h (Supp. Table 4). To calculate linear correlations with time, the timepoints (T24h-T5W) are used as time units, and thus not converted into hours. Compounds that are often below the detection limit were excluded from analysis. For Lake Rot this included brGDGTs IIIb, IIIb', IIC', IIIC, no compounds were excluded from the analysis for Sihl River. The correlation between inorganic parameters (pH, alkalinity, conductivity, water ions) and the concentration, fractional abundance of brGDGTs or brGDGT ratios were examined using linear regression methods including the Pearson correlation coefficient (r), and p-value of correlation test between paired samples (where p-values <0.05 are considered significant). To test whether the composition of the bacterial community in Lake Rot and Sihl River could potentially determine the variation in brGDGT variability, between a selected group of mesocosms with distinct MBT_{5ME} and IR values, a bio-indicator approach is used (De Jonge et al., 2019; Halffman et al., 2022). Here, bio-indicators that are significantly increased in the respective groups (p< 0.1) are reported, with the p-value for this group calculated after Sidak's correction for multiple testing. Downstream and statistical data analysis on brGDGTs and the OTU table were thus

performed using packages “phyloseq” (McMurdie and Holmes, 2013) “vegan” (Oksanen et al., 2013), “indicpecies” (De Cáceres, 2013), and “tidyverse” from R v4.1.2.

3. Results

To compare the seasonal variability (T0) with the changes caused by the mesocosm treatments, a comparison between initial (T0) measurements of water chemistry, bacterial community composition, and brGDGTs concentration in Sihl River and Lake Rot is followed by the experimental (mesocosm) results.

3.1. Water chemistry parameters

To ensure that the mesocosms T0 conditions reflect typical freshwater inorganic parameter values, several indicators of the water chemistry in Lake Rot and Sihl River is described.

The inorganic parameters in Lake Rot exhibit similar values in spring and summer, with conductivity of 267 and 249 in spring and summer ($\mu\text{S}/\text{cm}$), pH between 8-9, and cations such as Ca^{2+} (1059, 1063 mg L^{-1}) and Na^+ (222, 206 mg L^{-1} in spring and summer respectively) indicating typical freshwater conditions (Horne and Goldman, 1994; Weyhenmeyer et al., 2019; Rogora et al., 2015). The concentration of SO_4^{2-} in the lake water ($< 150 \text{ mg L}^{-1}$) is similar to other freshwater lakes (Zak et al., 2021), but the concentration of NO_3^- in spring (50 mg L^{-1}) slightly exceeds the average freshwater NO_3^- levels, as reported in other studies ($> 40 \text{ mg L}^{-1}$, James et al., 2005). Water alkalinity in Lake Rot is similar to other freshwater lakes in Europe ($< 100 \text{ mg L}^{-1}$, Llíró et al., 2014). However, these parameters (pH, alkalinity, conductivity, Na^+ , Ca^{2+} , SO_4^{2-} , NO_3^-) decrease during autumn when NO_3^- is below the detection limit ($< 12 \text{ mg/L}$). In Sihl River, most inorganic parameters exhibit comparable values in spring and summer, that are also similar to Lake Rot. In autumn, some parameters (alkalinity, Na^+ , SO_4^{2-} , NO_3^-) increase while pH (8.3) and Ca^{2+} (1430 mg L^{-1}) remain stable (Fig. 2). These parameters, nonetheless, remain within the boundaries of standard freshwater river conditions (Bódis et al., 2016). Following the initiation of the incubation period, the minor variability in the mesocosm water chemistry is summarized in Fig. 2. As the impact of the water chemistry parameters pH and conductivity on brGDGT distribution has been observed previously in lacustrine environments (Stefanescu et al., 2021; Wang et al., 2021), changes in the mesocosm water chemistry are tracked. First, the variation in control mesocosms will be evaluated to test H1. As the mesocosms have narrow pH ranges (7-8.5) and conductivity ($\sim 200\text{-}300 \mu\text{S}/\text{cm}$), temperature is the main parameter changing in the mesocosms, which will allow to test for H2. By determining the impact of several water chemistry parameters (Supp. Table 3) on brGDGT concentration and distribution, the mesocosms provide the

opportunity to evaluate whether temperature changes have a stronger impact on brGDGTs than changes in water chemistry (H3).

3.2. DNA quantification and sequencing data

To identify the bacteria community composition in our incubations that could be responsible for brGDGTs distribution variability and address (H4), the composition of the bacterial community is determined (Supp. Table 1).

For the individual T0 conditions, the composition of the 20 most abundant phyla and Acidobacteria is summarized in Supp. Fig. 3. With a fractional abundance of 36% of total reads, phylum Proteobacteria is the most abundant bacteria in both sites, followed by phylum Actinobacteriota with 25% of all rarefied reads. In Lake Rot T0, Actinobacteria (\bar{x} = 49%, σ = 21%) and Proteobacteria (\bar{x} = 24%, σ = 11%) are the most common phyla in all seasons. In Sihl River, phylum Bacteroidota is the most abundant in spring (43%) while in summer and autumn, Proteobacteria has the highest total reads (43%, 42%) respectively. Phylum

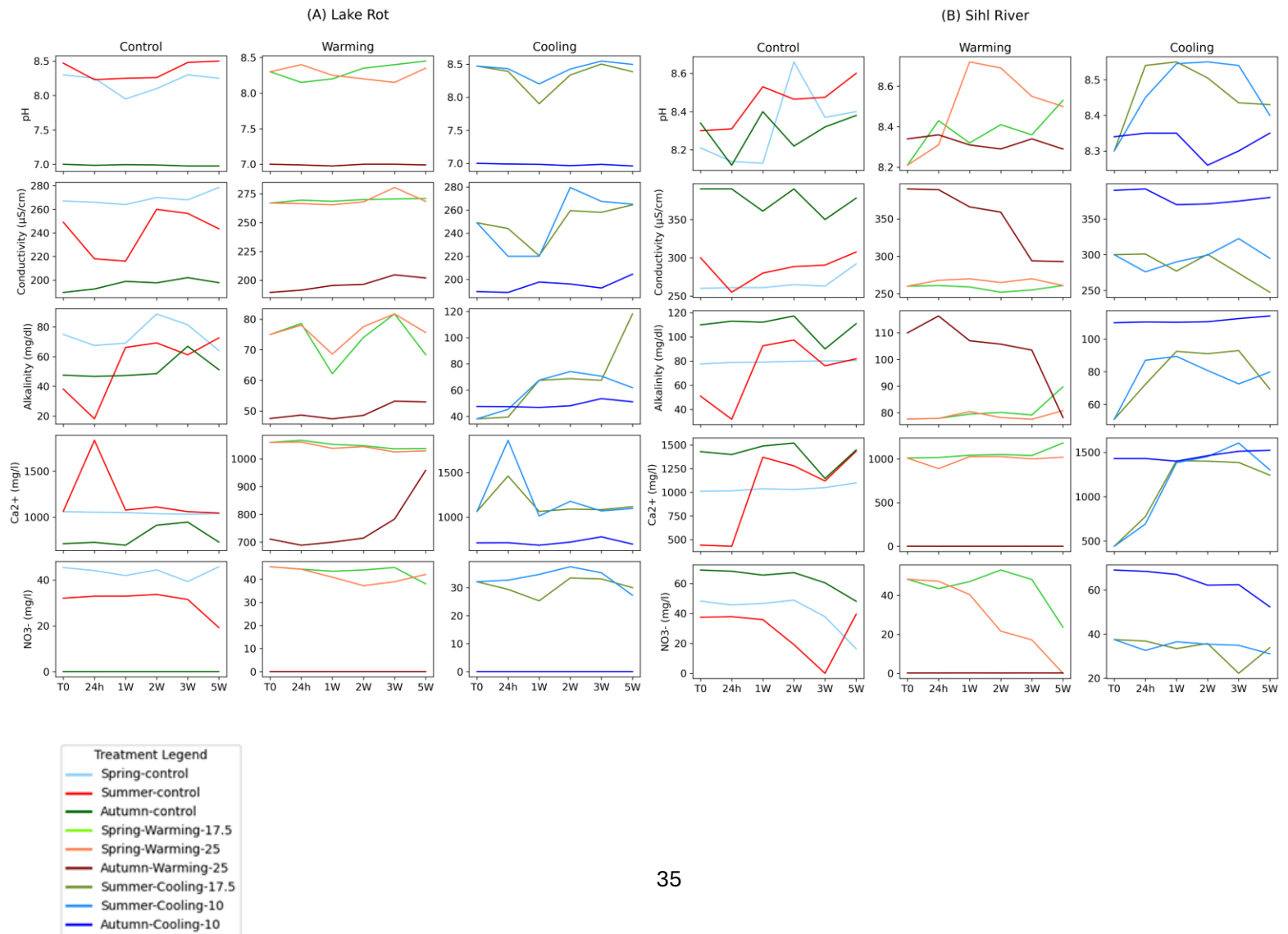


Fig. 2. Line plots representing changes with time of selected water chemistry parameters measured in Lake Rot and Sihl River T0 and mesocosms. Corresponding colors legend is valid for all brGDGT figures as well. [Color should be used for print version]

Acidobacteriota, whose members are shown to produce brGDGTs (Sinninghe Damste et al., 2018; Chen et al., 2022; Halamka et al., 2022), is represented in all samples with a low fractional abundance (<2%, LR:1-35, SR: 20-44 reads), with an increased occurrence in autumn (LR:35, SR:124 reads). OTUs that are typical for either Lake Rot or Sihl River (bio-indicator OTUs) have been determined (Supp Fig. 4). As represented in Supp. Fig. 3, there is significant variability in bacterial community composition after the start of the mesocosms in both Lake Rot and Sihl River over time and between treatments (control/cooling/warming). To summarize significant changes in bacterial composition, bacterial OTUs that are increased significantly in mesocosms with high MBT'_{5ME} in Lake Rot and increased IR in Sihl River are reported, after removing 5 OTUs that are potential contaminations. These OTUs are placed within the phyla Acidobacteria (Vicinamibacteria and Blastocatellia), Actinobacteriota (order Frankiales), Gammaproteobacteria (Burkholderiales), and Planctomycetota (order Planctomycetes and Phycisphaerae) for Lake Rot. For Sihl River 87 bio-indicator OTUs are identified within Actinobacteriota (order Microtrichales and Frankiales), Alphaproteobacteria (orders Acetobacterales, Caulobacterales, Reyranelles, and Rhodobacterales), Bacteroidota (order Chitinophagales), Cyanobacteria, Gammaproteobacteria (order Burkholderiales and Salinisphaerales) and Patescibacteria (Candidatus_Kaiserbacteri), Planctomycetota (order Pirellulales).

Changes in the bacterial community in control mesocosms will be described to test H1. With a distinct bacterial community between Lake Rot and Sihl River and described changes in the community composition with time, the bio-indicators identified will allow us to evaluate whether changes in bacterial community composition affect the brGDGTs ratios (H4).

3.3. BrGDGT concentration and distribution

3.3.1. Environmental distribution (T0)

Comparing brGDGT concentration at initial conditions (T0) (Fig. 3), brGDGTs were present at a high concentration in spring in Lake Rot and Sihl River (114 and 335 ng L⁻¹, respectively). In summer and autumn, both sites have noticeably lower brGDGT concentrations (generally <60 ng L⁻¹, Fig. 3, one-way ANOVA with $p < 0.001$). In addition to concentration changes, T0 brGDGT distribution is distinct between seasons. In Lake Rot, MBT'_{5ME} values increase from spring (0.41) to summer and autumn (0.48 and 0.44, respectively), reflecting a proportional increase of the fractional abundance of brGDGT Ia, compared to IIIa with increasing MBT'_{5ME} values (Supp. Table 2). This contrasts with Sihl River, where the MBT'_{5ME} in summer (0.44) and autumn (0.42) are slightly decreased compared to spring (0.48). Similarly, the change

in T0 MBT'_{5ME} values can mainly be tracked through changes in the fractional abundance of Ia compared to IIIa.

Similar to MBT'_{5ME}, variation in IR values between seasons are observed. Lake Rot summer IR (0.52) is decreased, compared to spring and autumn values (both 0.63), caused by a relative increase in brGDGT IIIa compared with IIa' and IIIa' in summer. In Sihl River, IR values are 0.38 for all seasons, representing stable fractional abundances of brGDGTs IIa, IIIa, IIa' and IIIa' (Supp. Table 2). Seasonal variation in distribution of GDGTs in T0 will be used to test H2.

3.3.2. Mesocosm distribution changes

The variation in the concentration and distribution of brGDGTs in the control, cooling, and warming treatments, is evaluated to determine the stability of control mesocosms, and the impact of temperature on brGDGT ratios (H1 and H2). Water collected at each starting condition

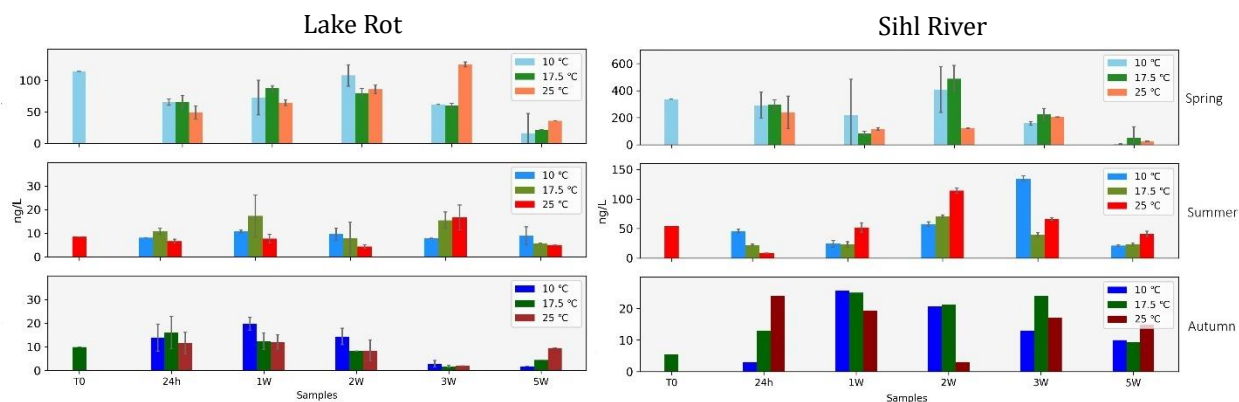
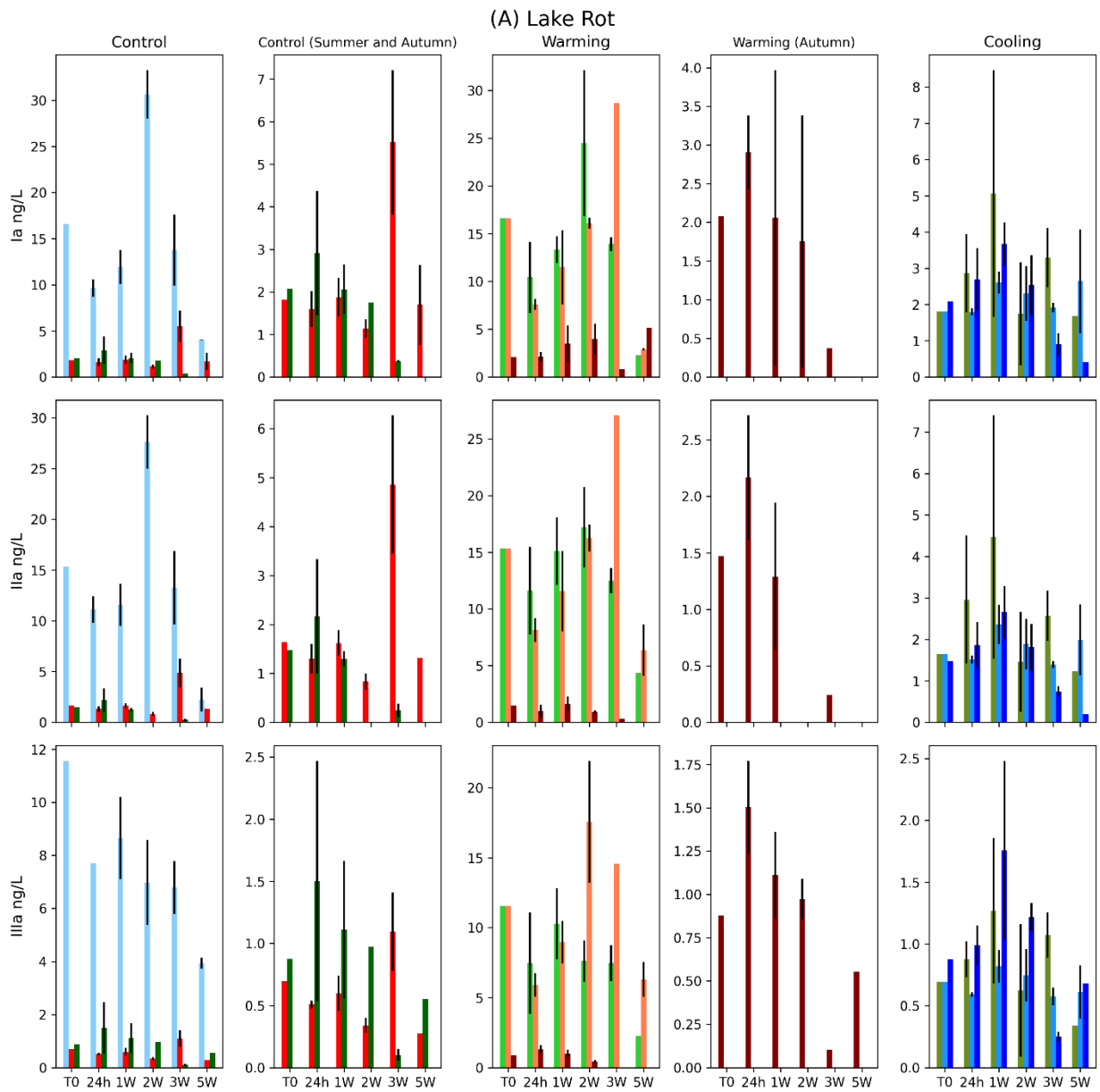


Fig. 3. Bar plots of summed concentration of brGDGTs from Lake Rot and Sihl River, with top, middle and bottom panels representing spring, summer and autumn, respectively. T0 values present concentration of brGDGTs filtered at site, timepoint values represent mesocosm samples filtered at each timepoint. Error bars reflect the standard deviation from mesocosm duplicates, with Sihl river autumn having no duplicate values. [Color should be used for print version]

contained viable GDGT producers, as the concentration of summed brGDGTs, compared to T24h, showed an initial increase after the beginning of the experiment, generally followed by a decrease in concentration (Fig. 3). In several mesocosm bottles the brGDGT concentration is increased compared to T0 (or T24h), 29 (40%) and 31 (52%) of Lake Rot and Sihl River, respectively. For those bottles where the summed concentration remained stable or decreased, a change in brGDGT distribution was considered to reflect the production of at least 1 brGDGT compound. With this selection process, summarized in Supp. Table 4, only 9 mesocosm bottles (all from Lake Rot) showed no evidence of brGDGT production, and were removed from the dataset, keeping 156 (86%) of all mesocosm for GDGT description and discussion. GDGT

distribution and concentration of either non-duplicate or average values of duplicate mesocosms are reported in Supp. Table 2.



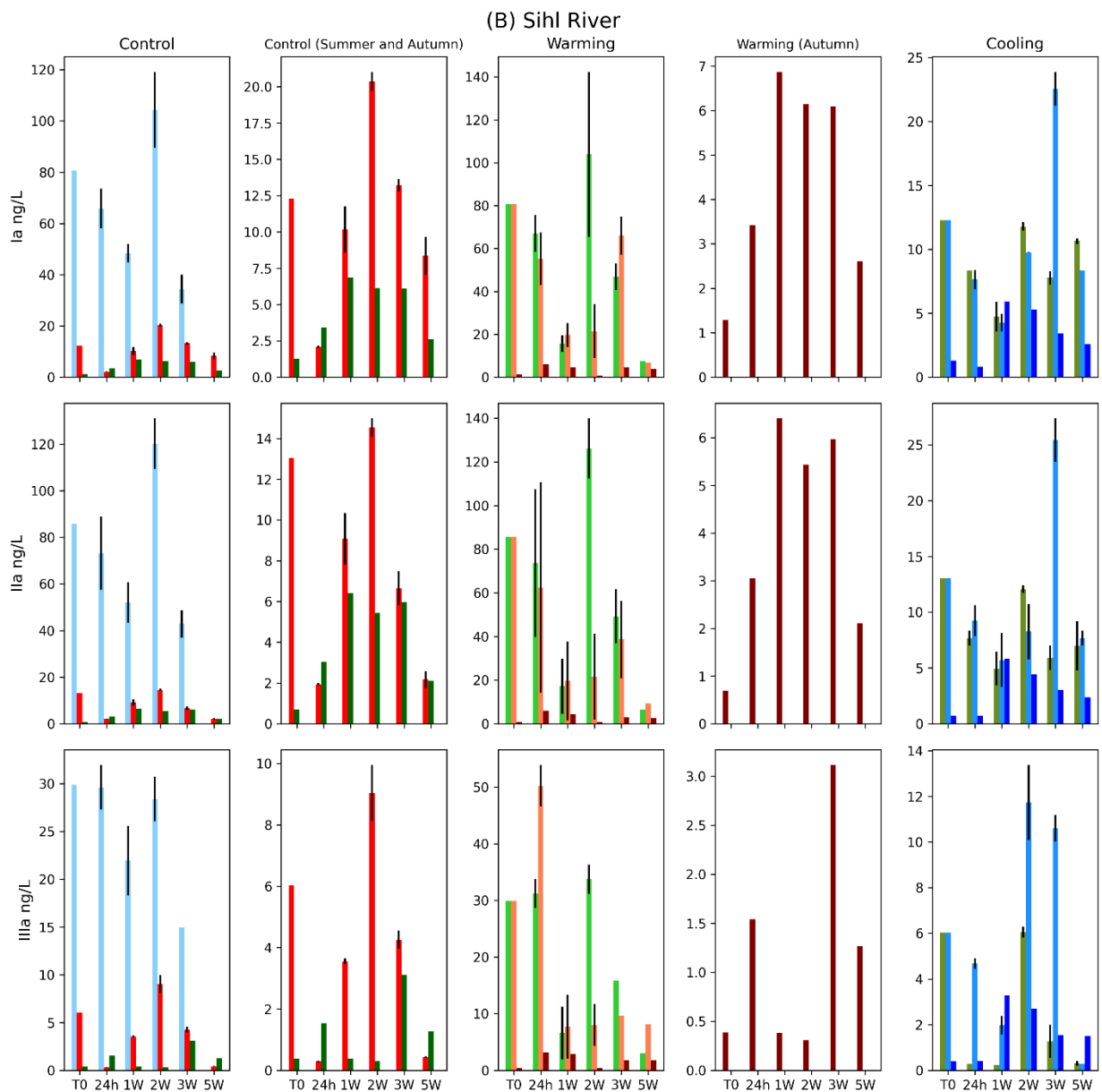


Fig. 4. Bar plots representing concentrations of individual brGDGTs Ia, IIa and IIIa in (A) Lake Rot and (B) Sihl River T0 and temperature treatment (control, cooling, and warming) mesocosms. Because of lower concentrations, subpanels “summer and autumn” and “autumn” present the values for these seasons on a magnified y-axis. Error bars reflect the standard deviation of mesocosm duplicates, with Sihl river autumn having no duplicate values. See Fig. 2 for the color legend for this Fig. [Color should be used for print version]

In Lake Rot mesocosms (Fig. 4A) control treatments, the concentration of brGDGTs generally decreases with time (however no negative correlation is present). In the temperature treatments, individual 5-methyl brGDGT compounds, show distinct concentration changes with time, often specific for individual seasons. Specifically, the concentration of brGDGT Ia and IIa (ng L^{-1}) increase the strongest in spring warming

treatments (25 °C) with timepoints ($r= 0.95, 0.96, p= 0.05$, respectively, Fig. 4A, orange bars). The concentration of brGDGT Ia also increases with time in the warming incubations (excluding T3W) of the autumn season ($r= 0.65, p< 0.2$, Fig. 4A, brown bars). In cooling treatments of summer and autumn, brGDGTs IIa and IIIa exhibit comparable concentration change through time, reflecting an initial increase followed by a decrease at T2W. In control treatments, the concentration of brGDGTs generally decreases with time (however no negative correlation is present). Because individual brGDGTs show different concentration variations in Lake Rot mesocosms, the fractional abundances of major brGDGTs Ia, IIa and IIIa vary between temperature treatments (Fig. 5A). The increase in GDGT concentration and change in their distributions and GDGT-based ratio in both control and temperature treatment experiments, will be discussed when testing H1 and H2. To address the temperature impact on GDGT ratios (H2) the MBT'_{5ME} and IR values are calculated.

As MBT'_{5ME} values are expected to respond to temperature, MBT'_{5ME} changes in the different temperature treatments are reported (control, cooling, warming; Supp. Table 2). With a range of 15-60%, brGDGT Ia has the highest fractional abundance across treatments of Lake Rot. In cooling incubations, the changes in fractional abundances of Ia and specially IIIa are limited in (Fig. 5A). A decrease in MBT'_{5ME} values is observed only for the last timepoint of the autumn season (T5W, Fig. 6A), driven by a sudden increase in the fractional abundance of IIIa (Fig. 5A). However, at the final time point (T5W) a significant reduction in the concentration of brGDGTs is observed compared to the initial conditions, where brGDGTs Ia and IIa fall below detection limit. Although degradation of individual compounds is not expected to influence the distribution (Yamamoto et al., 2016), changes in the composition can be caused by degradation.

In contrast, in the autumn warming incubation, Ia% increases and IIIa decreases (going below the detection limit with time), reaching a final value of 0 at 5 weeks (T5W). Hence, the MBT'_{5ME} values increase with time in the autumn season ($r= 0.97, p< 0.05$, excluding T3W). Also, in individual mesocosms of the spring warming treatments (Fig. 6A) MBT'_{5ME} values are increased, caused by elevated Ia% and IIa%. In Lake Rot control incubations, the fractional abundance of Ia marginally increases with time in spring mesocosms as reflected in the MBT'_{5ME} increase in these incubations. In summer and autumn, the variation in MBT'_{5ME} values is muted in control treatments, with diverging MBT'_{5ME} values observed at T5W (Fig. 6A).



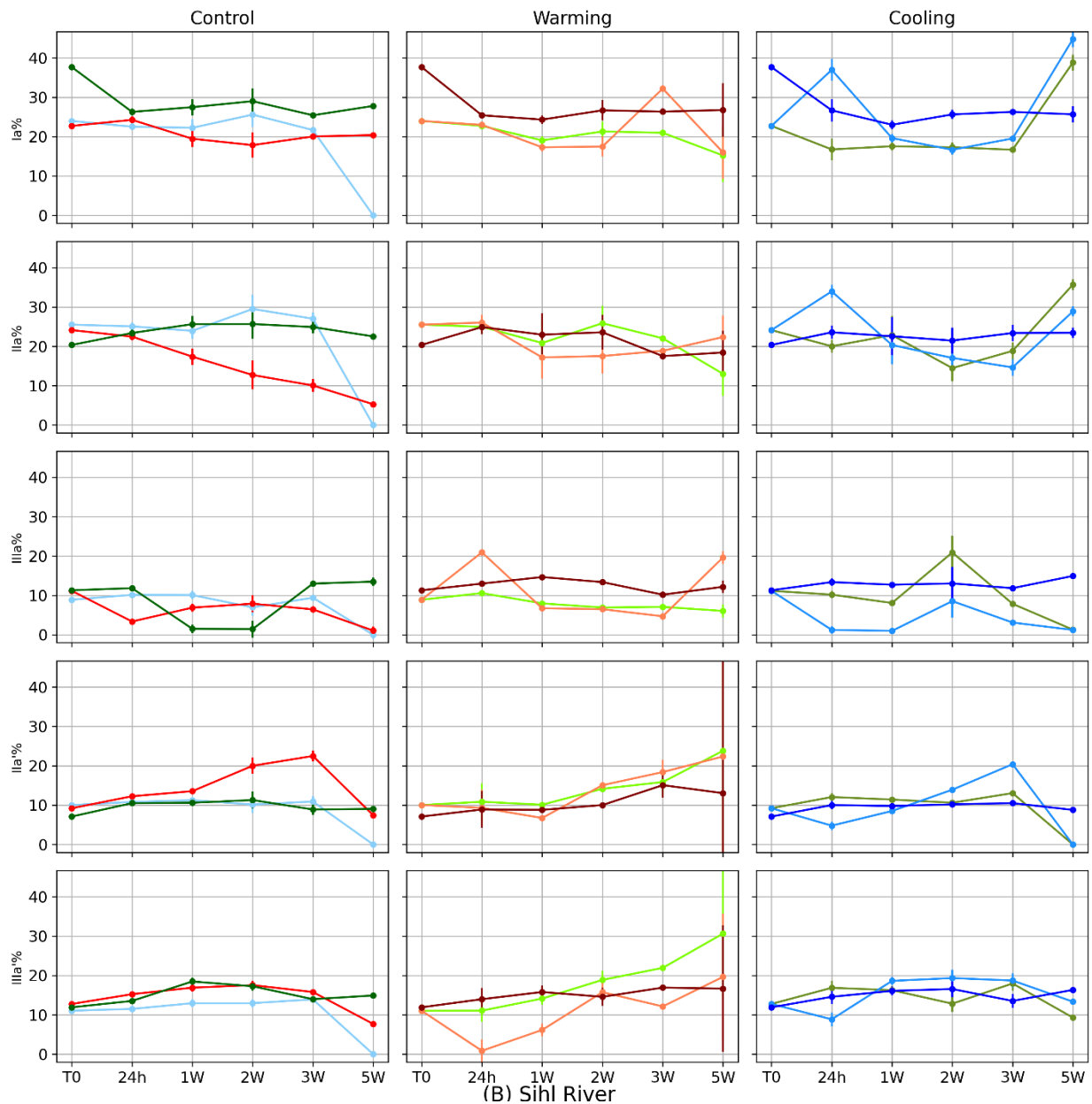
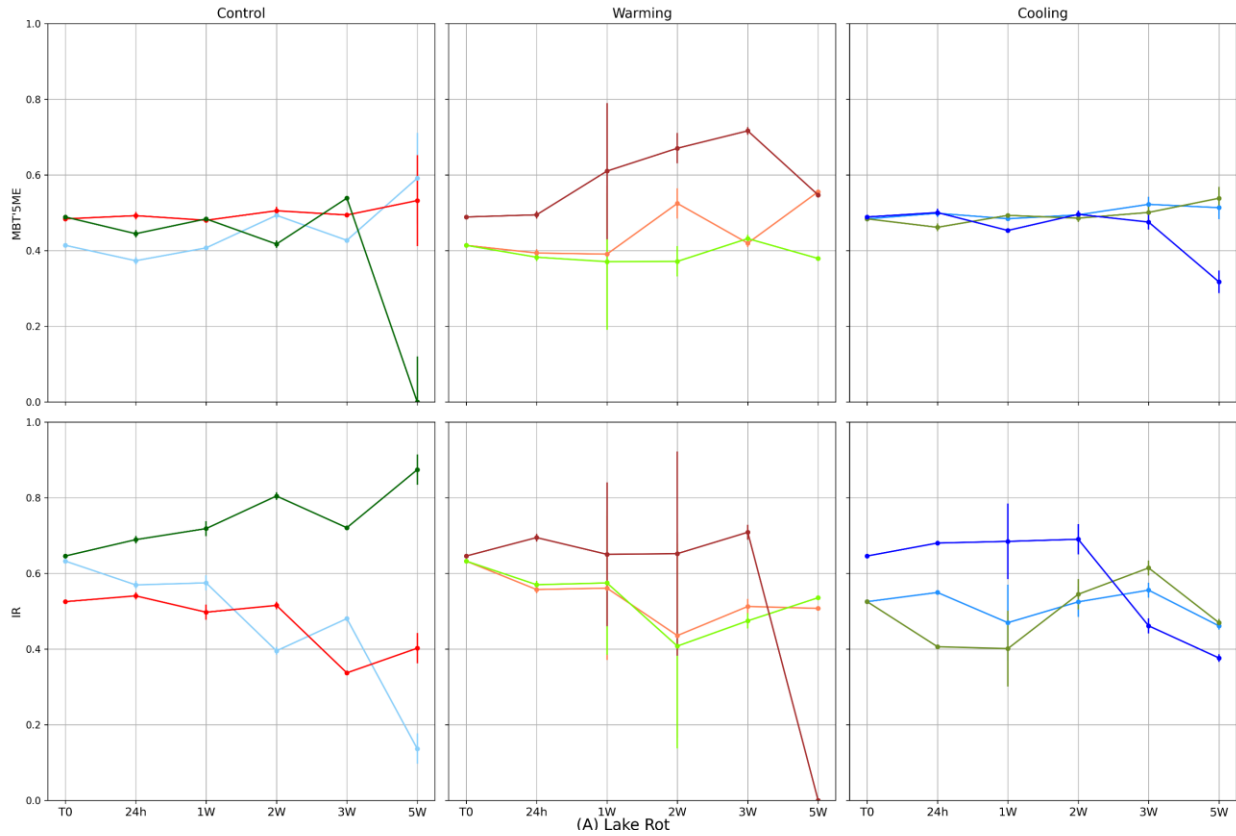


Fig. 5. Line plots of fractional abundance of brGDGTs Ia, IIa, IIIa, IIa' and IIIa' in (A) Lake Rot and (B) Sihl River T0 and mesocosms. Error bars reflect the standard deviation of mesocosm duplicates, with Sihl river autumn having no duplicate values. See Fig. 2 for the color legend for this Fig. [Color should be used for print version]

In Lake Rot mesocosms, the concentration of 6-methyl brGDGTs (ng L^{-1}) represents stable values in all individual temperature treatments (control, cooling and warming) of spring and summer (Fig. 7A). In autumn cooling and warming incubations, however, compound IIIa' gradually decreases, and is present below detection limit at end of the experiment. The increased fractional abundance of brGDGT IIa' in some mesocosms of Lake Rot (i.e., autumn warming T3W), is not caused by a concentration increase of this

compound but instead a decrease of IIIa'. For $T \leq T2W$ of Autumn control mesocosms, the fractional abundance of 6-methyl compounds is higher (25-40%) which is not observed in spring and summer control incubations (10-20%). This is reflected in the variability in autumn IR values (Fig. 6A), where in autumn control and warming incubations, IR remains high ($IR > 0.6$) for $T \leq T3W$. In the cooling treatment of autumn however, with a decrease in fractional abundance of brGDGT IIIa', IR decreases after T2W. In general, changes in the fractional abundance of 6-methyl GDGTs and the IR values are mainly driven by both 5-methyl and 6-methyl compounds.



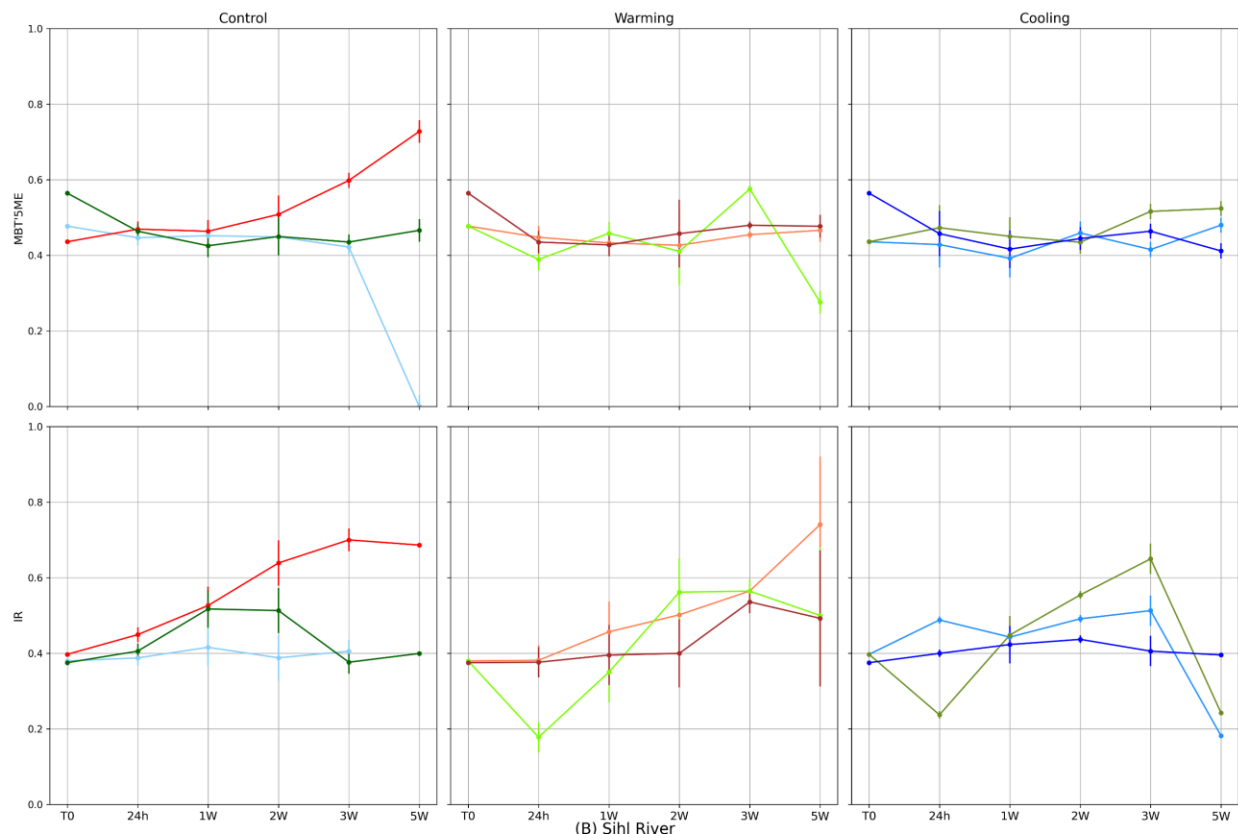


Fig. 6. Line plots displaying the brGDGT ratios MBT'_{5ME} and IR for (A) Lake Rot and (B) Sihl River T0 and mesocosms. Error bars reflect the standard deviation for mesocosm duplicates. See Fig. 2 for the color legend for this Fig. [Color should be used for print version]

In Sihl River mesocosms, the response of brGDGTs to temperature treatments is distinct from Lake Rot. The concentrations of brGDGT Ia, IIa and IIIa do not exhibit a uniform increase or decrease in any of the warming or cooling treatments (Fig. 4B), although there is variability in GDGT concentration and a good agreement in concentration changes between brGDGT Ia vs IIa ($R^2= 0.50, 0.72$, for warming and cooling, respectively). In spring and autumn control treatments, the variation in the fractional abundances of brGDGTs Ia, IIa, IIIa (Fig. 5B) results in minimal changes in MBT'_{5ME} values (Fig. 6B). However, MBT'_{5ME} increases in the summer control treatments, driven by a decrease in the fractional abundance of brGDGT IIa (although not observed in concentration of IIa compared to Ia). In the cooling treatments, no response of the MBT'_{5ME} with time is observed, although the variance in the summer cooling treatment (17.5 °C) increases with time (Fig. 6B). In the warming treatment (25 °C), spring MBT'_{5ME} values increase in individual mesocosm bottles, driven by an increase in brGDGT Ia fractional abundance (although minimally observed in the concentration of IIa compared to Ia). In addition to the 5-methyl brGDGTs, the concentration of 6-methyl compounds are variable in both the control and temperature treatments. Except

for the concentration of IIIa', which increases with time in the warming (25 °C) treatments of spring ($r=0.98$, $p<0.05$), generally 6-methyl brGDGT concentrations do not display a uniform trend with time. Reflecting the increase in concentration, brGDGT IIIa' fractional abundance increases with time in spring warming (17.5 °C and 25 °C) treatments ($r=0.97$, $r=0.98$ $p<0.05$, respectively, Fig. 5B). The fractional abundance of 6-methyl brGDGT IIa' increases with time (excluding T5W) in control and cooling (17.5 °C) treatments in summer ($r=0.97$, 0.99 , $p<0.05$, respectively for control and cooling; Fig. 5B), and in autumn ($r=0.82$, $p<0.1$) and spring (17.5 °C) warming treatments ($r=0.96$, $p<0.05$), resulting in IR values that increase with time in spring warming treatment (17.5 °C) ($r=0.96$, $p<0.05$, Fig. 6B).

Across both sites and all seasons, MBT'_{5ME} thus increases with time in 2 warming treatments, specifically Lake Rot spring (17.5 °C) and Lake Rot autumn (25 °C), and in the control treatments of Lake Rot spring and Sihl River summer. It does not increase or decrease in any cooling treatments. While the MBT'_{5ME} is the most temperature-sensitive proxy in Lake Rot, in Sihl River, IR represents the prominent temperature dependencies. As such, the discussion will explore the mechanisms behind the temperature-dependent variation in MBT'_{5ME} and IR values of Lake Rot and Sihl River.

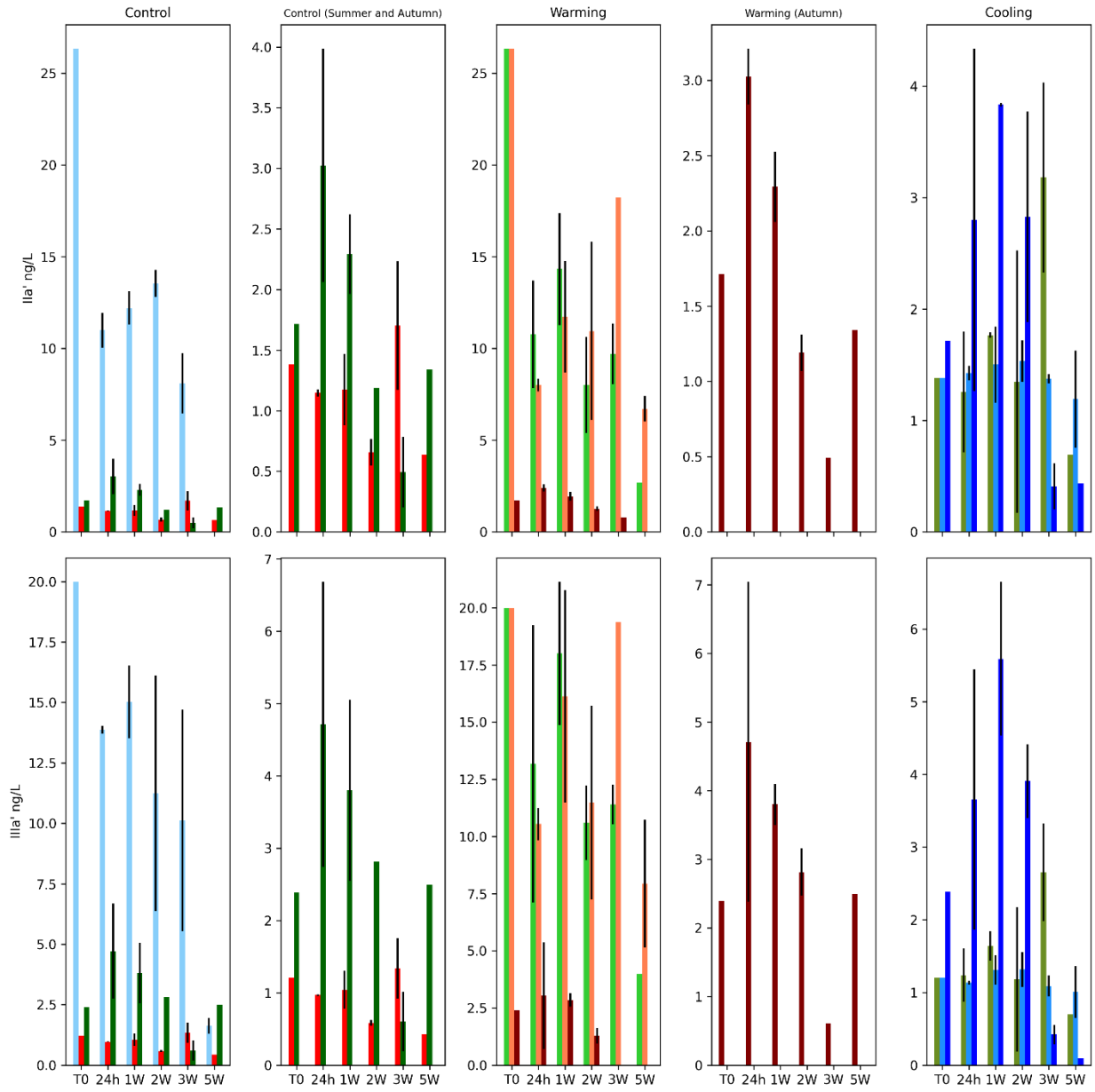
4. Discussion

4.1. Performance of mesocosms for brGDGTs production

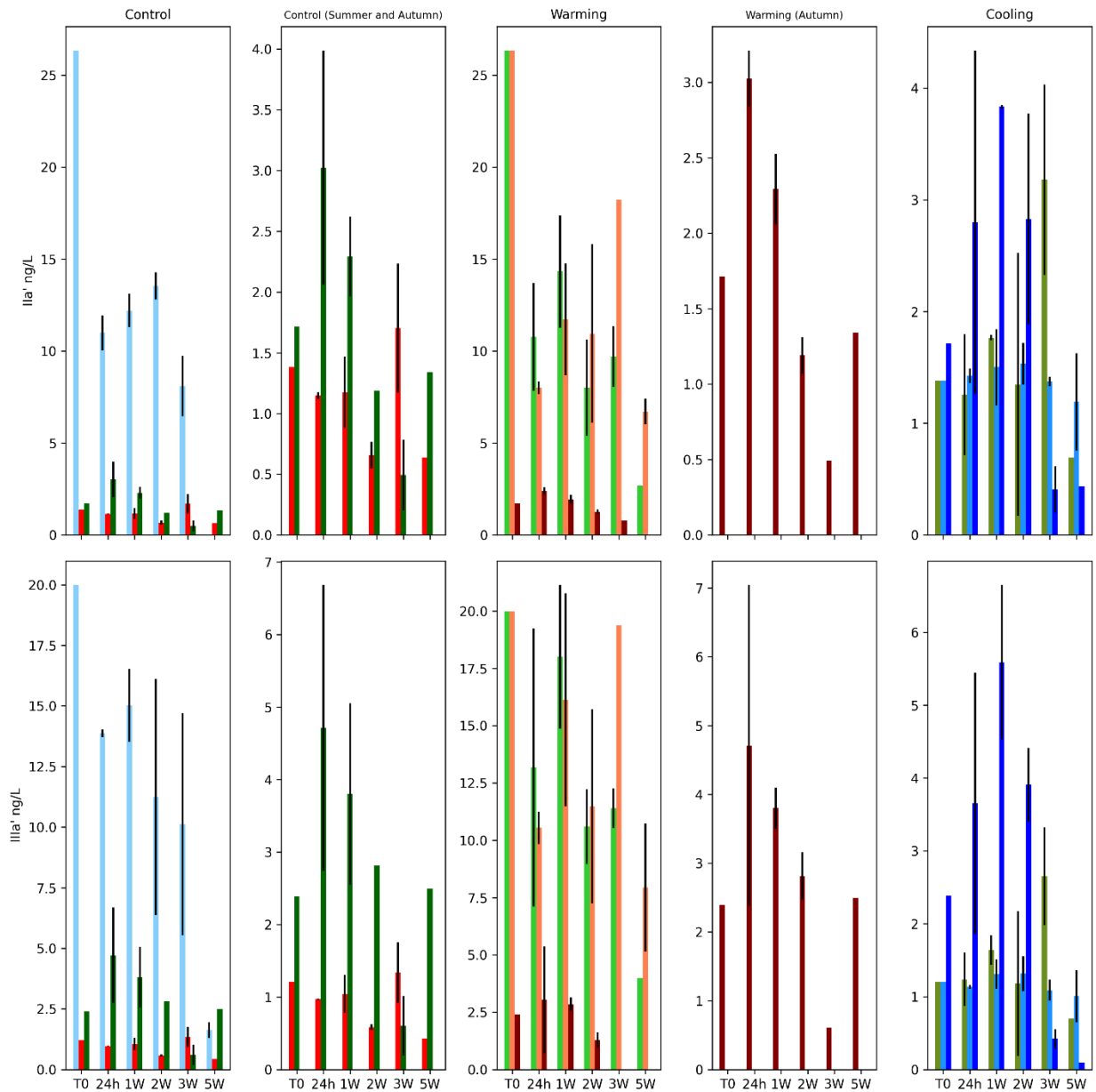
To evaluate whether control incubations were representative of natural conditions (H1), changes in chemistry, bacterial community and GDGTs are discussed. In both the control incubations of spring and autumn in Lake Rot and Sihl River, the chemistry variables (including pH, alkalinity, conductivity, and Ca²⁺) partially exhibit limited variability with time, but only across a small range (pH up to 0.25, alkalinity up to 35, conductivity up to 25, Ca²⁺ up to 250; Supp. Fig. 5). The control treatment therefore did not impact inorganic chemistry values strongly compared to initial natural conditions (T0). The NMDS plot of the control samples (Supp. Fig. 6) reveals limited but existing variability in the composition of the bacterial community, especially in the single successfully characterized sample taken at T5W. This suggests that while some changes are evident in the control incubations, the majority of the bacterial community exhibits a relatively consistent composition, indicating a limited degree of succession under control conditions.

Variations in GDGTs concentration (2-5 folds increase/decrease) and ratio (0.1-0.2 unit change in MBT'_{5ME}) were observed in the control treatments for all seasons at both sites (Supp. Fig. 7). This change in concentrations align with the variability reported by Martínez-Sosa et al. (2019) in concentration (2-4 folds change) and ratios (0.1-0.4) of their samples and can be attributed to possible increased biovolume in bacteria when relieved from grazing pressure in the mesocosm bottles (Pomeroy et al., 1994; García-Martín and Pérez-Lorenzo., 2011; Kunzmann et al., 2019). Observing this response in the control mesocosms,

shows that it is a temperature-independent effect. It is advisable to exercise caution when interpreting the initial changes in bacterial community composition and brGDGT concentration and distribution considering the so called “bottle effect”. This term refers to errors arising from sample containment. As such samples will practically capture only part of the natural community, excluding for instance grazers, this leads to changes in community composition and interactions (Pomeroy et al., 1994). Based on the control mesocosms, initial changes in the mesocosms can thus be attribute to the release of the grazing pressure. In addition, the controls indicate that after 5 weeks the bacterial communities undergo drastic changes that can be related to nutrient limitations. Furthermore, based on results from Martínez-Sosa et al., it takes 2-4 weeks before the background GDGT signal is overwritten and no instantaneous responses to the temperature change are thus expected. Consequently, although changes across all timepoints are discussed, the mesocosms that have had more time for acclimation (e.g., T2W, T3W) to the experimental temperature tests, may represent the most realistic response to temperature change.



(A) Lake Rot



(B) Sihl River

Fig. 7. Bar plots showing the concentration of individual 6-methyl brGDGTs Ila' and IIIa' in (A) Lake Rot and (B) Sihl River T0 and temperature treatment (control, cooling, and warming) mesocosms. magnified subpanels "summer and autumn" and "autumn" present the values for these seasons on smaller y-axis. Error bars reflect the standard deviation of mesocosm duplicates. For Autumn Sihl River, presented values are based on single measurements (no error bars). See Fig. 2 for the color legend for this Fig. [Color should be used for print version]

4.2. In-situ seasonal brGDGT signatures

The brGDGT concentrations in Lake Rot summer and autumn T0 measurements ($10 > \Sigma \text{brGDGT} > 8 \text{ ng L}^{-1}$) compare well with other freshwater lakes, namely, Lower King Pond and Lake Chala ($\Sigma \text{brGDGT} < 12 \text{ ng L}^{-1}$, Loomis et al., 2014, Van Bree et al., 2020, respectively). Similarly, summer T0 brGDGT concentration in Sihl River ($\Sigma \text{brGDGT} = 54 \text{ ng L}^{-1}$) is comparable with reports of brGDGT concentration from Yenisei River in east Siberia ($\Sigma \text{brGDGT} < 69 \text{ ng L}^{-1}$, collected in summer, De Jonge et al., 2014a). However, in eutrophic Lake Rot and Sihl River, brGDGTs spring in situ concentrations (LR- $\Sigma \text{brGDGT} = 114 \text{ ng L}^{-1}$, SR- $\Sigma \text{brGDGT} = 335 \text{ ng L}^{-1}$) exceed those reported in other lake and riverine systems (Martínez-Sosa et al., 2020; Van Bree et al., 2020). With comparable in situ MBT'_{5ME} values (0.41-0.48) across all seasons for both sites, the absolute values (12-14 °C) are comparable to the real-time day average air temperatures (8.4-10.3 °C). However, the small variability in reconstructed temperature ($T_{\text{rec.}}$) between seasons does not reflect the seasonal variability of in situ temperatures in both calibrations applied. Reconstructed temperatures derived from both Russell et al. (2018) and the average reconstruction from Martínez-Sosa et al. (2021) (Supp. Table 2) showed an offset of less than 2 degrees. The reported values are based on the Russell et al. (2018) calibration, as the in-situ measured temperatures generally were closer to this calibration. Spring and autumn reconstructed temperatures (Lake Rot: 12 °C and 14 °C, Sihl River: 14 °C and 12 °C) present an offset of 2 to 3 °C in spring and of 2 to 5 °C in autumn (measured air temperature of 8.4 °C and 10.3 °C in spring and 18.2 °C and 14.4 °C in autumn for Lake Rot and Sihl River, respectively). This offset is bigger (6 to 10 °C) for summer, where measured in situ air temperature is 20.5 °C for Lake Rot (reconstructed temperature = 14 °C), and 22.1 °C for Sihl River (reconstructed temperature = 13 °C), respectively. This muted variation in T0 MBT'_{5ME} values across seasons indicates that brGDGT producers in these systems are less sensitive to temperature changes, compared to what would be expected based on a global scale.

4.3. Impact of temperature on brGDGT distribution

Based on global calibrations we expect the MBT'_{5ME} to increase with warming, decrease with cooling and remain stable in control conditions, with step-sizes reflecting the variability present on the global scale (H2). In Lake Rot mesocosms, the variations in MBT'_{5ME} followed this response only in a subset of the treatments (Fig. 6A). In the autumn warming treatment, an increase in Ia concentration, and a decrease in IIIa causes the MBT'_{5ME} to increase with temperature, reaching 0.71 ($T_{\text{rec.}} = 22 \text{ °C}$) at T3W before dropping to 0.55 ($T_{\text{rec.}} = 16 \text{ °C}$) at T5W. The temperature dependency of brGDGTs in the autumn season is confirmed by the observation that the fractional abundance of brGDGT IIIa increases in the cold treatment, resulting in a decrease of the MBT'_{5ME} (0.32), with a reconstructed temperature (9 °C) similar to the cold incubation

temperature (10 °C). A second example of MBT'_{5ME} increases in response to warming, is observed in one of the warming incubations (17.5 °C) of spring, where MBT'_{5ME} values reach 0.56, reflecting reconstructed temperatures (16.8 °C) that are similar to the growth temperature. Although the increase of MBT'_{5ME} values aligns with a similar trend observed in mesocosms in a warm lake (AZ, USA) where, after 4-6 weeks of incubation at warmer temperatures (27 and 35 °C), MBT'_{5ME} values consistently increased with up to 0.5 MBT'_{5ME} units (Martínez-Sosa et al., 2020). However, in the Swiss mesocosms the response size is generally smaller (up to 0.3). Furthermore, the lack of response in some of our warming mesocosms is not observed at the warm Lake Kennedy mesocosms (Martínez-Sosa et al., 2020). Indeed, not all temperature and control treatments result in the expected response of the MBT'_{5ME} . In the warmest spring warming (25 °C) treatment, where the concentration of Ia shows a steady increase with time, MBT'_{5ME} does not increase. Ia concentration is indeed matched by an increase in the concentration of IIa and IIIa, which results in stable MBT'_{5ME} ratio values instead. In addition to an increase in the warming treatment, in the spring control treatment, the MBT'_{5ME} shows a muted but significant increase with time ($r= 0.83$, $p < 0.1$), caused by a higher fractional abundance of Ia, IIa, Ib and Ic (Supp. Table 2; Fig. 5A for Ia and IIa). There is thus seasonal variation in the temperature dependence of brGDGTs, with significant changes in the MBT'_{5ME} in autumn caused by changes in concentration and the fractional abundances of 5-methyl brGDGTs Ia and IIIa, while more muted changes in the spring season caused by the increased concentrations and fractional abundances of brGDGTs Ia and IIa.

Although MBT'_{5ME} is seen to increase in several warming but also control treatments, a decrease of MBT'_{5ME} values in cooling treatments is never observed, exemplified by the summer incubations where MBT'_{5ME} shows a low variability ($\bar{x}= 0.5$, $\sigma = 0.02$). This could indicate a limited response of brGDGTs producers to cooling temperatures, as bacterial activity is temperature-dependent (White et al., 1991). Still, even a slow decrease in MBT'_{5ME} values is not detected. This observation is consistent with the findings in the cooling mesocosms of Lake Kennedy, where MBT'_{5ME} also does not exhibit a decrease over time in incubations conducted at lower temperatures (9 and 18 °C), compared to their the in-situ environment (22 °C).

This absence of consistent increase/decrease in the fractional abundance of brGDGTs Ia and IIa or IIIa and the MBT'_{5ME} values in all warming incubations (Fig. 5A, Fig. 6B), challenges the proposed temperature dependency of these compounds in Lake Rot. In addition to the temperature dependency of the MBT'_{5ME} , we evaluate the temperature sensitivity of the IR. Tentative positive correlations between the IR and temperature based on large regional to global scale datasets have been put forward recently by Russell et al. (2018) and Martínez-Sosa et al. (2021) but were not reported as such by Raberg et al. (2021). In Lake Rot, the concentration of 6-methyl compounds (IIa', IIIa') increases with time in temperature treatments,

specifically some of the autumn cooling incubations, supporting the idea of a potential aquatic producer of 6-methyl brGDGT during autumn. In some warming treatments (autumn), an increase in the fractional abundance of Ila' is observed, but it is not caused by a clear increase in the concentration of brGDGT Ila'. An increase in IR values with time in the warm treatments is not observed (Fig. 6A).

Compared to lakes, the dependency between MBT'_{5ME} values and temperature in rivers is poorly constrained. Although the occurrence of in situ produced brGDGTs has been reported in river systems (De Jonge et al., 2014a; Zell et al., 2014; Kirkels et al., 2022), it remains unclear whether 5-methyl brGDGTs produced in fluvial systems show the same temperature response as brGDGTs produced in lakes. Instead, 6-methyl brGDGTs have been proposed to be indicative of in-situ production in rivers (Freymond et al., 2017; Kirkels et al., 2022). To test the temperature response of riverine brGDGTs, freshwater from Sihl River was subjected to the same temperature treatments as Lake Rot.

Only in the summer treatments, the MBT'_{5ME} values in the control incubations, which are only 2-3 °C warmer than in situ summer temperatures, portray a positive correlation ($r= 0.54$) with time, reaching a final (T5W) reconstructed temperature of 22.1°C, representing real-time summer in situ temperature. This elevated MBT'_{5ME} trend is reflected in the increase in fractional abundance of brGDGT Ia at a higher rate compared to Ila and IIIa (Fig. 5B). However, other than the concentration increase of brGDGT Ia in the summer control treatment, and a sporadic increase in the concentration of brGDGT IIIa in some incubations of spring warming treatment (25 °C), in general, 5-methyl brGDGTs show no concentration changes in Sihl River temperature treatments (Fig. 6B).

Instead, the majority of brGDGTs variation is observed as changes in the 6-methyl brGDGTs, and correspondingly the IR values (Fig. 6B). With the observed strong concentration increase of 6-methyl compounds in Sihl River mesocosms (especially in spring and summer), aquatic production of these compounds is confirmed, leading to changes in the fractional abundance of brGDGTs. In spring, the fractional abundance of 6-methyl brGDGTs increase in warming treatments, while remaining stable in the control treatment, indicating that temperature potentially has a direct effect on the production of Ila' and IIIa'. Supporting the production of 6-methyl brGDGTs at warm temperatures, is the observation that in summer incubations, Ila' and Iib' also increase in concentration with time (T24h to T2W) in control treatments, i.e., at a warm growth temperature. On the other hand, the concentration of brGDGT IIIa', shows a 3-fold increase with time (T24h-T3W) in the coldest treatment (10 °C) of summer, potentially reflecting an increase in hexamethylated brGDGTs when growth temperature drops strongly (here: 15 °C), and complicating the interpretation of temperature-dependence of this compound. In autumn, IR stays stable across different treatments with only the warming treatment (T>2W) showing a marginal increase in IR. As the temperature dependency of the fractional abundance of the 6-methyl brGDGTs and the IR is not uniform across temperature treatments and seasons, its application as a temperature proxy will be limited. However,

the use as a proxy for in situ production of brGDGTs in river systems, a process that is expected to be more intense when the temperature is warmer, is confirmed.

Across both sites, the response of either MBT'_{5ME} or IR on the temperature treatments, reveal a temperature dependency that is dominated by a response to warming, and absent or muted responses to cooling. This different environmental dependency of brGDGTs in fluvial and lacustrine settings can possibly impact the interpretation of the MBT'_{5ME} as a temperature proxy in sedimentary settings with substantial riverine input. The increase in concentration or fractional abundance of Ila' in warmer conditions (Fig. 5, 6), however, is shared between both sites presenting similarities in response of 6-methyl compounds to temperature irrespective of their aquatic source. Still, although the MBT'_{5ME} (in Lake Rot) and IR (in Sihl River) reflect a temperature dependency, not all variation in these proxies can currently be explained by the temperature treatments.

4.4. Impact of water chemistry on brGDGT variability

Although the mesocosm experiment aimed at keeping all other environmental variables constant to measure the impact of temperature, some variability in the inorganic water parameters is observed (Fig. 2). This variability can be explained by evaporation (conductivity and cations concentrations increase with time in some mesocosms), and a possible difference in the suspended mineral content (impacting cations concentrations) between mesocosm bottles during filling the mesocosm bottles. Furthermore, temperature can also accelerate chemical reactions in freshwater (Elser et al., 2007), potentially changing the mineral content concentrations of individual mesocosms. As for instance conductivity (Tierney et al., 2010; Shanahan et al., 2013; Loomis et al., 2014; Raberg et al., 2021) and nutrient availability (Loomis et al., 2014), have been reported to potentially control the brGDGTs distribution, these unintended changes in water chemistry have potentially impacted the brGDGT ratios. To statistically test for the impact of confounding parameters in addition to temperature, a factorial design should have been used (e.g., Collins et al., 2009). As this was not the case, we address H3 by performing a post hoc analysis of the variability of GDGTs and water chemistry, for Lake Rot and Sihl River separately.

As T0 water chemistry of spring and summer had comparable values at both sites, we look at common dependencies that act across these two seasons collectively, while keeping autumn as a separate season, generating 12 correlation matrices (2 locations, 2 season groups, contrasting 3 treatments (control, cooling and warming); Supp. Table 3A-B). In Lake Rot treatments, minimal correlations between brGDGT ratios and the inorganic parameters are observed, as is evident in the lack of a significant correlation between MBT'_{5ME} and water chemistry. Concerning the proxies that vary with chemistry in soils (CBT' and DC'; Naafs et al., 2017; De Jonge et al., 2021), only DC' increases in multiple treatments with pH (Supp. Table

3A). Although DC' does not correlate with dissolved Ca^{2+} , in warming incubations of Lake Rot (spring and autumn), the fractional abundance of Iib' correlates with dissolved Ca^{2+} ($r= 0.74$), which matches the previously described increase of 6-methyl brGDGTs with exchangeable Ca^{2+} in soils (Halffman et al., 2022). However, as DC' does not respond to pH in all mesocosm studies, and the dependency of Iib' on Ca^{2+} is not observed in control and cooling mesocosms, although a range in pH and Ca^{2+} values is present, the environmental dependency of the DC' remains poorly constrained based on the Lake Rot mesocosms. In Sihl River, however, multiple brGDGT ratios and fractional abundances of brGDGTs correlate with temperature and water chemistry (Supp. Table 3b), and we first discuss whether water chemistry drives variation in the IR, in addition to the temperature dependency. IR values correlate with water pH in summer cooling incubations ($r= 0.72$), which matches previous observations in soils (Naafs et al., 2017; Russell et al., 2018; De Jonge et al., 2021). The correlations between the fractional abundance of IIIa' and Iia with pH ($r= 0.65$, $r= -0.66$, respectively) cause the dependency between IR and pH. A more general dependency is observed between IR and water conductivity in control (spring and summer) and cooling (summer) incubations ($r= 0.70$, $r= 0.72$, respectively), which is based on correlations between conductivity and the fractional abundance of Iia ($r= -0.73$, $r= -0.74$, respectively), and 6-methyl compounds Iia' (Supp. Table 3B). This observation supports the correlation between IR and conductivity previously reported by Raberg et al. (2021). However, it is not observed in all mesocosms.

Similar to Lake Rot, in the cooling treatments of Sihl River ($n= 10$), DC' increases with water pH ($r= 0.73$), as does the fractional abundance of brGDGT Iib' (Supp. Table 3B), but not Ib or Iib compounds, promoting the idea of a strong impact of water pH on the 6-methyl cyclopentane containing brGDGT Iib' in freshwaters of both lakes and rivers. This observation is in general agreement with previously reported positive correlations of fractional abundances of monocyclopentane containing brGDGTs (Ib, Iib, Iib') and pH in lake sediments (Raberg et al., 2021).

In our seasonal dataset, multiple distinct correlations between brGDGTs ratios and inorganic environmental parameters are observed, particularly in Sihl River. However, no overarching driver of aquatic chemistry on brGDGT ratios could be identified. Based on the mesocosm studies, where the range in water chemistry values is minor and well-constrained, variations in the brGDGTs distribution are predominantly attributed to temperature changes. Nonetheless, our findings suggest that chemical environmental factors, particularly in riverine systems, can have the potential to affect brGDGTs ratios typically used for chemistry or conductivity reconstruction (IR, DC').

4.5. Bacterial community composition as a source of brGDGT variability

As several brGDGTs and brGDGT-based ratios showed variability in response to environmental drivers, coeval compositional changes in the bacterial community can be evaluated to constrain potential GDGT producers. As this is based on relative quantities, e.g., rarefied 16S rRNA gene counts, including strains that don't produce brGDGTs, we report correlations between brGDGT ratios and bacterial groups that show relative increases, without assigning bacterial groups as definite brGDGT producers.

In soils, large changes in the MBT'_{5ME} ratio and the IR, have been attributed to changes in the composition of the bacterial community (De Jonge et al., 2019; De Jonge et al., 2021). To elucidate whether a similar mechanism can explain the variation in brGDGT distribution, we use a bio-indicator approach. As the bacterial community composition for each T0 is different, we report significant changes in the fractional abundance of OTUs per season that are coeval with changes across a cut-off value in MBT'_{5ME} values (for Lake Rot) and IR values (for Sihl River), for those seasons where 16S-based community composition was reconstructed in sufficient samples. The cut-off values are determined to represent an average value of the selected treatment.

Specifically, we determine bio-indicators in Lake Rot autumn mesocosms (n= 5, cut-off value of MBT'_{5ME} = 0.50) and in the Sihl River spring mesocosms (n= 6, cut-off value of IR = 0.39). Firstly, in Lake Rot autumn, where a response of the MBT'_{5ME} values with warming is observed (MBT'_{5ME} ranges between 0.48 and 0.67), driven by a concentration increase of brGDGT Ia and a decrease of IIIa, we evaluate which bio-indicator OTUs are present in mesocosms with an elevated MBT'_{5ME} value (>0.5, n= 2), compared to background values (0.48-0.50, n= 3). The phylogenetic distribution of the OTUs that are increased in high MBT'_{5ME} mesocosms is represented by Actinobacteriota (order Frankiales and Micrococcales), and Gammaproteobacteria (order Burkholderiales) [Fig.8A]. Interestingly, no Acidobacterial OTUs were included in the bio-indicators. This aligns with previous observations of low abundance of Acidobacteria in freshwater settings, suggesting that sources other than Acidobacteria may potentially be responsible for brGDGT production in lakes. Evaluating the bio-indicators identified, Zeng et al. (2022) describe the presence of a Tes homologue in the genus Oxalobacteraceae (Bulkholderiales). As such, this OTU (8% of all reads) potentially contributes to the production of GDGTs in Lake Rot mesocosms. Secondly, IR bio-indicator OTUs are determined in the Sihl River spring mesocosms (n= 6, cut-off value of IR= 0.39), where brGDGT IIIa' shows variation in concentration. Several bio-indicator OTUs with a wide phylogenetic spread are determined (Fig. 8B). Among these, acidobacteriotal orders Vicinamibacteria (subgroup 6; 3 bio-indicator OTUs) and Blastocatellia (subgroup 4; 2 bio-indicator OTUs) have been shown to produce brGDGT precursor lipids (reviewed in Sinninghe Damste et al., 2018) and to increase in soils with increased pH and IR values (De Jonge et al., 2021). Furthermore, representatives of the following orders have been shown to carry a Tes homologue (Zeng et al., 2022); Chitinophagaceae (4 bio-indicator OTUs),

Saprospiraceae (1 bio-indicator OTU), Sphingobacteriaceae (2 bio-indicator OTUs) and Pirellulaceae (3 bio-indicator OTUs). These OTUs are generally present in low abundance, with the Sphingobacteriaceae bio-indicator OTUs as the most abundant clade, amounting up to 1.3% of OTU reads.

Although changes in the fractional abundance of Acidobacterial OTUs can be responsible for the observed changes in IR in Sihl River, a) the low abundance of Acidobacterial bio-indicator OTUs (0 to 0.5%), b) lack of detection of Acidobacteria orders in Lake Rot bio-indicator OTUs, c) as well as the detection of several other bio-indicator OTUs in both Lake Rot and Sihl River, imply that not all brGDGT producers may fall within this phylum. Further research aimed at identifying bacterial producers of brGDGTs in freshwater systems, should not only focus on identifying potential producers within the Acidobacteria phylum, but also explore other phyla that may be involved in the production of these biomarker lipids in freshwater systems.

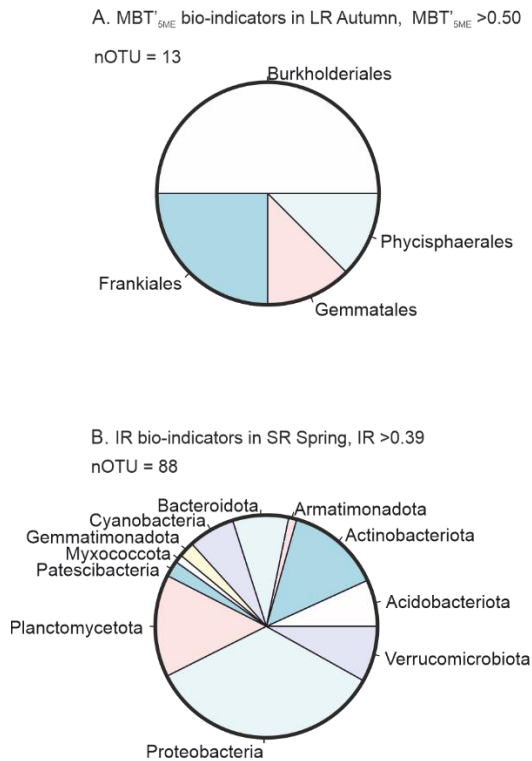


Fig. 8. Pie chart depicting the phylogenetic distribution of bio-indicator OTUs, (A) bio-indicator OTUs that are increased in Lake Rot autumn season mesocosms with $MBT'_{SME} > 0.5$, order level; (B) distribution of bio-indicator OTUs that are increased in Sihl River spring season mesocosms with $IR > 0.39$, phylum level.

4. Conclusions

The seasonal mesocosm dataset was used to test production of brGDGTs sourced from Lake Rot and Sihl River surface water under three different temperatures, providing insights into the drivers behind brGDGT variability in both a lake and river system. The hypotheses proposed can now be answered as follows:

(H1) While our oxic mesocosm setup revealed variations in brGDGTs concentration and/or distribution, evaluating the control set-ups highlighted those factors such as the removal of grazing microorganisms, change in nutrient availability, and the exclusion of sediment from freshwater introduce secondary effects, which limit the extent to which mesocosm can be seen as a replication of the natural environment. Furthermore, unintended small changes in the potentially confounding factors (pH, alkalinity, conductivity, Ca^{2+}) were measured, both in the control and in the temperature treatments, with specifically pH, alkalinity and conductivity showing correlations with GDGT-based ratios. To constrain the impacts of these parameters, a multifactorial design is needed. It is crucial for future incubation studies to exercise caution when considering the constraints of such setups and the potential sensitivity of specific microbial communities to temperature changes. Although the range of temperatures used was realistic, the sudden increase in temperature potentially impacted the $\text{MBT}'_{5\text{ME}}$ response for instance in the warmest spring mesocosm, and in the cold summer mesocosms. A modified set-up could include a more gradual increase or decrease of the growth temperature to test for this effect. Finally, employing more robust incubation setups like chemostats enables continuous monitoring of nutrient availability for microorganisms, reducing nutrient stress for bacteria.

(H2) A muted increase in situ $\text{MBT}'_{5\text{ME}}$ values with temperature was observed, with $T_{\text{rec.}}$ at both locations underestimating average temperature at time of sampling. The muted response of $\text{MBT}'_{5\text{ME}}$ in Lake Rot and Sihl River cooling and warming temperature treatments further highlights the limitations of this temperature proxy in our settings. Nonetheless, in certain mesocosms, $\text{MBT}'_{5\text{ME}}$ does show a response to warming temperatures.

(H3) Although water chemistry variables have the potential to affect brGDGT ratios (IR) in riverine systems, complicating the idea of a unidirectional temperature response of brGDGTs in the water column, temperature is still recognised as the primary driver behind brGDGT distribution changes. Therefore, the use of GDGT ratios as a paleotemperature application remains a reasonable and valuable approach.

(H4) A change in brGDGT distribution (specifically the IR in Sihl River) is indeed coeval with a change in bacterial community composition as revealed by the bio-indicator OTUs. This highlights the potential for the role of bacterial communities in driving changes in GDGT distributions.

In summary, the MBT'_{SME} is more strongly influenced by warming and may be insensitive to cold spells. Despite the observed limitation of MBT'_{SME} as a temperature proxy in Lake Rot and Sihl River, the increase in IR with warming temperature treatments in Sihl River suggests that the in-situ production of 6-methyl brGDGTs in rivers and their temperature sensitivity could be a promising area for further investigation.

Acknowledgement

This work was supported by the Swiss National Science Foundation [SNSF Project MiCoDy, grant PR00P2_179783]. In addition, the authors wish to express their gratitude for the assistance provided during the fieldwork of this project by Mr. Marco Bolandini, for the valuable support extended by the staff of the Genetic Diversity Center of ETH Zürich (GDC) in the laboratory work and the anonymous reviewers for their critical and constructive comments on an earlier version of this manuscript

Bibliography, Chapter 2

- Bódis, E., Tóth, B., and Sousa, R. (2016). Freshwater mollusc assemblages and habitat associations in the Danube River drainage, Hungary. *Aquatic Conservation: Marine and Freshwater Ecosystems*, 26(2), 319-332.
- Buckles, L. K., Weijers, J. W., Verschuren, D., and Sinninghe Damsté, J. S. (2014). Sources of core and intact branched tetraether membrane lipids in the lacustrine environment: Anatomy of Lake Challa and its catchment, equatorial East Africa. *Geochimica et Cosmochimica Acta*, 140, 106-126.
- Chen, Y., Zheng, F., Yang, H., Yang, W., Wu, R., Liu, X., Liang, H., Chen, H., Pei, H., Zhang, C., Pancost, R.D., Zeng, Z. (2022). The production of diverse brGDGTs by an *Acidobacterium* providing a physiological basis for paleoclimate proxies. *Geochimica et Cosmochimica Acta*, 337, 155-165.
- Collins, L. M., Dziak, J. J., and Li, R. (2009). Design of experiments with multiple independent variables: a resource management perspective on complete and reduced factorial designs. *Psychological methods*, 14(3), 202.
- Crampton-Flood, E. D., Tierney, J. E., Peterse, F., Kirkels, F. M., and Sinninghe Damsté, J. S. (2020). BayMBT: A Bayesian calibration model for branched glycerol dialkyl glycerol tetraethers in soils and peats. *Geochimica et Cosmochimica Acta*, 268, 142-159.
- De Cáceres, M. (2013). How to use the indicpecies package (ver. 1.7. 1). *R Proj*, 29.
- De Jonge, C., Hopmans, E. C., Stadnitskaia, A., Rijpstra, W. I. C., Hofland, R., Tegelaar, E., Sinninghe Damsté, J. S. (2013). Identification of novel penta- and hexamethylated branched glycerol dialkyl glycerol tetraethers in peat using HPLC–MS², GC–MS and GC–SMB–MS. *Organic geochemistry*, 54, 78-82.
- De Jonge, C., Stadnitskaia, A., Hopmans, E. C., Cherkashov, G., Fedotov, A., and Sinninghe Damsté, J. S. (2014a). In situ produced branched glycerol dialkyl glycerol tetraethers in suspended particulate matter from the Yenisei River, Eastern Siberia. *Geochimica et Cosmochimica Acta*, 125, 476-491.
- De Jonge, C., Hopmans, E. C., Zell, C. I., Kim, J. H., Schouten, S., and Sinninghe Damsté, J. S. (2014b). Occurrence and abundance of 6-methyl branched glycerol dialkyl glycerol tetraethers in soils: Implications for palaeoclimate reconstruction. *Geochimica et Cosmochimica Acta*, 141, 97-112.
- De Jonge, C., Radujković, D., Sigurdsson, B. D., Weedon, J. T., Janssens, I., and Peterse, F. (2019). Lipid biomarker temperature proxy responds to abrupt shift in the bacterial community composition in geothermally heated soils. *Organic Geochemistry*, 137, 103897.

- De Jonge, C., Kuramae, E. E., Radujković, D., Weedon, J. T., Janssens, I. A., and Peterse, F. (2021). The influence of soil chemistry on branched tetraether lipids in mid-and high latitude soils: Implications for brGDGT-based paleothermometry. *Geochimica et Cosmochimica Acta*, 310, 95-112.
- Dedysh, S. N., and Sinninghe Damsté, J. S. (2018). *Acidobacteria*. eLS, 1-10.
- Deng, L., Bölsterli, D., Kristensen, E., Meile, C., Su, C. C., Bernasconi, S. M., Seidenkrantz, M., Glombita, C., Lagostina, L., Han, X., Jørgensen, B.B., Røy, H., Lever, M. A. (2020). Macrofaunal control of microbial community structure in continental margin sediments. *Proceedings of the National Academy of Sciences*, 117(27), 15911-15922.
- Elser, J. J., Bracken, M. E., Cleland, E. E., Gruner, D. S., Harpole, W. S., Hillebrand, H., Ngai, J.T., Seabloom, E.W., Shurin, J.B., Smith, J. E. (2007). Global analysis of nitrogen and phosphorus limitation of primary producers in freshwater, marine and terrestrial ecosystems. *Ecology letters*, 10(12), 1135-1142.
- Freymond, Chantal V., Francien Peterse, Lorena V. Fischer, Florin Filip, Liviu Giosan, and Timothy I. Eglinton. "Branched GDGT signals in fluvial sediments of the Danube River basin: Method comparison and longitudinal evolution." *Organic Geochemistry* 103 (2017): 88-96.
- García-Martín, E. E., Serret, P., and Pérez-Lorenzo, M. (2011). Testing potential bias in marine plankton respiration rates by dark bottle incubations in the NW Iberian shelf: incubation time and bottle volume. *Continental Shelf Research*, 31(5), 496-506.d
- Guo, J., Ma, T., Liu, N., Zhang, X., Hu, H., Ma, W., ... and Peterse, F. (2022). Soil pH and aridity influence distributions of branched tetraether lipids in grassland soils along an aridity transect. *Organic Geochemistry*, 164, 104347.
- Halamka, T. A., Raberg, J. H., McFarlin, J. M., Younkin, A. D., Mulligan, C., Liu, X. L., and Kopf, S. H. (2022). Production of diverse brGDGTs by *Acidobacterium Solibacter usitatus* in response to temperature, pH, and O₂ provides a culturing perspective on br GDGT proxies and biosynthesis. *Geobiology*, 21(1), 102-118.
- Halfman, R., Lembrechts, J., Radujković, D., De Gruyter, J., Nijs, I., and De Jonge, C. (2022). Soil chemistry, temperature, and bacterial community composition drive brGDGT distributions along a subarctic elevation gradient. *Organic Geochemistry*, 163, 104346.
- Han, X., Schubert, C. J., Fiskal, A., Dubois, N., and Lever, M. A. (2020). Eutrophication as a driver of microbial community structure in lake sediments. *Environmental Microbiology*, 22(8), 3446-3462.

- Harning, D. J., Curtin, L., Geirsdóttir, Á., D'Andrea, W. J., Miller, G. H., and Sepúlveda, J. (2020). Lipid biomarkers quantify Holocene summer temperature and ice cap sensitivity in Icelandic lakes. *Geophysical Research Letters*, 47(3), e2019GL085728.
- Hopmans, E. C., Schouten, S., and Sinninghe Damsté, J. S. (2016). The effect of improved chromatography on GDGT-based palaeoproxies. *Organic Geochemistry*, 93, 1-6.
- Horne, A. J., and Goldman, C. R. (1994). *Limnology* (Vol. 2). New York: McGraw-Hill.
- Huguet, A., Francez, A. J., Jusselme, M. D., Fosse, C., and Derenne, S. (2014). A climatic chamber experiment to test the short-term effect of increasing temperature on branched GDGT distribution in Sphagnum peat. *Organic geochemistry*, 73, 109-112.
- Huguet, C., Hopmans, E. C., Febo-Ayala, W., Thompson, D. H., Sinninghe Damsté, J. S., and Schouten, S. (2006). An improved method to determine the absolute abundance of glycerol dibiphytanyl glycerol tetraether lipids. *Organic Geochemistry*, 37(9), 1036-1041.
- James, C., Fisher, J., Russell, V., Collings, S., and Moss, B. (2005). Nitrate availability and hydrophyte species richness in shallow lakes. *Freshwater biology*, 50(6), 1049-1063.
- Kirkels, F. M., Zwart, H. M., Usman, M. O., Hou, S., Ponton, C., Giosan, L., Eglinton, T.I., Peterse, F. (2022). From soil to sea: sources and transport of organic carbon traced by tetraether lipids in the monsoonal Godavari River, India. *Biogeosciences*, 19(17), 3979-4010.
- Kunzmann, A. J., Ehret, H., Yohannes, E., Straile, D., and Rothhaupt, K. O. (2019). Calanoid copepod grazing affects plankton size structure and composition in a deep, large lake. *Journal of Plankton Research*, 41(6), 955-966.
- Lever, M. A., Torti, A., Eickenbusch, P., Michaud, A. B., Šantl-Temkiv, T., and Jørgensen, B. B. (2015). A modular method for the extraction of DNA and RNA, and the separation of DNA pools from diverse environmental sample types. *Frontiers in microbiology*, 6, 476.
- Lliros, M., Inceoğlu, Ö., García-Armisen, T., Anzil, A., Leporcq, B., Pigneur, L. M., Viroux, L., Darchambeau, F., Descy, J., Servais, P. (2014). Bacterial community composition in three freshwater reservoirs of different alkalinity and trophic status. *PloS one*, 9(12), e116145.
- Loomis, S. E., Russell, J. M., Heures, A. M., D'Andrea, W. J., and Sinninghe Damsté, J. S. (2014). Seasonal variability of branched glycerol dialkyl glycerol tetraethers (brGDGTs) in a temperate lake system. *Geochimica et Cosmochimica Acta*, 144, 173-187.

Marcott, S. A., and Shakun, J. D. (2015). Holocene climate change and its context for the future. *Pages Mag.*, 23(1), 28-29.

Martínez-Sosa, P., and Tierney, J. E. (2019). Lacustrine brGDGT response to microcosm and mesocosm incubations. *Organic Geochemistry*, 127, 12-22.

Martínez-Sosa, P., Tierney, J. E., and Meredith, L. K. (2020). Controlled lacustrine microcosms show a brGDGT response to environmental perturbations. *Organic Geochemistry*, 145, 104041.

Martínez-Sosa, P., Tierney, J. E., Stefanescu, I. C., Crampton-Flood, E. D., Shuman, B. N., and Routson, C. (2021). A global Bayesian temperature calibration for lacustrine brGDGTs. *Geochimica et Cosmochimica Acta*, 305, 87-105.

McMurdie, P. J., and Holmes, S. (2013). phyloseq: an R package for reproducible interactive analysis and graphics of microbiome census data. *PloS one*, 8(4), e61217.

Miller, D. R., Habicht, M. H., Keisling, B. A., Castañeda, I. S., and Bradley, R. S. (2018). A 900-year New England temperature reconstruction from in situ seasonally produced branched glycerol dialkyl glycerol tetraethers (brGDGTs). *Climate of the Past*, 14(11), 1653-1667.

Naafs, B. D. A., Inglis, G. N., Zheng, Y., Amesbury, M. J., Biester, H., Bindler, R., Blewett, J., Burrows, M.A., del Castillo, T., Chambers, F.M., Cohen, A.D., Evershed, R. P., Feakins, S. J., Galka, M., Gallego-Sala, A., Gandois, L., Gray, D. M., Hatcher, P. G., Honorio Coronado, E. N., Hughes, P. D. M., Pancost, R. D. (2017). Introducing global peat-specific temperature and pH calibrations based on brGDGT bacterial lipids. *Geochimica et Cosmochimica Acta*, 208, 285-301.

Naafs, B. D. A., Oliveira, A. S. F., and Mulholland, A. J. (2021). Molecular dynamics simulations support the hypothesis that the brGDGT paleothermometer is based on homeoviscous adaptation. *Geochimica et Cosmochimica Acta*, 312, 44-56.

Naeher, S., Peterse, F., Smittenberg, R. H., Niemann, H., Zigah, P. K., and Schubert, C. J. (2014). Sources of glycerol dialkyl glycerol tetraethers (GDGTs) in catchment soils, water column and sediments of Lake Rotsee (Switzerland)—Implications for the application of GDGT-based proxies for lakes. *Organic Geochemistry*, 66, 164-173.

Oksanen, J., Blanchet, F. G., Kindt, R., Legendre, P., Minchin, P. R., O'hara, R. B., Simpson, G. L., Solymos [aut], P., Steven, M. H. H., Szoecs, E., Wagner, H., Barbour, M., Bedward, M., Bolker, B., Borcard, D., Carvalho, G., Chirico, M., De Caceres, M., Evangelista, D. S. H., Oksanen, M. J. (2013). Package 'vegan'. *Community ecology package*, version, 2(9), 1-295.

- Peterse, F., Kim, J. H., Schouten, S., Kristensen, D. K., Koç, N., and Sinninghe Damsté, J. S. (2009). Constraints on the application of the MBT/CBT palaeothermometer at high latitude environments (Svalbard, Norway). *Organic Geochemistry*, 40(6), 692-699.
- Peterse, F., Moy, C. M., and Eglinton, T. I. (2015). A laboratory experiment on the behaviour of soil-derived core and intact polar GDGTs in aquatic environments. *Biogeosciences*, 12(4), 933-943.
- Peterse, F., van der Meer, J., Schouten, S., Weijers, J. W., Fierer, N., Jackson, R. B., Kim, J., Sinninghe Damsté, J. S. (2012). Revised calibration of the MBT–CBT paleotemperature proxy based on branched tetraether membrane lipids in surface soils. *Geochimica et Cosmochimica Acta*, 96, 215-229.
- Pomeroy, L. R., Sheldon, J. E., and Sheldon Jr, W. M. (1994). Changes in bacterial numbers and leucine assimilation during estimations of microbial respiratory rates in seawater by the precision Winkler method. *Applied and environmental microbiology*, 60(1), 328-332.
- Raberg, J. H., Harning, D. J., Crump, S. E., de Wet, G., Blumm, A., Kopf, S., Geirsdóttir, Á., Miller, G. H., Sepúlveda, J. (2021). Revised fractional abundances and warm-season temperatures substantially improve brGDGT calibrations in lake sediments. *Biogeosciences*, 18(12), 3579-3603.
- Rogora, M., Mosello, R., Kamburska, L., Salmaso, N., Cerasino, L., Leoni, B., Garibaldi, L., Soler, V., Lepori, F., Colombo, L., Buzzi, F. (2015). Recent trends in chloride and sodium concentrations in the deep subalpine lakes (Northern Italy). *Environmental Science and Pollution Research*, 22, 19013-19026.
- Russell, J. M., Hopmans, E. C., Loomis, S. E., Liang, J., and Sinninghe Damsté, J. S. (2018). Distributions of 5-and 6-methyl branched glycerol dialkyl glycerol tetraethers (brGDGTs) in East African lake sediment: Effects of temperature, pH, and new lacustrine paleotemperature calibrations. *Organic Geochemistry*, 117, 56-69.
- Sahonero-Canavesi, D. X., Siliakus, M. F., Abdala Asbun, A., Koenen, M., von Meijenfildt, F. B., Boeren, S., Bale, N. J., Engelman, J. C., Fiege, C., Strack van Schijndel, L., Sinninghe Damsté, J. S., Villanueva, L. (2022). Disentangling the lipid divide: Identification of key enzymes for the biosynthesis of membrane-spanning and ether lipids in Bacteria. *Science advances*, 8(50), eabq8652.
- Schouten, S., Hopmans, E. C., Pancost, R. D., and Sinninghe Damsté, J. S. (2000). Widespread occurrence of structurally diverse tetraether membrane lipids: evidence for the ubiquitous presence of low-temperature relatives of hyperthermophiles. *Proceedings of the National Academy of Sciences*, 97(26), 14421-14426.
- Schouten, S., Hopmans, E. C., and Sinninghe Damsté, J. S. (2013). The organic geochemistry of glycerol dialkyl glycerol tetraether lipids: A review. *Organic geochemistry*, 54, 19-61.

- Schubert, C. J., Lucas, F. S., Durisch-Kaiser, E., Stierli, R., Diem, T., Scheidegger, O., Vazquez, F., Müller, B. (2010). Oxidation and emission of methane in a monomictic lake (Rotsee, Switzerland). *Aquatic sciences*, 72, 455-466.
- Schwab, M. S., Gies, H., Freymond, C. V., Lupker, M., Haghipour, N., and Eglinton, T. I. (2022). Environmental and hydrologic controls on sediment and organic carbon export from a subalpine catchment: insights from a time series. *Biogeosciences*, 19(23), 5591-5616.
- Shade, A., Kent, A. D., Jones, S. E., Newton, R. J., Triplett, E. W., and McMahon, K. D. (2007). Interannual dynamics and phenology of bacterial communities in a eutrophic lake. *Limnology and Oceanography*, 52(2), 487-494.
- Shanahan, T. M., Huguen, K. A., and Van Mooy, B. A. (2013). Temperature sensitivity of branched and isoprenoid GDGTs in Arctic lakes. *Organic Geochemistry*, 64, 119-128.
- Sinninghe Damsté, J. S., Hopmans, E. C., Pancost, R. D., Schouten, S., and Geenevasen, J. A. (2000). Newly discovered non-isoprenoid glycerol dialkyl glycerol tetraether lipids in sediments. *Chemical Communications*, (17), 1683-1684.
- Sinninghe Damsté, J. S., Rijpstra, W. I. C., Hopmans, E. C., Weijers, J. W., Foesel, B. U., Overmann, J., and Dedysh, S. N. (2011). 13, 16-Dimethyl octacosanedioic acid (iso-diabolic acid), a common membrane-spanning lipid of Acidobacteria subdivisions 1 and 3. *Applied and environmental microbiology*, 77(12), 4147-4154.
- Sinninghe Damsté, J. S., Rijpstra, W. I. C., Hopmans, E. C., Foesel, B. U., Wüst, P. K., Overmann, J., Tank, M., Bryant, D. A., Dunfield, P. F., Houghton, K., Stott, M. B. (2014). Ether-and ester-bound iso-diabolic acid and other lipids in members of Acidobacteria subdivision 4. *Applied and Environmental Microbiology*, 80(17), 5207-5218.
- Sinninghe Damsté, J. S., Rijpstra, W. I. C., Foesel, B. U., Huber, K. J., Overmann, J., Nakagawa, S., Kim, J. M., Dunfield, P. F., Dadysh, S. N., Villanueva, L. (2018). An overview of the occurrence of ether-and ester-linked iso-diabolic acid membrane lipids in microbial cultures of the Acidobacteria: Implications for brGDGT paleoproxies for temperature and pH. *Organic Geochemistry*, 124, 63-76.
- Smith, V. H., Tilman, G. D., and Nekola, J. C. (1999). Eutrophication: impacts of excess nutrient inputs on freshwater, marine, and terrestrial ecosystems. *Environmental pollution*, 100(1-3), 179-196.
- Stefanescu, I. C., Shuman, B. N., and Tierney, J. E. (2021). Temperature and water depth effects on brGDGT distributions in sub-alpine lakes of mid-latitude North America. *Organic Geochemistry*, 152, 104174.

- Su, Y., Lammers, M., Zhang, Y., van Bree, L., Liu, Z., Reichart, G. J., and Middelburg, J. J. (2017). Sources of organic matter for bacteria in sediments of Lake Rotsee, Switzerland. *Journal of Paleolimnology*, 58, 391-402.
- Tierney, J. E., and Russell, J. M. (2009). Distributions of branched GDGTs in a tropical lake system: implications for lacustrine application of the MBT/CBT paleoproxy. *Organic Geochemistry*, 40(9), 1032-1036.
- Tierney, J. E., Russell, J. M., Eggermont, H., Hopmans, E. C., Verschuren, D., and Sinninghe Damsté, J. S. (2010). Environmental controls on branched tetraether lipid distributions in tropical East African lake sediments. *Geochimica et Cosmochimica Acta*, 74(17), 4902-4918.
- Tierney, J. E., Poulsen, C. J., Montañez, I. P., Bhattacharya, T., Feng, R., Ford, H. L., Hönisch, B., Inglis, G. N., Petersen, S. V., Sagoo, N., Tabor, C. R., Thirumalai, K., Zhu, J., Burls, N. J., Foster, G. L., Godderis, Y., Huber, B. T., Ivany, L. C., Turner, S. K., Lunt, D. J., McElwain, J. C., Mills, B. J. W., Otto-Bliesner, B. L., Ridgeway, A., Zhang, Y. G. (2020). Past climates inform our future. *Science*, 370(6517), eaay3701.
- Van Bree, L. G., Peterse, F., Baxter, A. J., De Crop, W., Van Grinsven, S., Villanueva, L., Verschuren, D., Sinninghe Damsté, J. S. (2020). Seasonal variability and sources of in situ brGDGT production in a permanently stratified African crater lake. *Biogeosciences*, 17(21), 5443-5463.
- Wang, H., Liu, W., He, Y., Zhou, A., Zhao, H., Liu, H., Cao, Y., Hu, J., Meng, B., Jiang, J., Kolpakova, M., Krivonogov, S., Liu, Z. (2021). Salinity-controlled isomerization of lacustrine brGDGTs impacts the associated MBT5ME' terrestrial temperature index. *Geochimica et Cosmochimica Acta*, 305, 33-48.
- Weber, Y., Sinninghe Damsté, J. S., Hopmans, E. C., Lehmann, M. F., and Niemann, H. (2017). Incomplete recovery of intact polar glycerol dialkyl glycerol tetraethers from lacustrine suspended biomass. *Limnology and Oceanography: Methods*, 15(9), 782-793.
- Weber, Y., Sinninghe Damsté, J. S., Zopfi, J., De Jonge, C., Gilli, A., Schubert, C. J., Lepori, L., Lehmann, M. F., Niemann, H. (2018). Redox-dependent niche differentiation provides evidence for multiple bacterial sources of glycerol tetraether lipids in lakes. *Proceedings of the National Academy of Sciences*, 115(43), 10926-10931.
- Weijers, J. W., Schouten, S., Spaargaren, O. C., and Sinninghe Damsté, J. S. (2006). Occurrence and distribution of tetraether membrane lipids in soils: Implications for the use of the TEX86 proxy and the BIT index. *Organic Geochemistry*, 37(12), 1680-1693.

- Weijers, J. W., Schouten, S., van den Donker, J. C., Hopmans, E. C., and Sinninghe Damsté, J. S. (2007). Environmental controls on bacterial tetraether membrane lipid distribution in soils. *Geochimica et Cosmochimica Acta*, 71(3), 703-713.
- Weijers, J. W., Panoto, E., van Bleijswijk, J., Schouten, S., Rijpstra, W. I. C., Balk, M., Stams, A. J. M., Sinninghe Damsté, J. S. (2009). Constraints on the biological source (s) of the orphan branched tetraether membrane lipids. *Geomicrobiology Journal*, 26(6), 402-414.
- Weyhenmeyer, G. A., Hartmann, J., Hessen, D. O., Kopáček, J., Hejzlar, J., Jacquet, S., Hamilton, S. K., Verburg, P., Leach, T. H., Schmid, M., Flaim, G., Nöges, T., Nöges, P., Wentzky, V. C., Rogora, M., Rusak, J. A., Kosten, S., Paterson, A. M., Teubner, K., Higgins, S. N., Lawrence, G., Kangur, K., Kokorite, I., Cerasino, L., Funk, L., Harvey, R., Moatar, F., deWit, H. A., Zechmeister, T. (2019). Widespread diminishing anthropogenic effects on calcium in freshwaters. *Scientific Reports*, 9(1), 1-10.
- White, P.A., Kalff, J., Rasmussen, J.B., Gasol, J.M., 1991. The Effect of Temperature and Algal Biomass on Bacterial Production and Specific Growth Rate in Freshwater and Marine Habitats. *Microbial Ecology* 21, 99–118.
- Xiao, W., Wang, Y., Zhou, S., Hu, L., Yang, H., and Xu, Y. (2016). Ubiquitous production of branched glycerol dialkyl glycerol tetraethers (brGDGTs) in global marine environments: a new source indicator for brGDGTs. *Biogeosciences*, 13(20), 5883-5894.
- Yamamoto, M., Shimamoto, A., Fukuhara, T., and Tanaka, Y. (2016). Source, settling and degradation of branched glycerol dialkyl glycerol tetraethers in the marine water column. *Geochimica et Cosmochimica Acta*, 191, 239-254.
- Zak, D., Hupfer, M., Cabezas, A., Jurasinski, G., Audet, J., Kleeberg, A., McInnes, R., Kristiansen, S. M., Petersen, R. J., Liu, H., Goldhammer, T. (2021). Sulphate in freshwater ecosystems: A review of sources, biogeochemical cycles, ecotoxicological effects and bioremediation. *Earth-Science Reviews*, 212, 103446.
- Zang, J., Lei, Y., and Yang, H. (2018). Distribution of glycerol ethers in Turpan soils: implications for use of GDGT-based proxies in hot and dry regions. *Frontiers of Earth Science*, 12, 862-876.
- Zell, C., Kim, J. H., Hollander, D., Lorenzoni, L., Baker, P., Silva, C. G., Nittouer, C., Sinninghe Damsté, J. S. (2014). Sources and distributions of branched and isoprenoid tetraether lipids on the Amazon shelf and fan: Implications for the use of GDGT-based proxies in marine sediments. *Geochimica et Cosmochimica Acta*, 139, 293-312.

Zeng, Z., Chen, H., Yang, H., Chen, Y., Yang, W., Feng, X., Pei., H, and Welander, P. V. (2022). Identification of a protein responsible for the synthesis of archaeal membrane-spanning GDGT lipids. *Nature communications*, 13(1), 1545.

Supplementary materials, Chapter 2

Sample	Proteobacteria (%)	Actinobacteriota (%)	Cyanobacteria (%)	Bacteroidota (%)	Acidobacteriota (%)	fraction from total OTU reads (%)	Season	Treatment
LR-Spr-0	11.66666667	63.39215686	13.56862745	9.333333333	0	97.96078431	Spring	T0
LR-Sum-0	27.94117647	58.56862745	4.941176471	5.509803922	0.039215686	97	Summer	T0
LR-Aut-0	32.45098039	24.62745098	14.23529412	9.274509804	1.274509804	81.8627451	Autumn	T0
LR-Spr-3W-C	67.03921569	22.35294118	1.078431373	3.705882353	0.450980392	68.73170732	Spring	Control
LR-Sum-2W-C	11.1372549	2.431372549	54.01960784	1.058823529	0.117647059	68.76470588	Summer	Control
LR-Sum-3W-C	47.1372549	25.96078431	3.588235294	7.843137255	0.137254902	84.66666667	Summer	Control
LR-Aut-1W-C	33.39215686	22.84313725	17.35294118	6.470588235	0.431372549	81	Autumn	Control
LR-Aut-5W-C	80.80392157	0.490196078	0.568627451	9.019607843	0.411764706	90.6097561	Autumn	Control
LR-Sum-24h-T	34.43137255	3.470588235	13.33333333	0	0	93.95121951	Summer	Cooling
LR-Sum-1W-T	26.7254902	42.76470588	14	4.529411765	0.058823529	88.07843137	Summer	Cooling
LR-Aut-24h-Co	20.54901961	43.7254902	8.823529412	10.05882353	0.078431373	83.02439024	Autumn	Cooling
LR-Aut-1W-W	36.39215686	26.1372549	12.45098039	4.705882353	0.137254902	79.82352941	Autumn	Warming
LR-Aut-2W-W	20.49019608	46.35294118	9.392156863	6.098039216	0.078431373	82.41176471	Autumn	Warming
SR-Spr-0	32.37254902	7.862745098	3.470588235	43.03921569	1.117647059	87.8627451	Spring	T0
SR-Sum-0	42.92156863	20.74509804	2.470588235	22.82352941	0.529411765	89.49019608	Summer	T0
SR-Aut-0	42.2745098	12.64705882	15.70588235	8.333333333	3.235294118	82.19607843	Autumn	T0
SR-Spr-1W-C	54.58823529	7.705882353	2.921568627	20.25490196	0.68627451	86.15686275	Spring	Control
SR-Spr-3W-C	23.39215686	63.03921569	3.784313725	4.784313725	0.647058824	95.64705882	Spring	Control
SR-Aut-2W-C	40.35294118	25.82352941	5.68627451	14.03921569	0.098039216	86	Autumn	Control
SR-Aut-3W-C	41.54901961	17.68627451	14.94117647	16.80392157	0	90.98039216	Autumn	Control
SR-Spr-24h-T	21.74509804	39.43137255	10.07843137	10.92156863	0	82.17647059	Spring	Warming
SR-Spr-1W-W	53.17647059	2.705882353	0	2.215686275	0	58.09803922	Spring	Warming
SR-Aut-2W-W	32.58823529	11.54901961	3.803921569	2.529411765	0.156862745	50.62745098	Autumn	Warming

Supplementary Table 1. The fractional abundance (OTU reads %) of the major phyla and phylum Acidobacteria for the 25 samples that underwent successful 16S gene quantification and sequencing. OTU read % reflects the fraction of these major phyla out of the 5100 total rarefied OTUs. Successful quantification denotes samples that passed the Cp cut-off threshold of 27.

SPR Summer	lla	lla'	llla'	lllb'	lllc'	llld'	llle'	lla	llb	llc	llc'	lla	llb	llc	llc'	lla	llb	llc	llc'	lla	llb	llc	llc'	lla	llb	llc	llc'	lla	llb	llc	llc'	lla	llb	llc	llc'	lb	lc	2ng/L	MBT _{SKE}	IR	DC	CBP	Rec T (°C)-Russell et al., (2018) calibration	Rec a.e. T(°C)-Martinez-Sosa et al., (2021)	Temperature (°C)	Treatment	Timepoint						
T0	11.16	12.76	16.87±1.73	1.01±0.04	1.6±0.04	1.33	0.84	24.13	9.21	12.05±1.08	4.9±0.12	6.07±0.15	0.89±0.02	0.4±0.01	16.75±2.8	6.54±0.17	1.91±0.13	45.9±3.24	54.06	0.44	0.4	0.21	-0.11	12.92	12.04	23.00	Control	T0																									
24h10	10.2±0.93	12.4±0.11	8.86±0.07	b.d.l.	b.d.l.	0.4±0.01	0.39±0.01	20.03±1.62	12.05±1.08	4.9±0.12	6.07±0.15	0.89±0.02	0.4±0.01	16.75±2.8	6.54±0.17	1.91±0.13	45.9±3.24	54.06	0.44	0.4	0.21	-0.11	12.92	12.04	23.00	Control	T0																										
24h15	10.2±0.93	12.4±0.11	8.86±0.07	b.d.l.	b.d.l.	0.4±0.01	0.39±0.01	20.03±1.62	12.05±1.08	4.9±0.12	6.07±0.15	0.89±0.02	0.4±0.01	16.75±2.8	6.54±0.17	1.91±0.13	45.9±3.24	54.06	0.44	0.4	0.21	-0.11	12.92	12.04	23.00	Control	T0																										
24h25	3.77±0.38	15.25±0.08	b.d.l.	b.d.l.	b.d.l.	b.d.l.	b.d.l.	22.47±1.28	12.29±1.15	6.01±0.27	7.55±0.3	b.d.l.	b.d.l.	24.27±0.14	7.32±0.11	2.51	8.49±0.23	22.22±1.13	0.47±0.03	0.24	0.14	-0.5±0.3	14.12	12.97	17.50	Temperate	24h																										
1w10	8.08±0.09	16.27±1.06	1.04±0.14	1.75±0.17	0.41±0.04	0.41±0.04	0.41±0.04	22.85±4.85	11.41±0.17	4.7±0.45	6.24±0.59	0.44±0.04	0.57±0.11	17.57±1.06	6.32±0.16	1.99±0.28	24.28±5.33	10.53	0.47	0.45	0.02	-0.18	14.00	13.09	25.00	Control	24h																										
1w15	0.98±0.18	18.62±3.25	b.d.l.	b.d.l.	b.d.l.	b.d.l.	b.d.l.	20.34±7.24	8.51±0.04	8.62±0.04	8.57±0.04	b.d.l.	b.d.l.	19.63±0.96	11.34±0.05	3.39±0.03	22.22±4.66	10.53	0.47	0.45	0.02	-0.18	14.00	13.09	25.00	Control	1W																										
1w25	6.89±1.77	16.9±1.35	0.96±0.24	1.64±0.04	0.4±0.01	0.37±0.01	17.39±0.28	13.55±0.38	4.79±0.11	7.27±0.17	0.85±0.02	0.43±0.01	19.46±0.03	7.1±0.16	1.99±0.21	51.93±8.08	12.36	0.46	0.53	0.01	-0.05±0.02	13.82	12.46	17.50	Temperate	1W																											
2w10	20.91±4.21	12.84±2.1	0.92±0.07	1.51	0.35	0.36	14.47±3.32	10.61±0.36	4.7	6.61	0.96±0.12	0.4±0.04	17.31±1.18	6.26	1.8±0.25	57.66±3.81	12.46	0.46	0.53	0.01	-0.05±0.02	13.82	12.46	17.50	Control	1W																											
2w15	8.55±0.03	19.34±0.03	0.99±0.02	1.72±0.01	0.35	0.37	17.06±0.15	13.91±0.86	4.78±0.02	6.72±0.03	0.88	0.45	16.66±1.08	6.41±0.03	1.82±0.06	70.64±2.6	12.59	0.46	0.53	0.01	-0.05±0.02	13.82	12.59	17.50	Control	2W																											
2w25	7.9±0.47	17.55±1.35	0.78	1.43±0.02	0.28	0.31	12.72±0.14	20.0±0.04	3.6±0.04	7.9±0.09	0.71±0.01	0.42	17.85±1.34	6.98±0.08	1.57±0.06	114.11±4.83	11.84	0.51±0.02	0.64	0.27	0.1±0.02	15.27	14.74	25.00	Control	2W																											
3w10	7.86±0.7	17.97±1.79	0.98±0.07	1.76±0.02	0.34	0.41	18.84±2.1	13.05±0.33	5.02±0.05	7.21±0.07	0.92±0.01	0.5±0.01	16.67±0.42	6.55±0.07	1.9±0.05	134.46±4.63	14.48	0.42±0.02	0.51±0.04	0.28	0.04	-0.03±0.04	12.25	11.48	10.00	Cold	3W																										
3w15	3.11±1.54	18.72±4.49	0.87±0.02	1.51±0.01	0.31	0.36	14.65±1.4	20.4±4.39	4.1±0.04	7.17±0.06	0.72±0.01	0.41	19.54±3.13	6.36±0.06	1.79±0.08	39.77±3.65	14.53	0.52±0.08	0.65±0.06	0.25	0.06	0.09±0.02	15.52	14.53	17.50	Temperate	3W																										
3w25	6.45±0.2	15.8±0.6	0.66±0.01	1.45±0.09	0.21±0.01	0.24±0.02	10.06±0.89	22.49±0.11	2.63±0.16	9.72±0.61	0.61±0.04	0.43±0.03	20.04±0.1	7.69±0.48	1.53±0.06	65.99±2.49	16.97	0.61±0.01	0.7±0.01	0.28	0.01	0.15±0.01	18.18	16.97	25.00	Control	3W																										
5w10	1.3±0.11	9.3±0.31	b.d.l.	b.d.l.	b.d.l.	b.d.l.	35.68±1.32	b.d.l.	4.34±0.16	3.39±0.13	b.d.l.	b.d.l.	38.82±2.0	5.26±0.2	1.91	21.14±1.09	13.06	0.48±0.02	0.18	0.15	-0.76±0.02	14.35	13.06	10.00	Cold	5W																											
5w15	1.23±0.82	13.35±0.46	b.d.l.	b.d.l.	b.d.l.	b.d.l.	28.87±6.61	b.d.l.	2.14±1.56	4.86±0.17	b.d.l.	b.d.l.	44.78±5.23	2.04±0.32	2.73±0.03	23.3±2.2	14.44	0.52±0.11	0.24±0.08	0.11	0.08	-0.63±0.07	15.78	14.44	17.50	Temperate	5W																										
5w25	1.06±0.19	7.69±4.73	1.61±0.21	3.56±0.19	0.52±0.03	0.47±0.2	5.29±0.42	7.44±2.35	6.45±0.35	23.79±1.29	1.49±0.08	1.06±0.06	20.4±0.85	18.82±1.02	0.35±0.03	40.81±4.67	20.91	0.73	0.69±0.03	0.6	0.03	0.21±0.01	22.39	20.91	25.00	Control	5W																										
n-vialle																																																					
Temperature °C																																																					
pH																																																					
Conductivity																																																					
Alkalinity																																																					
Ca2+																																																					
Na+																																																					
NO3-																																																					
SO2-4																																																					

LR-Control																
Spring and Summer																
	MBT _{SME}	IR	DC	CBT	ng/L	I/la	II/a	III/a	IIa'	IIa'	IIa'	IIb'	IIb'	Ia	Ib	Ic
pH																
Conductivity																
Alkalinity																
Na ⁺ (mg/L)																
Ca ²⁺ (mg/L)			0.72		0.71											
NO ₃ ⁻ (mg/L)																
SO ₄ ²⁻ (mg/L)																

LR-Cooling																
Autumn																
	MBT _{SME}	IR	DC	CBT	ng/L	I/la	II/a	III/a	IIa'	IIa'	IIa'	IIb'	IIb'	Ia	Ib	Ic
pH																
Conductivity																
Alkalinity																
Na ⁺ (mg/L)																
Ca ²⁺ (mg/L)																
NO ₃ ⁻ (mg/L)																
SO ₄ ²⁻ (mg/L)																

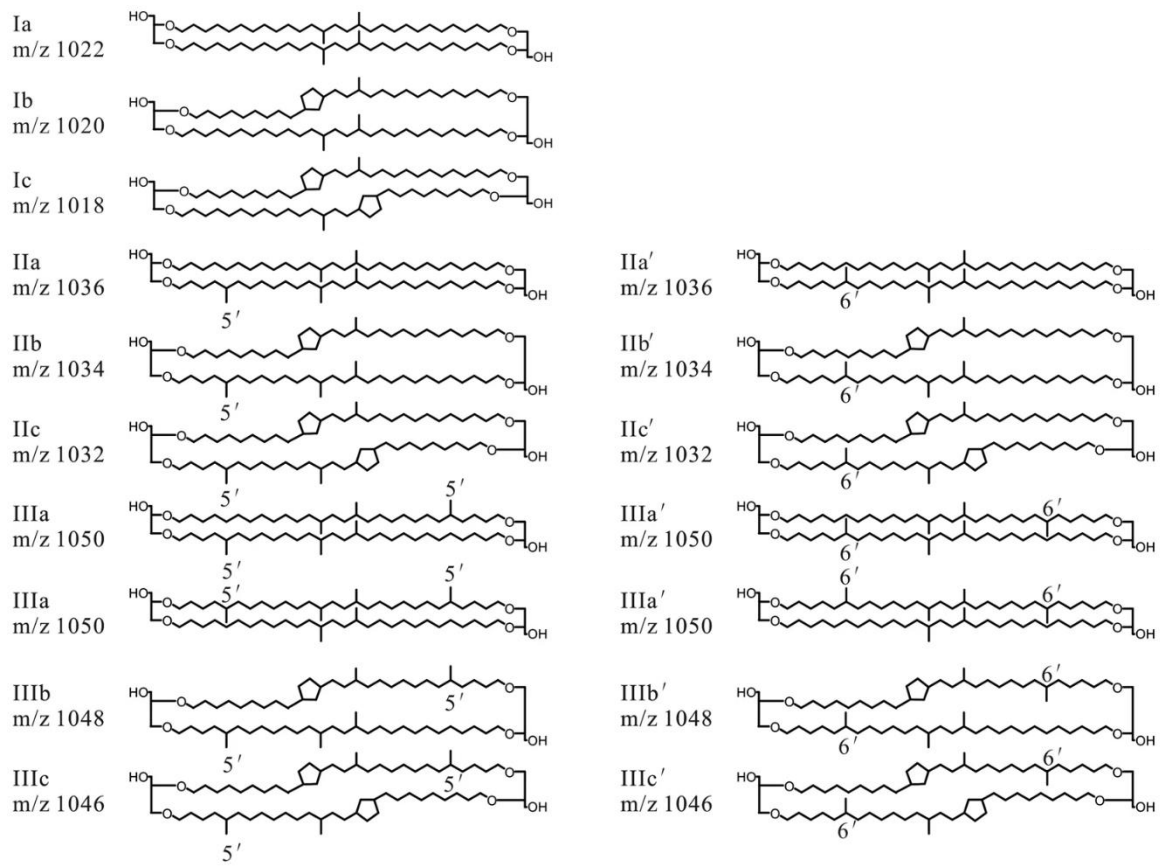
LR-warming																
Spring																
	MBT _{SME}	IR	DC	CBT	ng/L	I/la	II/a	III/a	IIa'	IIa'	IIa'	IIb'	IIb'	Ia	Ib	Ic
pH																
Conductivity																
Alkalinity																
Na ⁺ (mg/L)																
Ca ²⁺ (mg/L)																
NO ₃ ⁻ (mg/L)																
SO ₄ ²⁻ (mg/L)																

Supplementary Table 3A. Lake Rot correlation table of fractional abundance (%), concentration and ratios of brGDGTs grouped in seasonal groups and temperature treatments. Significant linear correlations (p<0.05) with environmental variables (temperature, pH, conductivity, alkalinity, Ca²⁺, Na⁺, NO₃⁻ and SO₄²⁻ are reported). Correlations with a p<0.01 are in **bold type**. As multiple autumn water chemistry parameters were distinctly different, correlation for this season is reported separately, with significant linear correlations reported for p<0.1.

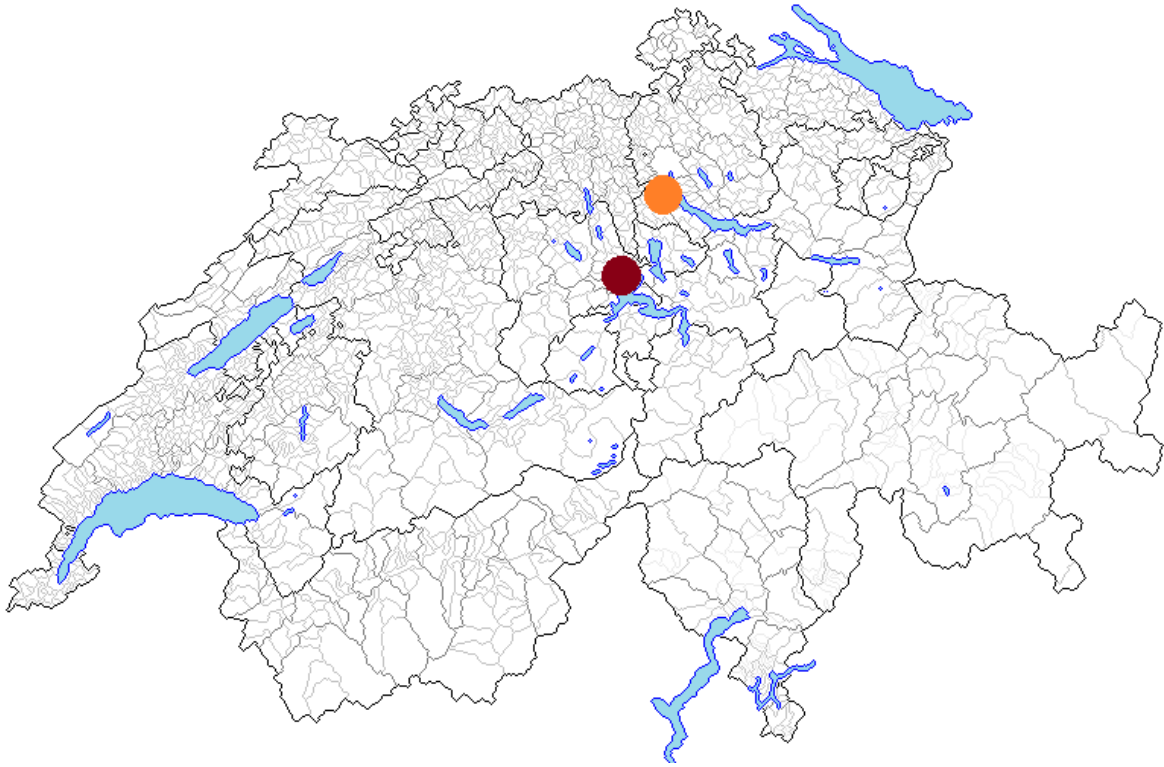
LR Spring	MBT¹_{SME} offset	IR offset
1w10	0.03	0.01
1w17.5	<i>0.00</i>	<i>0.00</i>
1w25	0.01	0.00
2w10	0.12	0.17
2w17.5	0.13	0.12
2w25	0.01	0.16
3w10	0.05	0.09
3w17.5	0.03	0.04
3w25	0.05	0.10
5w10	0.22	0.43
5w17.5	0.16	0.05
5w25	0.00	0.03
LR Summer		
1w10	0.01	0.08
1w17.5	0.03	0.01
1w25	0.01	0.04
2w10	0.00	0.02
2w17.5	0.02	0.14
2w25	0.01	0.03
3w10	0.02	0.01
3w17.5	0.04	0.21
3w25	0.00	0.20
5w10	0.01	0.09
5w17.5	0.08	0.06
5w25	0.04	0.14
LR Autumn		
1w10	0.05	0.00
1w17.5	0.04	0.03
1w25	0.12	0.04
2w10	0.00	0.01
2w17.5	0.03	0.12
2w25	0.18	0.04
3w10	0.03	0.22
3w17.5	0.09	0.03
3w25	0.22	0.01
5w10	0.18	0.30
5w17.5	0.44	0.18
5w25	0.05	0.69

SR Spring	MBT¹_{SME} offset	IR offset
1w10	0.01	0.03
1w17.5	0.01	0.08
1w25	0.07	0.17
2w10	<i>0.00</i>	<i>0.00</i>
2w17.5	0.02	0.12
2w25	0.02	0.38
3w10	0.02	0.02
3w17.5	0.01	0.18
3w25	0.19	0.39
5w10	0.45	0.39
5w17.5	0.02	0.36
5w25	0.11	0.32
SR Summer		
1w10	0.04	0.05
1w17.5	0.02	0.21
1w25	0.01	0.08
2w10	0.03	0.00
2w17.5	0.04	0.32
2w25	0.04	0.19
3w10	0.01	0.02
3w17.5	0.04	0.41
3w25	0.13	0.25
5w10	0.05	0.31
5w17.5	0.05	0.01
5w25	0.26	0.24
SR Autumn		
1w10	0.04	0.02
1w17.5	0.04	0.11
1w25	0.01	0.02
2w10	0.01	0.04
2w17.5	0.01	0.11
2w25	0.02	0.02
3w10	0.01	0.01
3w17.5	0.03	0.03
3w25	0.04	0.16
5w10	0.05	0.00
5w17.5	0.00	0.01
5w25	0.04	0.12

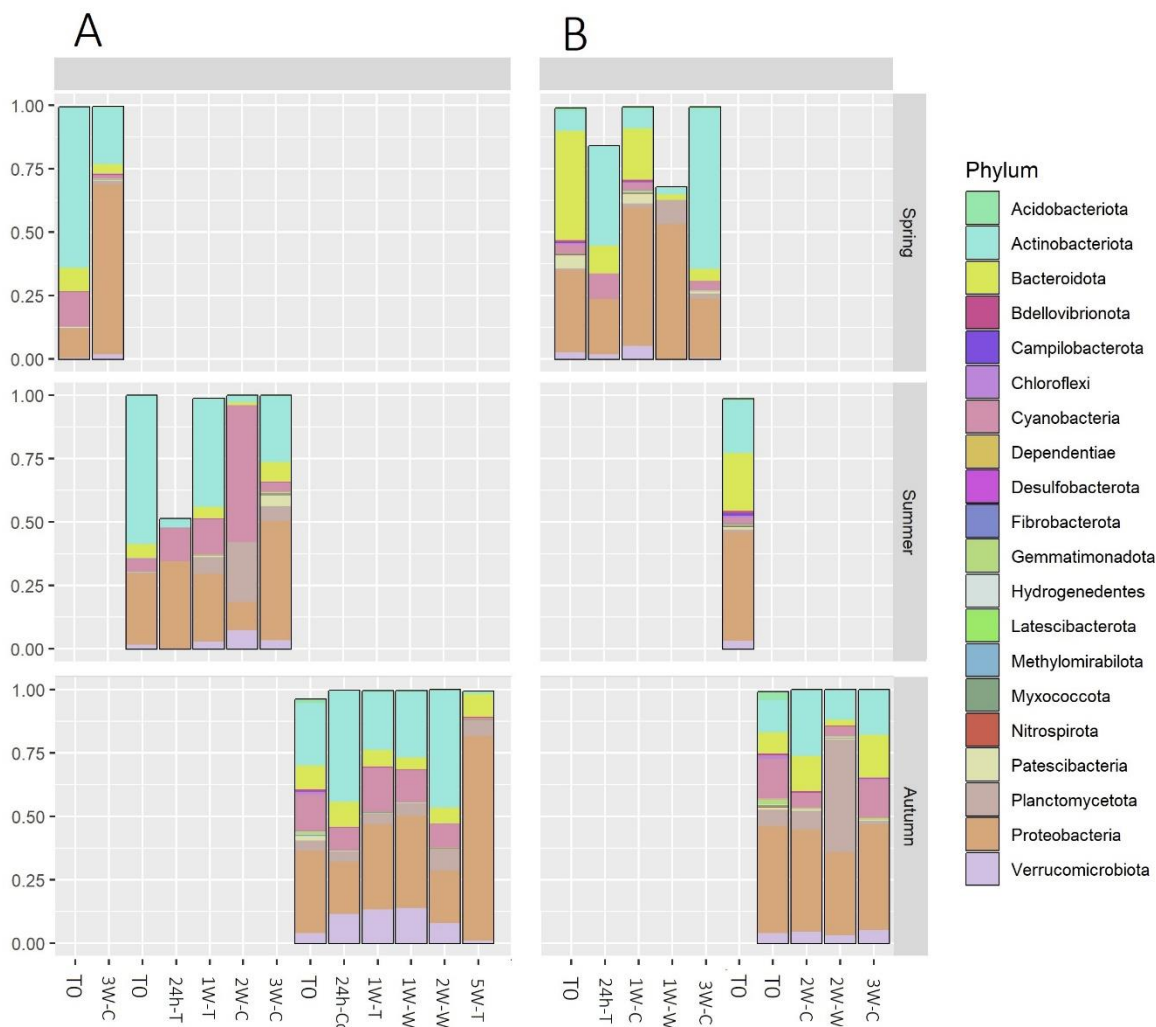
Supplementary Table 4. The mesocosm selection criteria based on offset values of MBT¹_{SME} and IR compared to the value at 24h for each treatment. For 2 italic samples "LR Spring-1w 17.5" and "SR Spring 2w 10", where both MBT¹_{SME} and IR showed no deviation compared to their 24h respective treatment, a change in CBT¹ showed an offset and hence, samples were kept for analysis.



Supp. Fig. 1: The structural diversity of brGDGTs (De Jonge et al., 2014).



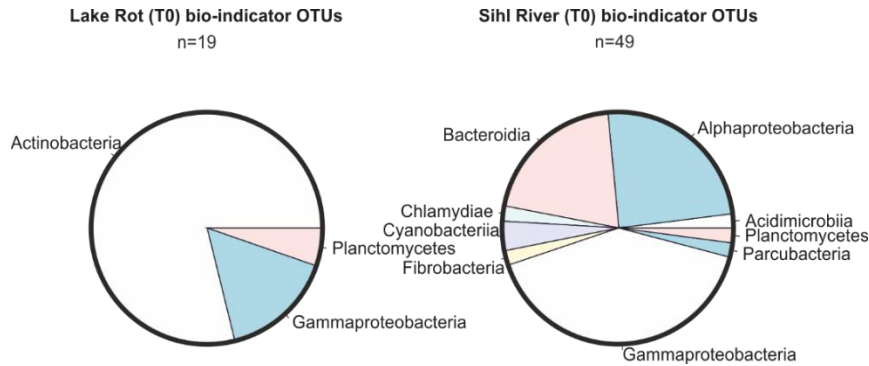
Supp. Fig. 2. Map of the freshwater bodies sampled in Switzerland. The orange sphere represents the location of Sihl River, with the red sphere showing the location of Lake Rot.



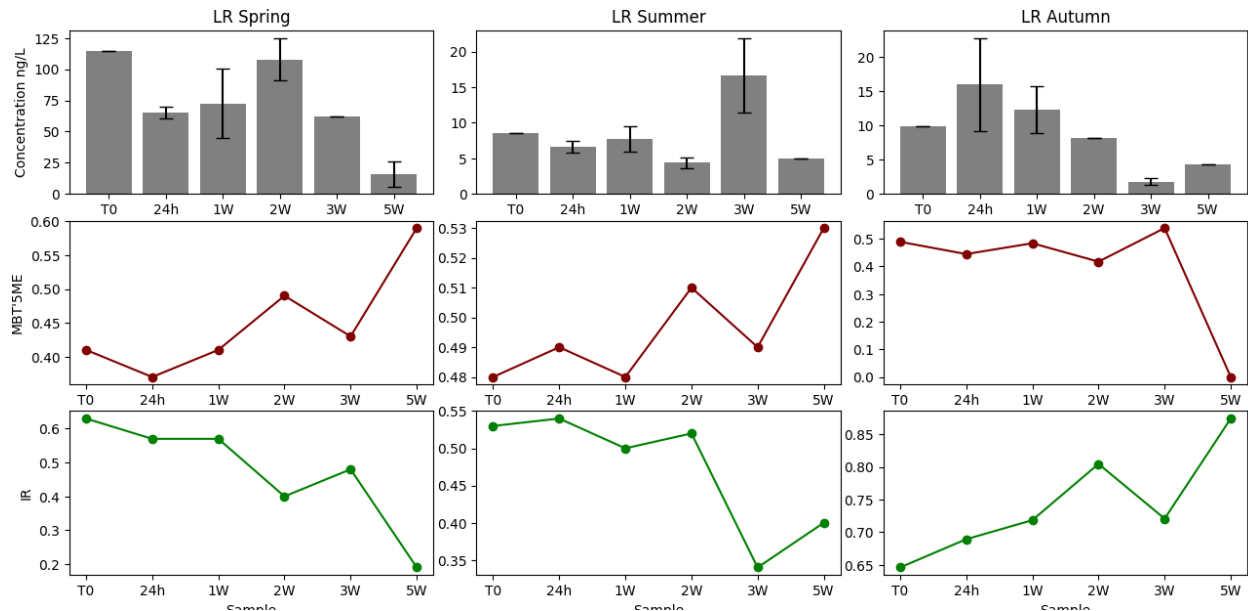
Supp. Fig. 3. Bar charts representing the relative abundance of top 20 phyla in sequenced samples ($n=23$) in (A) Lake Rot and (B) Sihl River with $cp \leq 27$. Corresponding full names of the mesocosm samples can be found in Supplementary table 1.

Results from the sequenced bacteria from our mesocosms show, in Lake Rot control mesocosm of spring (T3W), Proteobacteria has the highest count (67%), replacing the abundant Actinobacteria of T0 condition. Similarly in summer control mesocosms (T2W-T3W), Actinobacteria abundance of T0 is replaced by a noticeable Cyanobacteria presence (54%) at 2 weeks, while Proteobacteria takes over as the most abundant phyla at 3 weeks. In autumn control incubations, Proteobacteria has the highest OTU counts from beginning (T1W, 33%) to end of experiment (80%, T5W), similar to that of the T0 conditions. In the early stages of the cooling treatments (T1W, T24h, respectively for summer and autumn), Actinobacteria with a relative abundance of 42% ($\sigma = 1.5\%$), is the primary phylum in the bacteria community. In the warming mesocosms of autumn, with comparable OTU counts, Proteobacteria and Actinobacteriota alternate as most abundant phyla. In Sihl River, all control incubations for $T < 2W$ of spring and autumn show similar community

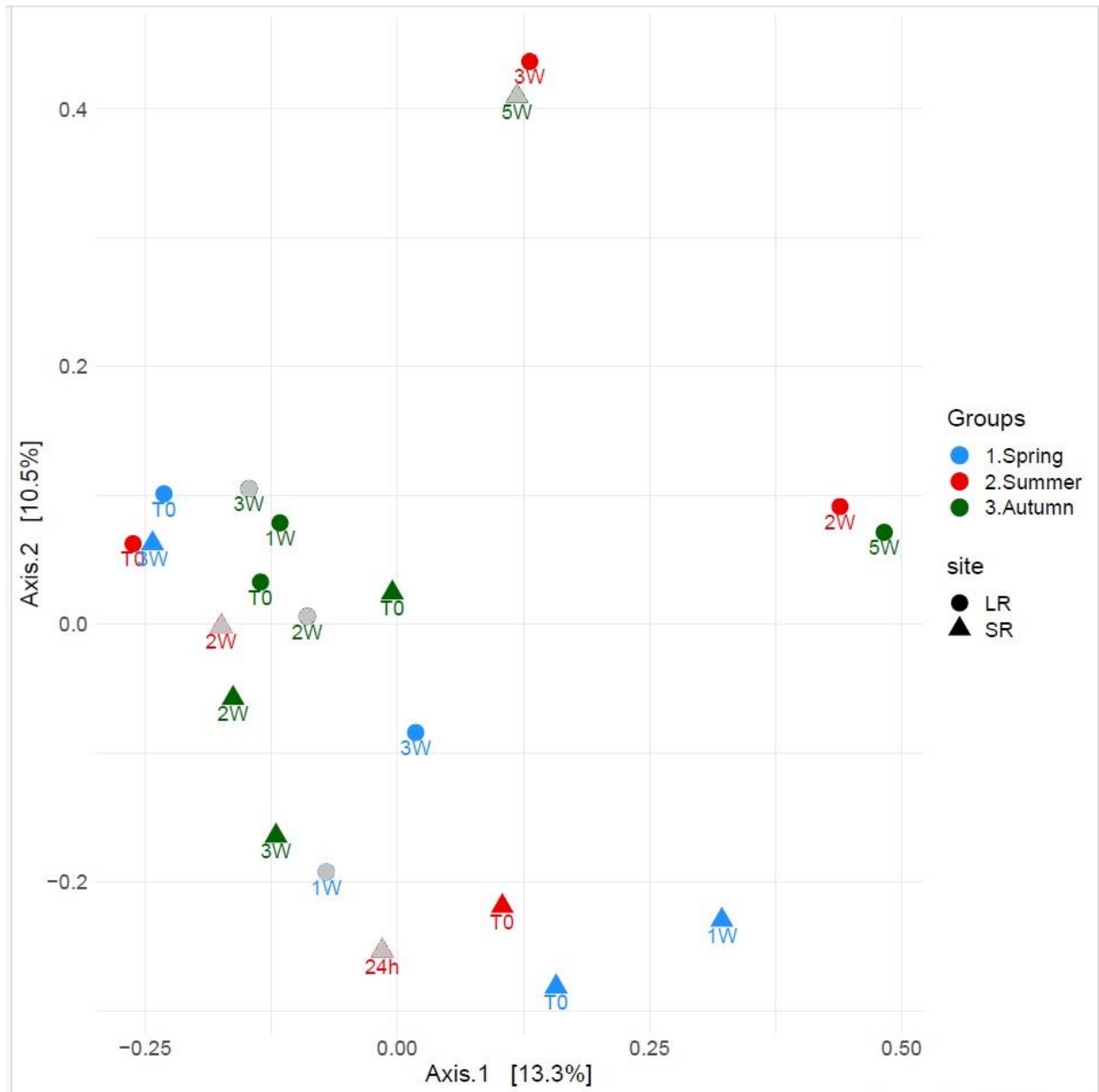
composition, with Proteobacteria being the prevalent group. Nonetheless in autumn control incubation after T2W, other phyla, i.e., Bacteroidota and Chloroflexi have marked presence (Table 1). In warming mesocosms (17.5 °C) of spring (T24h) Firmicutes has a noticeable abundance (17%) before disappearing (<1%, T2W). Planctomycetota with a relative abundance of 49% (T2W) is surprisingly the dominant group in autumn warming incubation. The relative abundance of Acidobacteriota remains low, at <1% of rarefied reads in all mesocosms.



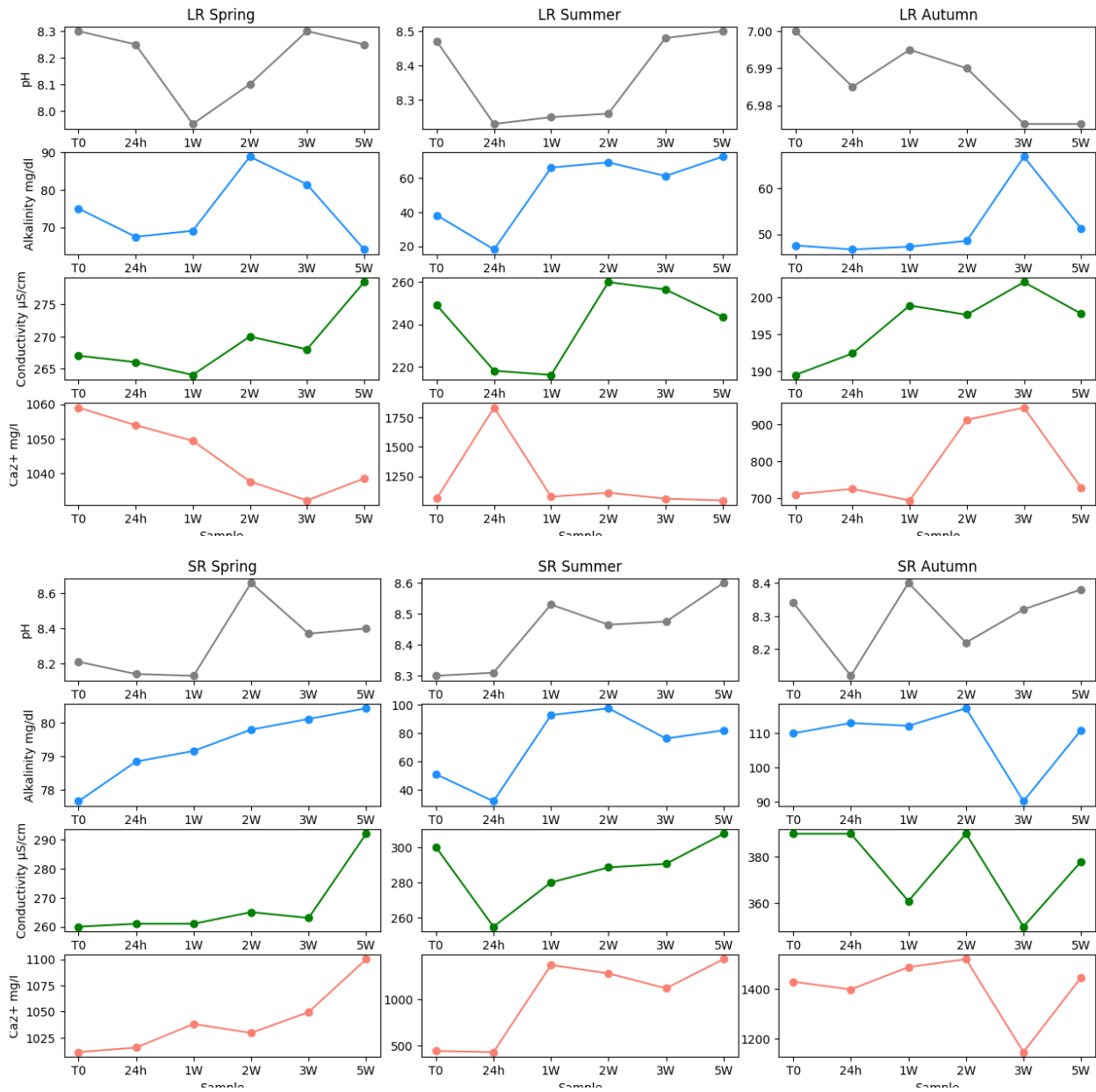
Supp. Fig. 4. Illustrating the bio-indicator OTUs of T0 conditions in Lake Rot and Sihl River



Supp. Fig. 5: Plotting the variability in concentration, MBT'_{5ME} and IR of brGDGTs in the T0 and control incubations over time.



Supp. Fig. 6: Illustrating the NMDS ordination of control incubations for the Lake Rot (LR) and Sihl River (SR). The color-coded spheres and triangles represent the different seasons. The grey samples show samples that were subsequently removed after rarefaction of OTU data, and therefore not included in the discussion.



Supp. Fig. 7: The variability of major water chemistry parameters in the control incubations of the different seasons.

Chapter 3

Controls on brGDGT distributions in the particulate matter of the seasonally anoxic water column of Lake Rot

F. Ajalloeian ^a, N. Dubois ^{a,b}, S. N. Ladd ^c, M. A. Lever ^{d,e}, C. J. Schubert ^{d,f}, C. De Jonge ^a

a Geological Institute, Earth Science Department, ETH Zurich, Sonneggstrasse 5, 8092 Zurich, Switzerland

b Swiss Federal Institute of Aquatic Science and Technology, Eawag, Überlandstrasse 133, 8600 Dübendorf, Switzerland

c Department of Environmental Science, University of Basel, Bernoullistrasse 30, 4056 Basel, Switzerland

d Institute of Biogeochemistry and Pollutant Dynamics, ETH Zurich, Universitätstrasse 16, 8092 Zürich, Switzerland

e Marine Science Institute, University of Texas at Austin, TX, 78373 Port Aransas, USA

f Swiss Federal Institute of Aquatic Science and Technology, Eawag, Seestrasse 79, 6047 Kastanienbaum, Switzerland

Correspondence to: Fatemeh Ajalloeian (fatemeh.ajalloeian@erdw.ethz.ch)

Abstract

Developing reliable methods for quantifying past temperature changes is essential for a more comprehensive understanding of Earth's climate evolution and provides the foundation for predicting future climatic shifts. The methylation of branched tetraethers (MBT'_{5ME}) of bacterial membrane lipids branched glycerol dialkyl glycerol tetraethers (brGDGTs) has become an accepted tool for lacustrine palaeothermometry in recent years. Here, we present a record of brGDGTs present in suspended particulate matter (SPM) in Lake Rot (Switzerland) epi- and hypolimnion over a 10-month period, contrasting GDGTs present as core lipids and intact polar lipid forms. Lake Rot water column exhibits significant variations in temperature, conductivity, and dissolved oxygen levels due to summer warming and stratification of the water column. In the oxic epilimnion, a muted increase in MBT'_{5ME} during stratified summer months, mainly associated with an increase in the concentration of brGDGT Ia was observed. However, the isomer ratio of brGDGTs (IR) rather than the MBT'_{5ME} demonstrated pronounced correlation with epilimnion temperature changes, highlighting the sensitivity of 6-methyl brGDGTs to mean annual temperatures. In the seasonally anoxic hypolimnion, MBT'_{5ME} correlated with water pH rather than temperature, indicating the influence of water chemistry on this ratio and complicating its interpretation as a temperature proxy. Production of IPL brGDGTs was exclusively observed in the anoxic hypolimnion during stratification confirming anoxia as a key trigger for GDGT production.

Lastly, surface sediment samples retrieved from the oxic, and seasonally anoxic lakebed exhibited distinct signals. Compared with the SPM, the sediment underlying the oxic water column displayed lower MBT'_{5ME} values, potentially caused by the sedimentary production of brGDGTs IIa and IIIa. The MBT'_{5ME} of sediments that underlie seasonally anoxic water, MBT'_{5ME} reflected the average values of the epilimnion SPM, suggesting a deposition of lake surface brGDGTs into the sediments. These findings present significant implications for the use of MBT'_{5ME} as a temperature proxy in stratified lake environments. In Lake Rot, temperature effects on MBT'_{5ME} and IR are clearly observable in the lake's epilimnion, however in the hypolimnion, where temperature variations are limited, water chemistry is the primary driver of brGDGT distributions. Last but not least, our results indicate that sedimentary brGDGT distribution can vary within a single lake due to the production of brGDGTs within the sediment itself; potentially complicating the interpretation of a paleotemperature signal.

1. Introduction

Developing reliable methods to determine past temperature changes (paleothermometry) is important for building a more comprehensive picture of the Earth's climate evolution. Moreover, knowing local climate variability provides a critical foundation for addressing the pressing climate challenges of the present and future (Kaufman et al., 2020), allowing geographically focused efforts to mitigate the effects of climate change. Bacterial membrane lipid biomarkers have emerged as a promising tool for paleothermometry (Russell et al., 2018). Branched glycerol dialkyl glycerol tetraethers (brGDGTs) are ubiquitous bacterial membrane-spanning lipids found in various environmental settings (Weijers et al., 2006). Initially discovered in peatlands (Sinninghe Damsté et al., 2000, Weijers et al., 2006), they have since been found in abundance in soils (Weijers et al., 2007a), aquatic sediments (Weijers et al., 2007b; Peterse et al., 2009; Tierney and Russell, 2009), and freshwater ecosystems (Tierney et al., 2010; De Jonge et al., 2014a; Russell et al., 2018; Martínez-Sosa et al., 2020). Their structural diversity (Supp. Fig. S1) comprises a change in the degree of methylation (4-6 branches), resulting in different forms known as tetra-, penta-, and hexamethylated brGDGTs. Additionally, internal cyclization of the methyl branches can lead to the formation of one or two cyclopentyl moieties in the molecules. BrGDGT compounds with the outer methyl branch(es) on α and/or $\omega 5$ are designated as 5-methyl brGDGTs, while those with the outer methyl branch(es) on α and/or $\omega 6$ are termed 6-methyl brGDGTs (De Jonge et al., 2013).

On a global scale, the structural diversity of brGDGTs varies along specific environmental gradients. In particular, the methylation of branched tetraethers index (defined originally as MBT and MBT', now MBT'_{5ME}) and the cyclization ratio of branched tetraethers (defined originally as CBT, now CBT') have been linked to air temperature and soil or lake water pH, respectively (Weijers et al., 2007b; Tierney and Russell, 2009; Peterse et al., 2012; De Jonge et al., 2014b; Russell et al., 2018; Martínez-Sosa et al., 2019; 2021). Similarly, the isomeration ratio of brGDGTs, which expresses the relative abundance of 6-methyl penta- and hexamethylated brGDGTs compared to their 5-methyl counterparts (summarized as IR), has been used as a proxy for soil or lake water pH (De Jonge et al., 2014b; Naafs et al., 2017; Russell et al., 2018; Halfman et al., 2022), and more recently lake water conductivity and salinity (Raberg et al., 2021; Wang et al., 2021, Kou et al., 2022). In lake water columns, changes in brGDGT distributions (including individual brGDGT compounds and brGDGT-based ratios (MBT'_{5ME}, CBT', IR) have been reported to vary with other environmental factors, such as dissolved oxygen (Colcord et al., 2017, Weber et al., 2018, Van Bree et al., 2020, Yao et al., 2020, Lattaud et al., 2021), seasonality changes in temperature and mixing regimes (Loomis et al., 2014a, Van Bree et al., 2020, Dearing Crampton-Flood et al., 2020), nutrient concentrations (Loomis et al., 2014a, Hu et al., 2016), pH (Weijers et al., 2007b) and alkalinity (Schoon et

al., 2013), complicating and potentially obfuscating any variations in brGDGT compositions associated with temperature changes. Additionally, as water column studies have shown that brGDGT concentrations increase under O₂ depletion, it is thought that brGDGTs are primarily produced in the anoxic portion of the hypolimnion (Bechtel et al., 2010; Blaga et al., 2011; Woltering et al., 2012; Buckles et al., 2014; Loomis et al., 2014b; Miller et al., 2018, Weber et al., 2018, Van Bree et al., 2020). Yet, the mechanics of brGDGT production in lakes remain poorly understood. This is illustrated in the diversity of lake-specific calibrations, which generally do not decrease the error associated with GDGT-based temperature reconstruction (Russell et al., 2018, Martínez-Sosa et al., 2021, Raberg et al., 2021).

Previous environmental studies have shown that Acidobacteria are potential producers of GDGTs in soils (Peterse et al., 2010; De Jonge et al., 2019). This is confirmed by reports of the presence of a potential precursor of brGDGT lipids, iso-diabolic acids (either as free acids or as mono-glycerol ethers), as membrane lipids in cell membranes of acidobacterial subgroups 1, 3, 4 and 6 (Sinninghe Damsté et al., 2011, 2014, 2018). Additionally, acidobacterial strain *A2-4c* and *E. aggregans Wbg-1* produce trace amounts of brGDGT Ia (Sinninghe Damsté et al., 2011), and pure culture experiments have demonstrated that *Solibacter usitatus*, a member of Acidobacteriaceae (Acidobacteria Subgroup 1), can produce brGDGTs Ia, IIa, IIIa, Ib, and IIb (Chen et al., 2022, Halamka et al., 2022). Nonetheless, not all 15 brGDGT compounds found in soil and aquatic ecosystems have been detected in pure cultures. Moreover, recent studies have identified biosynthetic genes with potential GDGT-producing pathways in a wide diversity of bacterial phyla (Sahonero-Canavesi et al., 2022; Zeng et al., 2022). The potential for multiple bacterial phyla to produce these lipids is especially relevant for assessing the sources of brGDGTs in lake water columns, where Acidobacteria are generally rare (Parfenova et al., 2013; Dedysh and Sinninghe Damsté, 2018; Weber et al., 2018; Van Bree et al., 2020). This leads to the general question whether changes in GDGT compositions are primarily driven by microbial community changes, as supported by certain environmental observations (Weber et al., 2018; De Jonge et al., 2019, 2021) and GDGT distributions among pure culture strains (Sinninghe Damsté et al., 2018), or reflect physiological adaptations of the same organisms to different temperature regimes. The ability of many bacteria to modify the chemical compositions of membrane lipids in response to temperature variations, a phenomenon known as “homeoviscous adaptation”, is well-known. Indeed, the modelled impact of GDGT compositions on membrane fluidity supports this second mechanism (Naafs et al., 2021).

To complicate things further, brGDGT concentrations and distributions in lakes can vary seasonally, with reported increases in brGDGT concentrations during spring and fall isothermal mixing (Loomis et al., 2014a; Miller et al., 2018). This can introduce a seasonal production bias (Loomis et al., 2014a; Miller et

al., 2018), and it remains unclear whether changes in water temperature, water chemistry (e.g., dissolved oxygen), or bacterial community composition are the underlying drivers (Shade et al., 2007). To elucidate which of these variables best explain seasonal variations in brGDGT concentrations and distributions, we examined water column and surface sediment samples from Lake Rot (Switzerland). This subalpine lake experiences strong seasonal changes that include pronounced bottom water anoxia during summer stratification (Fig. 1). brGDGT production was previously shown to occur in surface sediments (Naeher et al., 2014) and experimental mesocosms involving surface water samples from the lake (Ajallooeian et al., 2024).

2. Materials and Methods

2.1. Study site

Lake Rot (Rotsee, 47°21'05.8" N; 8°31'12.7" E) is a small subalpine lake with a surface area of 0.48 km² and maximum depth of 16 m. It is a naturally eutrophic, monomictic lake, that exhibits annual, thermal water column stratification during the warm season. During this stratification period, the absence of physical mixing-related O₂ inputs and high rates of aerobic mineralization of phytoplankton-derived organic matter (Schubert et al., 2010; Naeher et al., 2014) lead to bottom water anoxia (Fig. 1).

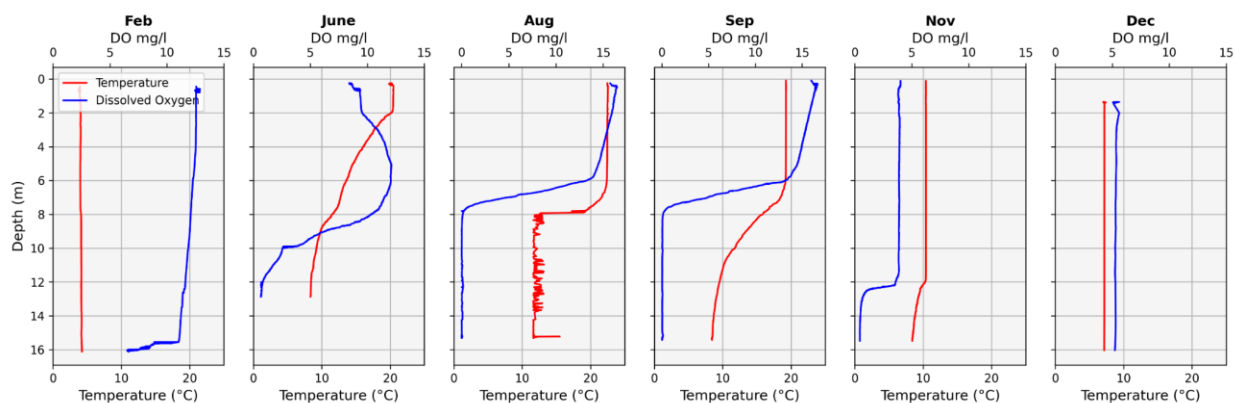


Fig. 1. Vertical profile of temperature (°C) and dissolved oxygen (mg/l) in the water column of Lake Rot during selected months illustrating i) isothermal mixing (December and February), ii) stratification onset (June), iii) stratified water column conditions (August and September) and iv) post-stratification (November).

2.2. Water column and surface sediment sampling

Starting in February 2019, water column samples were collected every two to four weeks. Water samples were taken using a 20 L Niskin water sampler at water depths of 0-1 m and 14-15 m (1 meter above the sediment surface), to represent the epilimnion and seasonally anoxic hypolimnion, respectively. Monthly time intervals until December 2019 (excluding April) were analyzed, resulting in a total of 10 time points. Concurrent with each water sampling, water column temperature, conductivity, pH, and dissolved oxygen were measured using a CTD scanner (SeaandSun Technology®, Germany). The mean annual air temperature (MAAT) was calculated based on the average measured air temperature on days of sampling.

Water alkalinity was determined by analyzing aliquots from each depth using an 862 Compact Titrosampler (Metrohm Inc., Switzerland, following the international standard organization method EN ISO 9963-1:1995). From February to August, aliquots of the water were, moreover, used to measure concentration of anions (Nitrate – NO_3^- , Sulfate – SO_4^{2-} , Chloride – Cl^-), and cations (Calcium – Ca^{2+} , Sodium – Na^+ , Ammonium – NH_4^+ , Potassium – K^+ , and Magnesium – Mg^{2+}) using a Compact Ion Chromatograph Pro, Model 881 (standard method from Metrohm Inc, Switzerland). Nutrients including total Phosphorous (total P) were measured on a Flow Injection Analyzer (SKALAR METHODS No. 461 (NO3/NO2/TN) and No. 503 (PO4/TP), instrument: SKALAR SAN++, Procon AG, Switzerland).

For each layer approximately 40 L of lake water was filtered (within 12h to 24h after sampling, stored at 4 °C) using a 0.7 µm GF/F filter (Durapore®, Germany) placed on a titanium tripod (cleaned with EtOH and MilliQ between samples; referred to as GF/F sample) to collect the suspended particulate matter (SPM). Subsequently, the filtered water underwent a second filtration step using a 0.22 µm PVDF filter (Durapore®, Germany) to capture smaller sized bacteria and associated lipids (referred to as PVDF sample). For some timepoints (17.07.2019, 14.08.2019, 18.12.2019), Aluminum Sulfate salt was used to coagulate the dissolved organic matter in the lake water that was previously filtered over a 0.22 µm filter and filtered once again over a 0.7 µm GF/F filter (referred to as DOM sample). This method has proven effective in flocculating organic matter (Masion et al., 2000). Filter samples were wrapped in aluminum foil and stored frozen at -20°C.

The dataset also includes two surface sediment samples (1 gram sampled from top surface sediment 0-2 cm) from Lake Rot. The “oxic” sample was collected from a shallower depth (water depth: 5.5 m, collection month: October) where it is exposed to a water column that stays oxic throughout the year. In contrast, the “seasonally anoxic” sample was obtained from a depth where it is exposed to a seasonally anoxic water column occurs (water depth: 14.5 m, collecting month: September). Important to note is, although the oxygen content of the sediment pore water was not measured, it is expected to be depleted at a shallow

depth at the oxic station (most likely within the top 0.5 cm of sediment), and to be fully absent from sediments of the anoxic station.

2.3. Lipid extraction

For the selected water column sample set ($n=20$), a known area of the filter ($\sim 16 \text{ mm}^2$) was stored for DNA analysis, before freeze-drying the remaining filter material. Then, each filter was cut into 3 equal sections, with split 1 (E1) of the water column extracted for core lipids (CL) using a modified Bligh-Dyer extraction (BDE+TCA) method with a mixture of methanol (MeOH), dichloromethane (DCM), and a phosphate-buffer (2:1:0.8, v/v/v) for the first round of ultrasonic extractions (3x), and subsequently substitution of phosphate-buffer with 5% trichloroacetic acid (TCA) for the second round of ultrasonic extractions (3x) (Sturt et al., 2004; Pitcher et al., 2009). Thereafter, DCM and phosphate-buffer or TCA was added (3x) to either the BDE or TCA extracts and after centrifugation at 2,000 rpm for 3 min, the DCM phase was collected and dried under a gentle stream of N_2 , providing the total lipid extract (TLE). The second split (E2, only water column samples) and the surface sediment samples ($n=2$) were subjected to acid hydrolysis to convert all intact polar lipid (IPL) GDGTs to core lipids (CL; Weber et al., 2017). Briefly, the filters or freeze-dried sediments were placed in centrifuge tubes and submerged in 1.5N HCl in MeOH (v/v). Tubes were capped and wrapped with Teflon tape and heated at 80°C for 2 hours. A last split (E3) was kept as an archive.

The TLEs were fractionated using a 3.4 cm column packed with activated aluminum oxide and eluted with three different solvent mixtures. The non-polar, ketone and polar fractions were collected using hexane/DCM 9:1 (v/v), hexane/DCM 1:1 (v/v), and DCM/methanol 1:1 (v/v), respectively. Before the analysis, 49.6 ng of GTGT internal standard (C46) (Huguet et al., 2006) was added to the polar fraction. The polar fraction was then filtered through a $0.45 \mu\text{m}$ PTFE filter, dried under N_2 , and re-dissolved in 50 μL of hexane/isopropanol (IPA) 99:1 (v/v). Subsequently, the samples were injected into a high-performance liquid chromatography–mass spectrometry (HPLC–MS) system (Agilent Technologies®-1200, USA) as described in Hopmans et al. (2016), using a modified column temperature of 40°C and an injection volume of 10 μL .

Instrument error in quantifying brGDGTs was determined to be 15 % for the freshwater column samples, which has been used as an error estimate for the CL GDGTs derived from E1. To calculate the quantity of IPL brGDGTs, the quantity of recovered brGDGTs from E1 (BDE+TCA: CL brGDGTs) was subtracted from the E2 extracts (AH: CL+IPL brGDGTs). The instrument error in quantification was propagated (17-21 %).

The MBT'_{5ME} (De Jonge et al., 2014b) and Isomer Ratio (IR) were calculated following the formulas defined by De Jonge et al. (2014b), where the IR reflects only compounds without cyclopentane moieties (De Jonge et al., 2015; Halffman et al., 2022). This method works well for cases where one to two cyclopentane-bearing hexamethylated compounds (IIIb, IIIc, and their isomers) are frequently below the detection limit, similar to this dataset. The IR has been known to vary with pH in soils (Yang et al., 2015, Naafs et al., 2017) and temperature in lakes (Russell et al., 2018, Martínez-Sosa et al., 2020). The estimation of water temperature and pH was performed using the calibrations proposed by Russell et al. (2018).

$$MBT'_{5ME} = \frac{Ia+Ib+Ic}{Ia+Ib+Ic+IIa+IIb+IIc+IIIa}$$

$$IR = \frac{IIa'+IIIa'}{IIa'+IIIa'+IIa+IIIa}$$

$$DC' = \frac{Ib+IIb+IIb'}{Ia+IIa+IIa'+Ib+IIb+IIb'}$$

$$CBT' = \log_{10} \frac{(Ic+IIa'+IIb'+IIc'+IIIa'+IIIb'+IIIc')}{Ia+IIa+IIIa}$$

$$\text{Mean Annual Temperature (MAT)} = -1.21 + 32.42 \times MBT'_{5ME} \quad (r^2= 0.92, p < 0.0001, \text{RMSE}= 2.44 \text{ } ^\circ\text{C})$$

$$\text{Surface Water pH} = 8.95 + 2.65 \times CBT' \quad (r^2= 0.57, p < 0.0001, \text{RMSE}= 0.80)$$

2.4. Quantification and sequencing of 16S rRNA Genes

To capture the bacterial community variability of the water column, a known fraction of the seasonal SPM water filters ($\sim 16 \text{ mm}^2$) was cut and stored in PCR-clean tubes at -20°C . These samples underwent DNA extraction following the modular protocol outlined by Lever et al. (2015) and performed previously (Ajallooeian et al., 2024). Briefly, to reduce DNA sorption, dNTP solution (10 mM) was added to samples, followed by addition of cell lysis solution I, and chemical lysis treatment on a shaker for 1 hour at 50°C to break down the cells and release the DNA, followed by separation of the DNA-containing supernatant from the residual sample material by centrifugation (10 mins at $14,000\text{xg}$). The DNA-containing supernatant was washed twice with cold chloroform-isoamyl alcohol (24:1) to remove non-polar fractions. DNA was then precipitated using NaCl, Linear Polyacrylamide (LPA; $20 \mu\text{g mL}^{-1}$ of extract), and ethanol (EtOH) in a dark environment at room temperature for 2 hours. DNA pellets were produced by centrifugation (20 mins at $14,000\text{xg}$), washed three times using 70% EtOH to remove excess NaCl, and dried before resuspension and dissolution in molecular biology grade water (H_2O).

The abundance of bacterial 16S rRNA genes was determined using a quantitative PCR (qPCR) assay conducted on a LightCycler 480 II instrument (Roche Life Science, Switzerland). The qPCR assay was

based on the protocols established by Lever et al., (2015). For the qPCR reaction, the 16S bacterial primers BAC908F (5'-AACTCAAAGGAATTGACGGG-3') and BAC1075R (5'-CACGAGCTGACGACARCC-3') were utilized (0.5 μ L of each primer). The qPCR reaction mixture included the addition of 5 μ L SYBR Green-I-based master mix (Taq DNA polymerase; Roche Life Sciences, Switzerland), enabling real-time monitoring of the amplification process, 1 μ L H₂O, and 1 μ L BSA. QPCR standards consisted of dilution series (10^1 - 10^7) of full-length 16S rRNA gene plasmids from *Rhodobacter sphaeroides*. As negative controls, molecular biology grade H₂O and extraction blanks, sample-free extractions that served as controls for contamination by reagents or during handling, were included. The average 16S rRNA gene copy number was ~1,000-fold lower in both forms of negative controls compared to Lake Rot samples.

Based on a subset of 18 samples that represent sampling dates throughout the year, a 16S rRNA gene amplicon sequence library was prepared using the workflow outlined in Deng et al., (2020). In short, amplicons of the bacterial 16S rRNA gene were obtained through PCR reactions using the primer pairs S-D-Bact-0341-b-S-17 (5'-CCTACGGGNGGCWGCAG-3') and S-D-Bact-0785-a-A-21 (5'-GACTACHVGGGTATCTAATCC-3'). Paired-end sequencing was performed using the Illumina MiSeq platform at the Genetic Diversity Centre (GDC) of ETH Zurich (<https://gdc.ethz.ch/>). To ensure the quality and reliability of the sequencing run, an Acidobacteria positive control (plasmids containing 16S rRNA gene sequences) from *Holophaga foetida*, was included, along with contamination controls, consisting of molecular grade H₂O and extraction blanks.

During the back-mapping process of the raw sequencing data, data loss was minimal (< 5%), with 14'608 zOTUs (denoised sequencing data, zero radius operational taxonomic units) identified. After exclusion of singletons, a total of 7,545,540 amplicon reads, representing 8301 zOTUs, were used for further analyses, which included operational taxonomic unit (OTU) clustering (97% identity threshold), and phylogenetic assignments using the SILVA database (<https://www.arb-silva.de/>; for further information, see Deng et al., 2020). The resulting OTU table contained 8,299 taxa across 18 samples. Subsequently, to avoid introducing biases based on differences in sequencing depths, the total reads were rarefied to 222,646 reads per sample resulting in retainment of 6,103 OTUs and 16 samples for analysis.

2.5. Statistical methods

The study assessed changes in brGDGT distributions between two extraction methods using average offset calculated on brGDGT fractional abundances. Mean (\bar{x}) and standard deviation (σ) of brGDGT fractional abundances and ratios were also determined to examine variability through time, separately for epi- and hypolimnion water, with compounds always below the detection limit (IIIc and IIIc') excluded from

calculations of PCA and linear correlations. To calculate weighted averages for brGDGT fractional abundances, ratios, and MAAT, the average values for March and May were used to represent the missing month of April in the dataset. Thereafter the lipid concentration data were normalized using min-max scaling to ensure comparability. Linear weighting was applied to months based on their normalized concentrations, with higher weights being assigned to months with higher concentrations. Finally, concentration-weighted averages of brGDGT ratios and fractional abundances were calculated, allowing the emphasis on the influence of months with greater lipid concentrations in the analysis. To assess the extent to which environmental variables account for variability in the brGDGT data, we conducted correlation analyses (Pearson correlation coefficients (r)) and Principal Component Analysis (PCA). Additionally, we calculated the variance explained by each environmental variable while considering the effects of other variables via a stepwise forward selection model (Dray et al., 2006, Legendre and Legendre, 2012, Russell et al., 2018). The stepwise forward selection process constructs a linear regression model, starting with the environmental variable that exhibits the strongest correlation (R^2) with the brGDGT data. Subsequently, it sequentially adds additional variables based on the significance of the F-statistic, determined through Monte-Carlo permutation tests (499 simulations). The process concludes when adding new variables no longer explains a significant fraction of the remaining variance, as established through permutation testing (Legendre and Legendre, 2012).

The environmental and microbiome data were analyzed using packages, "phyloseq" (McMurdie and Holmes, 2013) and "vegan" (Oksanen et al., 2013), implemented in R version 4.1.2. These packages are well-established tools for comprehensive analysis and manipulation of microbiome datasets. A bio-indicator approach was employed to explore whether the bacterial community in Lake Rot can potentially influence the brGDGT variability, using the package *indicspecies* (De Cáceres, 2013), as was done previously in De Jonge et al. (2019) and Halffman et al. (2022). This was performed to identify OTUs that are increased in either i) epilimnion or hypolimnion communities, or ii) in suboxic and anoxic hypolimnion conditions, compared with oxic hypolimnion conditions. Assignment of bio-indicator OTUs of these sample types, is based on analysis that determines whether frequency of the species in each site group is higher than random (permutation= 999, $p < 0.01$, p-value was corrected based on Sidak's correction for multiple testing).

Downstream and statistical data analysis were performed using the "scipy.stats" package, from Python, with packages "matplotlib", "seaborn" (python v.3.8.5) and "tidyverse", "ggplot2" (from R v.4.2.3) used for data visualization and general data manipulation tasks.

3. Results

3.1. Mixing regime and water chemistry of Lake Rot

In 2021, thermal stratification of Lake Rot started mid-May and the thermocline reached a maximum depth of 8m (Fig. 1). Following cooling down of the epilimnion, water column mixing first deepened the thermally stratified layer (September-November), with a fully mixed water column observed by December (Fig. 1). In the epilimnion of Lake Rot, temperature varied significantly (4-24 °C), with February and August as the coldest and warmest months, respectively. In the hypolimnion August also was the warmest month, however, year-round temperature variation was more limited (4-9 °C) (Fig. 2A). The seasonal mixing and development of a thermocline caused variation in Lake Rot's dissolved oxygen concentrations (Fig. 1). In the epilimnion, dissolved oxygen levels exhibited stable values during the winter-spring mixing season, averaging around 11 mg L⁻¹. During and following thermal stratification, oxygen concentration increased, reaching 15 mg L⁻¹ (Fig. 1). In November, following the onset of hypolimnion mixing, oxygen levels decreased. In the hypolimnion, dissolved oxygen levels were similar to those in the epilimnion during the winter mixing season before decreasing in May (1.57 mg L⁻¹), eventually leading to suboxic conditions ([DO]> 2 mg L⁻¹) in May, June and July and anoxic conditions ([DO]< 0.1 mg L⁻¹) in August, September and October (Fig. 1, Fig. 2E). Subsequently, oxygen levels increased during the autumn lake mixing, with December representing a fully mixed column.

Seasonal stratification impacted various inorganic chemistry parameters in the Lake Rot water column. In the epilimnion, these parameters are identified by a correlation with temperature, while in the hypolimnion, these parameters correlate with dissolved oxygen levels. Specifically, conductivity and total P showed significant correlations with temperature ($r= 0.66, -0.70$, respectively, $p< 0.05$) in the epilimnion, while in hypolimnion, conductivity, temperature, and alkalinity showed correlations with DO ($r= -0.89, -0.70, -0.60$, respectively, $p< 0.05$).

Conductivity in the lake's epilimnion is decreased during the stratification period with an average of 169 $\mu\text{S cm}^{-1}$ (Fig. 2B), while total P concentration increased ($> 20 \mu\text{g L}^{-1}$) in mixing months from a background average value of 15.14 $\mu\text{g L}^{-1}$. In contrast, with generally higher values (300-350 $\mu\text{S cm}^{-1}$), the bottom layer conductivity increased during stratification. This increase is most pronounced in September, where bottom waters had the highest measured conductivity values (368 $\mu\text{S cm}^{-1}$, Fig. 2B). The same trend is observed for Ca^{2+} and K^+ , that correlate with conductivity values in the hypolimnion ($r= 0.91, p< 0.05$ for Ca^{2+} and $r= 0.91, p< 0.05$ for K^+). Hypolimnion alkalinity (Fig. 2C) increases with the onset of bottom water anoxia (Fig. 2C), while epilimnion alkalinity concentrations decrease during the stratification (Fig. 2C). Ca^{2+} (Fig.

2C) correlated with alkalinity both in the epi and hypolimnion ($r= 0.85, 0.98, p< 0.05$). Similarly, K^+ and SO_4^{2-} , and total P correlated ($r= 0.92, -0.88, 0.69, p< 0.05$, respectively) with alkalinity in bottom waters (Fig. 2F, G, J).

Water pH, on the other hand, displayed stratification-independent oscillations (Fig. 2D). In the epilimnion of Lake Rot, it showed stable values for the period of spring mixing and stratification ($\bar{x}= 8.1, \sigma= 0.1$). With start of the autumn's isothermal mixing that disrupts the isolated water column, pH dropped in the epilimnion to 7.1 (Fig. 2D). In the hypolimnion the stratification onset results in reduced pH values, increasing in pH (8.8) during the onset of isothermal mixing, the so-called post-stratification period (Fig. 1).

To summarize the variance in the chemical parameters, a PCA ordination, based on water chemistry parameters (dissolved oxygen, conductivity, pH, alkalinity, and cations and anions) of surface and deep water respectively was performed (Supp. Fig. S2). This ordination illustrates a similar water chemistry for spring and summer months (March-June). September, is present as an outlier in the ordination space of bottom, driven mainly by changes in Cl^- and SO_4^{2-} values (Supp. Fig. S2).

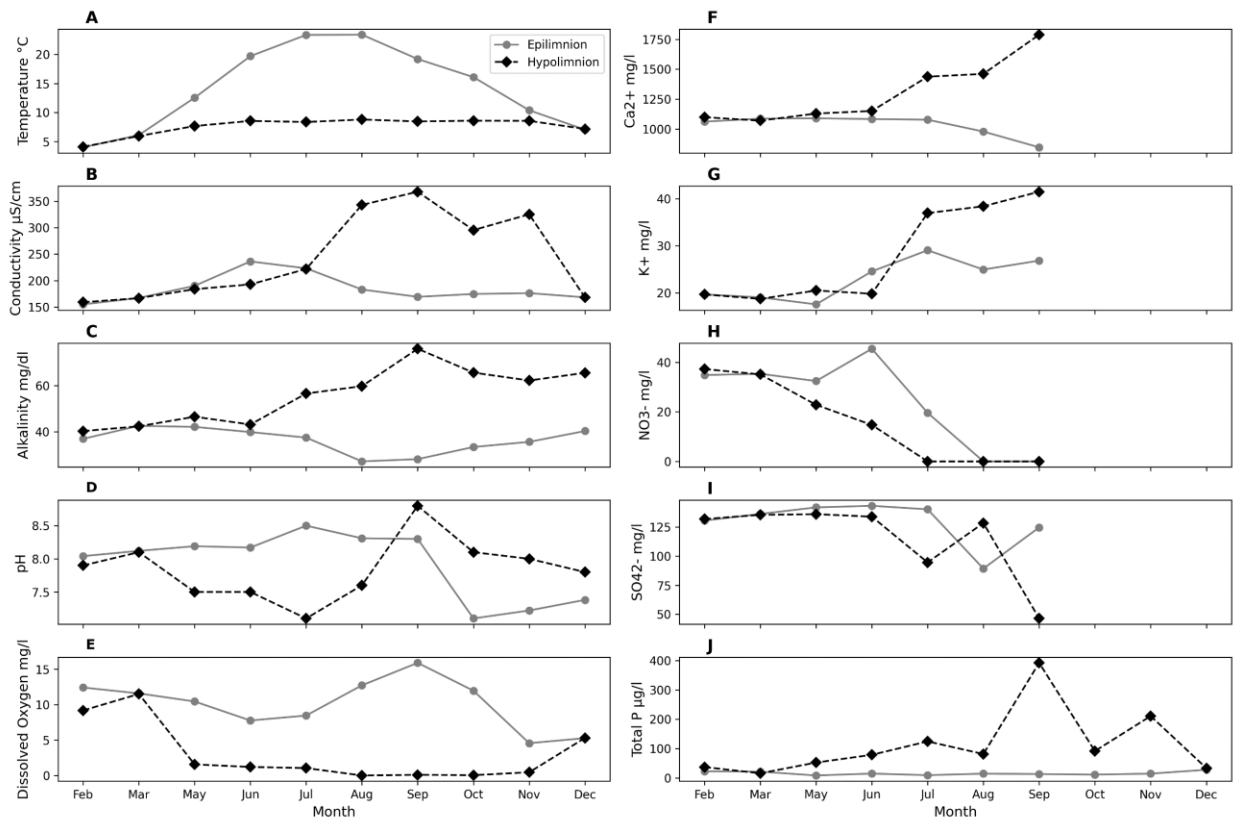


Fig. 2. The variability of inorganic parameters for epi- and hypolimnion of Lake Rot, with time. Specifically, temperature ($^{\circ}\text{C}$), conductivity ($\mu\text{S cm}^{-1}$), alkalinity (mg dl^{-1}), pH and dissolved oxygen (DO; mg L^{-1}), as well as cations (Ca^{2+} , K^{+}), anions (NO_3^{2-} , SO_4^{2-}) (mg L^{-1}) and Total Phosphorus (Total P) concentrations ($\mu\text{g L}^{-1}$). Dissolved cations and anions were not determined from October to December.

3.2. Patterns of brGDGTs in Lake Rot suspended particulate matter (SPM)

3.2.1. GDGT concentration variability

The PVDF and DOM samples yielded significantly lower summed concentrations in comparison to GF/F ($1 < \sum \bar{x} < 11 \text{ ng L}^{-1}$) samples (Supp. Table S1: $\sum \bar{x} < 0.45$ and $< 0.10 \text{ ng L}^{-1}$ for PVDF and DOM samples, respectively), and often only included the brGDGT compounds Ia, IIa and IIIa. As GF/F filters were thus able to collect 95% of brGDGT in the SPM, the results obtained from GF/F samples (Supp. Table S1) will be discussed from this point on.

The summed concentrations of CL brGDGTs varied between depths and with time (Supp. Table S1; Fig. 3A). Although the hypolimnion layer (bottom: $0.6\text{-}10.9 \pm 0.1\text{-}1.6 \text{ ng L}^{-1}$) exhibited generally higher summed concentrations in the first half of the year compared to the epilimnion (surface: $0.7\text{-}5.3 \pm 0.1\text{-}0.7 \text{ ng L}^{-1}$) in Lake Rot SPM, during isothermal stratification months (July, August, September, and October) epilimnion concentrations were higher than the concentrations measured in the hypolimnion (Fig. 3A). Similarly, in December the epilimnion concentration surpassed those of the hypolimnion (Fig. 3A). The IPL brGDGT concentration ranged from 0.1 to 2.4 ($\sigma = 0.7$) and from 0.02 to 3.6 ($\sigma = 1.2$) ng L^{-1} for epi- and hypolimnion, respectively (Supp. Table S1; Fig. 3A).

In the epilimnion, brGDGT Ia was the most abundant compound, with an increased concentration during the summer months, resulting in a maximum concentration in July of 0.85 ng L^{-1} (Fig. 3B). These elevated values for brGDGT Ia persisted until August, after which a general decrease was observed, reaching 0.22 ng L^{-1} in December. The concentration of brGDGT IIa remained stable throughout the year, correlating positively with the concentration of brGDGT Ia ($r = 0.67$, $p < 0.05$). In contrast, brGDGT IIIa was present at lower concentrations, with a stable average of around 0.47 ng L^{-1} until September. However, during the latter part of the year, it became more abundant, with an average of 0.70 ng L^{-1} (Fig. 3C). The opposing behavior between concentrations of brGDGT Ia and IIIa (Supp. Fig. S3A), however, does not lead to a significant anti-correlation.

Compared with their 5-methyl counterparts, 6-methyl brGDGTs consistently showed higher concentrations throughout the year in the Lake Rot epilimnion (Fig. 3B). Here, brGDGT IIa' was generally present at a lower concentration compared with brGDGT IIIa'. The maximum (0.94 ng L^{-1}) and minimum (0.26 ng L^{-1})

¹) concentrations of Ila' were observed in July and December, respectively, mirroring the pattern observed for compound Ia (Fig. 3B). On the other hand, brGDGT IIIa', with notably higher concentrations, experienced a significant peak in July (1.17 ng L⁻¹) and maintained relatively high concentrations (0.79-0.94) afterward, before declining to 0.37 ng L⁻¹ in December (Fig. 3B). This pattern matched the concentration changes observed for brGDGT Ia.

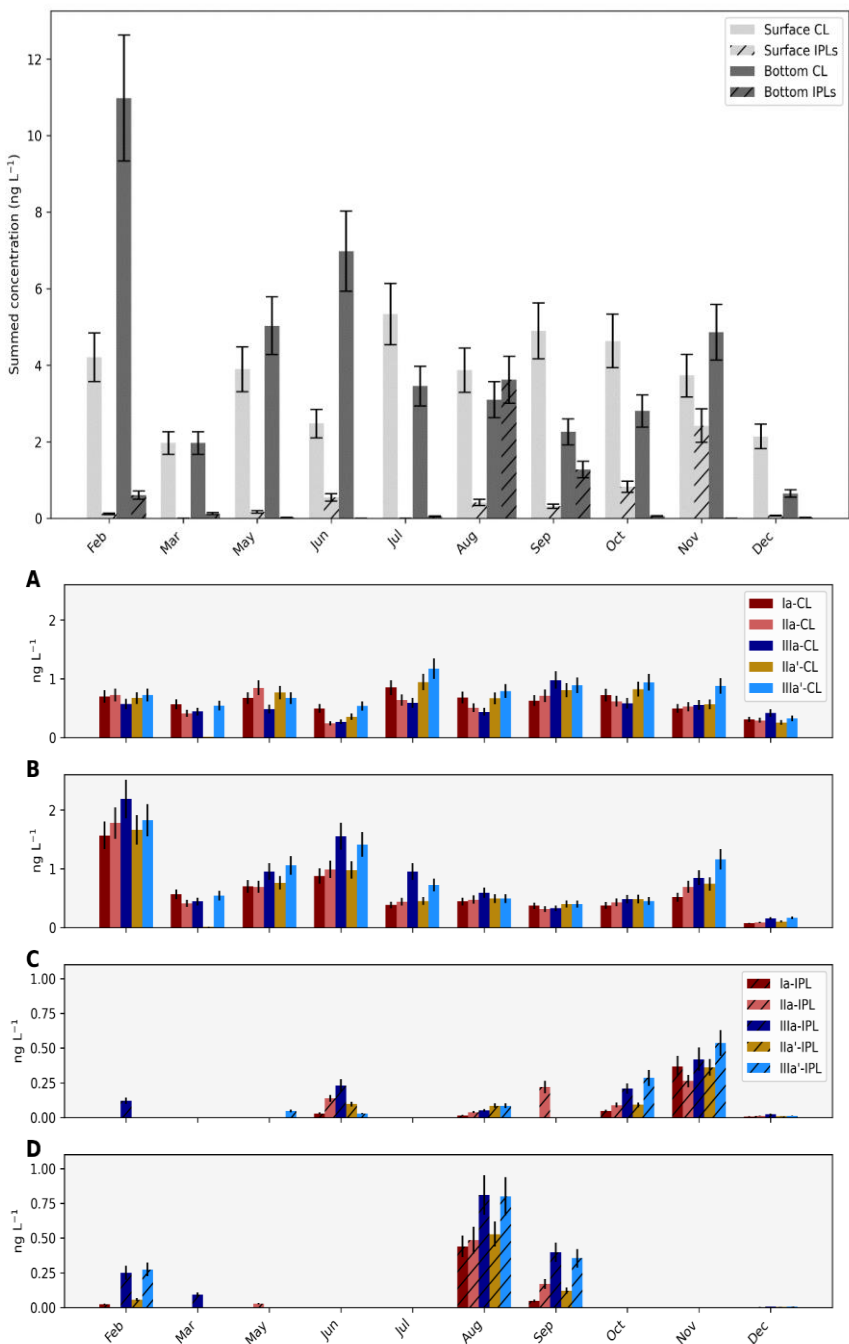


Fig. 3. Summed concentrations of brGDGTs through the year in Lake Rot. Light grey bars represent epilimnion, while dark grey display hypolimnion concentrations. CL and IPL GDGTs refer to core and intact polar lipids,

respectively. Error bars display the instrumental concentration error (15%). In the subplots the concentration of the five most abundant individual brGDGTs in Lake Rot SPM are plotted. Panel A and B show GDGTs present as core lipid (CL) and panel C and D show GDGTs present as intact polar lipids (IPL). Panels A and C represent epilimnion values, while panels B and D represent hypolimnion concentrations.

In the seasonally anoxic hypolimnion, brGDGT IIIa was the most abundant brGDGT compound, ranging from 0.1 to 2.1 ng L⁻¹ (Fig. 3C). In contrast to the epilimnion, a significant positive correlation was observed between the concentrations of brGDGT Ia and IIIa ($r=0.93$, $p=0.00$). Similarly, a strong positive correlation was observed between the concentrations of Ia and IIa ($r=0.98$, $p=0.00$) (Supp. Fig. S3A). The 6-methyl isomers (IIa', IIIa') did not reach the same concentration as observed in the surface waters. Nevertheless, brGDGT IIIa' remained one of the prevalent compounds, with an average concentration (\bar{x}) of 0.8 ng L⁻¹ ($\sigma=0.5$ ng L⁻¹, Fig. 3C).

For the IPL brGDGTs, only the predominant compounds (brGDGTs Ia, IIa, IIIa, IIa', and IIIa') were present above detection limit during specific periods (Fig. 3D-E). These periods included June, August, October, and November in the epilimnion, and February, August, and September in the hypolimnion (Fig. 3D-E). Notably, hypolimnion IPL brGDGT concentrations exhibited exceptionally high values in August, reaching 3.62 ng L⁻¹. BrGDGT Ia, was never the most abundant compound in either surface (4-12%) or bottom waters (3-15%) (Supp. Table S1), which contrasts with the CL distribution. For the epilimnion, the summed 6-methyl brGDGTs represent the largest fraction of IPL GDGTs (21-29%) while in the hypolimnion, the hexamethylated 5-methyl GDGT (IIIa, 38%) represented the largest fraction of IPLs (Fig. 3D-E, Supp. Table S1). In the sediment, the oxic sample displayed an approximately six-fold higher total concentration of CL brGDGTs compared to the seasonally anoxic surface sediment (Supp. Table S1), with the full suite of brGDGT compounds present in both samples. The dominant brGDGT compound is IIa and IIa' for the "oxic" and "seasonally anoxic" sediments, respectively. 6-methyls are more abundant than their 5-methyl counterparts in the "seasonally anoxic" sediment.

3.2.2. GDGT distribution variability

The seasonal changes in the concentration of CL brGDGTs in the epi- and hypolimnion of Lake Rot result in distributional changes that are summarized as variations in brGDGT ratios MBT'_{5ME}, IR and CBT', and MBT'_{5ME}-based reconstructed temperatures (T_{rec}). In the surface layer, MBT'_{5ME} varied between 0.22-0.53, with a weighted average value of 0.39 (Fig. 4A). The variation in MBT'_{5ME} generally exhibited small changes from February to May (0.38-0.39), caused by a stable fractional abundance of the major brGDGTs Ia, IIa and IIIa (Fig. 4C). In June, the CL MBT'_{5ME} showed a significant increase (T_{rec} : 15.8°C), attributed

to the high fractional abundance of brGDGTs Ia (20%) and Ib (8%) (Supp. Table S1), which continued until August. In September, a drop in MBT'_{5ME} value (0.31) was coeval with an increased fractional abundance of brGDGTs IIb (> 6%) and IIIa (20%), while in December,

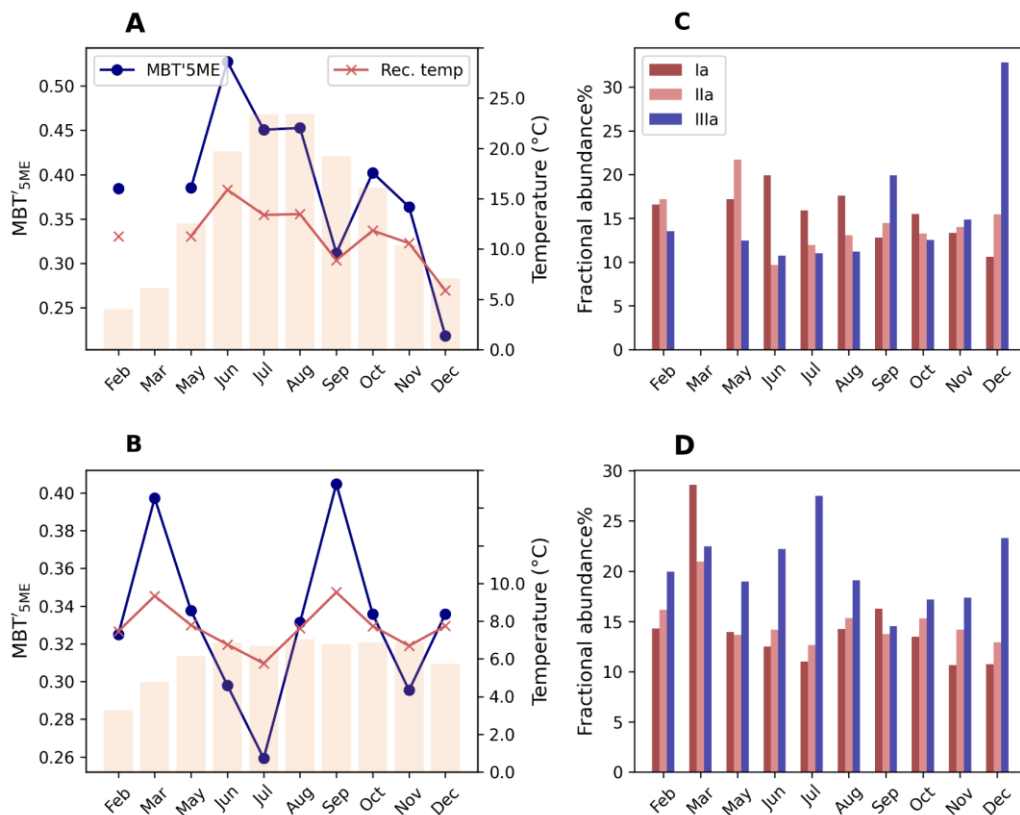


Fig. 4. Comparing brGDGT based ratio MBT'_{5ME} (blue) and the MBT'_{5ME}-based reconstructed temperature (red), with measured water temperature at the depth of sampling (shaded bars; panel A for epilimnion, B for hypolimnion). The fractional abundance of brGDGTs Ia, IIa and IIIa is plotted in panels C and D for epilimnion and hypolimnion, respectively.

where MBT'_{5ME} also declined (0.22), the lower fractional abundance of brGDGTs Ia (< 15%), Ib (< 4%), along with the increased fractional abundance of IIIa (> 30%), contributed to this shift (Supp. Table S1).

In the hypolimnion, the range of MBT'_{5ME} (0.25-0.40) was narrower compared to the epilimnion (Fig. 4B). The MBT'_{5ME} showed maxima in March and September and decreased in June-July and Nov-Dec (Fig. 4B). While in March a high fractional abundance in Ia was responsible for the elevated MBT'_{5ME}, in September the decreased IIIa% along with increased Ib% accounted for the increase in MBT'_{5ME} value (Fig. 4D or Supp. Table S1). In July, the low fractional abundance of brGDGT Ia and high fractional abundance of IIIa, drive the minimum MBT'_{5ME} value (< 0.25). Reflecting the relative contribution of 5 and 6-methyl

brGDGTs, the epilimnion showed low variability in IR values ($\bar{x}=0.56$, $\sigma=0.06$; Fig. 5A), indicating similar fractional abundances of brGDGT IIIa ($\bar{x}=16\%$, $\sigma=2\%$), and IIIa' ($\bar{x}=20\%$, $\sigma=2\%$). In the hypolimnion (Fig. 5B), similar IR values compared to the surface were observed. March stands out with a noticeably low IR value (0.38) caused by a low (< 2%) fractional abundance of IIIa'. In July and September, variability in the IR values was caused by either an increased or decreased fractional abundance of IIIa (30 and 14%, respectively). Reflecting the same structural variability as the IR, the CBT' showed constrained changes ($\bar{x}=-0.03$, -0.06 ; $\sigma=0.09$, 0.04) in both the epi- and hypolimnion of Lake Rot (Supp. Fig. 4). Although DC' exhibited a slightly larger range in the epilimnion ($\bar{x}=0.25$, $\sigma=0.05$) compared to the hypolimnion ($\bar{x}=0.23$, $\sigma=0.01$, Supp. Fig. 4), the fractional abundances of compounds Ib, IIb, and IIb' remained similar across both layers (Supp. Table S1).

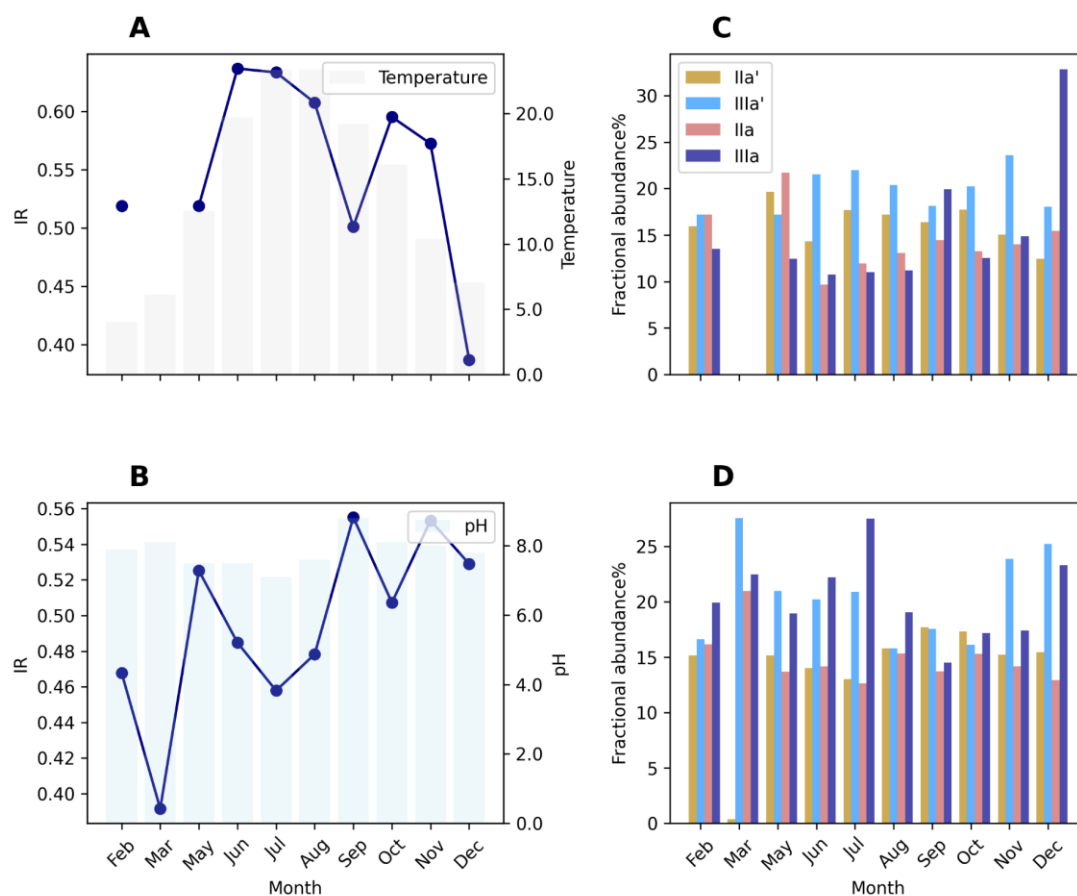


Fig. 5. Plotting brGDGT Isomer ratio (IR) values for Lake Rot (A) epilimnion and (B) hypolimnion (blue line). Measured epilimnion temperature is plotted as grey bars (A), and hypolimnion pH plotted in light blue (B). Panel C and D represent the fractional abundance of brGDGTs IIIa', IIIa, IIa, and IIIa' for epi- and hypolimnion, respectively.

In the surface sediment of Lake Rot, there was a significant difference in MBT'_{5ME} between the oxic and the seasonally anoxic setting. The “oxic” sediment exhibited an MBT'_{5ME} value of 0.28 ($T_{rec}= 7.7^{\circ}C$), while the “seasonally anoxic” sample displayed a higher MBT'_{5ME} value of 0.43, resulting in a higher reconstructed temperature ($12.7^{\circ}C$). Additionally, the “oxic” sample had a lower IR value (0.44) compared to the “seasonally anoxic” (0.54). Conversely, CBT' and DC' showed higher values (-0.1, 0.33) for the “oxic” sediment. A PCA is used to summarize changes in the brGDGT fractional abundance in Lake Rot SPM and surface sediments (Fig. 6A). As distinct brGDGT interdependencies are observed, separate ordinations are also performed based on epilimnion and hypolimnion SPM respectively (Fig. 6B-C).

3.3. Lake Rot 16S rRNA Gene-based bacterial community

The qPCR-derived 16S mean gene copies ($m L^{-1}$) of the seasonal SPM exhibited unsystematic concentration fluctuations throughout the year, showing increases and decreases in stratified and mixing months of both epi- and hypolimnion (Supp. Fig. S5). Similarly, the composition of the 16S rRNA gene-based bacterial community displayed seasonal variations. NMDS analysis highlighted these seasonal shifts in bacterial composition in both the epi- and hypolimnion (Fig. 7; Supp. Fig. S6). The community composition of each layer was similar during months with isothermal mixing. The most significant contrast between the epilimnion and hypolimnion was observed during the stratified summer months (Fig. 7). Bio-indicator OTUs for the epi- and hypolimnion are reported in Supp. Table 3A-B. For the epilimnion these include members from the orders Burkholderiales, Sphingomonadales (Proteobacteria), Chloroplast (Cyanobacteria), Flavobacteriales, Chitinophagales (Bacteroidota), Frankiales (Actinobacteria) (non-exhaustive, see Supp. Table 3B). For the hypolimnion, bio-indicator OTUs are representatives from the orders Chromatiales, Burkholderiales (Proteobacteria), Gaiellales (Actinobacteria), Omnitrophales (Verrucomicrobiota), Saccharimonadales (Paterscibacteria) (non-exhaustive, see Supp. Table 3B).

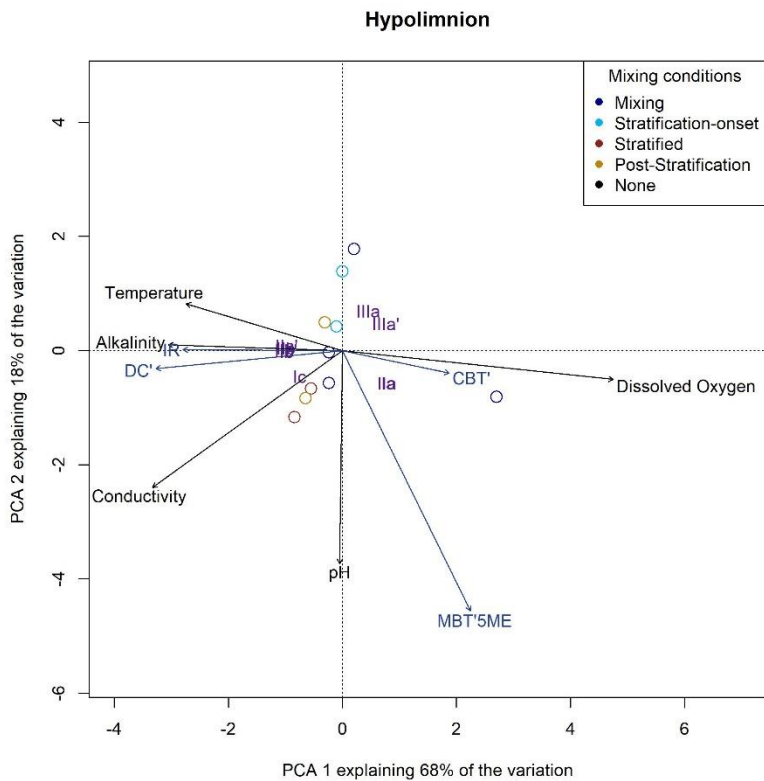
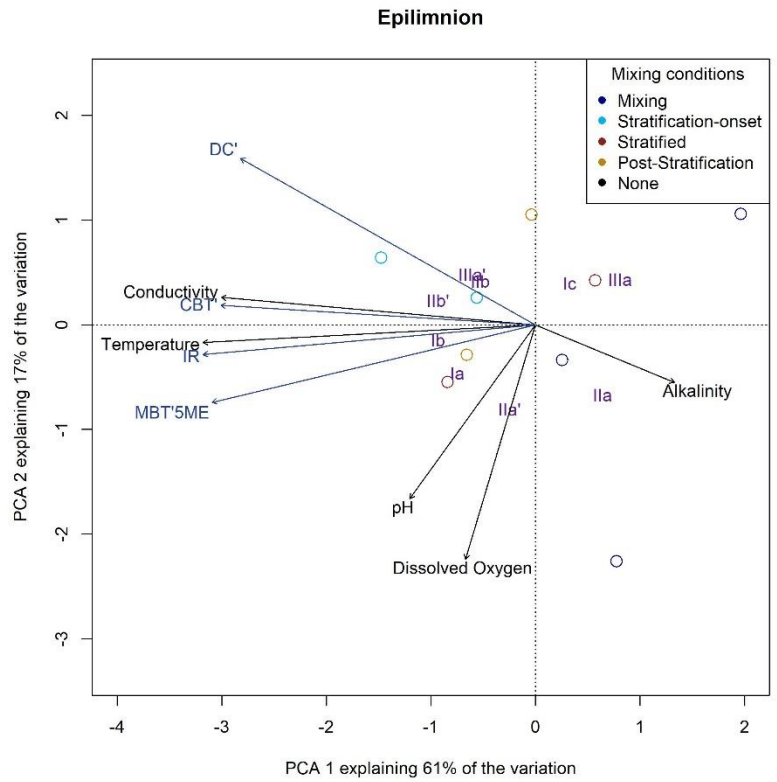
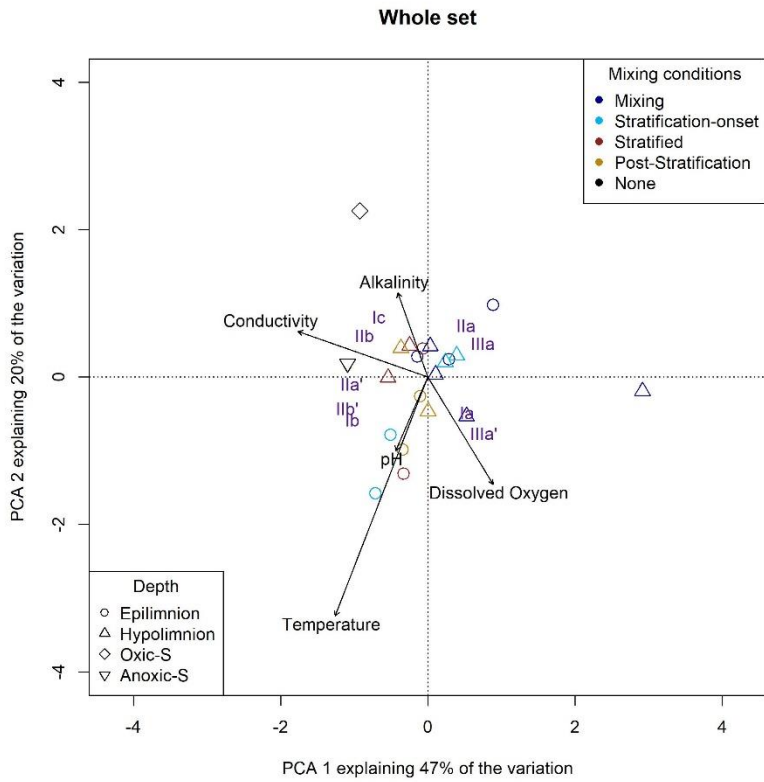


Fig. 6. An unconstrained principal component analysis (PCA) of 13 CL brGDGTs (excluding IIIc and IIIc') based on their standardized fractional abundance in (A) Lake Rot suspended particulate matter (SPM) and surface sediments, (B) Lake Rot epilimnion SPM and (C) Lake Rot hypolimnion SPM. The symbol color code of the SPM samples reflects different seasons. To avoid overlapping only more abundant brGDGTs (Ia, Ib, Ic, IIa, IIIa, IIa' and IIIa') are plotted. The environmental variables and GDGT-based ratios plotted a posteriori in the ordination space.

4. Discussion

In the following discussion, the impact of the measured environmental variables on individual brGDGTs and ratios variability is thoroughly discussed. While temperature plays a vital role in determining MBT'_{5ME} and IR changes in the epilimnion of Lake Rot, the isothermal water column stratification that leads to hypolimnion anoxia is a significant driver of brGDGT signal variability. Similarly, distinct dependencies between GDGTs and temperature-independent variables is observed in the hypolimnion. Moreover, the observed pronounced production of IPL GDGTs in the anoxic hypolimnion further confirms previous association of living microbial IPL GDGT producers with oxygen-depleted environments. The examination of the surface sediment samples also yields significant implications for MBT'_{5ME}-based paleothermometry.

4.1. Abiotic and biotic drivers of brGDGTs production in the lake water column

In Lake Rot, seasonal temperature changes and stratification results in variable brGDGT concentrations and distributions. Specifically, marked changes in brGDGT concentration are observed in the stratified summer months, during warming of the epilimnion and development of hypolimnion anoxia, coeval with changes in the bacterial community composition. With isothermal mixing, the distinct signature of summer epi- and hypolimnion is averaged out, resulting in similar brGDGT distribution between surface and bottom water before and after stratification. When discussing production of brGDGTs, IPL brGDGTs are often considered as markers of living (or recently active) GDGT-producing microbes that transform into more resistant CL GDGTs over time upon cell lysis (Lengger et al., 2013, 2014). In Rotsee, this process is observed for the conversion of hypolimnion August IPL brGDGT to epilimnion November CL brGDGTs. However, also instances of increased CL brGDGTs concentrations that do not correspond to concurrent increases in IPLs, for instance the increase of brGDGT Ia in surface water are observed. And conversely, instances of elevated IPLs that do not manifest in increased CL brGDGTs, for instance in Lake Rot anoxic bottom water. This discrepancy suggests that distinct drivers may underlie the production of CL and IPL brGDGTs in freshwater environments, and they are therefore discussed separately. Furthermore, the fluctuations in concentration patterns of both CL and IPL GDGTs do not follow or correlate with changes in the overall bacterial load as determined by qPCR.

Globally, brGDGT Ia is characterized by an increase in fractional abundance at warmer temperatures while brGDGT IIIa dominates the GDGT distribution in colder and/or deeper waters (Russell et al., 2018; Weber et al., 2018; Yao et al., 2020; Stefanescu et al., 2021). Temperature-sensitive production of CL is indeed evidenced from the increase in concentration of brGDGT Ia in the warmed and stratified summer months and brGDGT IIIa in colder mixing months in Lake Rot. Also 6-methyl brGDGT IIIa' is apparently produced in the warmer summer months, which supports its interpretation as a marker for aquatic production (De Jonge et al., 2014; Guo et al., 2020; Chapter 2). The production of CL brGDGT Ia coincides with an increase

in the number of epilimnion bio-indicator OTUs in June and July (Fig. 8A). These bacterial taxa that notably exclude Acidobacteria, include the orders Burkholderiales (Proteobacteria), Flavobacteriales, Chitinophagales (Bacteroidota), and Cyanobacteriales (Cyanobacteria) (see Supp. Table S1). These bacterial orders have been reported to contain members that possess “TES”, a protein homologue (Zeng et al., 2022), which is a key homologue responsible for bacterial membrane spanning lipid synthesis and are thus potential candidate orders for harbouring brGDGT producers.

In the epilimnion a significant increase in surface IPL brGDGT concentrations occurred in November, during a period of deepening of the thermocline in surface waters and lower oxygen content (Fig. 1; Fig. 2B). These elevated surface IPL brGDGT concentrations in October and November in Lake Rot’s epilimnion are attributed to the onset of the mixing season, leading to the upwelling of bottom water to the epilimnion during these months, bringing IPLs produced in the hypolimnion to the surface. This is confirmed by the presence of hypolimnion bio-indicators in the epilimnion at this timepoint (Fig. 8A).

The production of IPL brGDGTs in the hypolimnion is limited to anoxic conditions. This finding unequivocally highlights the role of anoxia as a key trigger for in-situ IPL brGDGT production. Culture studies have similarly reported the favorable production of brGDGTs (measured as CL GDGTs) under oxygen-limited conditions (Chen et al., 2022; Halamka et al., 2021, 2022). Both in the epi- and hypolimnion SPM brGDGT IIIa and IIIa’ dominate the distribution of IPL brGDGTs, hinting at the possibility that suboxic to anoxic conditions could promote the production of hexamethylated brGDGTs. The increase in the concentration of brGDGT IIIa (and compound IIIa’ which was not observed in Lake Rot) in suboxic to anoxic water columns have also previously been observed (Weber et al., 2018). However, this increase in IPL brGDGTs is not reflected in a concentration increase of CL brGDGTs. In addition, the distribution from the anoxic IPLs is distinct from that of the CL fraction (Fig. 3C and E). As CL brGDGT concentrations in the bottom layer during these anoxic periods were lower than those in the epilimnion and in the oxic period preceding stratification, the role of anoxia on CL brGDGTs needs to be seen independently from their IPL counterparts in lake systems. Hypolimnion IPL brGDGT production coincides with the increase of bio-indicator OTUs for these anoxic and suboxic months (Fig. 8). Several of these OTUs belong to distinct non-Acidobacteria taxa, specifically within the phyla Firmicutes (e.g., Clostridia, Monoglobales), Proteobacteria (e.g., Burkholderiales, Acetobacterales), Chloroflexi (e.g., Anaerolineales, Chloroflexales), and Actinobacteriota (e.g., Microtrichales) (non-exhaustive, see Supp. Table S3A-B). Several of these phyla have members that have previously been observed to possess the ether bond-forming enzyme known as “Ger,” that is involved in the synthesis of membrane-spanning lipids in bacteria in anoxic conditions (Sahonero-Canavesi et al., 2022). This strengthens the interpretation that the appearance of specific strains of anoxic bacteria (Supp. Table S1) are a potential source of IPL GDGTs.

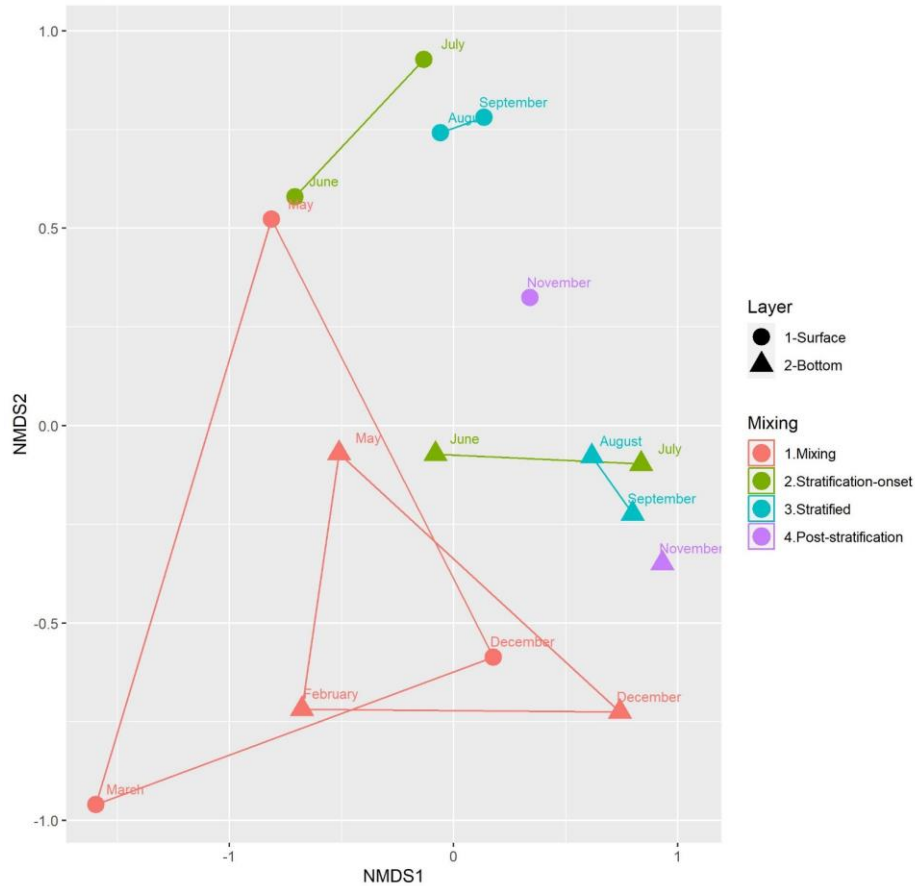


Fig. 7. Non-metric multidimensional scaling (NMDS) of Lake Rot 16S rRNA genes based bacterial community composition, with the shortest distance calculated as a polygon. The color code of the sample scores reflects the season of sampling, with symbol shapes representing sampling depth; epilimnion (sphere) or hypolimnion (triangle).

4.2. Environmental drivers on brGDGTs concentration and distribution

4.2.1. Proposed temperature-sensitive brGDGTs Ia, IIa and IIIa and ratios

In Lake Rot, depth-dependent production of CL brGDGTs in the epi- and hypolimnion is observed, highlighting the distinct dependencies of brGDGTs on selected environmental variables such as temperature, conductivity, alkalinity, pH, and dissolved oxygen. These variables account for 86% of the variation in brGDGT distribution in the hypolimnion and 67% in the epilimnion (Supp. Table S4). To understand the environmental drivers on brGDGTs, we will separately discuss their impact on the epilimnion and hypolimnion.

BrGDGT Ia is typically associated with temperature sensitivity, as observed in globally distributed lake sediments where its fractional abundance increases in surface sediments with warmer temperatures (Russell et al., 2018; Martínez-Sosa et al., 2021; Raberg et al., 2021). In Lake Rot, increased production of brGDGT Ia during the warm summer months (Fig. 3B, Fig. 4C) is observed, supporting this interpretation in our local study. Additionally, the concentration of brGDGT Ib, another compound known to increase with temperature in lake sediments globally (e.g., Raberg et al., 2021), shows a significant correlation with temperature ($r=0.61$, $p<0.05$). However, brGDGTs IIa and IIIa, while not showing a direct correlation with temperature in terms of concentration, exhibit a negative relationship with temperature in their fractional abundances (Supp. Table S4), which is also reflected in the PCA (Fig. 6B).

Throughout the remainder of the year (autumn and winter), as temperatures steadily decrease, the concentration of Ia generally declines (Fig. 3B). This behavior aligns with the expected response of this compound to the cooling temperatures typical of the colder months. However, in addition to a direct impact of temperature, the impact of lake water column mixing needs to be considered. During the epilimnion mixing season, distribution changes of brGDGTs is observed. Specifically, a decrease in brGDGT Ia and an increase in brGDGT IIIa, reflect a change to the GDGT distribution found in the hypolimnion (Fig. 3C). With the deepening of the thermocline (October-November) and onset of full water column mixing (November and December), the brGDGT lipids typical for the hypolimnion are brought to the epilimnion. Therefore, no direct impact of cooling on brGDGT Ia is observed in Lake Rot. For brGDGT IIIa, in contrast, the increase in concentration and fractional abundance (Fig. 3B, Fig. 4) during the colder November and December months in epilimnion is not derived from a bottom water signal, indicating the cold-induced production of this compound. However, although the increase in concentration of Ia is observed in warm stratified months in the epilimnion, the absence of a correlation between Ia and temperature during colder months, contributes to the non-significant dependency between MBT'_{SME} and temperature ($r=0.59$, $p=0.10$). In addition, MBT'_{SME} responds to the stratification-dependent conductivity, showing a correlation of $r=0.71$ ($p<0.05$).

Although 6-methyl compounds are not traditionally associated with temperature sensitivity, an increased IIIa' concentration, in response to warmer temperatures is notably visible in July (Fig. 3B), reflected in a dependency between the fractional abundance of IIIa' and temperature between May and September ($r=0.80$, $p=0.07$). Furthermore, the negative loadings of brGDGT IIIa' on epilimnion PCA axis 1 (Ia: -0.24, IIIa': -0.28) align with the loading of the temperature vector (Fig. 6B). This temperature dependency of the fractional abundance of brGDGT IIIa' agrees with recent studies (Russell et al., 2018; Martínez Sosa et al., 2020) that have observed positive correlations between the fractional abundances of brGDGTs IIa' and IIIa' and growth temperature in aquatic environments. Interestingly, the IR, as evident from Fig. 5A,

demonstrates a more robust correlation with temperature in surface waters ($r= 0.68$, $p< 0.05$), compared with MBT'_{5ME} . Furthermore, the stepwise forward selection model reinforces temperature as the primary environmental variable, explaining 46% of the variance in IR in the lake's epilimnion (Supp. Table S4). The addition of conductivity only marginally increases the explained variability by an extra 7% (resulting in a marginal effect variance of 53%). This suggests that, while there is a significant linear correlation between IR and conductivity ($r= 0.65$, $p< 0.05$) that matches previous global observations (Raberg et al., 2021), temperature (with a 20 °C annual range) may be the primary driver for variance in IR values, as supported by previous findings (Russell et al., 2018; Martínez-Sosa et al., 2020; Ajallooeian et al., (Chapter 2, under review)). Nevertheless, the observed correlation between IR and conductivity further indicates that in lakes where conductivity is temperature-dependent, distinguishing the direct influences of conductivity and/or temperature on IR can be challenging.

Overall, in the epilimnion Lake Rot, temperature does not significantly explain the variation in MBT'_{5ME} , but it is a statistically significant predictor for IR (adj. $r^2=0.46$, $p= 0.04$). In this context, we explore the potential impact of temperature on the hypolimnion brGDGTs.

In the hypolimnion, a more muted variability in temperature (4-9 °C; Fig. 2A) is present. Hence, the reported linear correlations and stepwise forward selection models report a larger impact of stratification-independent water chemistry parameters on GDGTs compared to temperature. In the hypolimnion, both the concentration of brGDGT Ia and IIIa' show a negative correlation with water alkalinity ($r= -0.73$, -0.69 , $p< 0.05$; Supp. Fig. S8). As alkalinity and temperature show a dependency ($r= 0.59$, $p< 0.1$) the concentration of brGDGT Ia even displays a reverse correlation with temperature ($r= -0.66$, $p< 0.05$). Similarly, IIIa concentration, exhibits a correlation with water alkalinity ($r= -0.70$, $p< 0.05$) but not temperature. The lack of a temperature response in the bottom water GDGTs can potentially be attributed to the presence of distinct temperature dependent GDGT-producing bacteria in the epilimnion, and their absence in the hypolimnion (Fig. 8). In the hypolimnion MBT'_{5ME} shows a strong correlation with pH ($r= 0.80$, $p< 0.01$), highlighting the various influences on this proxy in settings that do not experience a large temperature fluctuation.

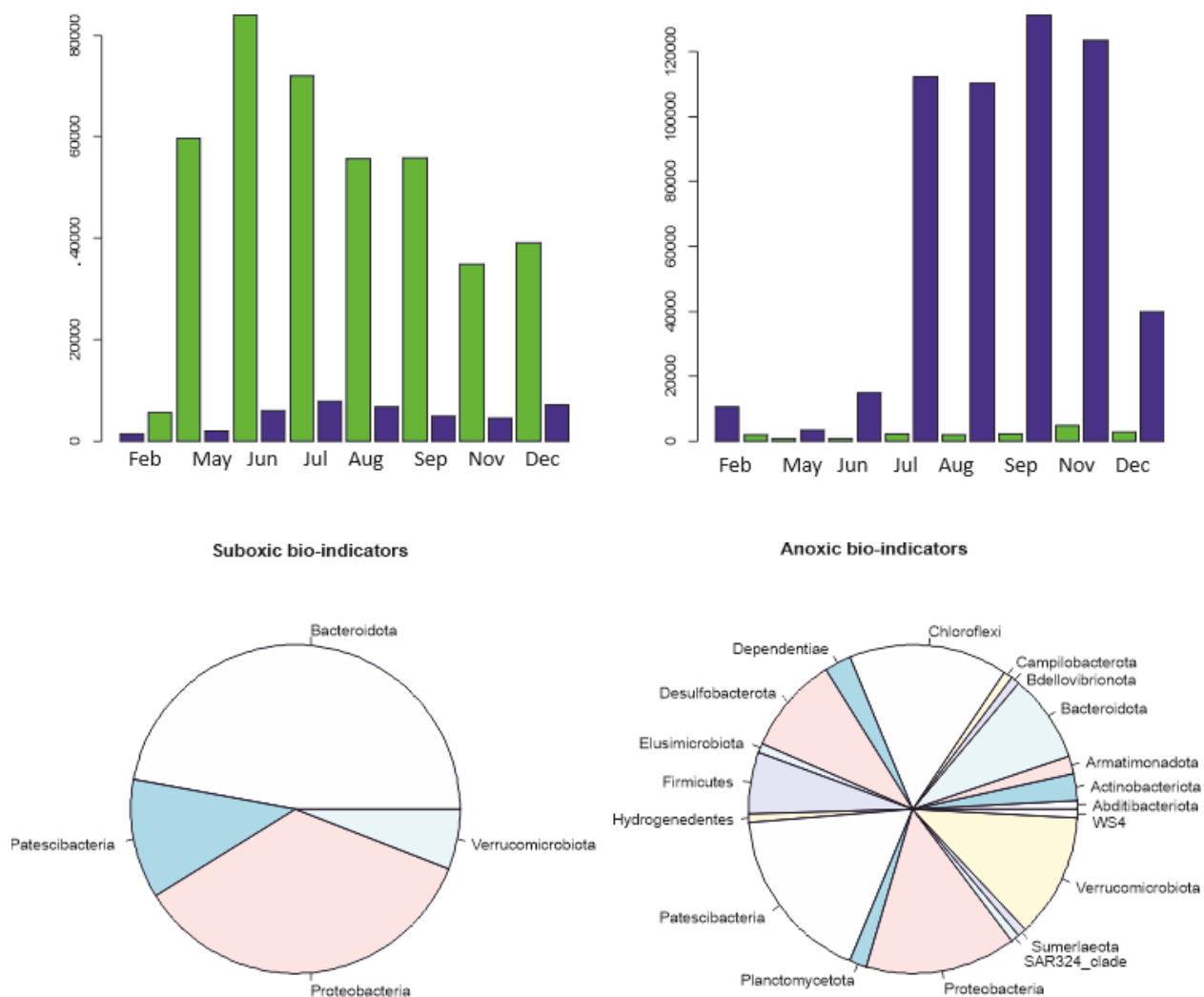


Fig. 8. The count of (A) epilimnion and (B) hypolimnion bio-indicator OTU reads for Lake Rot epilimnion (green) and hypolimnion (blue), respectively. (The phylogenetic diversity of the bio-indicator OTUs can be found in Supp. Table S3A-B. Panel C shows 2 pie charts illustrating the composition of bio-indicator OTUs identified for the suboxic (dissolved oxygen (DO) <math>< 2 \text{ mg L}^{-1}</math>; May, June, July) and anoxic (DO <math>< 0.1 \text{ mg L}^{-1}</math>; August, September) hypolimnion of Lake Rot.

4.2.2. Chemistry-sensitive 6-methyl and cyclopentane-containing brGDGTs, IR, CBT' and DC'

Chemistry brGDGT ratios including CBT' and DC' do not exhibit any dependency on the water chemistry of epilimnion (Supp. Table S2), instead CBT' correlates with temperature ($r = 0.66$, $p < 0.05$). The absence of a correlation between CBT' and pH particularly contrasts with previous lacustrine studies, where CBT'

was found to correlate with pH in oxic water layers (Zhang et al., 2016) and lake sediments (Martínez-Sosa et al., 2021).

In Lake Rot hypolimnion however, lake chemistry parameters dissolved oxygen (and conductivity and alkalinity to a lesser extent) drive increases in cyclopentane-containing and 6-methyl brGDGTs (Supp. Table S2). While the individual concentration of 5- and 6-methyl brGDGTs do not exhibit a direct correlation with the varying dissolved oxygen levels in the hypolimnion, the fractional abundance of cyclopentane containing brGDGTs Iib, Ib and Ic and 6-methyl brGDGTs Iia' and Iib' correlates with DO ($r = -0.64$ to -0.80 , $p < 0.05$), as well as the IR, CBT' and DC' ($r = -0.65$ to -0.78 , $p < 0.05$). This correlation is also observed in the IR ($r = -0.64$, $r = 0.66$, $p < 0.05$, for dissolved oxygen and alkalinity respectively). This aligns with findings from several studies (Dang et al., 2018; Russell et al., 2018; Weber et al., 2018; Van Bree et al., 2020), which have reported a similar anti-correlation between the fractional abundance of 6-methyl brGDGTs or IR and DO. On the other hand, other studies (Yao et al., 2020; Qian et al., 2019) have argued for a positive relationship between 6-methyl compounds and dissolved oxygen. Furthermore, as a correlation between alkalinity and total P was observed, IR correlates with total P ($r = 0.60$, $P < 0.05$), suggesting that with increasing nutrients in the seasonally anoxic hypolimnion 6-methyls proportions also increased. However, this correlation is not observed with individual fractional abundances of IR compounds.

In summary, similar to global observations, brGDGT Ia responds rapidly to warm summer temperatures and brGDGT IIIa is increased in the deep and/or cold waters. A closer examination of brGDGT ratio variation reveals dependencies on different environmental variables between the epi- and hypolimnion. In the hypolimnion, brGDGT ratios exhibit dependency on water chemistry parameters pH, alkalinity, and dissolved oxygen (Supp. Table S2), whereas at the surface, temperature remains the primary driver of variation (explaining ~50% of variability). This distinction is important when considering the brGDGT signal deposited into sediments and its sensitivity to environmental influences.

In section 4.3, we discuss surface sediment samples collected from both oxic and seasonally anoxic water column regimes, providing insight into the signal that will be incorporated in the sedimentary archive.

4.3. Implications for paleoclimate records

The 'oxic' sediment contains higher brGDGT concentrations (Supp. Table S1) compared to the 'seasonally anoxic' sediment, which is contrary to previous reports (Weber et al., 2018; Van Bree et al., 2020). While the 'oxic' sediment is expected to receive brGDGTs dominantly produced in the epilimnion, a cold MBT'_{5ME} signal of 0.27 is observed that is lower than the water column's weighted average signal of either

the stratified or mixed epilimnion ($MBT'_{5ME} = 0.40, 0.38$ for stratified and mixed epilimnion, respectively; Supp. Fig. S8). In addition, the PCA analysis (Fig. 6A) illustrates that this ‘oxic’ sediment has a unique brGDGT distribution compared to any of the water column samples. The high fractional abundance of brGDGT IIa and IIIa (33%) in this sediment sample suggests a possible in-situ brGDGT production of penta- and hexamethylated brGDGTs in the sediment, a phenomenon not observed in the epilimnion. The colder signal of MBT'_{5ME} observed in the ‘oxic’ sample aligns with earlier findings in other studies (Zhao et al., 2021 and references therein) that reported a cold signal in the top-cores.

On the other hand, the fractional abundances of Ia, IIa and IIIa in the ‘seasonally anoxic’ sediment sample corresponds best with the average signal of the stratified and/or mixed epilimnion (Supp. Fig. S8), leading to a warmer MBT'_{5ME} signal of 0.44 ($T_{rec} = 13$ °C) in this ‘seasonally anoxic’ sediment. The MBT'_{5ME} of the ‘seasonally anoxic’ sediment overestimates the water column reconstructed mean annual temperature (MAT) by 2 degrees yet matches the current mean annual air temperature (MAAT: 14 °C) at Lake Rot. The higher fractional abundance of brGDGT IIa’ in the anoxic sediment, compared to the epilimnion, points to the potential influence of sedimentary production of brGDGT IIa’ in the ‘seasonally anoxic’ sediment.

Although the distribution in the seasonally anoxic sediment mirrors the epilimnion SPM generally, efforts need to be made to constrain the potential contribution of hypolimnion SPM. Based on the correlation observed in the hypolimnion, MBT'_{5ME} produced in the hypolimnion record muted temperature variability and can even be impacted by pH changes. Considering these distinct observations, the choice of coring location is crucial when intending to apply MBT'_{5ME} -based temperatures as a paleotemperature indicator for lacustrine settings. To identify GDGT distributions that are sourced from the epilimnion, both MBT'_{5ME} and IR can be determined in parallel, as a good correlation is expected when brGDGTs are sourced from the epilimnion. Furthermore, the interdependencies of brGDGTs downcore can be compared with patterns observed in the epi- and hypolimnion (e.g. Fig. 6, Supp. Fig. 3B). As several of the environmental dependencies we observe within Lake Rot have been observed on a global scale, this approach has potential to be used globally on distributed lakes with a thermally isolated hypolimnion. Its applicability through time should however be tested in follow-up research.

5. Conclusions

In Lake Rot, although the water column seasonal stratification causes variability in epilimnion temperature, changes in MBT'_{5ME} underestimate the measured temperature fluctuations (by 0-7 °C), resulting in a subdued reconstructed temperature. The isomer ratio (IR) of brGDGTs however represent a stronger

dependency on temperature highlighting the potential of 6-methyl brGDGTs in stratified lakes as paleothermometer-indicative compounds. In the hypolimnion, with a limited temperature range (4-9 °C), and seasonal anoxia, MBT'_{5ME} does not correlate with temperature but rather with water pH. Similarly, the maximum flux of IPL GDGTs is observed in the anoxic hypolimnion along with a strong correlation between IR and dissolved oxygen, confirming prior reports on dissolved oxygen role as a trigger for production of 6-methyl brGDGTs.

The two surface sediments retrieved from the “oxic”, and “seasonally anoxic” sections of the lake put forward significant implications for paleotemperature reconstructions in lacustrine settings. While the observed core-top production of brGDGT IIIa can complicate the interpretation of the MBT'_{5ME} signal in the “oxic” sediments; recording mostly an epilimnion signal, MBT'_{5ME} along with IR in this location hold promise as temperature indicators. This is especially the case for IR, as the observed temperature dependency of IR is exclusively observed in lake’s epilimnion. However, in seasonally anoxic sediments of the lake, the temperature signal of MBT'_{5ME} although matches the epilimnion, can become complicated by the input of hypolimnion chemistry-influenced MBT'_{5ME}. This suggests that paleotemperature studies based on brGDGTs recovered from cores collected from “anoxic” part of stratified lakes may exhibit a muted temperature response, potentially complicated by water chemistry. Consequently, the authors suggest testing the applicability of coupled MBT'_{5ME} and IR in parallel as a tool to recognize an epilimnion GDGT input in the sedimentary records of stratified lakes. This approach has potential to be used globally on distributed lakes with a thermally isolated hypolimnion.

Last but not least, based on a bio-indicator statistical approach, bacterial groups exclusively outside Acidobacteria, are highlighted as *potential* brGDGT producers especially in stratified water column of Lake Rot.

Acknowledgments

This work was supported by the Swiss National Science Foundation [SNSF Project MiCoDy, grant PR00P2_179783]. In addition, the authors wish to express their gratitude for the assistance provided during the fieldwork of this project by Patrick Kathriner, Karin Beck, Nina Studhalter, Sandra Schmid, Alois Zwysig and for the valuable support extended by the staff of the Genetic Diversity Center of ETH Zürich (GDC) in the laboratory work.

Bibliography, Chapter 3

- Bechtel, A., Smittenberg, R. H., Bernasconi, S. M., and Schubert, C. J. (2010). Distribution of branched and isoprenoid tetraether lipids in an oligotrophic and a eutrophic Swiss lake: insights into sources and GDGT-based proxies. *Organic Geochemistry*, 41(8), 822-832.
- Bлага, C. I., Reichart, G. J., Vissers, E. W., Lotter, A. F., Anselmetti, F. S., and Sinninghe Damsté, J. S. (2011). Seasonal changes in glycerol dialkyl glycerol tetraether concentrations and fluxes in a perialpine lake: Implications for the use of the TEX86 and BIT proxies. *Geochimica et Cosmochimica Acta*, 75(21), 6416-6428.
- Buckles, L. K., Weijers, J. W., Verschuren, D., and Sinninghe Damsté, J. S. (2014). Sources of core and intact branched tetraether membrane lipids in the lacustrine environment: Anatomy of Lake Challa and its catchment, equatorial East Africa. *Geochimica et Cosmochimica Acta*, 140, 106-126.
- Chen, Y., Zheng, F., Yang, H., Yang, W., Wu, R., Liu, X., Liang, H., Chen, H., Pei, H., Zhang, C., Pancost, R.D., Zeng, Z. (2022). The production of diverse brGDGTs by an *Acidobacterium* providing a physiological basis for paleoclimate proxies. *Geochimica et Cosmochimica Acta*, 337, 155-165.
- Colcord, D. E., Pearson, A., and Brassell, S. C. (2017). Carbon isotopic composition of intact branched GDGT core lipids in Greenland lake sediments and soils. *Organic Geochemistry*, 110, 25-32.
- Crampton-Flood, E. D., Tierney, J. E., Peterse, F., Kirkels, F. M., and Sinninghe Damsté, J. S. (2020). BayMBT: A Bayesian calibration model for branched glycerol dialkyl glycerol tetraethers in soils and peats. *Geochimica et Cosmochimica Acta*, 268, 142-159.
- Dang, X., Yang, H., Naafs, B. D. A., Pancost, R. D., and Xie, S. (2016). Evidence of moisture control on the methylation of branched glycerol dialkyl glycerol tetraethers in semi-arid and arid soils. *Geochimica et Cosmochimica Acta*, 189, 24-36.
- De Cáceres, M. (2013). How to use the *indicpecies* package (ver. 1.7. 1). *R Proj*, 29.
- De Jonge, C., Hopmans, E. C., Stadnitskaia, A., Rijpstra, W. I. C., Hofland, R., Tegelaar, E., Sinninghe Damsté, J. S. (2013). Identification of novel penta- and hexamethylated branched glycerol dialkyl glycerol tetraethers in peat using HPLC–MS2, GC–MS and GC–SMB-MS. *Organic geochemistry*, 54, 78-82.
- De Jonge, C., Hopmans, E. C., Zell, C. I., Kim, J. H., Schouten, S., and Sinninghe Damsté, J. S. (2014b). Occurrence and abundance of 6-methyl branched glycerol dialkyl glycerol tetraethers in soils: Implications for palaeoclimate reconstruction. *Geochimica et Cosmochimica Acta*, 141, 97-112.

- De Jonge, C., Kuramae, E. E., Radujković, D., Weedon, J. T., Janssens, I. A., and Peterse, F. (2021). The influence of soil chemistry on branched tetraether lipids in mid-and high latitude soils: Implications for brGDGT-based paleothermometry. *Geochimica et Cosmochimica Acta*, 310, 95-112.
- De Jonge, C., Radujković, D., Sigurdsson, B. D., Weedon, J. T., Janssens, I., and Peterse, F. (2019). Lipid biomarker temperature proxy responds to abrupt shift in the bacterial community composition in geothermally heated soils. *Organic Geochemistry*, 137, 103897.
- De Jonge, C., Stadnitskaia, A., Hopmans, E. C., Cherkashov, G., Fedotov, A., and Sinninghe Damsté, J. S. S. (2014a). In situ produced branched glycerol dialkyl glycerol tetraethers in suspended particulate matter from the Yenisei River, Eastern Siberia. *Geochimica et Cosmochimica Acta*, 125, 476-491.
- Dedysh, S. N., and Sinninghe Damsté, J. S. (2018). *Acidobacteria*. eLS, 1-10.
- Deng, L., Bölsterli, D., Kristensen, E., Meile, C., Su, C. C., Bernasconi, S. M., Seidenkrantz, M., Glombita, C., Lagostina, L., Han, X., Jørgensen, B.B., Røy, H., Lever, M. A. (2020). Macrofaunal control of microbial community structure in continental margin sediments. *Proceedings of the National Academy of Sciences*, 117(27), 15911-15922.
- Dray, S., Legendre, P., and Peres-Neto, P. R. (2006). Spatial modelling: a comprehensive framework for principal coordinate analysis of neighbour matrices (PCNM). *Ecological modelling*, 196(3-4), 483-493.
- Duan, Y., Sun, Q., Werne, J. P., Yang, H., Jia, J., Wang, L., Xie, H. and Chen, F. (2020). Soil pH dominates the distributions of both 5-and 6-methyl branched tetraethers in arid regions. *Journal of Geophysical Research: Biogeosciences*, 125(10), e2019JG005356.
- Guo, J., Glendell, M., Meersmans, J., Kirkels, F., Middelburg, J. J., and Peterse, F. (2020). Assessing branched tetraether lipids as tracers of soil organic carbon transport through the Carminowe Creek catchment (southwest England). *Biogeosciences*, 17(12), 3183-3201.
- Halamka, T. A., McFarlin, J. M., Younkin, A. D., Depoy, J., Dildar, N., & Kopf, S. H. (2021). Oxygen limitation can trigger the production of branched GDGTs in culture. *Geochemical Perspectives Letters*.
- Halamka, T. A., Raberg, J. H., McFarlin, J. M., Younkin, A. D., Mulligan, C., Liu, X. L., and Kopf, S. H. (2022). Production of diverse brGDGTs by *Acidobacterium Solibacter usitatus* in response to temperature, pH, and O₂ provides a culturing perspective on brGDGT proxies and biosynthesis. *Geobiology*, 21(1), 102-118.

Halfman, R., Lembrechts, J., Radujković, D., De Gruyter, J., Nijs, I., and De Jonge, C. (2022). Soil chemistry, temperature, and bacterial community composition drive brGDGT distributions along a subarctic elevation gradient. *Organic Geochemistry*, 163, 104346.

Hopmans, E. C., Schouten, S., and Sinninghe Damsté, J. S. (2016). The effect of improved chromatography on GDGT-based palaeoproxies. *Organic Geochemistry*, 93, 1-6.

Hu, J., Zhou, H., and Spiro, B. (2016). Seasonal variability in concentrations and fluxes of glycerol dialkyl glycerol tetraethers in Huguangyan Maar Lake, SE China: Implications for the applicability of the MBT–CBT paleotemperature proxy in lacustrine settings. *Chemical Geology*, 420, 200-212.

Huguet, C., Hopmans, E. C., Febo-Ayala, W., Thompson, D. H., Sinninghe Damsté, J. S., and Schouten, S. (2006). An improved method to determine the absolute abundance of glycerol dibiphytanyl glycerol tetraether lipids. *Organic Geochemistry*, 37(9), 1036-1041.

Kaufman, D., McKay, N., Routson, C., Erb, M., Davis, B., Heiri, O., Jaccard, S., Tierney, J., Dätwyler, C., Axford, Y., Brussel, T., Cartapanis, O., Chase, B., Dawson, A., de Vernal, A., Engels, S., Jonkers, L., Marsicek, J., Moffa-Sánchez, P., Morrill, C., Orsi, A., Rehfeld, K., Saunders, K., Sommer, P. S., Thomas, E., Tonello, M., Tóth, M., Vachula, R., Andreev, A., Bertrand, S., Biskaborn, B., Bringué, M., Brooks, S., Caniupán, M., Chevalier, M., Cwynar, L., Emile-Geay, J., Fegyveresi, J., Feurdean, A., Finsinger, W., Fortin, M.-C., Foster, L., Fox, M., Gajewski, K., Grosjean, M., Hausmann, S., Heinrichs, M., Holmes, N., Ilyashuk, B., Ilyashuk, E., Juggins, S., Khider, D., Koinig, K., Langdon, P., Larocque-Tobler, I., Li, J., Lotter, A., Luoto, T., Mackay, A., Magyari, E., Malevich, S., Mark, B., Massaferró, J., Montade, V., Nazarova, L., Novenko, E., Pařil, P., Pearson, E., Peros, M., Pienitz, R., Plóciennik, M., Porinchu, D., Potito, A., Rees, A., Reinemann, S., Roberts, S., Rolland, N., Salonen, S., Self, A., Seppä, H., Shala, S., St-Jacques, J.-M., Stenni, B., Syrykh, L., Tarrats, P., Taylor, K., van den Bos, V., Velle, G., Wahl, E., Walker, I., Wilmshurst, J., Zhang, E., Zhilich, S. (2020). Holocene global mean surface temperature, a multi-method reconstruction approach. *Scientific data*, 7(1), 201.

Kou, Q., Zhu, L., Ju, J., Wang, J., Xu, T., Li, C., and Ma, Q. (2022). Influence of salinity on glycerol dialkyl glycerol tetraether-based indicators in Tibetan Plateau lakes: Implications for paleotemperature and paleosalinity reconstructions. *Palaeogeography, Palaeoclimatology, Palaeoecology*, 601, 111127.

Lattaud, J., De Jonge, C., Pearson, A., Elling, F. J., and Eglinton, T. I. (2021). Microbial lipid signatures in Arctic deltaic sediments—Insights into methane cycling and climate variability. *Organic Geochemistry*, 157, 104242.

Legendre, P. and Legendre, L. (2012). *Numerical ecology*. Elsevier.

- Lengger, S. K., Hopmans, E. C., Sinninghe Damsté, J. S., and Schouten, S. (2014). Impact of sedimentary degradation and deep water column production on GDGT abundance and distribution in surface sediments in the Arabian Sea: Implications for the TEX86 paleothermometer. *Geochimica et Cosmochimica Acta*, 142, 386-399.
- Lengger, S. K., Kraaij, M., Tjallingii, R., Baas, M., Stuut, J. B., Hopmans, E. C., Sinninghe Damsté, J. S., and Schouten, S. (2013). Differential degradation of intact polar and core glycerol dialkyl glycerol tetraether lipids upon post-depositional oxidation. *Organic Geochemistry*, 65, 83-93.
- Lever, M. A., Torti, A., Eickenbusch, P., Michaud, A. B., Šantl-Temkiv, T., and Jørgensen, B. B. (2015). A modular method for the extraction of DNA and RNA, and the separation of DNA pools from diverse environmental sample types. *Frontiers in microbiology*, 6, 476.
- Loomis, S. E., Russell, J. M., Eggermont, H., Verschuren, D., and Sinninghe Damsté, J. S. (2014). Effects of temperature, pH and nutrient concentration on branched GDGT distributions in East African lakes: Implications for paleoenvironmental reconstruction. *Organic Geochemistry*, 66, 25-37.
- Loomis, S. E., Russell, J. M., Heurreux, A. M., D'Andrea, W. J., and Sinninghe Damsté, J. S. (2014). Seasonal variability of branched glycerol dialkyl glycerol tetraethers (brGDGTs) in a temperate lake system. *Geochimica et Cosmochimica Acta*, 144, 173-187.
- Martínez-Sosa, P., and Tierney, J. E. (2019). Lacustrine brGDGT response to microcosm and mesocosm incubations. *Organic Geochemistry*, 127, 12-22.
- Martínez-Sosa, P., Tierney, J. E., and Meredith, L. K. (2020). Controlled lacustrine microcosms show a brGDGT response to environmental perturbations. *Organic Geochemistry*, 145, 104041.
- Martínez-Sosa, P., Tierney, J. E., Stefanescu, I. C., Crampton-Flood, E. D., Shuman, B. N., and Routson, C. (2021). A global Bayesian temperature calibration for lacustrine brGDGTs. *Geochimica et Cosmochimica Acta*, 305, 87-105.
- Masion, A., Vilg -Ritter, A., Rose, J., Stone, W. E., Teppen, B. J., Rybacki, D., and Bottero, J. Y. (2000). Coagulation-flocculation of natural organic matter with Al salts: Speciation and structure of the aggregates. *Environmental Science and Technology*, 34(15), 3242-3246.
- McMurdie, P. J., and Holmes, S. (2013). phyloseq: an R package for reproducible interactive analysis and graphics of microbiome census data. *PloS one*, 8(4), e61217.

- Miller, D. R., Habicht, M. H., Keisling, B. A., Castañeda, I. S., and Bradley, R. S. (2018). A 900-year New England temperature reconstruction from in situ seasonally produced branched glycerol dialkyl glycerol tetraethers (brGDGTs). *Climate of the Past*, 14(11), 1653-1667.
- Naafs, B. D. A., Inglis, G. N., Zheng, Y., Amesbury, M. J., Biester, H., Bindler, R., Blewett, J., Burrows, M.A., del Castillo, T., Chambers, F.M., Cohen, A.D., Evershed, R. P., Feakins, S. J., Galka, M., Gallego-Sala, A., Gandois, L., Gray, D. M., Hatcher, P. G., Honorio Coronado, E. N., Hughes, P. D. M., Pancost, R. D. (2017). Introducing global peat-specific temperature and pH calibrations based on brGDGT bacterial lipids. *Geochimica et Cosmochimica Acta*, 208, 285-301.
- Naafs, B. D. A., Oliveira, A. S. F., and Mulholland, A. J. (2021). Molecular dynamics simulations support the hypothesis that the brGDGT paleothermometer is based on homeoviscous adaptation. *Geochimica et Cosmochimica Acta*, 312, 44-56.
- Naeher, S., Peterse, F., Smittenberg, R. H., Niemann, H., Zigah, P. K., and Schubert, C. J. (2014). Sources of glycerol dialkyl glycerol tetraethers (GDGTs) in catchment soils, water column and sediments of Lake Rotsee (Switzerland)—Implications for the application of GDGT-based proxies for lakes. *Organic Geochemistry*, 66, 164-173.
- Oksanen, J., Blanchet, F. G., Kindt, R., Legendre, P., Minchin, P. R., O'hara, R. B., Simpson, G. L., Solymos [aut], P., Steven, M. H. H., Szoecs, E., Wagner, H., Barbour, M., Bedward, M., Bolker, B., Borcard, D., Carvalho, G., Chirico, M., De Caceres, M., Evangelista, D. S. H., Oksanen, M. J. (2013). Package 'vegan'. *Community ecology package*, version, 2(9), 1-295.
- Parfenova, V. V., Gladkikh, A. S., and Belykh, O. I. (2013). Comparative analysis of biodiversity in the planktonic and biofilm bacterial communities in Lake Baikal. *Microbiology*, 82, 91-101.
- Peterse, F., Kim, J. H., Schouten, S., Kristensen, D. K., Koç, N., and Sinninghe Damsté, J. S. (2009). Constraints on the application of the MBT/CBT palaeothermometer at high latitude environments (Svalbard, Norway). *Organic Geochemistry*, 40(6), 692-699.
- Peterse, F., Nicol, G. W., Schouten, S., and Sinninghe Damsté, J. S. (2010). Influence of soil pH on the abundance and distribution of core and intact polar lipid-derived branched GDGTs in soil. *Organic Geochemistry*, 41(10), 1171-1175.
- Peterse, F., van der Meer, J., Schouten, S., Weijers, J. W., Fierer, N., Jackson, R. B., Kim, J., Sinninghe Damsté, J. S. (2012). Revised calibration of the MBT–CBT paleotemperature proxy based on branched tetraether membrane lipids in surface soils. *Geochimica et Cosmochimica Acta*, 96, 215-229.

- Pitcher, A., Hopmans, E. C., Schouten, S., and Sinninghe Damsté, J. S. (2009). Separation of core and intact polar archaeal tetraether lipids using silica columns: insights into living and fossil biomass contributions. *Organic Geochemistry*, 40(1), 12-19.
- Qian, S., Yang, H., Dong, C., Wang, Y., Wu, J., Pei, H., Dang, X., Lu, J., Zhao, S., and Xie, S. (2019). Rapid response of fossil tetraether lipids in lake sediments to seasonal environmental variables in a shallow lake in central China: Implications for the use of tetraether-based proxies. *Organic Geochemistry*, 128, 108-121.
- Raberg, J. H., Harning, D. J., Crump, S. E., de Wet, G., Blumm, A., Kopf, S., Geirsdóttir, Á., Miller, G. H., Sepúlveda, J. (2021). Revised fractional abundances and warm-season temperatures substantially improve brGDGT calibrations in lake sediments. *Biogeosciences*, 18(12), 3579-3603.
- Russell, J. M., Hopmans, E. C., Loomis, S. E., Liang, J., and Sinninghe Damsté, J. S. (2018). Distributions of 5- and 6-methyl branched glycerol dialkyl glycerol tetraethers (brGDGTs) in East African lake sediment: Effects of temperature, pH, and new lacustrine paleotemperature calibrations. *Organic Geochemistry*, 117, 56-69.
- Sahonero-Canavesi, D. X., Siliakus, M. F., Abdala Asbun, A., Koenen, M., von Meijenfeldt, F. B., Boeren, S., Bale, N. J., Engelman, J. C., Fiege, C., Strack van Schijndel, L., Sinninghe Damsté, J. S., Villanueva, L. (2022). Disentangling the lipid divide: Identification of key enzymes for the biosynthesis of membrane-spanning and ether lipids in Bacteria. *Science advances*, 8(50), eabq8652.
- Schoon, P. L., De Kluijver, A., Middelburg, J. J., Downing, J. A., Sinninghe Damsté, J. S., and Schouten, S. (2013). Influence of lake water pH and alkalinity on the distribution of core and intact polar branched glycerol dialkyl glycerol tetraethers (GDGTs) in lakes. *Organic Geochemistry*, 60, 72-82.
- Schubert, C. J., Lucas, F. S., Durisch-Kaiser, E., Stierli, R., Diem, T., Scheidegger, O., Vazquez, F., Müller, B. (2010). Oxidation and emission of methane in a monomictic lake (Rotsee, Switzerland). *Aquatic sciences*, 72, 455-466.
- Shade, A., Kent, A. D., Jones, S. E., Newton, R. J., Triplett, E. W., and McMahon, K. D. (2007). Interannual dynamics and phenology of bacterial communities in a eutrophic lake. *Limnology and Oceanography*, 52(2), 487-494.
- Sinninghe Damsté, J. S., Hopmans, E. C., Pancost, R. D., Schouten, S., and Geenevasen, J. A. (2000). Newly discovered non-isoprenoid glycerol dialkyl glycerol tetraether lipids in sediments. *Chemical Communications*, (17), 1683-1684.

Sinninghe Damsté, J. S., Rijpstra, W. I. C., Foesel, B. U., Huber, K. J., Overmann, J., Nakagawa, S., Kim, J. M., Dunfield, P. F., Dadysh, S. N., Villanueva, L. (2018). An overview of the occurrence of ether-and ester-linked iso-diabolic acid membrane lipids in microbial cultures of the Acidobacteria: Implications for brGDGT paleoproxies for temperature and pH. *Organic Geochemistry*, 124, 63-76.

Sinninghe Damsté, J. S., Rijpstra, W. I. C., Hopmans, E. C., Foesel, B. U., Wüst, P. K., Overmann, J., Tank, M., Bryant, D. A., Dunfield, P. F., Houghton, K., Stott, M. B. (2014). Ether-and ester-bound iso-diabolic acid and other lipids in members of Acidobacteria subdivision 4. *Applied and Environmental Microbiology*, 80(17), 5207-5218.

Sinninghe Damsté, J. S., Rijpstra, W. I. C., Hopmans, E. C., Weijers, J. W., Foesel, B. U., Overmann, J., and Dedysh, S. N. (2011). 13, 16-Dimethyl octacosanedioic acid (iso-diabolic acid), a common membrane-spanning lipid of Acidobacteria subdivisions 1 and 3. *Applied and environmental microbiology*, 77(12), 4147-4154.

Staufferl, R. E. (1990). Alkalinities of Maine lakes: Are they really changing? *Limnology and oceanography*, 35(6), 1238-1257.

Stefanescu, I. C., Shuman, B. N., and Tierney, J. E. (2021). Temperature and water depth effects on brGDGT distributions in sub-alpine lakes of mid-latitude North America. *Organic Geochemistry*, 152, 104174.

Sturt, H. F., Summons, R. E., Smith, K., Elvert, M., and Hinrichs, K. U. (2004). Intact polar membrane lipids in prokaryotes and sediments deciphered by high-performance liquid chromatography/electrospray ionization multistage mass spectrometry—new biomarkers for biogeochemistry and microbial ecology. *Rapid communications in mass spectrometry*, 18(6), 617-628.

Su, Y., Lammers, M., Zhang, Y., van Bree, L., Liu, Z., Reichart, G. J., and Middelburg, J. J. (2017). Sources of organic matter for bacteria in sediments of Lake Rotsee, Switzerland. *Journal of Paleolimnology*, 58, 391-402.

Tierney, J. E., and Russell, J. M. (2009). Distributions of branched GDGTs in a tropical lake system: implications for lacustrine application of the MBT/CBT paleoproxy. *Organic Geochemistry*, 40(9), 1032-1036.

Tierney, J. E., Poulsen, C. J., Montañez, I. P., Bhattacharya, T., Feng, R., Ford, H. L., Hönisch, B., Inglis, G. N., Petersen, S. V., Sagoo, N., Tabor, C. R., Thirumalai, K., Zhu, J., Burls, N. J., Foster, G. L., Godderis, Y., Huber, B. T., Ivany, L. C., Turner, S. K., Lunt, D. J., McElwain, J. C., Mills, B. J. W., Otto-Bliesner, B. L., Ridgeway, A., Zhang, Y. G. (2020). Past climates inform our future. *Science*, 370(6517), eaay3701.

- Tierney, J. E., Russell, J. M., Eggermont, H., Hopmans, E. C., Verschuren, D., and Sinninghe Damsté, J. S. (2010). Environmental controls on branched tetraether lipid distributions in tropical East African lake sediments. *Geochimica et Cosmochimica Acta*, 74(17), 4902-4918.
- Van Bree, L. G., Peterse, F., Baxter, A. J., De Crop, W., Van Grinsven, S., Villanueva, L., Verschuren, D., Sinninghe Damsté, J. S. (2020). Seasonal variability and sources of in situ brGDGT production in a permanently stratified African crater lake. *Biogeosciences*, 17(21), 5443-5463.
- Wang, H., Liu, W., He, Y., Zhou, A., Zhao, H., Liu, H., Cao, Y., Hu, J., Meng, B., Jiang, J., Kolpakova, M., Krivonogov, S., Liu, Z. (2021). Salinity-controlled isomerization of lacustrine brGDGTs impacts the associated MBT5ME'terrestrial temperature index. *Geochimica et Cosmochimica Acta*, 305, 33-48.
- Weber, Y., Sinninghe Damsté, J. S., Hopmans, E. C., Lehmann, M. F., and Niemann, H. (2017). Incomplete recovery of intact polar glycerol dialkyl glycerol tetraethers from lacustrine suspended biomass. *Limnology and Oceanography: Methods*, 15(9), 782-793.
- Weber, Y., Sinninghe Damsté, J. S., Zopfi, J., De Jonge, C., Gilli, A., Schubert, C. J., Lepori, L., Lehmann, M. F., Niemann, H. (2018). Redox-dependent niche differentiation provides evidence for multiple bacterial sources of glycerol tetraether lipids in lakes. *Proceedings of the National Academy of Sciences*, 115(43), 10926-10931.
- Weijers, J. W., Schouten, S., Hopmans, E. C., Geenevasen, J. A., David, O. R., Coleman, J. M., ... and Sinninghe Damsté, J. S. (2006). Membrane lipids of mesophilic anaerobic bacteria thriving in peats have typical archaeal traits. *Environmental Microbiology*, 8(4), 648-657.
- Weijers, J. W., Schouten, S., van den Donker, J. C., Hopmans, E. C., and Sinninghe Damsté, J. S. (2007a). Environmental controls on bacterial tetraether membrane lipid distribution in soils. *Geochimica et Cosmochimica Acta*, 71(3), 703-713.
- Weijers, J. W., Schefuß, E., Schouten, S., and Sinninghe Damsté, J. S. (2007b). Coupled thermal and hydrological evolution of tropical Africa over the last deglaciation. *Science*, 315(5819), 1701-1704.
- Woltering, M., Werne, J. P., Kish, J. L., Hicks, R., Sinninghe Damsté, J. S., and Schouten, S. (2012). Vertical and temporal variability in concentration and distribution of thaumarchaeotal tetraether lipids in Lake Superior and the implications for the application of the TEX86 temperature proxy. *Geochimica et Cosmochimica Acta*, 87, 136-153.

Yang, H., Lü, X., Ding, W., Lei, Y., Dang, X., and Xie, S. (2015). The 6-methyl branched tetraethers significantly affect the performance of the methylation index (MBT') in soils from an altitudinal transect at Mount Shennongjia. *Organic Geochemistry*, 82, 42-53.

Yao, Y., Zhao, J., Vachula, R. S., Werne, J. P., Wu, J., Song, X., and Huang, Y. (2020). Correlation between the ratio of 5-methyl hexamethylated to pentamethylated branched GDGTs (HP5) and water depth reflects redox variations in stratified lakes. *Organic Geochemistry*, 147, 104076.

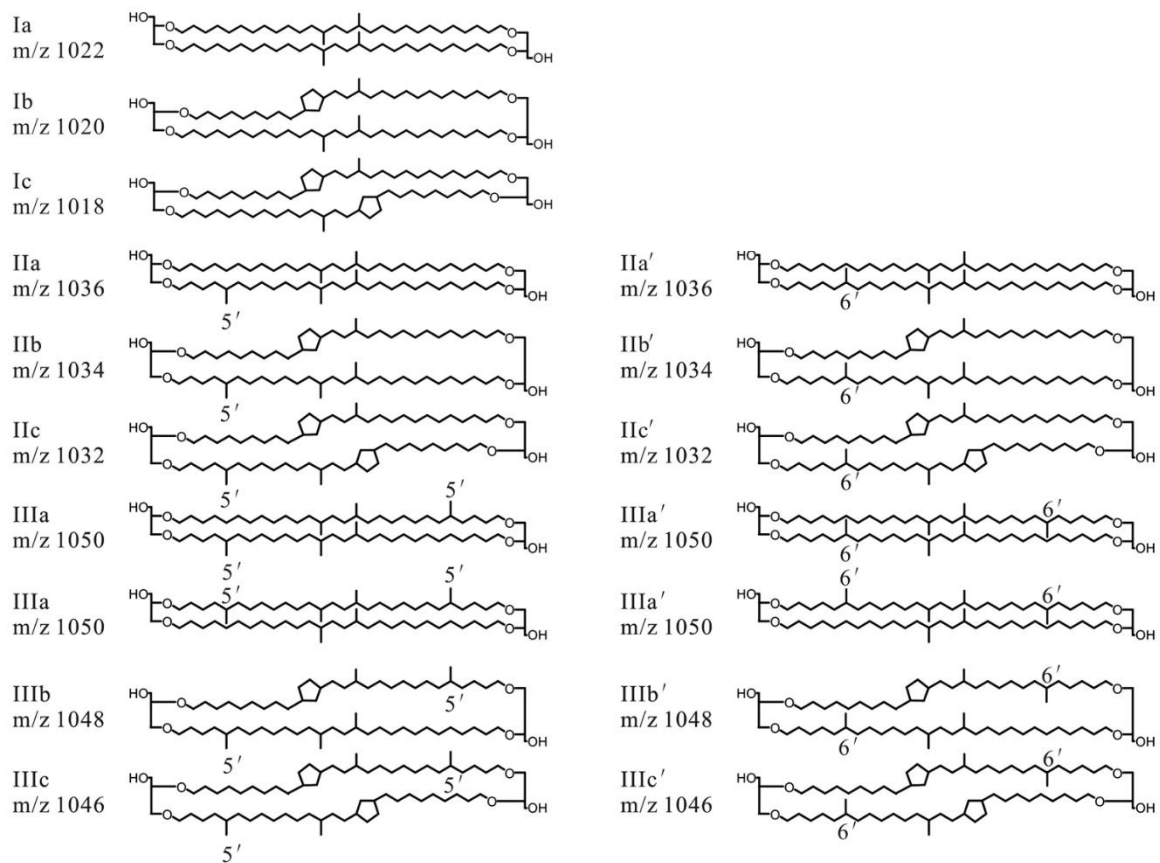
Zang, J., Lei, Y., and Yang, H. (2018). Distribution of glycerol ethers in Turpan soils: implications for use of GDGT-based proxies in hot and dry regions. *Frontiers of Earth Science*, 12, 862-876.

Zeng, Z., Chen, H., Yang, H., Chen, Y., Yang, W., Feng, X., Pei, H., and Welander, P. V. (2022). Identification of a protein responsible for the synthesis of archaeal membrane-spanning GDGT lipids. *Nature communications*, 13(1), 1545.

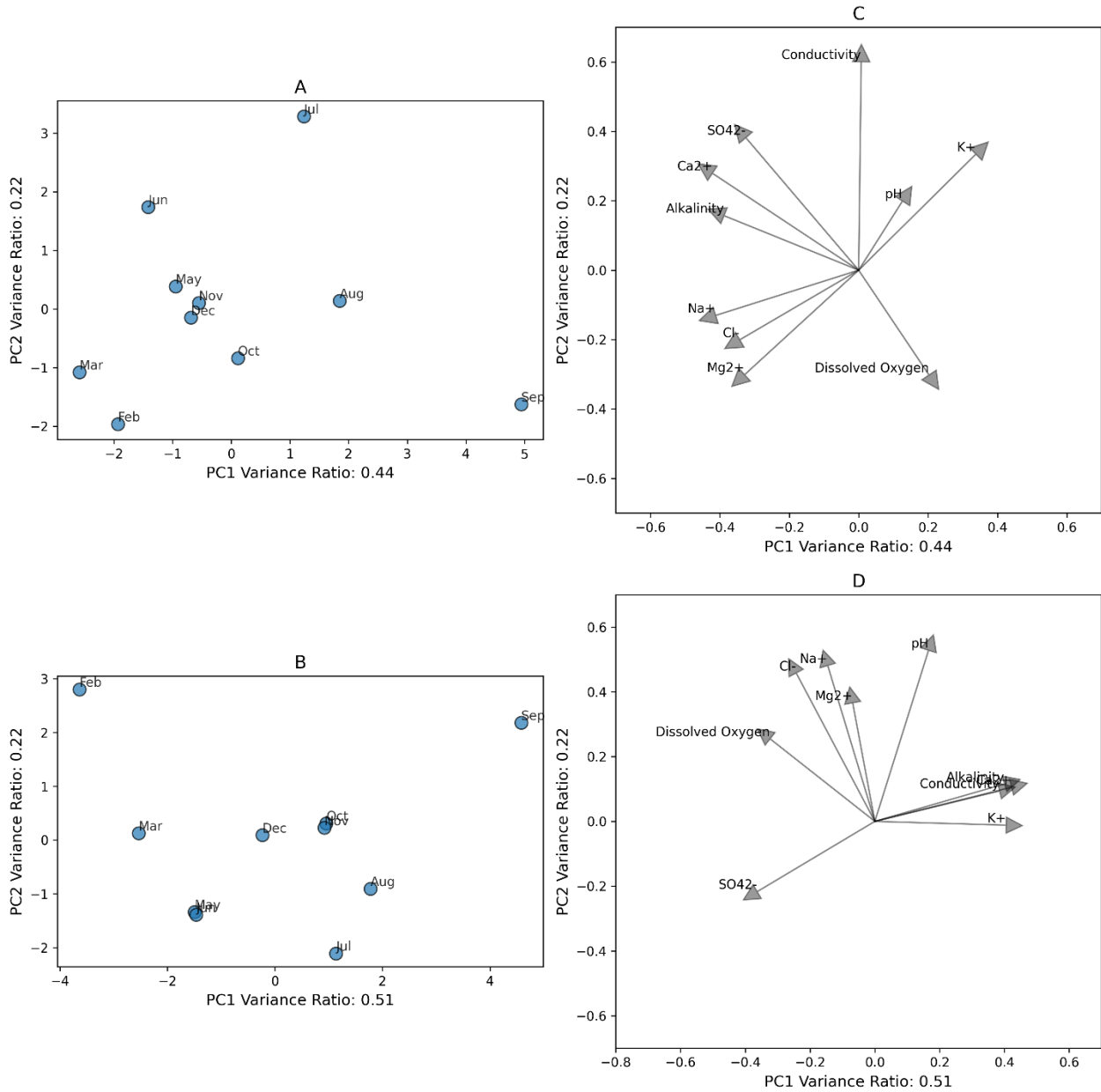
Zhang, Z., Smittenberg, R. H., and Bradley, R. S. (2016). GDGT distribution in a stratified lake and implications for the application of TEX86 in paleoenvironmental reconstructions. *Scientific reports*, 6(1), 34465.

Zhao, B., Castañeda, I. S., Bradley, R. S., Salacup, J. M., de Wet, G. A., Daniels, W. C., and Schneider, T. (2021). Development of an in situ branched GDGT calibration in Lake 578, southern Greenland. *Organic Geochemistry*, 152, 104168.

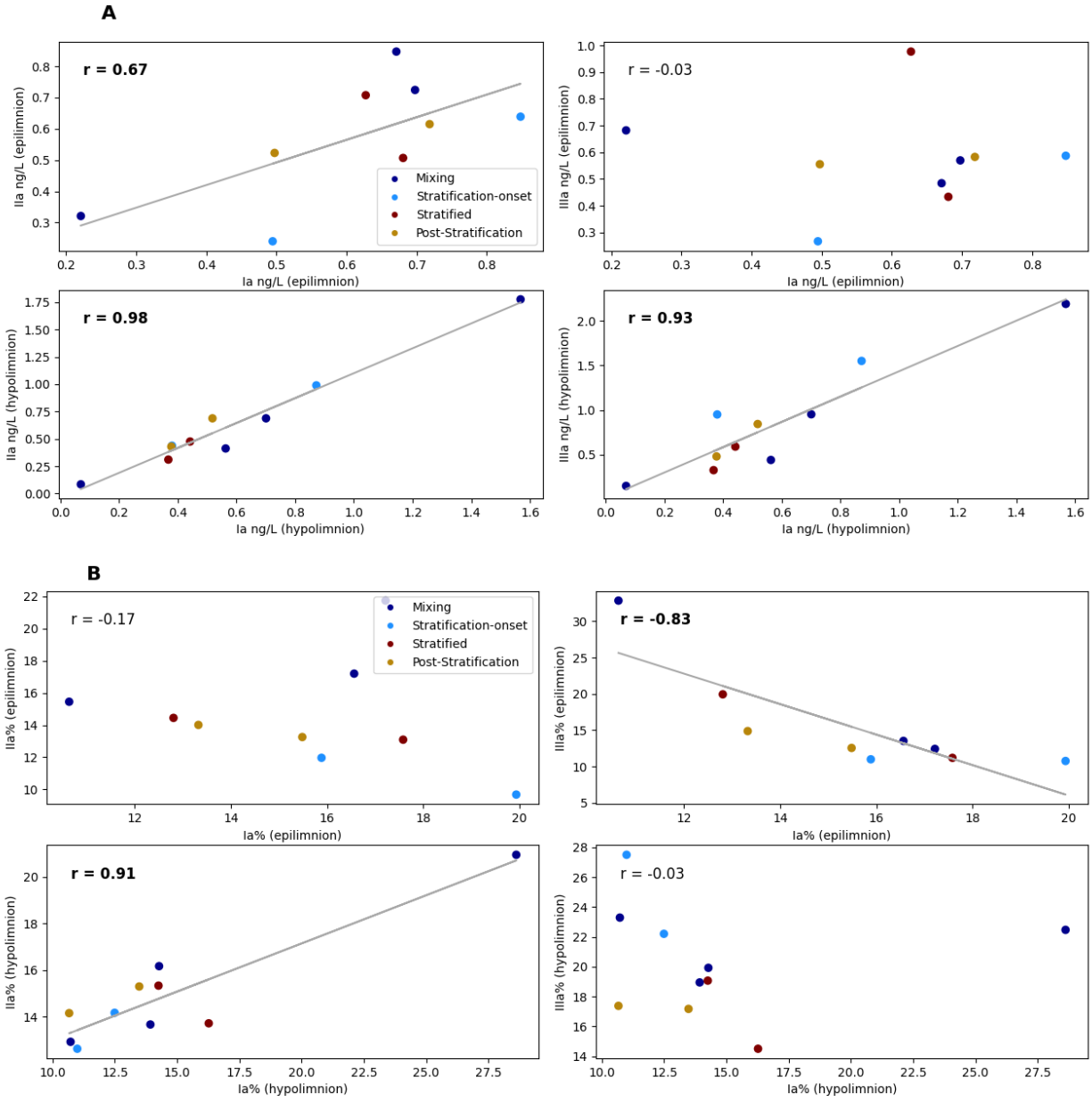
Supplementary Materials, Chapter 3



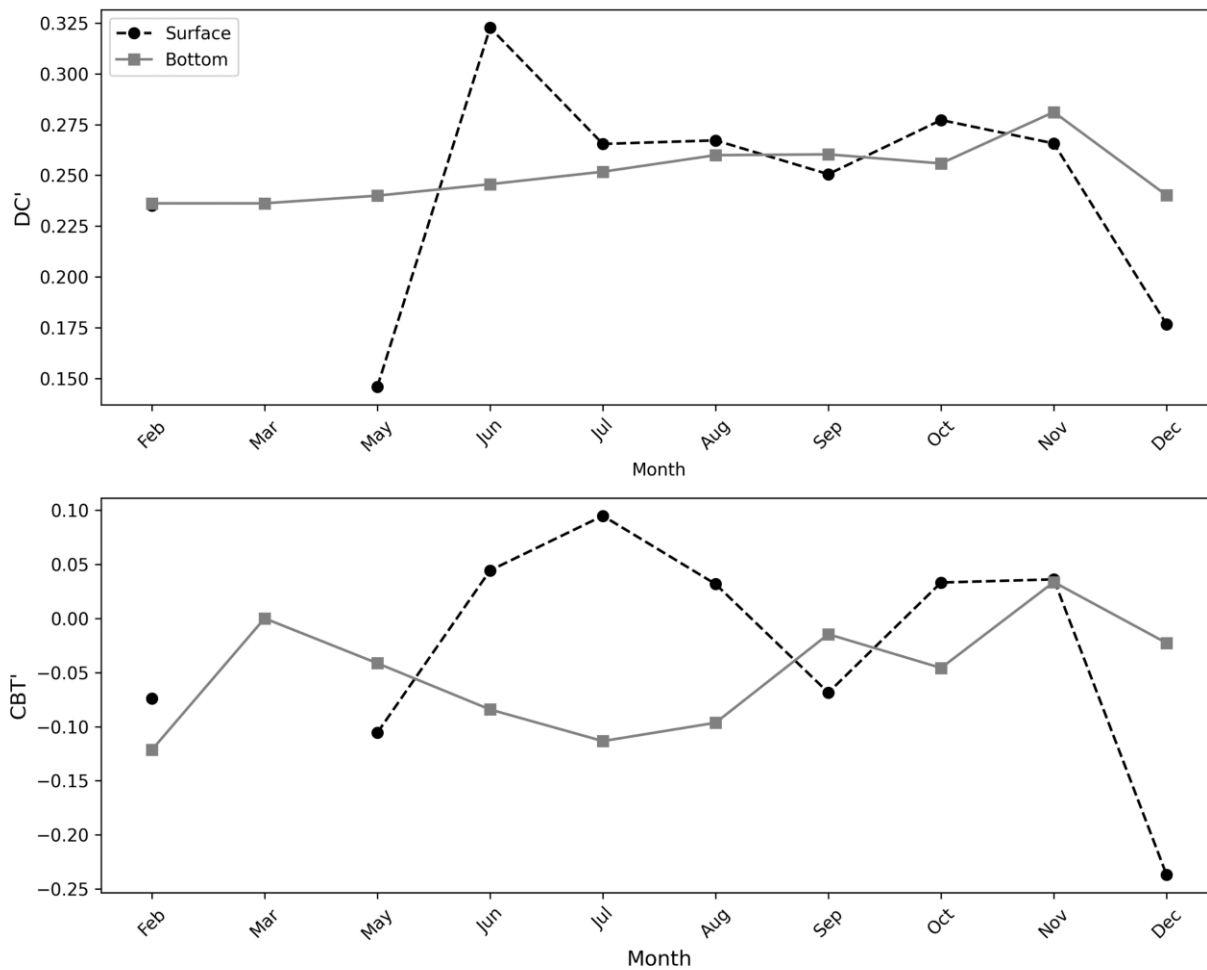
Supp. Fig. S1: The structural diversity of brGDGTs (De Jonge et al., 2014).



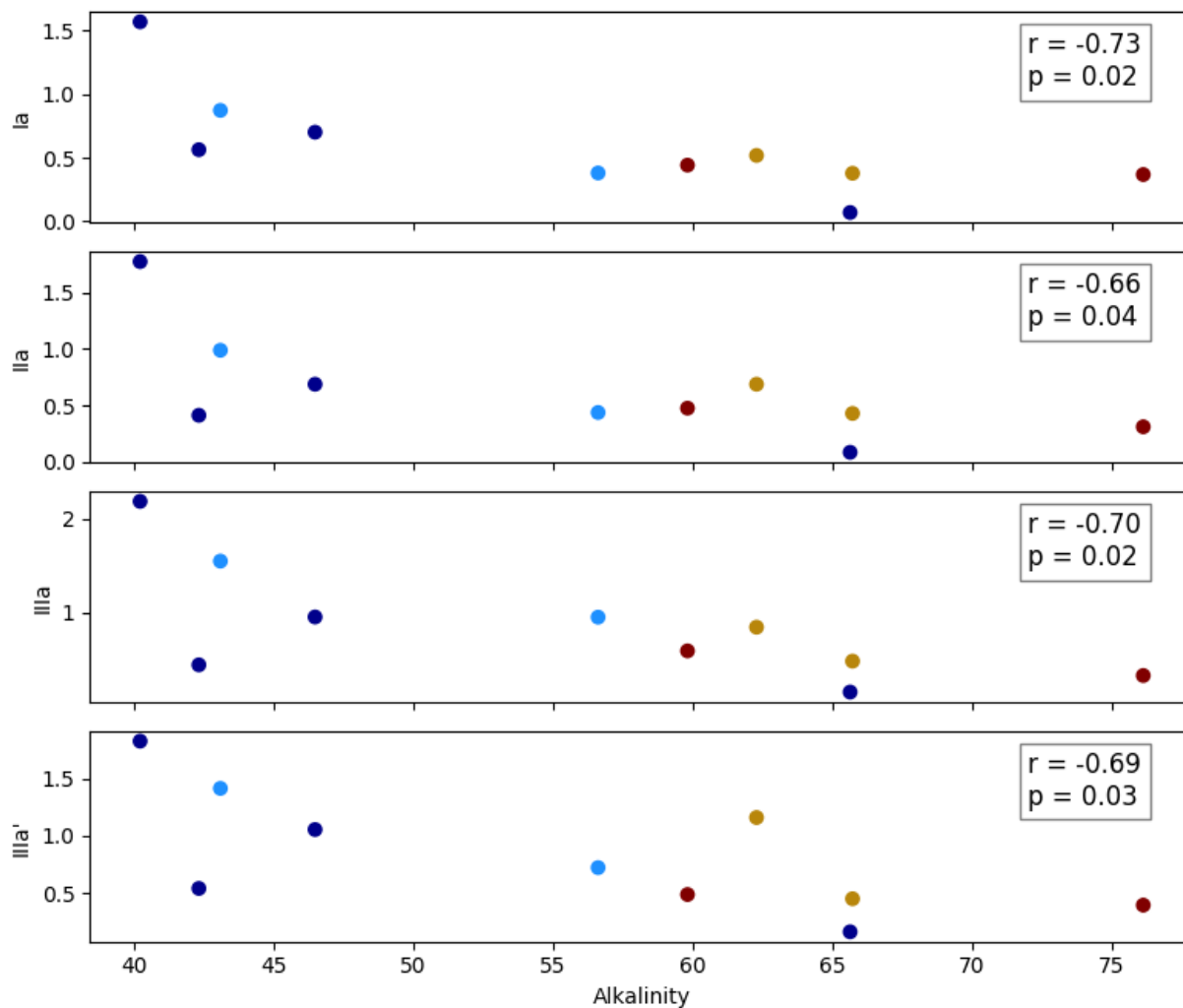
Supp. Fig. S2: unconstrained principal component analysis (PCA) based on the standardized values of the inorganic parameters of Lake Rot in (A-C) epi- and (B-D) hypolimnion, with site scores of individual months (A, B) and species scores (C and D) plotted.



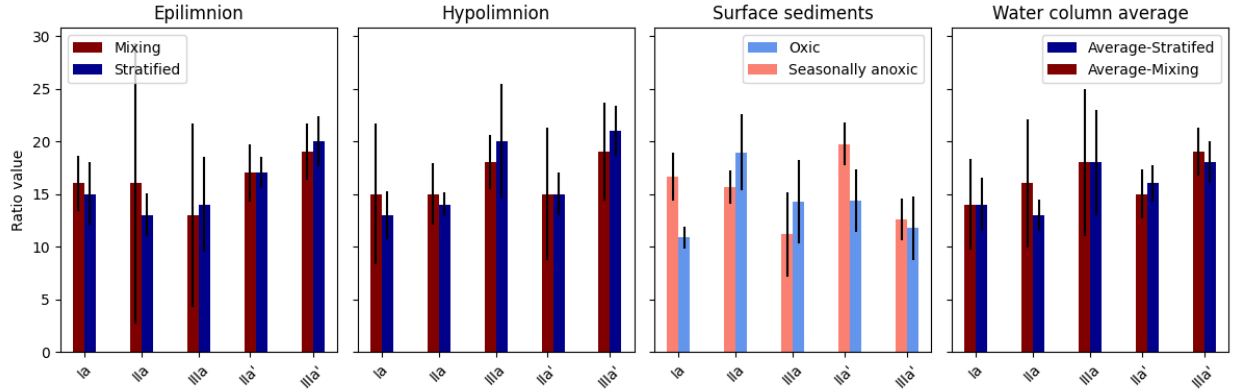
Supp. Fig. S3 A) A scatterplot (so-called diagnostic plot; De Jonge et al., 2021) of concentration of brGDGTs Ia, IIa and IIIa in Lake Rot suspended particulate matter (SPM) and B) the fractional abundance of brGDGTs Ia, IIa and IIIa in Lake Rot SPM.



Supp. Fig. S4. BrGDGT-based ratios DC' and CBT' plotted for Lake Rot epilimnion and hypolimnion SPM (top and bottom panel, respectively).



Supp. Fig. S5: Concentration (ng L⁻¹) of individual brGDGTs in the hypolimnion plotted against measured alkalinity values.



Supp. Fig. S6: The fractional abundances of brGDGTs Ia, IIa and IIIa in the (A) epilimnion and (B) hypolimnion suspended particulate matter (SPM) during stratified (June-September) and isothermally mixing months (February-March, October-December). Panel C shows the GDGT distribution in the sediments that underlie oxic and seasonally anoxic water column. In panel D, the SPM average represents the average of stratified and isothermally mixing months of the whole water column. The error bars in panel A, B and D represent the standard deviation.

SPM	IIa-CL	IIIa-CL	IIb-CL	IIIb-CL	IIIc-CL	IIc-CL	IIId-CL	IIIe-CL	IIIf-CL	IIIg-CL	IIh-CL	IIi-CL	IIj-CL	IIk-CL	IIl-CL	IIm-CL	IIo-CL	IIp-CL	IIq-CL	IIr-CL	IIs-CL	IIt-CL	IIu-CL	IIv-CL	IIw-CL	IIx-CL	IIy-CL	IIz-CL	Σ CL brGDGT concentration (ng/l)			
Feb-S	13.53	17.21	0.62	0.77	0.27	0.41	17.20	15.93	17.20	15.93	5.96	3.83	0.49	0.57	16.56	5.48	1.16	4.21														
May-S	12.43	17.22	0.27	0.00	0.00	0.00	21.74	19.66	21.74	19.66	2.31	2.48	0.51	0.22	17.22	5.23	0.72	3.90														
Jun-S	10.77	21.52	1.06	0.95	b.d.l.	b.d.l.	9.68	14.31	9.68	14.31	5.58	7.09	b.d.l.	b.d.l.	19.94	8.26	0.84	2.48														
Jul-S	11.00	21.98	1.12	1.01	0.82	b.d.l.	11.97	17.69	11.97	17.69	4.68	5.94	0.38	0.43	15.89	5.83	1.26	5.34														
Aug-S	11.20	20.40	0.62	1.08	0.38	0.23	13.09	17.19	13.09	17.19	4.81	5.81	0.44	0.34	17.58	6.84	b.d.l.	3.87														
Sep-S	19.94	18.15	0.76	0.63	0.28	0.15	14.45	16.40	14.45	16.40	6.16	3.70	0.58	0.17	12.81	4.73	1.09	4.90														
Oct-S	12.56	20.24	0.80	0.82	0.46	b.d.l.	13.26	17.71	13.26	17.71	6.07	5.45	0.50	0.35	15.49	6.29	b.d.l.	4.64														
Nov-S	14.88	23.60	0.75	0.90	b.d.l.	b.d.l.	14.01	15.06	14.01	15.06	5.39	4.68	0.50	0.33	13.32	5.27	1.28	3.73														
Dec-S	32.84	18.04	0.48	0.47	b.d.l.	b.d.l.	15.45	12.44	15.45	12.44	3.15	2.24	0.40	b.d.l.	10.64	2.89	0.97	2.08														
Feb-B	19.93	16.61	0.71	0.74	0.27	0.31	16.18	15.14	16.18	15.14	5.17	4.10	0.53	0.18	14.28	4.84	1.02	10.98														
Mar-B	22.47	27.56	0.00	0.00	b.d.l.	b.d.l.	20.96	0.39	0.00	0.00	0.00	0.00	0.00	28.62	0.00	b.d.l.	1.97															
May-B	18.95	20.96	0.92	0.65	0.18	0.26	13.67	15.14	13.67	15.14	5.09	3.98	0.52	0.19	13.93	4.42	1.14	5.03														
Jun-B	22.21	20.23	0.85	0.82	0.24	0.12	14.17	14.00	14.17	14.00	5.03	3.90	0.43	0.23	12.49	4.32	0.96	6.98														
Jul-B	27.50	20.90	0.60	0.51	b.d.l.	b.d.l.	12.63	13.00	12.63	13.00	4.58	3.94	0.51	b.d.l.	10.99	3.81	1.04	3.46														
Aug-B	19.07	15.77	0.88	0.75	b.d.l.	b.d.l.	15.34	15.78	15.34	15.78	6.06	4.99	0.53	0.52	14.25	4.89	1.17	3.10														
Sep-B	14.51	17.54	0.54	0.69	b.d.l.	b.d.l.	13.72	17.70	13.72	17.70	5.76	5.36	0.50	0.21	16.27	5.66	1.53	2.26														
Oct-B	17.18	16.13	0.99	0.87	0.32	0.22	15.31	17.32	15.31	17.32	5.95	4.96	0.47	0.62	13.48	4.94	1.24	2.80														
Nov-B	17.38	23.86	0.76	0.91	b.d.l.	b.d.l.	14.16	15.23	14.16	15.23	5.45	4.73	0.51	0.33	10.66	5.48	0.53	4.86														
Dec-B	23.29	25.23	b.d.l.	b.d.l.	b.d.l.	b.d.l.	12.93	15.46	12.93	15.46	4.68	3.86	b.d.l.	b.d.l.	10.72	3.83	b.d.l.	0.65														
Sediment	IIa-CL+IPL	IIIa-CL+IPL	IIb-CL+IPL	IIIb-CL+IPL	IIIc-CL+IPL	IIc-CL+IPL	IIId-CL+IPL	IIIe-CL+IPL	IIIf-CL+IPL	IIIg-CL+IPL	IIh-CL+IPL	IIi-CL+IPL	IIj-CL+IPL	IIk-CL+IPL	IIl-CL+IPL	IIm-CL+IPL	IIo-CL+IPL	IIp-CL+IPL	IIq-CL+IPL	IIr-CL+IPL	IIs-CL+IPL	IIt-CL+IPL	IIu-CL+IPL	IIv-CL+IPL	IIw-CL+IPL	IIx-CL+IPL	IIy-CL+IPL	IIz-CL+IPL	Σ CL brGDGT concentration (ng/l)			
SS-Oxic	14.26	11.75	1.58	1.06	0.21	0.07	18.95	14.37	18.95	14.37	13.93	4.85	1.47	0.38	10.85	3.91	2.36	8491.65														
SS-Seasonally-Anoxic	11.15	12.60	0.64	1.02	0.13	0.15	15.66	19.74	15.66	19.74	6.06	6.56	0.61	0.46	16.62	6.92	1.68	1254.89														

Supp. Table S1: Fractional abundances, summed brGDGT concentrations (CL, IPL) and brGDGT ratios for Lake Rot water column and surface sediment samples.

SPM	IR	MBT'5ME	CBT'	DC'	Depth	Water column regime
Feb-S	0.52	0.38	-0.07	0.24	Epilimnion	Mixing
May-S	0.52	0.39	-0.11	0.15	Epilimnion	Mixing
Jun-S	0.64	0.53	0.04	0.32	Epilimnion	Stratification-onset
Jul-S	0.63	0.45	0.09	0.27	Epilimnion	Stratification-onset
Aug-S	0.61	0.45	0.03	0.27	Epilimnion	Stratified
Sep-S	0.50	0.31	-0.07	0.25	Epilimnion	Stratified
Oct-S	0.60	0.40	0.03	0.28	Epilimnion	Post-Stratification
Nov-S	0.57	0.36	0.04	0.27	Epilimnion	Post-Stratification
Dec-S	0.39	0.22	-0.24	0.18	Epilimnion	Mixing
Feb-B	0.47	0.32	-0.12	0.24	Hypolimnion	Mixing
Mar-B	0.52	0.43	-0.11	0.24	Hypolimnion	Mixing
May-B	0.53	0.34	-0.04	0.24	Hypolimnion	Mixing
Jun-B	0.48	0.30	-0.08	0.25	Hypolimnion	Stratification-onset
Jul-B	0.46	0.26	-0.11	0.25	Hypolimnion	Stratification-onset
Aug-B	0.48	0.33	-0.10	0.26	Hypolimnion	Stratified
Sep-B	0.56	0.40	-0.01	0.26	Hypolimnion	Stratified
Oct-B	0.51	0.34	-0.05	0.26	Hypolimnion	Post-Stratification
Nov-B	0.55	0.31	0.03	0.28	Hypolimnion	Post-Stratification
Dec-B	0.53	0.26	-0.02	0.24	Hypolimnion	Mixing
Sediment	IR	MBT'5ME	CBT'	DC'		
SS-Oxic	0.44	0.26	-0.10	0.34		
SS-Seasonally-Anoxic	0.55	0.43	-0.01	0.27		

Supp. Table S1: Fractional abundances, summed brGDGT concentrations (CL, IPL) and brGDGT ratios for Lake Rot water column and surface sediment samples.

SPM	<i>IIIa</i> -'IPL	<i>IIIb</i> -'IPL	<i>IIIc</i> -'IPL	<i>IIId</i> -'IPL	<i>IIIE</i> -'IPL	<i>IIIf</i> -'IPL	<i>IIIg</i> -'IPL	<i>IIiH</i> -'IPL	<i>IIiI</i> -'IPL	<i>IIiJ</i> -'IPL	<i>IIiK</i> -'IPL	<i>IIiL</i> -'IPL	<i>IIiM</i> -'IPL	<i>IIiN</i> -'IPL	<i>IIiO</i> -'IPL	<i>IIiP</i> -'IPL	<i>IIiQ</i> -'IPL	<i>IIiR</i> -'IPL	<i>IIiS</i> -'IPL	<i>IIiT</i> -'IPL	<i>IIiU</i> -'IPL	<i>IIiV</i> -'IPL	<i>IIiW</i> -'IPL	<i>IIiX</i> -'IPL	<i>IIiY</i> -'IPL	<i>IIiZ</i> -'IPL	Depth	Water column regime
Feb-S	99.33	b. d. l.	b. d. l.	b. d. l.	b. d. l.	b. d. l.	b. d. l.	b. d. l.	b. d. l.	b. d. l.	b. d. l.	b. d. l.	b. d. l.	b. d. l.	b. d. l.	b. d. l.	b. d. l.	b. d. l.	b. d. l.	b. d. l.	b. d. l.	b. d. l.	b. d. l.	b. d. l.	b. d. l.	b. d. l.	Epilimnion	Mixing
May-S	b. d. l.	28.57	4.72	15.54	b. d. l.	b. d. l.	b. d. l.	b. d. l.	b. d. l.	b. d. l.	b. d. l.	b. d. l.	b. d. l.	b. d. l.	b. d. l.	b. d. l.	b. d. l.	b. d. l.	b. d. l.	b. d. l.	b. d. l.	b. d. l.	b. d. l.	b. d. l.	b. d. l.	b. d. l.	Epilimnion	Mixing
Jun-S	41.89	5.26	b. d. l.	1.17	b. d. l.	b. d. l.	b. d. l.	25.24	17.63	3.40	b. d. l.	b. d. l.	b. d. l.	b. d. l.	b. d. l.	b. d. l.	b. d. l.	b. d. l.	b. d. l.	b. d. l.	b. d. l.	b. d. l.	b. d. l.	b. d. l.	b. d. l.	b. d. l.	Epilimnion	Stratification-onset
Jul-S	b. d. l.	b. d. l.	b. d. l.	b. d. l.	b. d. l.	b. d. l.	b. d. l.	b. d. l.	b. d. l.	b. d. l.	b. d. l.	b. d. l.	b. d. l.	b. d. l.	b. d. l.	b. d. l.	b. d. l.	b. d. l.	b. d. l.	b. d. l.	b. d. l.	b. d. l.	b. d. l.	b. d. l.	b. d. l.	b. d. l.	Epilimnion	Stratification-onset
Aug-S	12.31	20.26	0.61	b. d. l.	1.69	4.64	9.36	20.43	2.94	8.50	b. d. l.	b. d. l.	b. d. l.	b. d. l.	b. d. l.	b. d. l.	b. d. l.	b. d. l.	b. d. l.	b. d. l.	b. d. l.	b. d. l.	b. d. l.	b. d. l.	b. d. l.	b. d. l.	Epilimnion	Stratified
Sep-S	b. d. l.	b. d. l.	8.17	b. d. l.	20.59	1.60	69.63	b. d. l.	b. d. l.	b. d. l.	b. d. l.	b. d. l.	b. d. l.	b. d. l.	b. d. l.	b. d. l.	b. d. l.	b. d. l.	b. d. l.	b. d. l.	b. d. l.	b. d. l.	b. d. l.	b. d. l.	b. d. l.	b. d. l.	Epilimnion	Stratified
Oct-S	24.98	34.48	0.03	b. d. l.	b. d. l.	b. d. l.	10.84	11.00	3.69	2.82	b. d. l.	b. d. l.	b. d. l.	b. d. l.	b. d. l.	b. d. l.	b. d. l.	b. d. l.	b. d. l.	b. d. l.	b. d. l.	b. d. l.	b. d. l.	b. d. l.	b. d. l.	b. d. l.	Epilimnion	Post-Stratification
Nov-S	17.32	22.16	0.72	0.77	b. d. l.	b. d. l.	10.84	14.87	5.70	5.13	0.40	0.30	0.40	0.30	15.22	5.53	1.05	2.42									Epilimnion	Post-Stratification
Dec-S	32.84	18.04	0.48	0.47	b. d. l.	b. d. l.	15.45	12.44	3.15	2.24	0.40	0.40	b. d. l.	b. d. l.	10.64	2.89	0.97	b. d. l.									Epilimnion	Mixing
Feb-B	40.83	44.78	b. d. l.	b. d. l.	b. d. l.	b. d. l.	b. d. l.	9.20	b. d. l.	b. d. l.	b. d. l.	b. d. l.	b. d. l.	b. d. l.	4.06	b. d. l.	1.13	0.61									Hypolimnion	Mixing
Mar-B	72.42	b. d. l.	b. d. l.	b. d. l.	b. d. l.	b. d. l.	b. d. l.	1.39	b. d. l.	b. d. l.	b. d. l.	b. d. l.	b. d. l.	b. d. l.	b. d. l.	b. d. l.	26.18	0.13									Hypolimnion	Mixing
May-B	b. d. l.	b. d. l.	b. d. l.	b. d. l.	b. d. l.	b. d. l.	b. d. l.	b. d. l.	b. d. l.	b. d. l.	b. d. l.	b. d. l.	b. d. l.	b. d. l.	b. d. l.	b. d. l.	0.00	0.03									Hypolimnion	Mixing
Jun-B	b. d. l.	b. d. l.	b. d. l.	b. d. l.	b. d. l.	b. d. l.	b. d. l.	b. d. l.	b. d. l.	b. d. l.	b. d. l.	b. d. l.	b. d. l.	b. d. l.	b. d. l.	b. d. l.	b. d. l.	b. d. l.	b. d. l.	b. d. l.	b. d. l.	b. d. l.	b. d. l.	b. d. l.	b. d. l.	b. d. l.	Hypolimnion	Stratification-onset
Jul-B	b. d. l.	b. d. l.	b. d. l.	b. d. l.	79.22	b. d. l.	b. d. l.	b. d. l.	b. d. l.	b. d. l.	b. d. l.	b. d. l.	20.78	b. d. l.	b. d. l.	b. d. l.	b. d. l.	0.05									Hypolimnion	Stratification-onset
Aug-B	22.37	22.12	0.32	0.67	b. d. l.	b. d. l.	13.40	14.59	4.30	3.04	0.39	2.22	12.14	3.65	0.80	3.62											Hypolimnion	Stratified
Sep-B	31.12	27.85	0.97	0.55	5.62	b. d. l.	13.32	9.45	3.70	2.24	0.36	0.22	3.80	0.80	b. d. l.	1.28											Hypolimnion	Stratified
Oct-B	b. d. l.	b. d. l.	b. d. l.	b. d. l.	63.91	b. d. l.	b. d. l.	b. d. l.	b. d. l.	b. d. l.	b. d. l.	b. d. l.	36.09	b. d. l.	b. d. l.	b. d. l.	0.06										Hypolimnion	Post-Stratification
Nov-B	b. d. l.	b. d. l.	b. d. l.	b. d. l.	b. d. l.	b. d. l.	b. d. l.	b. d. l.	b. d. l.	b. d. l.	b. d. l.	b. d. l.	b. d. l.	b. d. l.	b. d. l.	b. d. l.	b. d. l.	b. d. l.	b. d. l.	b. d. l.	b. d. l.	b. d. l.	b. d. l.	b. d. l.	b. d. l.	b. d. l.	Hypolimnion	Post-Stratification
Dec-B	23.29	25.23	b. d. l.	b. d. l.	b. d. l.	b. d. l.	12.93	15.46	4.68	3.86	b. d. l.	b. d. l.	b. d. l.	b. d. l.	10.72	3.83	b. d. l.	0.03									Hypolimnion	Mixing

Supp. Table S1: Fractional abundances, summed brGDGT concentrations (CL, IPL) and brGDGT ratios for Lake Rot water column and surface sediment samples.

<i>Epilimnion</i>	<i>Illa (FA)</i>	<i>IIla' (FA)</i>	<i>IIa (FA)</i>	<i>IIa' (FA)</i>	<i>IIb (FA)</i>	<i>IIb' (FA)</i>	<i>Ia (FA)</i>	<i>Ib (FA)</i>	<i>Ic (FA)</i>	<i>MBT'5ME</i>	<i>IR</i>	<i>CBT'</i>	<i>DC'</i>
Temperature			0.61				0.68	0.57		0.59	0.68	0.66	
Dissolved Oxygen							0.66	0.59	0.63	0.72	0.65		
Conductivity													
pH													
Alkalinity													
<i>Hypolimnion</i>	<i>Illa (FA)</i>	<i>IIla' (FA)</i>	<i>IIa (FA)</i>	<i>IIa' (FA)</i>	<i>IIb (FA)</i>	<i>IIb' (FA)</i>	<i>Ia (FA)</i>	<i>Ib (FA)</i>	<i>Ic (FA)</i>	<i>MBT'5ME</i>	<i>IR</i>	<i>CBT'</i>	<i>DC'</i>
Temperature													
Dissolved Oxygen			0.72	-0.72	-0.77	-0.80	0.65	-0.73	-0.64		-0.65	-0.75	-0.78
Conductivity		-0.65				0.63							
pH		-0.75								0.79			
Alkalinity						0.60					0.66		

Supp. Table S2: Correlation matrix between fractional abundances of selected brGDGT in Lake Rot epi- and hypolimnion and temperature, dissolved oxygen and water chemistry parameters. Only significant r-values with p-values < 0.05 are reported

<i>Bacteria groups (Zang et al., 2022)</i>			<i>This study</i>		
Phylum	Class/order	Tes Homologue in genome	Detected in water column	Detected as a bio-indicator	Order(s) detected
Proteobacteria	Acidithiobacilia				
	Alphaproteobacteria	x	x	x	x
	Betaproteobacteria	x			
	Deltaproteobacteria	x			
	Epsilonproteobacteria	x			
	Gammaproteobacteria	x	x	x	x
	Hydrogenophilalia				
Acidobacteria	Zetaproteobacteria				
	Acidobacteriales	x	x		
	Bryobacterales	x	x		
	Blastocatellales	x	x		
	Acanthopleuribacterales	x			
	Holophagales	x	x	x	x
	Thermotomaculales				
Thermoanaeobaculales		x			
Actinobacteria		x	x	x	x
Armanimonatedes		x	x		
Chloroflexi		x	x	x	x
Cyanobacteria		x	x		
Firmicutes		x	x	x	x
Bacteroidetes		x	x		
Chlamydiae		x	x		x
Planctomycetes		x	x	x	x
Verrucomicrobia		x	x		
Gracilibacteria		x	x	x	x
Parcubacteria		x	x	x	x
Saccharibacteria			x		
Omnitrophica		x	x		
Gemmatimonadetes		x			
Chlorobi		x	x		
Fibrobacteres		x	x		

<i>Bacteria groups (Sahonero-Canavesi et al., 2022)</i>		<i>This study</i>		
Phylum	Ger Homologue in genome	Detected in water column	Detected as a bio-indicator	Order(s) detected
Acidobacteria	x	x	x	x
Actinobacteria	x	x	x	x
Armanimonatedes	x	x		
Chloroflexi	x	x	x	x
Firmicutes	x	x	x	x
Elusimicrobia	x	x		
Fusobacteria	x	x	x	x
Nitrospirae	x	x		
Synergistetes	x			
Thermodesulfobacteria	x			
Thermotogae	x	x		

Supp. Table S3a: Summary of bio-indicator taxa found in water column of Lake Rot with those bacterial taxa reported previously in Zeng et al., (2022) and Sahonero-Canavesi et al., (2022) to possess the ether-bond synthesizing enzymes. For the complete phylogenetic information of identified bio-indicators refer to Supp. Table. S3B.

	IMBT ⁵ SME - Epilimnion		IR - Epilimnion		MBT ⁵ SME - Hypolimnion		IR - Hypolimnion	
	Var. explained	P-value	Var. explained	P-value	Var. explained	P-value	Var. explained	P-value
Temperature	71%	> 0.05	46%	0.04	54%	0.01	67%	> 0.05
Dissolved Oxygen	59%	> 0.05	68%	> 0.05	78%	> 0.05	54%	0.04
Conductivity	51%	0.02	53%	0.04	75%	> 0.05	70%	> 0.05
pH	72%	> 0.05	66%	> 0.05	76%	> 0.05	79%	> 0.05
Alkalinity	61%	> 0.05	64%	> 0.05	67%	> 0.05	43%	0.03

Supp. Table. S4: Results from the stepwise forward selection regression model for Lake Rot SPM epi- and hypolimnion. The variability in the brGDGT ratios MBT⁵SME and IR were tested against each reported environmental parameters. Variance explained is reported with significant results indicated in bold.

Chapter 4

Provenance and Drivers of brGDGTs in Lake Rot Sediments (manuscript in preparation)

F. Ajallooeian ^{a*}, T. I. Eglinton ^a, N. Dubois ^b, N. Haghypour ^a, S.N. Ladd ^c, M. A. Lever ^{d, e}, C. J. Schubert ^{a, f}, C. De Jonge ^a

*Corresponding author: F. Ajallooeian– Fatemeh.ajallooeian@erdw.ethz.ch

a Geological Institute, Earth Science Department, ETH Zurich. Sonneggstrasse 5, 8092 Zurich, Switzerland

b Swiss Federal Institute of Aquatic Science and Technology, Eawag, Uberlandstrasse 133, 8600 Dubendorf, Switzerland

c Department of Environmental Science, University of Basel, Bernoullistrasse 30, 4056 Basel, Switzerland

d Institute of Biogeochemistry and Pollutant Dynamics, ETH Zurich, Universtatstrasse 16, 8092 Zürich, Switzerland

e Marine Science Institute, University of Texas at Austin, TX, 78373 Port Aransas, USA

f Swiss Federal Institute of Aquatic Science and Technology, Eawag, Seestrasse 79, 6047 Kastanienbaum, Switzerland

Abstract

Branched GDGTs are a set of membrane-spanning lipids produced by bacteria. They are at the basis of the MBT'_{5ME} and isomer ratio (IR), biomarker ratios that are commonly used as paleotemperature and chemistry proxies, respectively. Previous work on the seasonal temperature variability of the MBT'_{5ME} and IR ratio within seasonally stratified lake (Lake Rot) revealed a distinct temperature response. While the MBT'_{5ME} responded to the onset of stratification, the IR showed a sustained response to increased summer temperatures. Now, the downcore record of this lake allows to shed light on the climate dependencies and change in provenance of brGDGTs. .

Based on the MBT'_{5ME}, colder temperatures are recorded in the Late Glacial Stadial and Younger Dryas. Throughout the Holocene, the presence of water column stratification is recorded by the MBT'_{5ME}, driven by the higher fractional abundance of brGDGT Ia, especially during the early Holocene (11.7-7.4 cal. ka BP). The abundance of brGDGT Ia, which is typically found in thermally stratified surface summer water, indicates that the MBT'_{5ME} temperature proxy is primarily influenced by thermal stratification rather than solely reflecting mean annual temperature. On the other hand, IR shows promise as a tracker of mean annual temperature.

The influence of brGDGTs sourced from the anoxic hypolimnion is reconstructed by evaluating brGDGT IR values. Only a muted influence from seasonal or permanent lake water anoxia was observed on the sedimentary IR signal, even during periods of documented anoxia based on XRF ratio values. Moreover, the concentration changes and interdependencies of brGDGTs during the oligotrophic phase of the lake mimicked the epilimnion conditions. The provenance of Lake Rot sedimentary brGDGTs is thus dominantly from the epilimnion, where MBT'_{5ME} and IR respond to temperature. This suggests that coring at the oxic depth of (seasonally) anoxic lakes can prove successful for using MBT'_{5ME} as a lake surface paleothermometer. These findings have substantial implications for paleoclimate studies. It is apparent that the development of seasonal stratification plays a crucial role in influencing MBT'_{5ME} values. However, it's worth noting that a predominant mixing water column fingerprint is evident for most of the Holocene climate, as indicated by the prevalence of intermediate values for brGDGT Ia.

1. Introduction

Understanding past climate variations and their underlying causes is essential for assessing the magnitude of future climate change crises (Tierney et al., 2020). By providing quantitative data for past climates, biomarker proxies play a pivotal role for enabling validation and refinement of climate models (Summons et al., 2022). The integration of various biomarkers, retrieved and quantified in dated geological records such as river outflow, marine and lake sediments allow for a comprehensive and multifaceted understanding of past climate systems. However, a crucial initial step in paleoclimate reconstruction is acquiring a comprehensive understanding of the mechanisms governing the proxy response to environmental changes. Branched glycerol dialkyl glycerol tetraethers, so-called brGDGTs, are increasingly used as a potent biomarker proxy for reconstructing soil or lake temperature changes through time (Weijers et al., 2007; Peterse et al., 2012; De Jonge et al., 2014a; Loomis et al., 2014; Li et al., 2016). These organic compounds are membrane-spanning lipids characterized by a wide range of structural diversity (Supp. Fig. 1), produced by a suite of partially identified heterotrophic bacteria. This structural diversity encompasses a change in the degree of methylation (4-6 branches), resulting in three different compound groups, tetra- penta- and hexamethylated GDGTs, where penta- and hexamethylated compounds have 1 or 2 additional outer branches, respectively. Additionally, internal cyclisation can generate 1-2 cyclopentane moieties in these molecules (Weijers et al., 2006). BrGDGT compounds with outer methyl branches located on α and/or ω_5 are referred to as 5-methyl brGDGTs, while those with the outer methyl branches on α and/or ω_6 are termed 6-methyl brGDGTs (De Jonge et al., 2013). In recent years, global studies on brGDGTs have revealed their ubiquity across various environments, including soils and peats (e.g., Peterse et al., 2014; Wei et al., 2022), lake sediments (Russell et al., 2018), and the water column of freshwater systems such as lakes and rivers (i.e., Loomis et al., 2014). Their in-situ production in the water column has been confirmed by several studies (e.g., De Jonge et al., 2014b; Martínez-Sosa et al., 2019), prior to their settling and incorporation in lake sediments. When their distributional changes on the global or continental scale are summarized, using either the MBT' or more recently MBT'_{5ME} (De Jonge et al., 2014; Russell et al., 2018; Dang et al., 2018; Martínez-Sosa et al., 2021), forward selection models of fractional abundances (e.g. Russell et al., 2018, Bauersachs et al., 2024) and other brGDGT ratios (Raberg et al., 2021), a good dependency on mean air temperature (a proxy for lake temperature) is observed. To explain offsets between reconstructed and measured temperatures, confounding factors are proposed that include the physical and chemical characteristics of lakes (Zhao et al., 2023), soil input (Martínez-Sosa et al., 2021), sedimentation rates in lakes (Zhao et al., 2021), and the possibility of a warm season bias in mid to high latitude lakes (Raberg et al., 2021). Moreover, the increased production of 6-methyl isomers (IR > 0.5), possibly originating from distinct bacterial producers, has been suggested to introduce an additional influence on the

MBT'_{5ME} temperature calibrations in mid-latitude alpine settings. This phenomenon is observed to induce a pronounced seasonality effect in lakes situated at higher altitudes (Bauersachs et al., 2024).

Complicating a straightforward interpretation of MBT'_{5ME} ratio values generated within a single lake system, are temperature-independent changes in brGDGTs distribution observed in individual lakes or across small temperature gradients. This includes individual brGDGT compounds and GDGT-based ratios (i.e. MBT'_{5ME}, CBT', IR). Specifically, GDGTs can be influenced by dissolved oxygen (Weber et al., 2018; Van Bree et al., 2020; Yao et al., 2020; Lattaud et al., 2021) and pH and alkalinity (Schoon et al., 2013) in the lake water column, with production in anoxic hypolimnion conditions confirmed by depleted $\delta^{13}\text{C}$ GDGT (Colcord et al., 2017). Furthermore, seasonal changes that include temperature and mixing regime impact the MBT'_{5ME} (Loomis et al., 2014a, Van Bree et al., 2020, Zhao et al., 2021). Furthermore, it has been observed that brGDGT concentrations increase with increasing hypoxia in the water column, suggesting that brGDGTs are primarily produced in the anoxic portion of the water column (Bechtel et al., 2010; Blaga et al., 2011; Woltering et al., 2012; Buckles et al., 2014; Loomis et al., 2014b; Miller et al., 2018, Weber et al., 2018, Van Bree et al., 2020). The lack of a comprehensive understanding of the mechanisms governing brGDGT production in lakes is reflected in the diversity of lake-specific calibrations.

In lacustrine settings where MBT'_{5ME}-based transfer functions have been employed for Holocene temperature reconstructions, other confounding factors beyond temperatures have been observed to impact the MBT'_{5ME}. These uncontrolled variables encompass terrigenous or soil organic matter input (Warden et al., 2018; Martin et al., 2020; Ramos-Roman et al., 2022).

While the number of lacustrine calibrations designed to capture large scale (global or regional) temperature variability continues to grow, the error associated with the temperature proxy MBT'_{5ME} remains stable (1.47-2.9°C). This illustrates that a lack of mechanistic understanding of the environmental drivers of MBT'_{5ME} variability in lake sediments remains. It raises questions about whether the interpreted signal exclusively reflects temperature change caused by overlying air temperature change, or whether confounding factors such as stratification and water chemistry could potentially alter the MBT'_{5ME} sensitivity to temperature.

Here, we investigate changes in the quantity and distribution of brGDGTs in a late glacial and Holocene sediment core from a temperate lake in Switzerland, which currently experiences seasonal bottom water anoxia. We build on previous water column studies of the same lake to explain variation in GDGT-based ratios, and an existing environmental reconstruction based on bulk and geochemical sedimentary

parameters, to determine how climate sensitive parameters like stratification and anoxia drive variation in MBT_{SME} values.

2. Material and Methods

Lake Rot (Rotsee, 47°21'05.8"N and 8°31'12.7"E), is a small prealpine lake with a surface area spanning 0.48 km² and a maximum depth of 16 m (Fig. 1). It exhibits a monomictic mixing regime and has been eutrophic for at least the last 100 years (Zullig and Rheineck, 1985). The formation of Lake Rot basin can be traced back to the regression of the Reuss glacier following the last interglacial period (Frey et al., 1907). The presence of dense vegetation surrounding the lake limits the influx of wind, facilitating the development of a stable water column stratification during the warm season (Schubert et al., 2010).

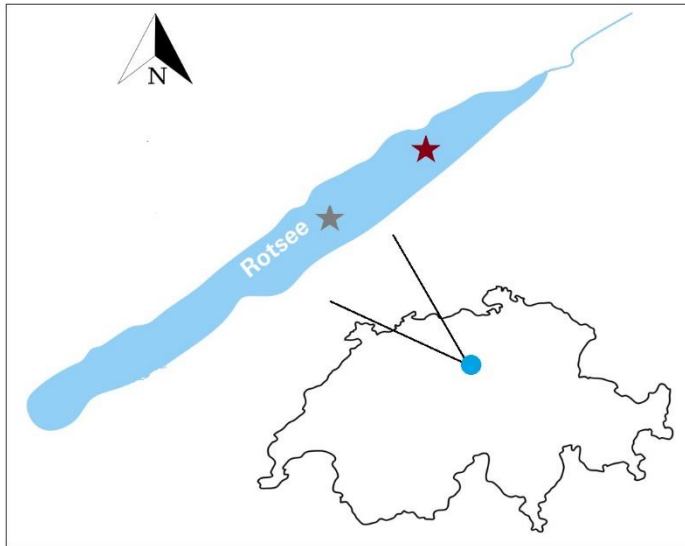


Fig. 1. Map of Lake Rot in Switzerland with the location of Rotsee indicated. Within the Rotsee outline red and grey stars mark the location of Rot21-1 core and water column sample sites, respectively.

2.1. Known paleoclimatic variability of Lake Rot system

Lake Rot climate variability has previously been reconstructed based on pollen (Lotter et al., 1989) and $\delta^{18}\text{O}$ analysis of chironomid capsules (Verbruggen et al., 2010), and discussed in the framework of other Central European sites. Specifically, it was recorded that the late Glacial interstadial occurred at Lake Rot between 14 650 and 12 860 cal. a BP, after which a colder Younger Dryas period is recorded between 12 860 and 11 610 cal. ka BP (Verbruggen et al., 2010).

Lotter et al. (1989) subsequently reported mild Holocene temperatures, with a mid-Holocene period characterized by warmer summer temperatures.

2.2. Core sedimentology and Age-Depth Model

In October 2021, a sediment core with a length of 1400 cm (Rot21-1) was recovered from Rotsee (N 47° 04' 27.81"; E 008° 19' 25.77; Fig. 1) from a water depth of 5.5 m, using an UWITEC piston corer operated from a platform fixed by 4 shoreline anchors. Two parallel holes were drilled, to allow the generation of a continuous sediment record. After splitting the cores, one half was subsampled at ~10 cm intervals for biomarkers and bulk geochemical analyses.

Radiocarbon dating was based on 18 macrofossils (e.g., seeds, leaf remains, and twigs) samples selected from Rotsee sediments. After wet sieving, the macrofossils underwent a room temperature acid-alkali-acid treatment (Norris et al., 2020) to remove carbonates, acid-soluble humic material, and humic acids. At 20 depths, bulk sediments were acidified using fumigation (Haas et al., 2019) and weighed prior to additional bulk sediment ¹⁴C dating. ¹⁴C measurements were conducted using the MIni CARbon DAting System (MICADAS) on an Accelerator Mass 1 Spectrometer (AMS) equipped with an Elemental Analyzer unit (EA) (company, country) at the radiocarbon facility of ETH Zurich. The radiocarbon ages were converted into calendar ages using the INtCal13 calibration curve via the Bayesian modelling R-package rbacon (RStudio Version 1.3.1093; R Development Core Team, 2015; Blaauw and Christen, 2011).

2.3. XRF elemental composition and bulk organic measurements

X-ray fluorescence (XRF) measurements were conducted on an AVAATECH core scanner at 5 mm resolution to identify the elemental composition of the sediment core. The cores were scanned both at 10 kV (Mg, Al, Si, S, K, Ca, Ti, Cr, Mn, RhLa Inc), and at 30 kV (Fe, Co, Ni, Cu, Zn, Rb, Sr, Zr, RhKa Inc and Pb). Of these, Mn, Fe and sedimentary P are used to calculate elemental ratios for redox reconstruction. To determine the sources of organic matter (OM) in the sediment core, Total Organic Carbon (TOC) and Total Nitrogen (TN) were analyzed. For this purpose, 2 cm wide sediment subsamples (n=100) were freeze-dried and homogenized using a pestle and mortar. Subsequently, for TOC% measurements, 30-80 mg of homogenized and weighed sediment was directly loaded into the instrument auto-sampler and analyzed at 400°C using the Soli TOC® Cube elemental analyzer (Elementar Analysensysteme GmbH, Langenselbold, Germany). The amount of CO₂ produced from this carbon fraction was measured used for

TOC% values. TN% was determined using EA-IRMS (Vario Pyro Cube, Elementar, Germany), following the protocol reported by Haas et al. (2019).

2.4. Lipid extraction and brGDGT indices calculation

The sediment subsamples used for lipid analysis, from a 2cm wide sediment subsample adjacent to the subsample taken for bulk sediments (n= 93) were homogenized and freeze-dried prior to lipid extraction. The total lipid extraction (TLE) was performed using an accelerated solvent extractor (ASE) system (Dionex 350, Thermofischer Scientific, Switzerland) with a pressure of 100 bar at a temperature of 100°C (5x) using a solvent mixture of dichloromethane (DCM) to Methanol (MeOH) 9:1 (v/v).

The TLEs were then subjected to column separation over an activated SiO_x column using three solvent mixtures hexane, hexane:DCM (9:1, v/v), and DCM:MeOH (1:1, v/v) to collect apolar, ketone and polar fractions of the TLEs, respectively. After drying the polar fraction under a gentle N₂ stream, 49.6 ng of the GTGT internal standard-C46- (Huguet et al., 2006) was added to the polar fraction. This fraction was subsequently filtered through a 0.45 µm PTFE filter, dried under a gentle N₂ stream, and re-dissolved in 50 µL of hexane/isopropanol (IPA) 99:1 (v/v). GDGT analysis was done by a high-performance liquid chromatography–mass spectrometry (HPLC–MS, Agilent Technologies®, USA) system, as outlined in Hopmans et al. (2016), with a modified column temperature of 40°C and an injection volume of 10 µL. As quantification of GDGTs using an internal standard is semi-quantitative (reference), a lab-specific instrument error of 15% for concentration determination was previously determined. Concentrations and fractional abundances of GDGTs are reported in Supp. Table 1. The calculation of MBT'_{5ME} (De Jonge et al., 2014a), CBT' and Isomer Ratio (IR) followed De Jonge et al. (2014a), where the IR reflects only compounds without cyclopentane moieties (De Jonge et al., 2015; Halfman et al., 2022). DC' is calculated following the modified (De Jonge et al., 2021) ratio (Sinninghe Damste et al., 2009). The GDGT-based reconstruction of temperature and pH was carried out using the Martínez-Sosa et al. (2018) and Bauersachs et al. (2022) calibrations. From these calibrations, the median values calculated using the regression model outlined by Martínez-Sosa et al. (2021) provided the closest reconstructed MAAT of the top core (recent sediment) to that of the current MAAT, and therefore, these values are reported (Supp. Table S1). The indices discussed in this chapter are presented in Table 1.

Ratio	Source
$MBT'_{SME} = \frac{Ia + Ib + Ic}{Ia + Ib + Ic + IIa + IIb + IIc + IIIa}$	Originally: Weijers et al., (2007) Modified: De Jonge et al., (2014a)
$IR = \frac{IIa' + IIIa'}{IIa' + IIIa' + IIa + IIIa}$	De Jonge et al., (2014a, 2015)
$CBT' = \log_{10} \frac{(Ic + IIa' + IIb' + IIc' + IIIa' + IIIb' + IIIc')}{Ia + IIa + IIIa}$	Originally: Weijers et al., (2007) Modified: De Jonge et al., (2014a)
$DC' = \frac{Ib + IIb + IIb'}{Ia + IIa + IIa' + Ib + IIb + IIb'}$	Originally: Sinninghe Damsté et al., (2009) Modified: De Jonge et al., (2021)
$pHrec = 8.95 + 2.65 \times CBT'$ (RMSE = 0.80)	Russell et al., (2018)
$y = X\beta + \epsilon$ $\epsilon \sim N(0, \sigma^2)$	Martinez-Sosa et al., (2021, for information on the regression model please refer to the paper)
$MAAT (^{\circ}C) = 7.11 + 67.66 \times Ib - 13.54 \times IIIa$	Bauersachs et al., (2024)

Table 1. Equations for brGDGTs discussed.

2.5. Statistical analysis

Statistical analysis was an integral part of this study, and various techniques were employed to explore the relationships between brGDGT compounds and MBT'_{SME} . Pearson correlation coefficients (r-value) and associated p-values for correlation tests between paired samples are reported (Supp. Table 2, Fig. 5-Fig. 7). Specifically, changes in concentration and fractional abundance of specific brGDGTs are analysed using scatterplots and so-called diagnostic plots (De Jonge et al., 2019). Principal Components Analysis (PCA) were performed using Python (python v.3.8.) libraries: 'scipy-stats' (Virtanen et al., 2020) and 'sklearn' (Pedregosa et al., 2011). Libraries "matplotlib" and "seaborn" (python v.3.8.5) were used for data visualization.

3. Results

3.1. Chemistry and Age-Depth Model

The age-depth model shows that the sediment core deepest section dates back to approximately 17 cal. ka BP (Fig. 2). Overlying these glacial clays are three peat sections that are dated to be formed during the Glacial interstadial, and the Younger Dryas (12.95 – 13.36 cal. ka BP). The bulk of the Younger Dryas is represented by lacustrine sediments, that represent the sediments between 964.8 ± 20 up to 923 ± 20 cm blf. The overlying sediments (923 to 0 cm blf) represent the Holocene period, with a Holocene onset dated at 11610 cal. BP in Rotsee (Verbruggen et al., 2010). According to the age-depth model (Fig. 2), the upper section of the core (0-800 cm) displays a consistent sedimentation rate, with no recorded sediment reversals. Downcore changes will therefore be reported as cal. ^{14}C ages BP.

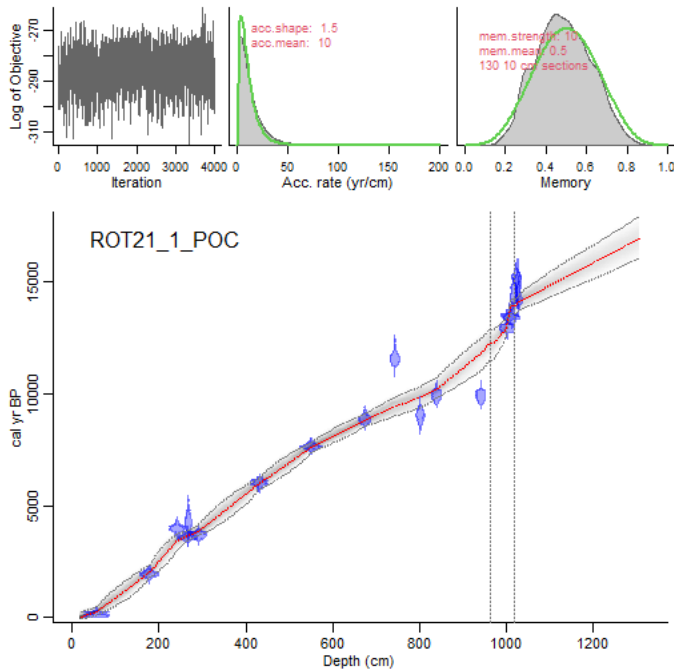


Fig. 2. The Bayesian age-depth model of Rot21-1 sediment core. See Supp. Table 1 for specific information about the radiocarbon samples.

To describe the amount and type of organic matter, the TOC content and C/N values are evaluated. The TOC% content of the sediment core exhibits large variation (5-25%), generally increasing with time before declining in late Holocene (~ 2.5 cal. ka BP, Fig. 3A). The Holocene C/N ratio ($\bar{x}= 10.9$, $\sigma= 2.6$) suggests that the organic matter primarily originates from a lacustrine autochthonous source (Fig. 3B).

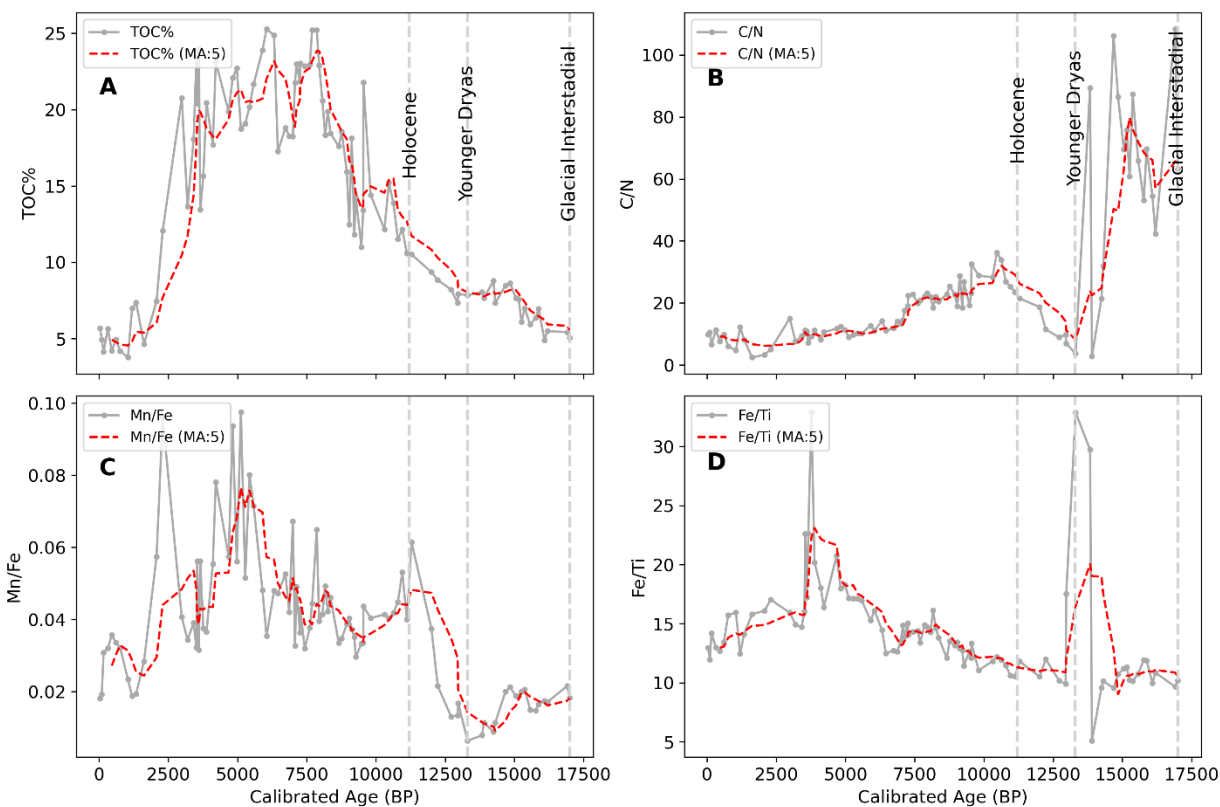


Fig. 3. Bulk sedimentary parameters TOC% (A) and C/N (B) plotted against time (cal. ^{14}C a BP). Panel C and D plot XRF-based elemental composition ratios Mn/Fe and Fe/Ti. The grey horizontal lines indicate measured values while the dashed red line displays a moving average (window= 5) for each parameter. The onset of the 3 time periods recorded in the sediments are indicated over the vertical dashed grey lines.

To describe high-resolution changes in sedimentary elemental composition, XRF-based elemental ratios like Mn/Fe can track the lake and sediment redox conditions in the record (Naeher et al., 2013; Makri et al., 2021). The Mn/Fe ratio is interpreted as reflecting conditions of seasonal anoxia (De Jonge et al., unpublished). Its values remain low (< 0.02) through the glacial sediments and starts to increase (0.06) at the onset of Holocene epoch at 11.3 cal. ka BP (Fig. 3C). Thereafter Mn/Fe remains stable between 0.04-0.06, increasing (0.08-0.10) during 2.5-2.6 cal. ka BP, indicating periods of seasonally anoxic hypolimnion. These prolonged periods of seasonally anoxic hypolimnion conditions potentially extended to permanent anoxia during 2.9-3.6 cal. ka BP. At this depth, Mn/Fe values are decreased, which matches a permanently anoxic hypolimnion (Makri et al., 2021). This transition is supported by the increased presence of both Fe and P, indicating the possible presence of Fe in the form of $\text{PO}_4\text{-Fe}$ (De Jonge et al., unpublished; Fig. 3D).

Hence, following the sedimentary description, three water column states are defined within the Holocene period based on TOC and XRF ratio data (De Jonge et al., unpublished); an oligotrophic state without evidence of hypolimnion anoxia (11.2-7.1 cal. ka BP), a eutrophic state with seasonal to permanent anoxia (7.1-1.3 cal. ka BP) and a mesotrophic state with variable redox conditions in the water column (1.3 cal. ka BP -present).

3.2. Variability in brGDGT concentration and distribution

The summed concentration of brGDGTs (normalized per g TOC) exhibits variations throughout the core (Fig. 4), decreasing over time. During the late Glacial interstadial (> 12 cal. ka BP), higher values (> 20 $\mu\text{g/g}$ TOC) are observed (Fig. 4. secondary-y axes). Subsequently, in the lacustrine sediments of the Younger Dryas and Holocene, brGDGT concentrations steadily decline, although

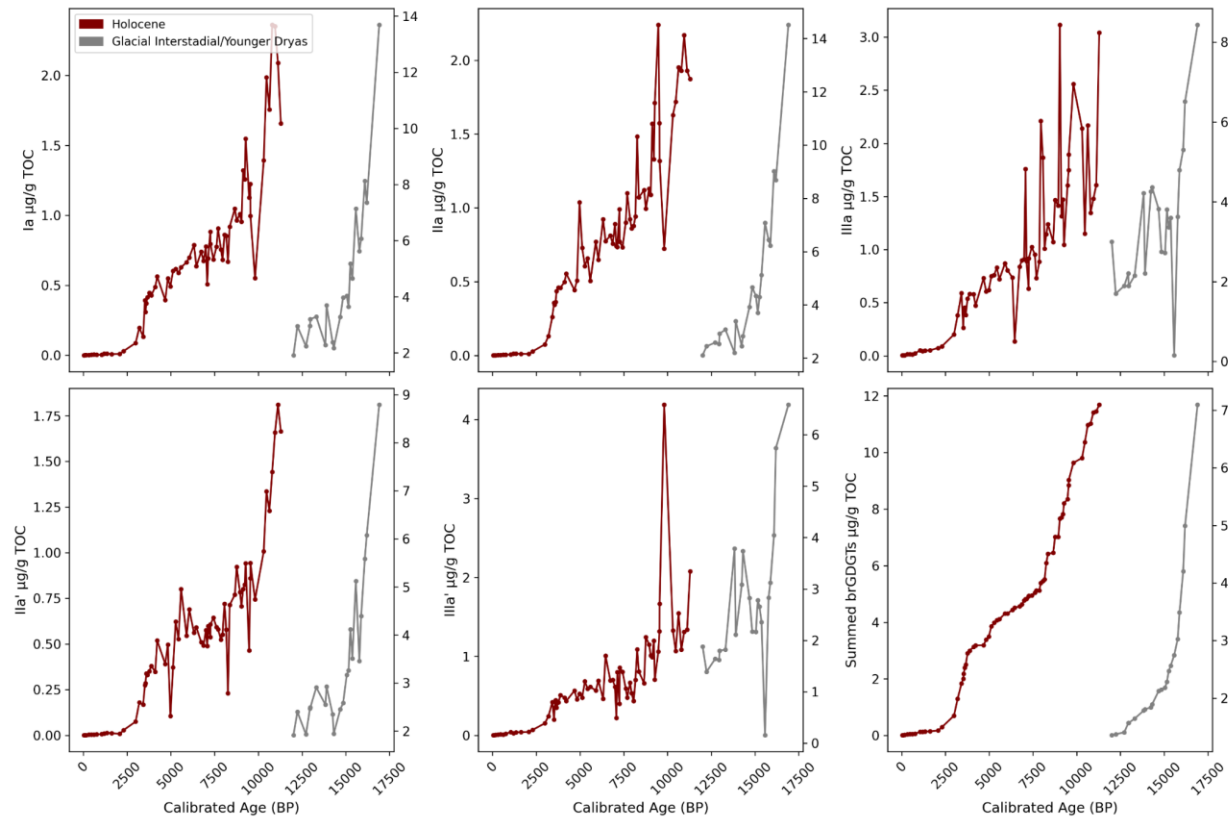


Fig. 4. The concentration ($\mu\text{g/g}$ TOC) of abundant brGDGTs (Ia, IIa, IIIa, IIa' and IIIa') in the core Rot21-1. The red lines depict the Holocene concentrations plotted on the primary y-axis; grey lines depict the late Glacial period on the secondary y-axis.

exhibiting variations at multiple time points (Fig. 4A-E). During the mid- to late-Holocene, concentrations decrease further, generally ranging from 0-2 $\mu\text{g/g}$ TOC. In the most recent 3000 years, TOC-normalized

brGDGT concentrations are low (\bar{x} = 0.14 $\mu\text{g/g TOC}$, σ = 0.17 $\mu\text{g/g TOC}$), with a 14-fold decrease compared to the Holocene average (5 $\mu\text{g/g TOC}$, σ = 3.38 $\mu\text{g/g TOC}$). Concentrations of major brGDGTs Ia, IIa and IIIa generally increase together, with an excellent correlation observed between brGDGT Ia and IIa (r = 0.99, p < 0.01; Fig. 5E) and a good correlation that reflects more scatter between brGDGT Ia and IIIa (r = 0.82, p < 0.05; Fig. 5F).

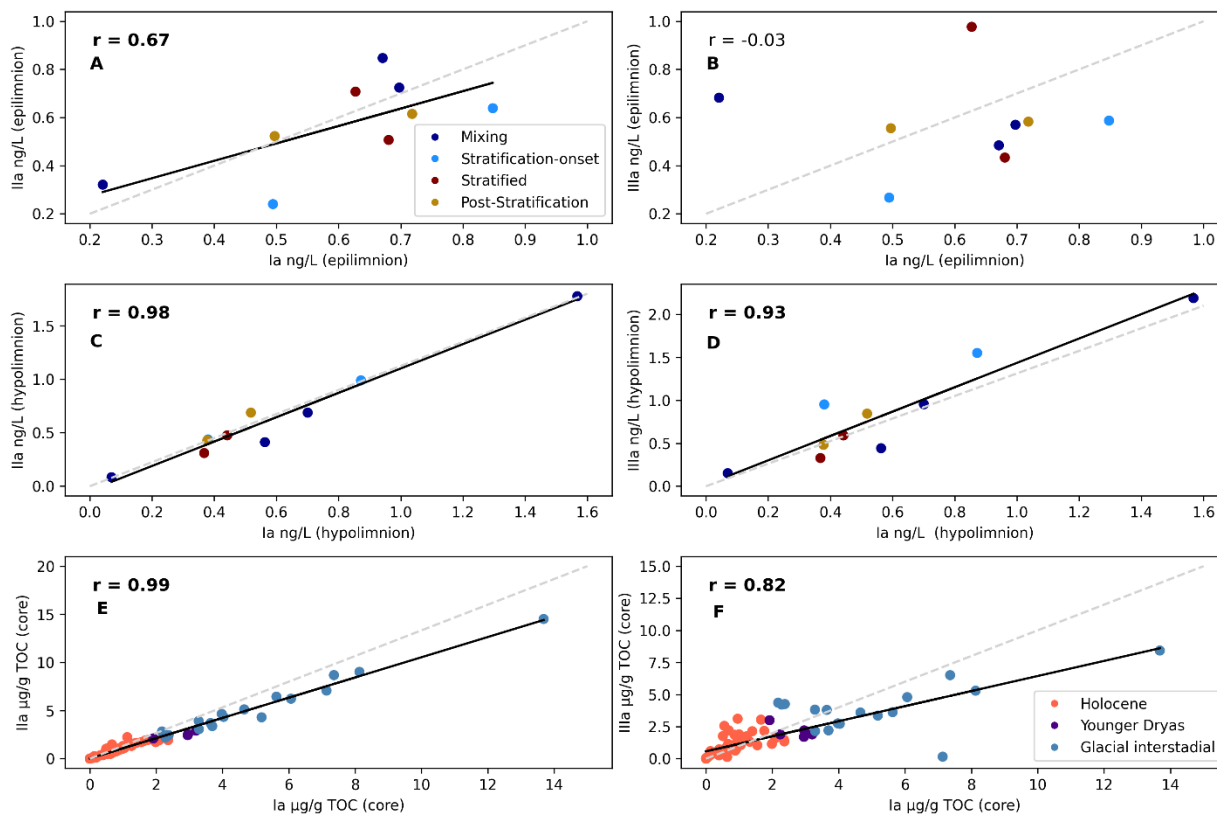


Fig. 5. Scatterplots depicting the concentration of brGDGTs Ia, IIa and IIIa in both the water column (epilimnion/hypolimnion) and the sediment core of Lake Rot. Note the varying scales and concentration units used in the plots. The color legend in the water column section is based on the mixing characteristics of the water column at time of sampling, while in the core section, it represents the different climate zones. Regression lines (black) and 1:1 line (dashed-grey) plotted.

The brGDGT compound IIa (t-test, P < 0.01) is the dominant compound throughout the core, with concentrations between 0-14 $\mu\text{g/g TOC}$. Specifically, brGDGTs Ia, IIa, and IIIa exhibit average concentrations of 1.63, 1.74, 1.53, (σ = (2.17, 2.30, 1.54) $\mu\text{g/g TOC}$), respectively. Their 6-methyl counterparts, IIa' and IIIa', show average concentrations of 0.76, 1.17 (σ = 1.09, 1.24) $\mu\text{g/g TOC}$, respectively (Fig. 4).

As individual brGDGTs show concentration changes throughout the core, the fractional abundance of brGDGTs Ia, IIa, and IIIa also varies, with values spanning from 5-20%, 5-30%, and 5-42%, for brGDGT Ia, IIa and IIIa respectively (Supp. Table S1). Variation in fractional abundances of these GDGTs is observed both within and between climate zones (Fig. 6A).

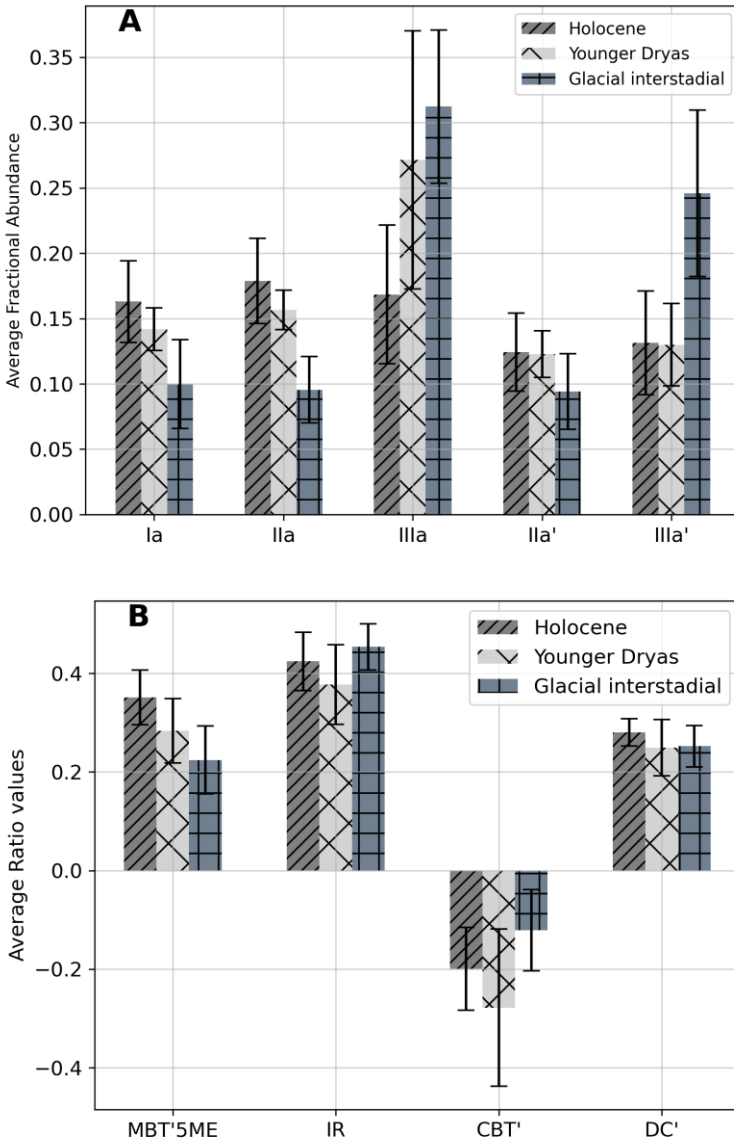


Fig. 6. (A) Bar charts depicting the average (A) fractional abundance of abundant brGDGTs and (B) ratios for the different core sediment types (Holocene, Younger Dryas and Glacial interstadial). Error bars represent the standard deviation.

A positive correlation exists between Ia% and IIa% in the Lake Rot sediments ($r = 0.72$, $p < 0.0001$; Fig. 7A), and a negative correlation between the fractional abundance of Ia and IIIa ($r = -0.83$, $p < 0.0001$; Fig. 7B). For both these correlations, the dataset exhibits a more pronounced scatter when brGDGT Ia is below $\sim 17\%$ (17% visually chosen as a cut-off value). Below this value there is a weaker correlation between Ia and IIa ($r = 0.64$, $p < 0.0001$) and Ia and IIIa ($r = -0.72$, $p < 0.0001$). Specifically, sediments with brGDGT Ia $> 17\%$ show a strong correlation between Ia and IIIa ($r = -0.89$, $p < 0.0001$). In general, samples with low brGDGT Ia ($< 10\%$) are derived from the Glacial interstadial clays, but not exclusively (Fig. 7A).

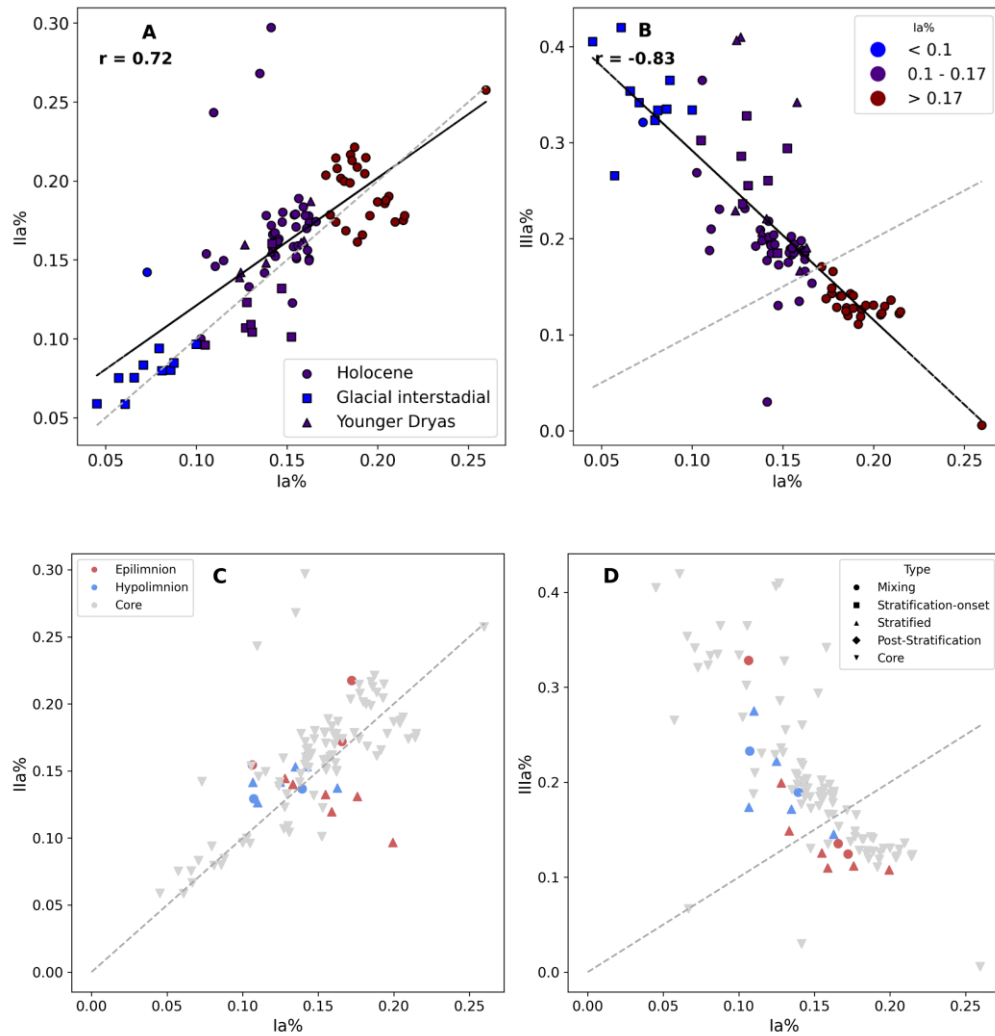


Fig. 7. (A) scatter (Diagnostic plot, after De Jonge et al., 2021) exhibiting the fractional abundances of brGDGTs Ia vs IIa and (B) Ia vs IIIa. The different symbols represent the climate zones (Holocene, Younger Dryas and Glacial interstadial) while the colors denote the classification of samples based on their Ia% values as discussed in text. Regression line (black), r -value for each subplot and 1:1 line (dashed-grey) plotted. For subpanel (C) and (D)

fractional abundances of brGDGTs Ia vs IIa and Ia vs IIIa are plotted, respectively, for both SPM and core samples. 1:1 line plotted (dashed-grey).

The MBT'_{5ME} values exhibit a substantial range of variation within the sediment core, spanning from 0.10 to 0.50 (Supp. Table S1, Fig. 8A, Fig. 9A). However, the majority of this variation during the Holocene period falls within a more constrained range of 0.30 to 0.45 (Fig. 8A, Fig. 9A). MBT'_{5ME} values and the fractional abundance of the major brGDGT Ia and IIa display strong positive correlations ($r = 0.94$ and 0.64 , $p < 0.01$, for brGDGT Ia and IIa respectively, Fig. 8A). A negative dependency between MBT'_{5ME} and the fractional abundance of brGDGT IIIa is observed ($r = -0.92$, $p < 0.01$; Fig. 8A).

The IR of the Rot core exhibits a muted (0.38-0.48) range during the Holocene period (Supp. Table S1, Fig. 8B, Fig. 9B), in contrast to the Younger Dryas and Glacial interstadial, where a broader IR range (0.28-0.50) is evident (Fig. 9B). The chemistry ratio CBT' exhibits a broader range (-0.49-0.13). In contrast, DC', another chemistry proxy, increases with time (Supp. Table S1), starting in the Holocene period with values ranging from 0.22 and reaching 0.35 in recent sediments (Supp. Fig. S3D).

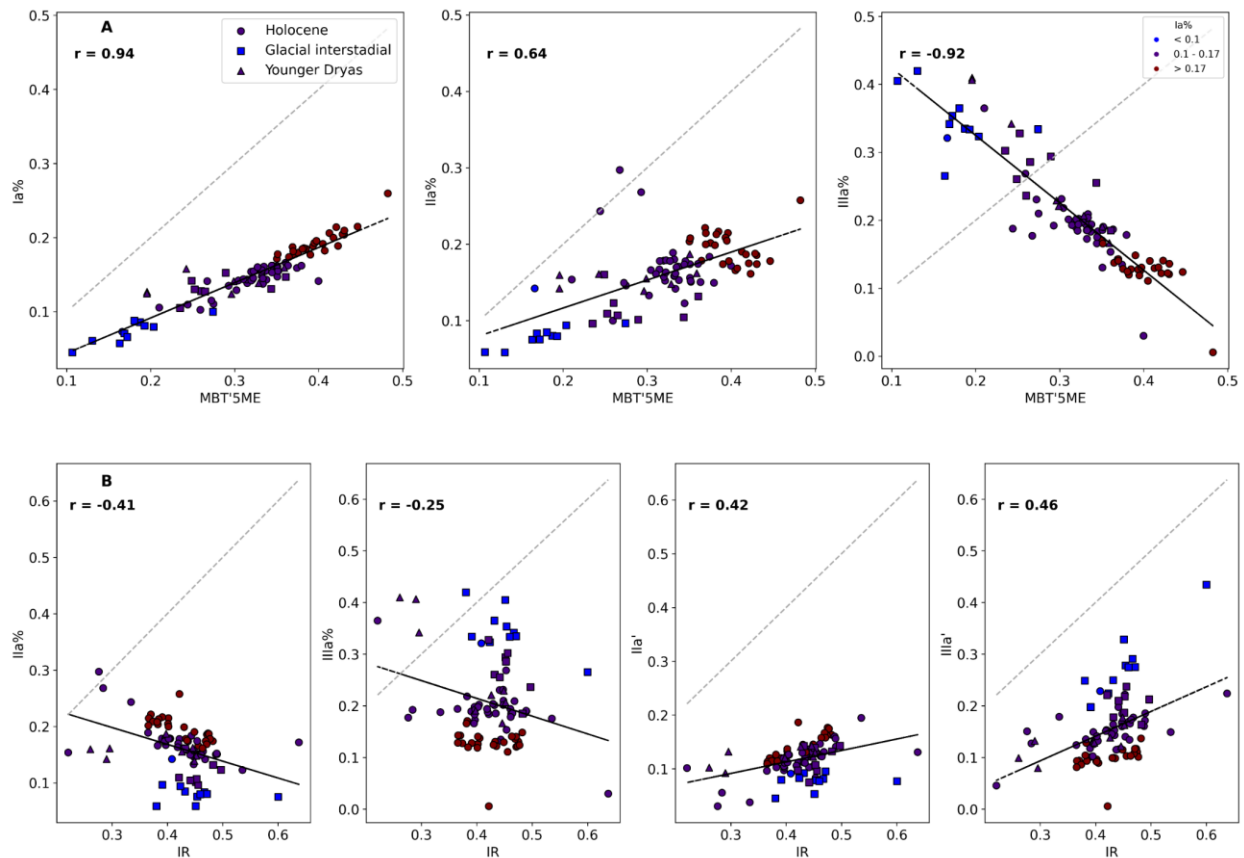


Fig. 8. Scatterplots comparing GDGT ratios with GDGT fractional abundance. (A) MBT'_{5ME} values against fractional abundances of brGDGTs Ia, IIa and IIIa and (B) brGDGTs IR vs fractional abundances of brGDGTs IIa, IIIa, IIa' and IIIa'. The symbols represent the climate zones (Holocene, Younger Dryas and Glacial Interstadial) while the colors denote the classification of samples based on their fractional abundance of brGDGT Ia (Ia%) values. Regression line (black), *r*-value for each subplot and 1:1 line (dashed-grey) plotted.

4. Discussion

4.1. Provenance and environmental drivers of sedimentary GDGTs

The core is sampled at a depth of 5.5 m, which is currently above the depth of seasonal anoxia. This location was informed by the variability in Lake Rot water column brGDGTs (Chapter 3) and selected with the aim to avoid a large contribution of brGDGT produced in the hypolimnion, as the Lake Rot MBT'_{5ME} values produced in the hypolimnion are determined by pH (Ajallooeian et al., Chapter 3). To confirm that the sediments were not influenced by anoxic bottom water throughout the entire sedimentary sequence, the provenance, and environmental drivers of Lake Rot sedimentary brGDGTs are discussed in the framework of the water column variability. Within the sediments, the observed correlation between the concentrations of Ia versus IIa and Ia versus IIIa (Fig. 5E-F) in the lacustrine sediments follows a pattern matching both the epi- and hypolimnion of Lake Rot (Fig. 5A-D). Thus, concentration changes alone do not allow to distinguish between an epi- or hypolimnion source. However, the temperature dependent production of brGDGT Ia and IIIa, as observed in the Rotsee epilimnion (Fig. 7B), still slightly impacts the concentration (Fig. 5F) of these compounds in the sediments. At several depths the additional production of brGDGT IIIa, can be seen as an offset from the 1/1 line (Fig. 5F). Furthermore, the production of brGDGTs Ia is observed as change in concentration (Fig. 5F) but especially as an increase in the fractional abundance (Fig. 7C-D) in Rotsee sediments. Further epilimnion characteristics are the observation that MBT'_{5ME} and the IR correlate ($r = 0.92$, $p < 0.01$) as both are driven by temperature, while the MBT'_{5ME} in the hypolimnion is driven by pH (Ajallooeian et al., Chapter 3), and the IR by dissolved oxygen and alkalinity (no correlation between MBT'_{5ME} and IR in hypolimnion). The provenance of sedimentary brGDGTs will now be discussed for each climate zone.

Starting around 16 cal. Ka BP, the Glacial interstadial sediments ($n = 18$) are characterized by low TOC and fully oxygenated sediments (Fig. 3). They have generally high brGDGT concentrations, indicating that bacterial-derived OM represent a large fraction of the sedimentary organic carbon. The concentration of individual brGDGTs (Ia, IIa, and IIIa) demonstrate positive correlations (Fig. 5). Specifically, the concentration increases in brGDGT Ia versus IIa ($r = 0.98$, $p < 0.001$) exhibits a stronger and more robust

correlation than that of Ia versus IIIa ($r= 0.56$, $p< 0.001$), with concentration of brGDGT IIIa consistently plotting above the 1:1 line (Fig. 5F). As the Glacial interstadial is the coldest period recorded in the Lake Rot sediments, this observation is explained by the production of brGDGT IIIa in cold conditions. As such, the Glacial interstadial can distinctly be identified by the lower fractional abundance of brGDGT Ia and IIa (< 0.1 , < 0.1 , respectively) and the higher fractional abundance of IIIa (> 0.25) (Supp. Table S1, Fig. 7A-B). MBT'_{SME} values are determined by the fractional abundance of brGDGT Ia and IIIa in Glacial interstadial sediments, with a comparatively weaker dependency between MBT'_{SME} and fractional abundance of IIa ($r= 0.74$, $p= 0.00$) in comparison to Ia ($r= 0.89$, $p= 0.00$) and IIIa ($r= -0.79$, $p= 0.00$) (Fig. 8A). The production of brGDGT IIIa thus causes the cold MBT'_{SME} values observed during this period, ultimately reconstructing an average Mean Annual Temperature (MAAT) of $5.6\text{ }^{\circ}\text{C}$ ($\sigma= 1.8$, Martínez-Sosa et al., 2021) or $4.8\text{ }^{\circ}\text{C}$ ($\sigma= 1.7$, Bauersachs et al., 2024; Supp. Table S1).

The IR ratio is driven by hexamethylated compounds that are present in large fractional abundances compared to the pentamethylated compounds (Fig. 8B). The hexamethylated compounds exhibit more pronounced variation in the glacial clays (Fig. 5A) compared to the Holocene. In contrast to what is observed in modern Lake Rot SPM, there is no correlation present between the IR and the MBT'_{SME} . The sedimentary setting during the Glacial interstadial, described as an organic matter poor and clastic material rich deposit, is consequently, distinct from the current lacustrine system.

In the sediments from the Younger Dryas period ($n= 8$), which include both peat ($n= 6$) and lacustrine sediments ($n= 2$) (marked on Supp. Fig. S4), an intermediate range in fractional abundance of brGDGT Ia, IIa, and IIIa (Fig. 7A-B) is observed. While the fractional abundances of brGDGT Ia and IIa exhibit a mild variation between the peat and lacustrine samples from the Younger Dryas, with a noticeable decrease, the fractional abundance of brGDGT IIIa exhibits a more pronounced variation when the peat layer transitions to lacustrine sediments (marked on Supp. Fig. S4). Subsequently, this period is characterized by a poor correlation between the fractional abundance of brGDGT Ia and IIa and between Ia and IIIa (Fig. 7A-B).

This is distinct from what is expected based on the different temperature dependency of soil and lacustrine GDGTs. However, the phenomenon that waterlogged soils represent a GDGT distribution that is similar to nearby lakes was described before by Loomis et al., (2011). However, the lower IR observed for this period (Supp. Fig. S3B) indicates a lower pH environment in the peat and lake environment of the Younger Dryas (De Jonge et al., 2021; Wei et al., 2022). The variability in IR of the Younger Dryas is determined by both penta- and hexamethylated brGDGTs (Fig. 8B).

Within the Holocene ($n= 66$), sedimentary brGDGT distributions align closely with the yearly range of values observed in the thermally stratified epilimnion of Lake Rot (Fig. 7C-D). As water column conditions

with a fractional abundance of Ia > 17% are only observed in thermally stratified water, the sedimentary variability in the fractional abundance of Ia can potentially be interpreted as a proxy for the presence of warm, thermally stratified surface water. In the diagnostic plots (Fig. 7C-D) the Holocene sediments show a strong anti-correlation between brGDGT Ia and IIIa, that aligns well with the variability in brGDGT Ia and IIIa in the Lake Rot epilimnion (Fig. 7C-D). However, there is also overlap with the mixed and post-stratified hypolimnion SPM, and the provenance (epi- and hypolimnion) of brGDGTs in the Holocene is expected to vary with time.

During the oligotrophic phase of the lacustrine Holocene sediments (11.3-7 cal. Ka. BP), XRF profiles revealed no signs of water column anoxia. In some samples, the elevated fractional abundance of brGDGT Ia (> 17%) mirrors the thermal stratification typical of Lake Rot's epilimnion, indicative of warmer temperatures (Fig. 9A). However, for the majority of this period, where Ia fractional abundance averages between 0.10-0.17, declines in MBT'_{5ME} suggests a decrease in temperature and/or the absence of stratification. A positive correlation between MBT'_{5ME} and IR ($r= 0.47$, $p< 0.01$) is observed during this period, matching the correlation observed exclusively in Lake Rot's surface SPM. This correlation provides further evidence of the presence of a warmed water column in the early Holocene, and the absence of hypolimnion-derived brGDGTs.

During the eutrophic phase of Lake Rot (11.3-7 cal. Ka. BP), the fractional abundance of brGDGT Ia remained similar to the oligotrophic period, indicating a prolonged presence of the stratified epilimnion signal in the lake (Fig. 9A). While both MBT'_{5ME} and IR values decrease, suggesting a colder water column compared to the oligotrophic phase, it's important to note that several samples within this phase indicate concurrent increases in both MBT'_{5ME} and IR, supporting episodes of warmer temperatures (e.g., at 6.3, 4.2, 2.2 cal. Ka BP). However, when considering all samples from this period, a correlation between MBT'_{5ME} and IR is not observed, which indicates that a contribution of hypolimnion brGDGTs is possible. As the IR increases in SPM during hypolimnion anoxia, for periods where an increase in only IR (and not MBT'_{5ME}) is observed (e.g., at 4.8, 3.4, 2 cal. Ka BP), a potential hypolimnion input is suggested. For certain periods, this matches permanent anoxic periods as recorded in the XRF profile (Fig. 9B, areas marked with Asterisk). For periods with decreased IR and without a corresponding decrease in MBT'_{5ME} values (e.g., 5.9, 3.5-3.6, 2.9 cal. Ka BP), the interpretation of the sources of the GDGTs becomes more complex. Some of these samples fall within periods of prolonged anoxia yet display surprisingly lower IR values (< 0.39) suggesting parameters other than lake water anoxia impacted the brGDGTs.

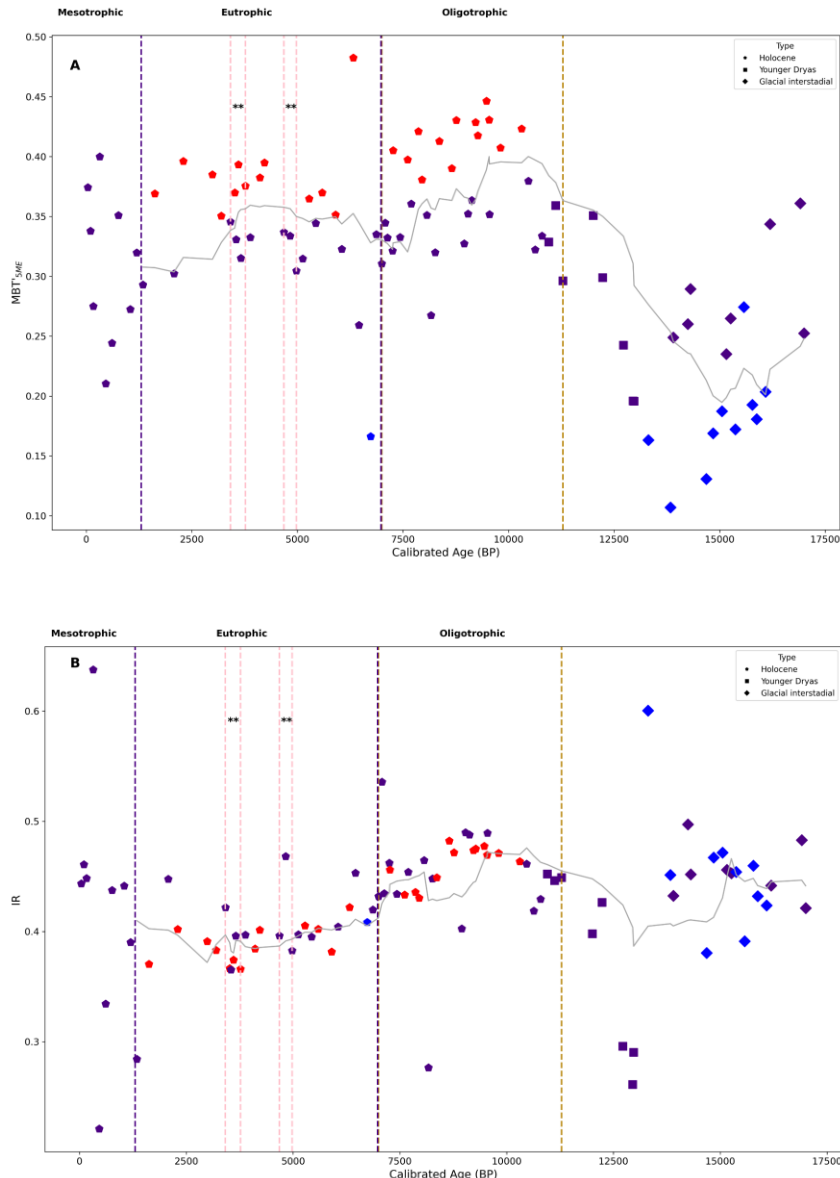


Fig. 9. (A) MBT'_{5ME} values of the different core sediment types through time. The symbols represent the climate zones (Holocene, Younger Dryas and Glacial Interstadial) while the colors denote the classification of samples based on their fractional abundance of brGDGT Ia ($Ia\%$) values (blue: $Ia\% < 0.10$, purple: $0.10 < Ia\% < 0.17$, red: $Ia\% > 0.17$). The areas between the dashed lines are characterized by the water column status (oligotrophic, eutrophic, mesotrophic). The area between purple dashed lines indicates periods of extended seasonal anoxia. The small pink areas marked with asterisks (*) on the graph represent periods with permanent anoxia. The moving average (window=10) for MBT'_{5ME} and IR plotted as a grey line.

The mesotrophic period (1.3 cal. Ka BP to the present, Fig. 9) of Lake Rot is characterized by increased variability in XRF profiles and a notable influx of terrigenous materials (De Jonge et al., unsubmitted). This observation suggests significant changes in nutrient balance and lake mixing, possibly linked to increased

human activity and agriculture (De Jonge et al., unsubmitted manuscript). Similar to the current surface sediment in Rotsee that underlie the oxic water column (Chapter 3), the fractional abundance of brGDGT IIIa is increased at these depths (Supp. Fig. S4). Because of the offset with the GDGT distribution in suspended particulate material, sedimentary production of brGDGT IIIa was suggested (Ajallooeian et al., Chapter 3). This phenomenon is observed in many lacustrine core-top sediments (Zhao et al., 2021; Raberg et al., 2022 and references therein) and has the potential to mask the water column signal if it persists. However, based on the sedimentary profile, this sedimentary GDGT production was limited to the last 1.3 ka. An alternative interpretation is that the in-situ produced sediment signal is degraded at depth, similar to labile bacterial compounds such as esters-containing compounds that are only present in the most recent 300 year of Rotsee sediments (De Jonge et al., unpublished).

4.2. Implications for GDGT-based paleoclimate reconstructions

The in-depth description of GDGT provenance in Rotsee sediments shows that the impact of GDGTs produced in anoxic bottom waters only occurs during specific time periods. Removing those samples with a clear impact of hypolimnion brGDGTs, can improve the accuracy of temperature reconstructions. The development of seasonal stratification has a large impact on the MBT'_{5ME} . In Rotsee, increased abundance of brGDGT Ia is used to identify conditions with well-developed stratification. Diagnostic plots are proposed as a tool to determine this temperature impact. The increased scatter in the Ia vs. IIa dependency in the oligotrophic phase, suggests a potential temperature signal. Specifically, when they deviate below the 1:1 line, it indicates evidence for thermal stratification as observable in Fig 7D where the higher Ia% (> 0.17) samples closely match the epilimnion conditions. Consequently, the MBT'_{5ME} potentially mirrors summer temperatures in conditions where thermal stratification takes place. However, also the temperature of the mixed season water column can change with time. Based on Lake Rot SPM analyses (Chapter 3), this temperature change in the mixed water column is reflected better by the IR than by the MBT'_{5ME} ratio.

4.3. Quantitative climate reconstruction of Lake Rot sediments

After excluding the most recent samples and sediments that likely exhibited a hypolimnetic influence on MBT'_{5ME} and IR, a quantitative paleotemperature reconstruction was conducted using the calibrations developed by Martínez-Sosa et al. (2021) and Bauersachs et al. (2024) (Fig. 10), reconstructing a Mean Annual Temperature above freezing ($MAAT_0$) and MAAT respectively. Both calibrations demonstrate generally corresponding trends, revealing an average temperature of 5.5 °C during the Glacial interstadial (Fig. 10). In contrast, the Holocene MAAT displays warmer temperatures, fluctuating between 7-12 °C,

with several warming and cooling events documented. Temperatures were generally above average between 7 and 11 ka BP, indicating the presence of an early Holocene thermal maximum. During this period, the record includes notable cooling events of 2-3 °C (MAAT₀) or 2 °C (MAAT) around 9.55, 9.00 at 8.17 cal. Ka BP, where the coldest event at 8.2 is consistent with previous findings (Von Grafenstein et al., 1998; Galaasen et al., 2014; Paus et al., 2019; Wilcox et al., 2020). Additionally, a warming episode is evident at 6.3-6.4 cal. Ka BP, also reported in the lacustrine systems of France (Martin et al., 2020), supporting the possibility of a Mid-Holocene thermal maximum.

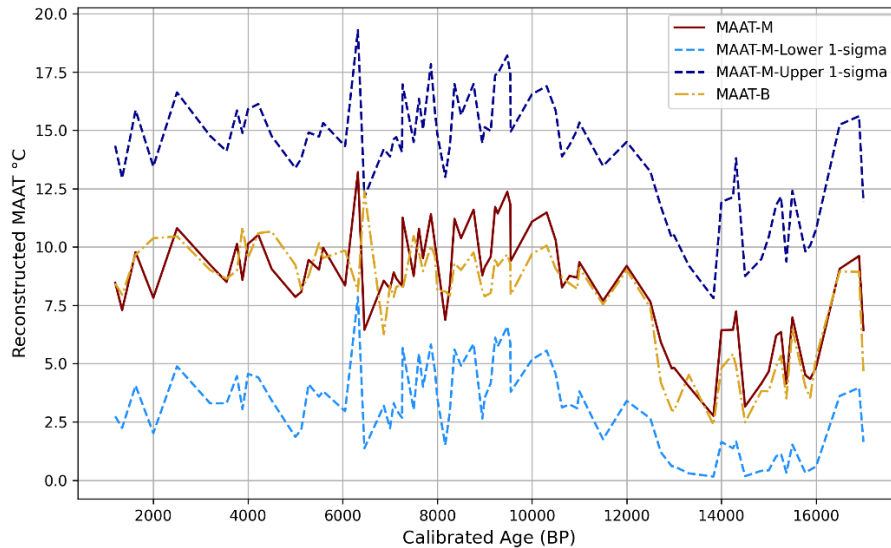


Fig. 10. Reconstructed mean annual air temperature (MAAT, °C) for Rot21-1 sediment core. MAAT-M represents the median age derived from calibration developed by Martínez-Sosa et al. (2021), with the 1 σ boundaries indicated. MAAT-B represents the MAAT based on the forward selection model developed by Bauersachs et al. (2024).

While the mechanism behind the variation in MBT'_{5ME} is proposed to be in response to lake stratification, an examination of the summer solar insolation during the Holocene reveals additional insights. Notably, the observed variability in MBT'_{5ME} closely mirrors changes in summer insolation (Fig. 11). This finding strongly suggests that the periods of lake stratification, marked by higher values in MBT'_{5ME}, are closely linked to the rise in summer insolation during the middle Holocene, promoting warmer summers. Similarly, it is noteworthy that the temperature variations during the period of summer solar insolation minima cover a range of 7.5-10 °C over the last 6 cal. ka BP in the record (Fig. 10-11). This range consistently underestimates the current Mean Annual Air Temperature (MAAT) of the region, which currently stands at 14 °C. MBT'_{5ME} based temperatures thus reconstruct expected climate variability in the Holocene. Based on the in-depth study of the Lake Rot system, the reconstructed temperatures are expected to be skewed towards summer temperatures instead of representing an average annual signal.

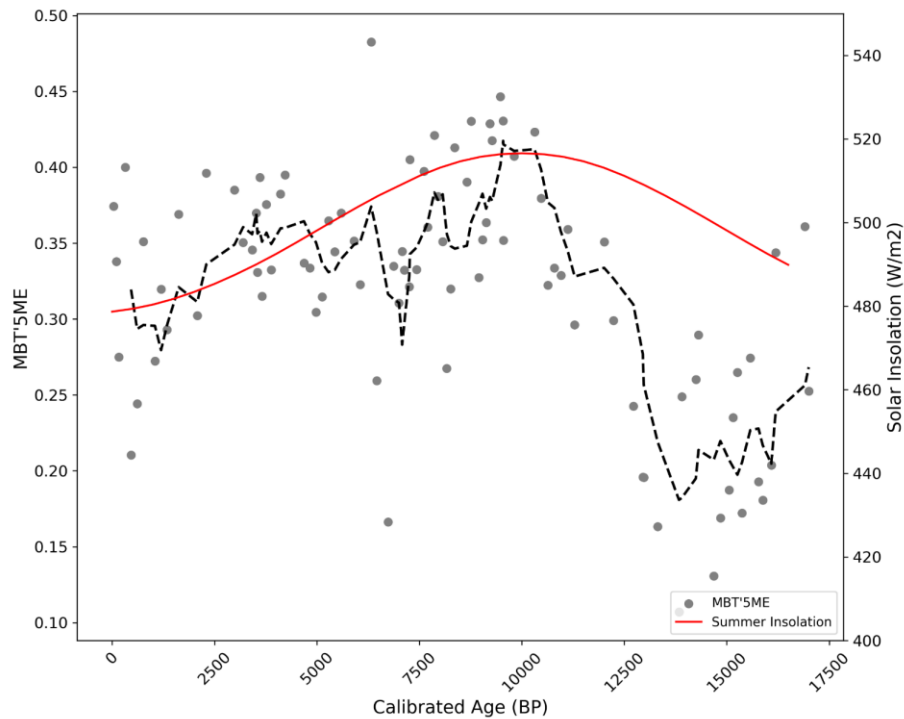


Fig. 11. Depicting the MBT'_{5ME} values of Rot21-1 sediment core against time (Cal. ^{14}C a BP), with the dashed black line representing moving average of MBT'_{5ME} . Secondary y-axis represents the solar insolation for summer at geographical position of Lake Rot (N 47° 04' 27.81"; E 08° 19' 25.77").

5. Conclusions

The analysis of temporal variations in brGDGTs within the Lake Rot sediment core has provided valuable insights into the lake's environmental history and the interdependencies of brGDGTs reflected in the paleotemperature proxy MBT'_{5ME} . The sediment core spans three distinct climate periods: the Glacial interstadial, Younger Dryas, and Holocene. Within the Holocene, variations in brGDGTs are further categorized based on the lake's mixing regime, revealing that water column stratification especially during the oligotrophic period of the Lake is recorded in the higher fractional abundance of brGDGT Ia. The provenance and environmental drivers of the sedimentary GDGTs have been identified and show a muted influence from seasonal or permanent lake water anoxia in the IR.

Generally, with the lake epilimnion showing a dependency between MBT'_{5ME} and temperature (and the lack of hypolimnion MBT'_{5ME} dependency on temperature), the concentration changes and interdependencies of brGDGTs mimic the epilimnion conditions, suggesting that coring at the oxic depth of Lake Rot proved successful for using MBT'_{5ME} as a paleothermometer. The presence of brGDGT Ia,

typical for thermally stratified summer water, further supports this observation and indicates a temperature proxy related to thermal stratification.

The implications for paleoclimate studies are significant. The development of seasonal stratification appears essential for impacting MBT'_{5ME} values. Nevertheless, with the majority of brGDGT Ia falling within intermediate values, a dominant mixing water column fingerprint is observed for much of the Holocene climate. The observed variability in MBT'_{5ME} further closely tracks changes in summer solar insolation, highlighting the influence of insolation on lake stratification and temperature signals.

Finally, the increase in the sedimentary signal of brGDGT IIIa, a common phenomenon in lacustrine core-top sediments, is also observed for Lake Rot, but it does not persist over longer periods. This emphasizes the importance of considering this variation in core-tops, as it may not be reflective of extended time periods in paleoclimatic reconstructions.

Bibliography, Chapter 4

Bauersachs, T., Schubert, C. J., Mayr, C., Gilli, A., and Schwark, L. (2024). Branched GDGT-based temperature calibrations from Central European lakes. *Science of The Total Environment*, 906, 167724.

Bechtel, A., Smittenberg, R. H., Bernasconi, S. M., and Schubert, C. J. (2010). Distribution of branched and isoprenoid tetraether lipids in an oligotrophic and a eutrophic Swiss lake: insights into sources and GDGT-based proxies. *Organic Geochemistry*, 41(8), 822-832.

Blaauw, M., and Christen, J. A. (2011). Flexible paleoclimate age-depth models using an autoregressive gamma process.

Blaga, C. I., Reichart, G. J., Vissers, E. W., Lotter, A. F., Anselmetti, F. S., and Sinninghe Damsté, J. S. (2011). Seasonal changes in glycerol dialkyl glycerol tetraether concentrations and fluxes in a perialpine lake: Implications for the use of the TEX86 and BIT proxies. *Geochimica et Cosmochimica Acta*, 75(21), 6416-6428.

Buckles, L. K., Weijers, J. W. H., Tran, X. M., Waldron, S., and Sinninghe Damsté, J. S. (2014). Provenance of tetraether membrane lipids in a large temperate lake (Loch Lomond, UK): implications for glycerol dialkyl glycerol tetraether (GDGT)-based palaeothermometry. *Biogeosciences*, 11(19), 5539-5563.

Colcord, D. E., Pearson, A., and Brassell, S. C. (2017). Carbon isotopic composition of intact branched GDGT core lipids in Greenland lake sediments and soils. *Organic Geochemistry*, 110, 25-32.

Cuven, S., Francus, P., and Lamoureux, S. F. (2010). Estimation of grain size variability with micro-X-ray fluorescence in laminated lacustrine sediments, Cape Bounty, Canadian High Arctic. *Journal of Paleolimnology*, 44, 803-817.

De Jonge, C., Hopmans, E. C., Stadnitskaia, A., Rijpstra, W. I. C., Hofland, R., Tegelaar, E., and Sinninghe Damsté, J. S. (2013). Identification of novel penta- and hexamethylated branched glycerol dialkyl glycerol tetraethers in peat using HPLC-MS², GC-MS and GC-SMB-MS. *Organic geochemistry*, 54, 78-82.

De Jonge, C., Stadnitskaia, A., Hopmans, E. C., Cherkashov, G., Fedotov, A., and Sinninghe Damsté, J. S. (2014a). In situ produced branched glycerol dialkyl glycerol tetraethers in suspended particulate matter from the Yenisei River, Eastern Siberia. *Geochimica et Cosmochimica Acta*, 125, 476-491.

De Jonge, C., Hopmans, E. C., Zell, C. I., Kim, J. H., Schouten, S., and Sinninghe Damsté, J. S. (2014b). Occurrence and abundance of 6-methyl branched glycerol dialkyl glycerol tetraethers in soils: Implications for palaeoclimate reconstruction. *Geochimica et Cosmochimica Acta*, 141, 97-112.

De Jonge, C., Radujković, D., Sigurdsson, B. D., Weedon, J. T., Janssens, I., and Peterse, F. (2019). Lipid biomarker temperature proxy responds to abrupt shift in the bacterial community composition in geothermally heated soils. *Organic Geochemistry*, 137, 103897.

De Jonge, C., Kuramae, E. E., Radujković, D., Weedon, J. T., Janssens, I. A., and Peterse, F. (2021). The influence of soil chemistry on branched tetraether lipids in mid-and high latitude soils: Implications for brGDGT-based paleothermometry. *Geochimica et Cosmochimica Acta*, 310, 95-112.

Galaasen, E. V., Ninnemann, U.S., Irvall, N., Kleiven, H. K. F., Rosenthal, Y., Kissel, C. and Hodell, D. A., 2014. Rapid reductions in North Atlantic Deep Water during the peak of the last interglacial period. *Science*, 343(6175), pp.1129-1132.

Haas, M., Baumann, F., Castella, D., Haghipour, N., Reusch, A., Strasser, M., and Dubois, N. (2019). Roman-driven cultural eutrophication of Lake Murten, Switzerland. *Earth and Planetary Science*

Halfman, R., Lembrechts, J., Radujković, D., De Gruyter, J., Nijs, I., and De Jonge, C. (2022). Soil chemistry, temperature, and bacterial community composition drive brGDGT distributions along a subarctic elevation gradient. *Organic Geochemistry*, 163, 104346.

Hopmans, E. C., Schouten, S., and Sinninghe Damsté, J. S. (2016). The effect of improved chromatography on GDGT-based palaeoproxies. *Organic Geochemistry*, 93, 1-6.

Huguet, C., Hopmans, E. C., Febo-Ayala, W., Thompson, D. H., Sinninghe Damsté, J. S., and Schouten, S. (2006). An improved method to determine the absolute abundance of glycerol dibiphytanyl glycerol tetraether lipids. *Organic Geochemistry*, 37(9), 1036-1041.

Lattaud, J., De Jonge, C., Pearson, A., Elling, F. J., and Eglinton, T. I. (2021). Microbial lipid signatures in Arctic deltaic sediments—Insights into methane cycling and climate variability. *Organic Geochemistry*, 157, 104242.

Li, J., Pancost, R. D., Naafs, B. D. A., Yang, H., Zhao, C., and Xie, S. (2016). Distribution of glycerol dialkyl glycerol tetraether (GDGT) lipids in a hypersaline lake system. *Organic Geochemistry*, 99, 113-124.

Loomis, S. E., Russell, J. M., and Sinninghe Damsté, J. S. (2011). Distributions of branched GDGTs in soils and lake sediments from western Uganda: Implications for a lacustrine paleothermometer. *Organic Geochemistry*, 42(7), 739-751. Loomis et al., 2014a

- Loomis, S. E., Russell, J. M., Heurreux, A. M., D'Andrea, W. J., and Sinninghe Damsté, J. S. (2014a). Seasonal variability of branched glycerol dialkyl glycerol tetraethers (brGDGTs) in a temperate lake system. *Geochimica et Cosmochimica Acta*, 144, 173-187.
- Loomis, S. E., Russell, J. M., Eggermont, H., Verschuren, D., and Sinninghe Damsté, J. S. (2014b). Effects of temperature, pH and nutrient concentration on branched GDGT distributions in East African lakes: Implications for paleoenvironmental reconstruction. *Organic Geochemistry*, 66, 25-37.
- Lotter, A. F., and Zbinden, H. (1989). Late-Glacial pollen analysis, oxygen-isotope record, and radiocarbon stratigraphy from Rotsee (Lucerne), Central Swiss Plateau. *Eclogae Geologicae Helvetiae*, 82(1), 191-201.
- Makri, S., Wienhues, G., Bigalke, M., Gilli, A., Rey, F., Tinner, W., and Grosjean, M. (2021). Variations of sedimentary Fe and Mn fractions under changing lake mixing regimes, oxygenation and land surface processes during Late-glacial and Holocene times. *Science of the total environment*, 755, 143418.
- Martin, C., Menot, G., Thouveny, N., Peyron, O., Andrieu-Ponel, V., Montade, V., and Bard, E. (2020). Early Holocene thermal maximum recorded by branched tetraethers and pollen in western Europe (massif central, France). *Quaternary Science Reviews*, 228, 106109.
- Martínez-Sosa, P., Tierney, J. E., Stefanescu, I. C., Crampton-Flood, E. D., Shuman, B. N., and Routson, C. (2021). A global Bayesian temperature calibration for lacustrine brGDGTs. *Geochimica et Cosmochimica Acta*, 305, 87-105.
- Miller, D. R., Habicht, M. H., Keisling, B. A., Castañeda, I. S., and Bradley, R. S. (2018). A 900-year New England temperature reconstruction from in situ seasonally produced branched glycerol dialkyl glycerol tetraethers (brGDGTs). *Climate of the Past*, 14(11), 1653-1667.
- Naeher, S., Schaeffer, P., Adam, P., and Schubert, C. J. (2013). Maleimides in recent sediments—Using chlorophyll degradation products for palaeoenvironmental reconstructions. *Geochimica et Cosmochimica Acta*, 119, 248-263.
- Naeher, S., Peterse, F., Smittenberg, R. H., Niemann, H., Zigah, P. K., and Schubert, C. J. (2014). Sources of glycerol dialkyl glycerol tetraethers (GDGTs) in catchment soils, water column and sediments of Lake Rotsee (Switzerland)—Implications for the application of GDGT-based proxies for lakes. *Organic Geochemistry*, 66, 164-173.
- Norris, M. W., Turnbull, J. C., Howarth, J. D., and Vandergoes, M. J. (2020). Pretreatment of terrestrial microfossils. *Radiocarbon*, 62(2), 349-360.

- Paus, A., Hafliðason, H., Routh, J., Naafs, B. D. A., and Thoen, M. W. (2019). Environmental responses to the 9.7 and 8.2 cold events at two ecotonal sites in the Dovre mountains, mid-Norway. *Quaternary Science Reviews*, 205, 45-61.
- Pedregosa, F., Varoquaux, G., Gramfort, A., Michel, V., Thirion, B., Grisel, O., ... and Duchesnay, É. (2011). Scikit-learn: Machine learning in Python. *the Journal of machine Learning research*, 12, 2825-2830.
- Raberg, J. H., Harning, D. J., Crump, S. E., de Wet, G., Blumm, A., Kopf, S., Geirsdóttir, Á., Miller, G. H., Sepúlveda, J. (2021). Revised fractional abundances and warm-season temperatures substantially improve brGDGT calibrations in lake sediments. *Biogeosciences*, 18(12), 3579-3603.
- Ramos-Roman, M. J., De Jonge, C., Magyari, E., Veres, D., Ilvonen, L., Develle, A. L., and Seppä, H. (2022). Lipid biomarker (brGDGT)-and pollen-based reconstruction of temperature change during the Middle to Late Holocene transition in the Carpathians. *Global and Planetary Change*, 215, 103859.
- Russell, J. M., Hopmans, E. C., Loomis, S. E., Liang, J., and Sinninghe Damsté, J. S. (2018). Distributions of 5-and 6-methyl branched glycerol dialkyl glycerol tetraethers (brGDGTs) in East African lake sediment: Effects of temperature, pH, and new lacustrine paleotemperature calibrations. *Organic Geochemistry*, 117, 56-69.
- Schoon, P. L., De Kluijver, A., Middelburg, J. J., Downing, J. A., Sinninghe Damsté, J. S., and Schouten, S. (2013). Influence of lake water pH and alkalinity on the distribution of core and intact polar branched glycerol dialkyl glycerol tetraethers (GDGTs) in lakes. *Organic Geochemistry*, 60, 72-82.
- Schubert, C. J., Lucas, F. S., Durisch-Kaiser, E., Stierli, R., Diem, T., Scheidegger, O., Vazquez, F. and Müller, B., 2010. Oxidation and emission of methane in a monomictic lake (Rotsee, Switzerland). *Aquatic sciences*, 72, pp.455-466.
- Seabold, S., and Perktold, J. (2010, June). Statsmodels: Econometric and statistical modeling with python. In *Proceedings of the 9th Python in Science Conference* (Vol. 57, No. 61, pp. 10-25080).
- Sinninghe Damsté, J. S., Ossebaar, J., Abbas, B., Schouten, S., and Verschuren, D. (2009). Fluxes and distribution of tetraether lipids in an equatorial African lake: constraints on the application of the TEX86 palaeothermometer and BIT index in lacustrine settings. *Geochimica et Cosmochimica Acta*, 73(14), 4232-4249.
- Summons, R. E., Welander, P. V., and Gold, D. A. (2022). Lipid biomarkers: molecular tools for illuminating the history of microbial life. *Nature Reviews Microbiology*, 20(3), 174-185.

Stefanescu, I. C., Shuman, B. N., and Tierney, J. E. (2021). Temperature and water depth effects on brGDGT distributions in sub-alpine lakes of mid-latitude North America. *Organic Geochemistry*, 152, 104174.

Tierney, J. E., Zhu, J., King, J., Malevich, S. B., Hakim, G. J., and Poulsen, C. J. (2020). Glacial cooling and climate sensitivity revisited. *Nature*, 584(7822), 569-573.

van Bree, L.G., Peterse, F., Baxter, A.J., De Crop, W., Van Grinsven, S., Villanueva, L., Verschuren, D. and Sinninghe Damsté, J.S., 2020. Seasonal variability and sources of in situ brGDGT production in a permanently stratified African crater lake. *Biogeosciences Discussions*, 2020, pp.1-36.

Verbruggen, F., Heiri, O., Reichert, G. J., and Lotter, A. F. (2010). Chironomid $\delta^{18}\text{O}$ as a proxy for past lake water $\delta^{18}\text{O}$: a Lateglacial record from Rotsee (Switzerland). *Quaternary Science Reviews*, 29(17-18), 2271-2279.

Virtanen, P., Gommers, R., Oliphant, T. E., Haberland, M., Reddy, T., Cournapeau, D., Burovski, E., Peterson, P., Weckesser, W., Bright, J. and Van Der Walt, S. J., 2020. SciPy 1.0: fundamental algorithms for scientific computing in Python. *Nature methods*, 17(3), pp.261-272.

Von Grafenstein, U., Erlenkeuser, H., Müller, J., Jouzel, J. and Johnsen, S., 1998. The cold event 8200 years ago documented in oxygen isotope records of precipitation in Europe and Greenland. *Climate dynamics*, 14, pp.73-81.

Warden, L., Moros, M., Weber, Y., and Sinninghe Damsté, J. S. (2018). Change in provenance of branched glycerol dialkyl glycerol tetraethers over the Holocene in the Baltic Sea and its impact on continental climate reconstruction. *Organic Geochemistry*, 121, 138-154.

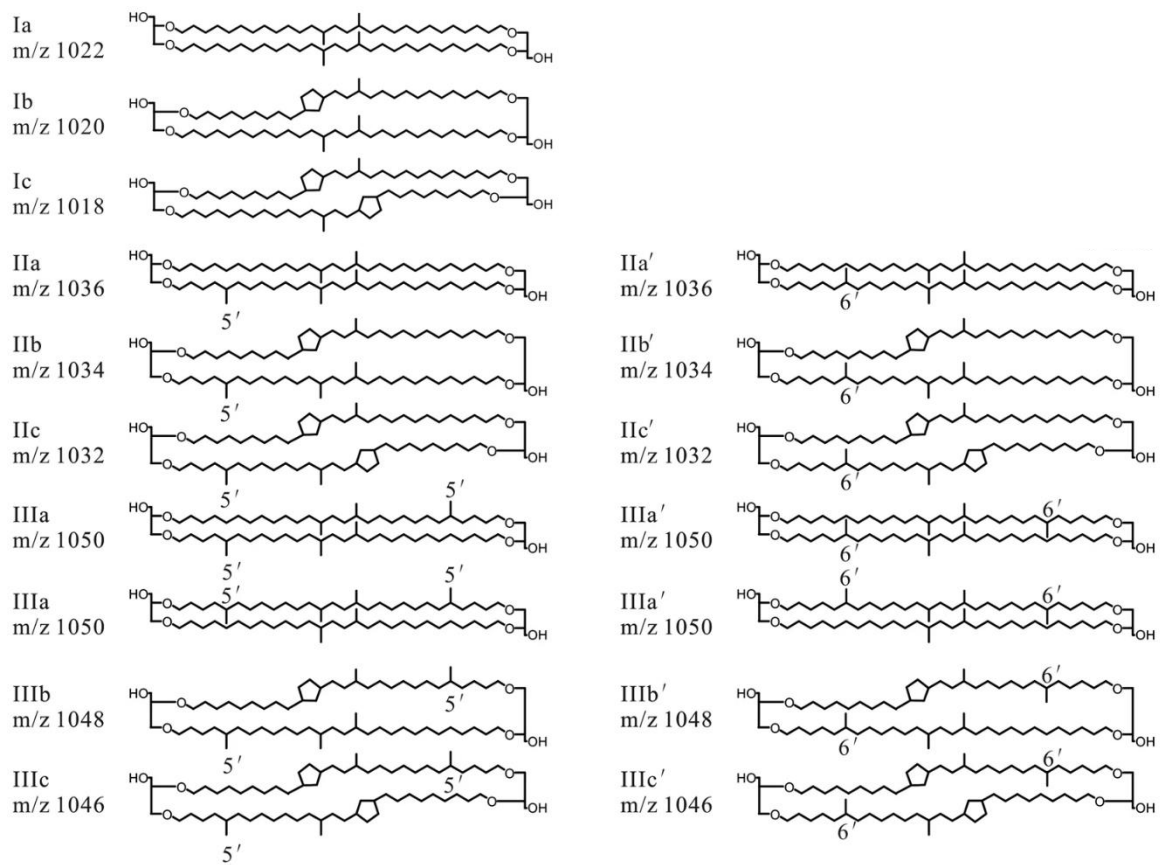
Weber, Y., Sinninghe Damsté, J.S., Zopfi, J., De Jonge, C., Gilli, A., Schubert, C.J., Lepori, F., Lehmann, M.F. and Niemann, H., 2018. Redox-dependent niche differentiation provides evidence for multiple bacterial sources of glycerol tetraether lipids in lakes. *Proceedings of the National Academy of Sciences*, 115(43), pp.10926-10931.

Wei, S., Rao, Z., Cao, J., Jia, G., Li, Y., Guo, H., Feng, Z., Guang, K., Qin, Q., Tian, Y. and Li, J., 2023. Holocene warming trend based on peat brGDGTs records from southeastern humid to northwestern arid China. *Palaeogeography, Palaeoclimatology, Palaeoecology*, 619, p.111528.

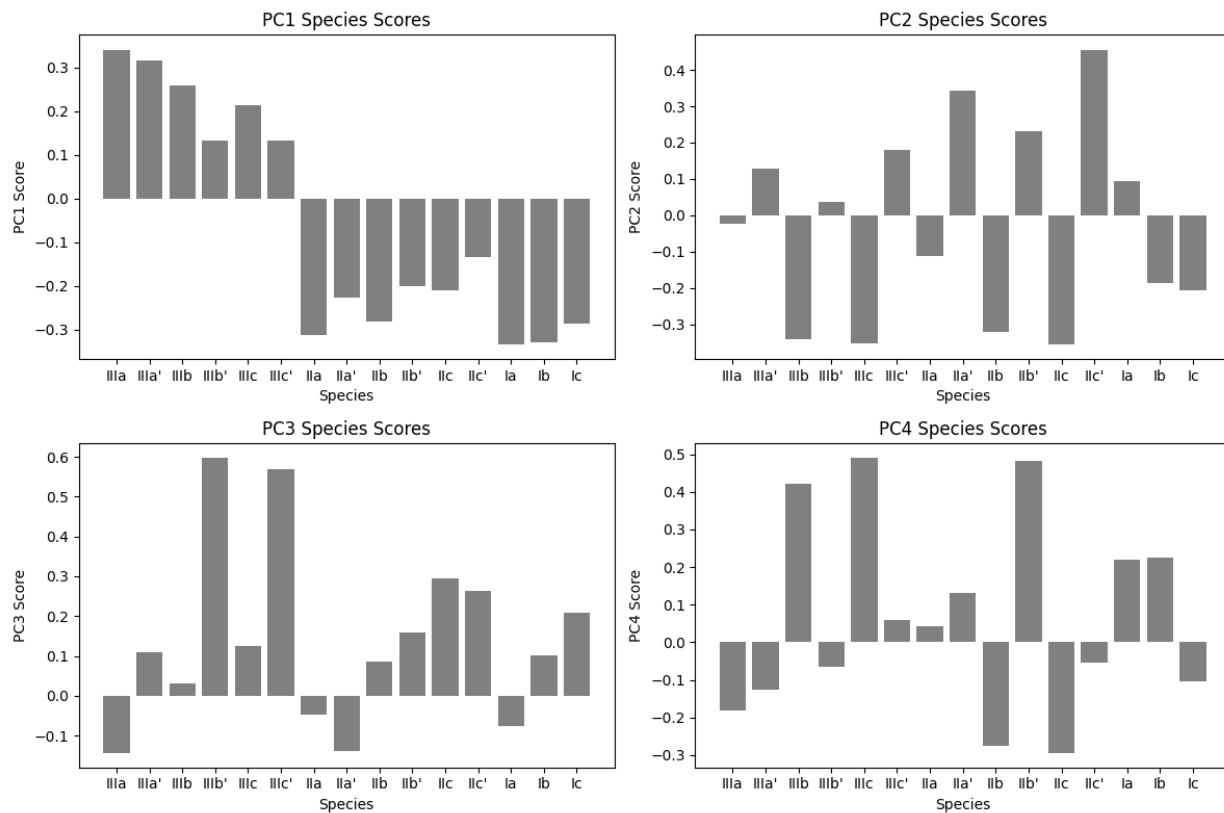
Weijers, J.W., Schouten, S., Hopmans, E.C., Geenevasen, J.A., David, O.R., Coleman, J.M., Pancost, R.D. and Sinninghe Damsté, J.S., 2006. Membrane lipids of mesophilic anaerobic bacteria thriving in peats have typical archaeal traits. *Environmental Microbiology*, 8(4), pp.648-657.

- Weijers, J. W., Schouten, S., van den Donker, J. C., Hopmans, E. C., and Sinninghe Damsté, J. S. (2007a). Environmental controls on bacterial tetraether membrane lipid distribution in soils. *Geochimica et Cosmochimica Acta*, 71(3), 703-713.
- Weijers, J. W., Schefuß, E., Schouten, S., and Sinninghe Damsté, J. S. (2007b). Coupled thermal and hydrological evolution of tropical Africa over the last deglaciation. *Science*, 315(5819), 1701-1704.
- Wilcox, P. S., Honiat, C., Trüssel, M., Edwards, R. L., and Spötl, C. (2020). Exceptional warmth and climate instability occurred in the European Alps during the Last Interglacial period. *Communications Earth and Environment*, 1(1), 57. Yao et al., 2020
- Woltering, M., Werne, J. P., Kish, J. L., Hicks, R., Sinninghe Damsté, J. S., and Schouten, S. (2012). Vertical and temporal variability in concentration and distribution of thaumarchaeotal tetraether lipids in Lake Superior and the implications for the application of the TEX86 temperature proxy. *Geochimica et Cosmochimica Acta*, 87, 136-153.
- Yang, H., Lü, X., Ding, W., Lei, Y., Dang, X., and Xie, S. (2015). The 6-methyl branched tetraethers significantly affect the performance of the methylation index (MBT') in soils from an altitudinal transect at Mount Shennongjia. *Organic Geochemistry*, 82, 42-53.
- Yao, Y., Zhao, J., Vachula, R. S., Werne, J. P., Wu, J., Song, X., and Huang, Y. (2020). Correlation between the ratio of 5-methyl hexamethylated to pentamethylated branched GDGTs (HP5) and water depth reflects redox variations in stratified lakes. *Organic Geochemistry*, 147, 104076.
- Zhao, B., Castañeda, I. S., Bradley, R. S., Salacup, J. M., de Wet, G. A., Daniels, W. C., and Schneider, T. (2021). Development of an in situ branched GDGT calibration in Lake 578, southern Greenland. *Organic Geochemistry*, 152, 104168.
- Zhao, B., Russell, J.M., Tsai, V.C., Blaus, A., Parish, M.C., Liang, J., Wilk, A., Du, X. and Bush, M.B., 2023. Evaluating global temperature calibrations for lacustrine branched GDGTs: Seasonal variability, paleoclimate implications, and future directions. *Quaternary Science Reviews*, 310, p.108124.

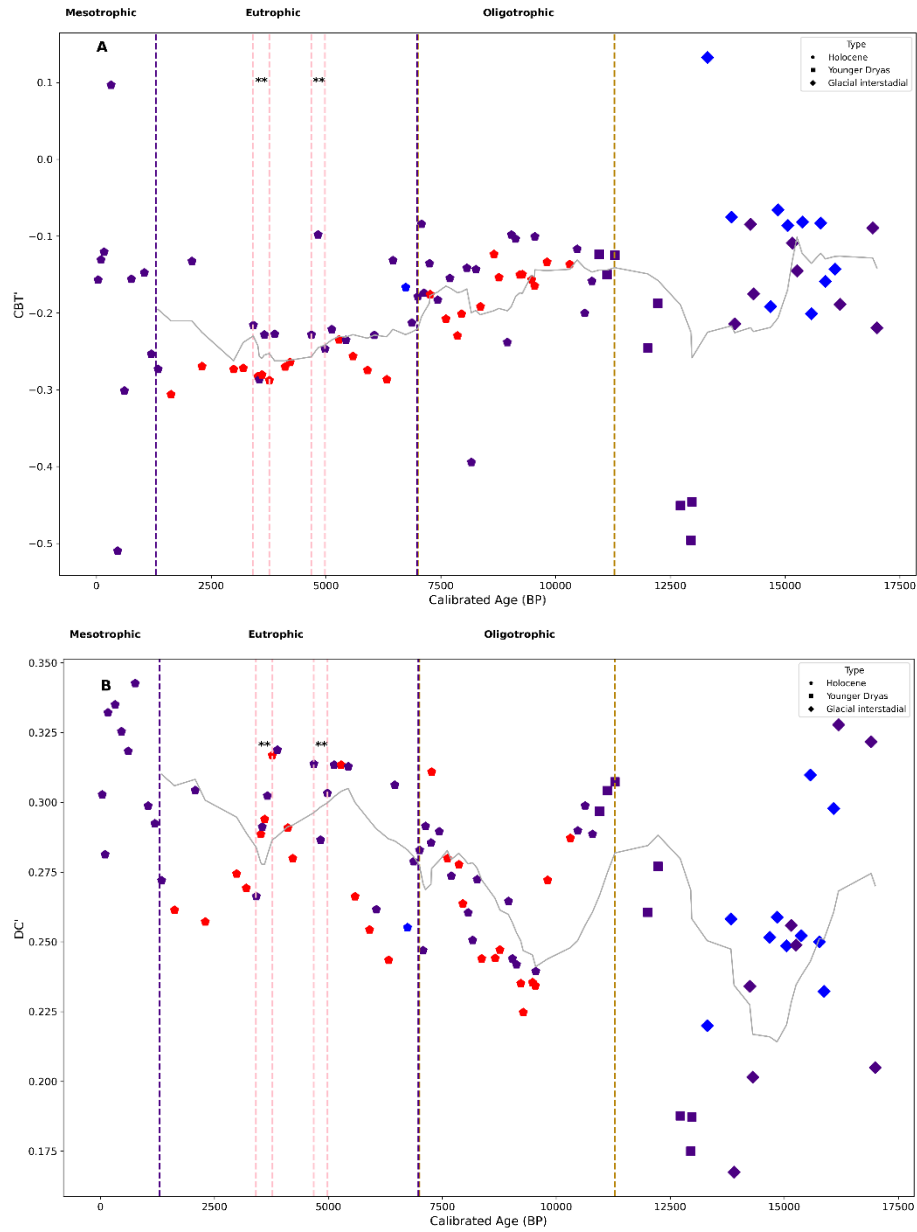
Supplementary materials, Chapter 4



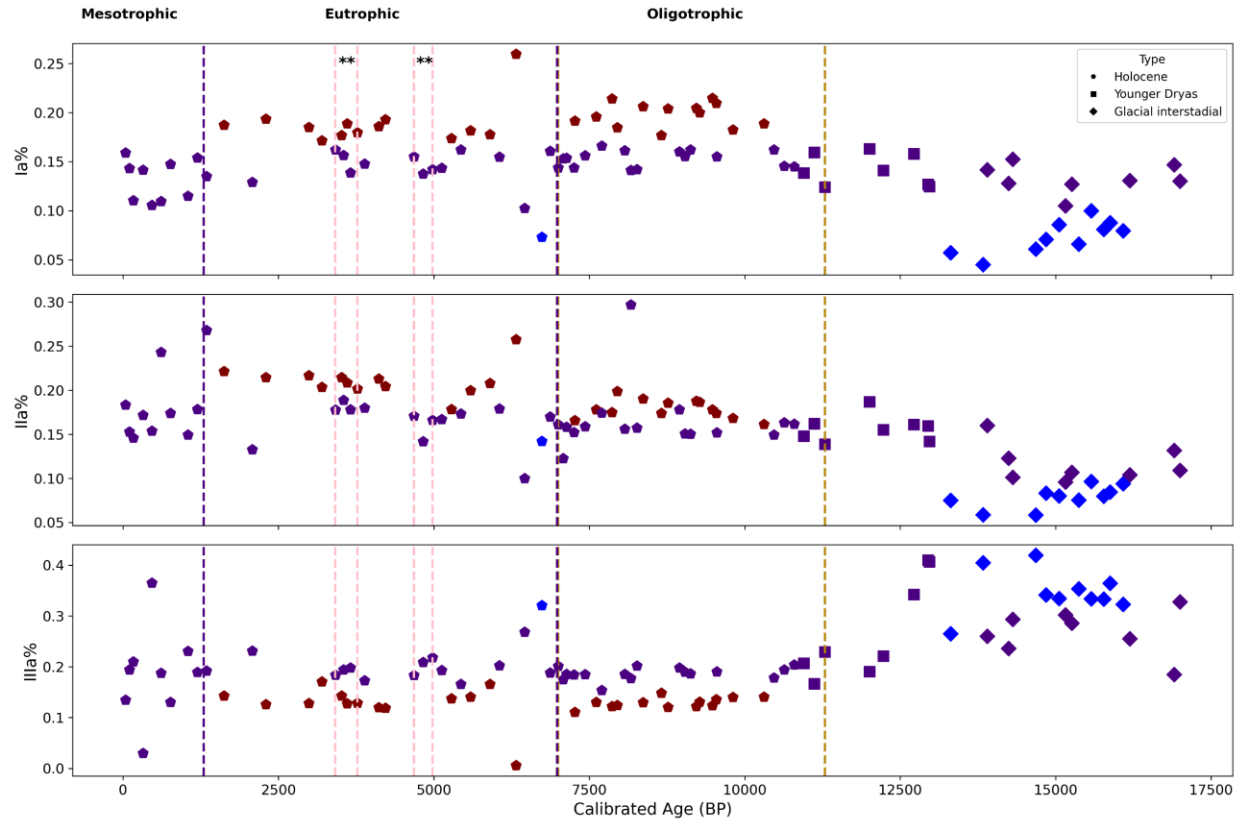
Supp. Fig. S1: The structural diversity of brGDGTs (De Jonge et al., 2014).



Supp. Fig. S2: The scores on principal component (PC) 1-4, based on an unconstrained principal component analysis based on standardized brGDGT fractional abundances.



Supp. Fig. S3: Variability of brGDGT ratios (A) CBT' and (B) DC' through time in the sediment core Rot 21-1. The symbols represent the climate zones (Holocene, Younger Dryas and Glacial Interstadial) while the colors denote the classification of samples based on their fractional abundance of brGDGT Ia (Ia%) values (blue: Ia% < 0.10, purple: 0.10 < Ia% < 0.17, red: Ia% > 0.17).



Supp. Fig. S4: Fractional abundance of brGDGTs Ia, IIa and IIIa through time in Lake Rot sediments (blue: $Ia\% < 0.10$, purple: $0.10 < Ia\% < 0.17$, red: $Ia\% > 0.17$).

Depth (cm blf)	Sediment type	Calibrated Age (14C age BP)	BrGDGTs (%)														Σ brGDGTs µg/g TOC	
			Ia	Ib	Ic	Ila	Ila'	Ilb	Ilb'	Ilc	Ilc'	IIla	IIla'	IIlb	IIlb'	IIlc		IIlc'
19.3	Lacustrine	38	0.16	0.07	0.02	0.18	0.14	0.09	0.04	0.01	b.d.l.	0.13	0.12	0.01	0.01	b.d.l.	b.d.l.	23.78
29.3	Lacustrine	101	0.14	0.06	0.02	0.15	0.13	0.07	0.04	0.01	b.d.l.	0.19	0.17	0.01	0.01	b.d.l.	b.d.l.	14.40
39.3	Lacustrine	165	0.11	0.05	0.01	0.15	0.10	0.09	0.04	0.02	b.d.l.	0.21	0.18	0.01	0.01	b.d.l.	b.d.l.	6.00
59.3	Lacustrine	320	0.14	0.07	0.02	0.17	0.13	0.11	0.04	0.03	b.d.l.	0.03	0.22	0.02	0.01	b.d.l.	b.d.l.	6.69
69.3	Lacustrine	462	0.11	0.05	0.01	0.15	0.10	0.10	0.03	0.02	b.d.l.	0.36	0.05	0.01	0.01	b.d.l.	b.d.l.	4.22
79.3	Lacustrine	611	0.11	0.05	0.01	0.24	0.04	0.10	0.03	0.02	b.d.l.	0.19	0.18	0.01	0.01	b.d.l.	b.d.l.	34.93
89.3	Lacustrine	763	0.15	0.07	0.02	0.17	0.12	0.11	0.04	0.03	b.d.l.	0.13	0.11	0.02	0.01	0.01	b.d.l.	192.93
109.3	Lacustrine	1044	0.12	0.05	0.01	0.15	0.10	0.08	0.03	0.01	b.d.l.	0.23	0.20	0.01	0.01	b.d.l.	b.d.l.	34.33
119.8	Lacustrine	1195	0.15	0.06	0.01	0.18	0.12	0.10	0.03	0.02	b.d.l.	0.19	0.12	0.01	0.01	b.d.l.	b.d.l.	33.08
129.8	Lacustrine	1341	0.14	0.05	0.01	0.27	0.06	0.01	0.11	0.01	b.d.l.	0.19	0.13	0.01	0.01	b.d.l.	b.d.l.	158.43
149.8	Lacustrine	1625	0.19	0.07	0.02	0.22	0.12	0.09	0.03	0.01	b.d.l.	0.14	0.09	0.01	0.01	b.d.l.	b.d.l.	62.13
179.8	Lacustrine	2079	0.13	0.05	0.01	0.13	0.13	0.07	0.04	0.01	b.d.l.	0.23	0.17	0.01	0.01	b.d.l.	b.d.l.	13.13
189.8	Lacustrine	2299	0.19	0.07	0.02	0.21	0.13	0.08	0.03	0.01	b.d.l.	0.13	0.10	0.01	0.01	b.d.l.	b.d.l.	73.12
219.8	Lacustrine	2988	0.19	0.08	0.02	0.22	0.12	0.09	0.03	0.01	b.d.l.	0.13	0.10	0.01	0.01	b.d.l.	b.d.l.	65.40
229.8	Lacustrine	3198	0.17	0.06	0.02	0.20	0.10	0.08	0.03	0.01	b.d.l.	0.17	0.13	0.01	0.01	b.d.l.	b.d.l.	10.44
239.8	Lacustrine	3417	0.16	0.06	0.02	0.18	0.11	0.08	0.03	0.01	b.d.l.	0.18	0.15	0.01	0.01	b.d.l.	b.d.l.	22.84
249.8	Lacustrine	3517	0.18	0.07	0.02	0.21	0.11	0.09	0.04	0.01	b.d.l.	0.14	0.09	0.01	0.01	b.d.l.	b.d.l.	5.04
253.4	Lacustrine	3547.5	0.16	0.07	0.02	0.19	0.10	0.08	0.03	0.02	b.d.l.	0.19	0.12	0.01	0.01	b.d.l.	b.d.l.	25.27
259.8	Lacustrine	3604	0.19	0.08	0.02	0.21	0.11	0.09	0.04	0.02	b.d.l.	0.13	0.09	0.01	0.01	b.d.l.	b.d.l.	13.21
266.1	Lacustrine	3659	0.14	0.07	0.02	0.18	0.10	0.08	0.03	0.02	b.d.l.	0.20	0.15	0.01	0.01	b.d.l.	b.d.l.	40.47
278.8	Lacustrine	3767	0.18	0.08	0.02	0.20	0.11	0.10	0.04	0.03	b.d.l.	0.13	0.08	0.01	0.01	b.d.l.	b.d.l.	9.54
291.6	Lacustrine	3883	0.15	0.07	0.02	0.18	0.10	0.09	0.04	0.02	b.d.l.	0.17	0.13	0.01	0.01	b.d.l.	b.d.l.	8.63
307.2	Lacustrine	4111	0.19	0.08	0.02	0.21	0.11	0.09	0.04	0.02	b.d.l.	0.12	0.09	0.01	0.01	b.d.l.	b.d.l.	63.70
313.9	Lacustrine	4218	0.19	0.08	0.02	0.20	0.12	0.09	0.04	0.02	b.d.l.	0.12	0.09	0.01	0.01	b.d.l.	b.d.l.	114.49
345.3	Lacustrine	4681	0.15	0.07	0.01	0.17	0.10	0.09	0.04	0.02	b.d.l.	0.18	0.13	0.01	0.01	b.d.l.	b.d.l.	13.84
355.3	Lacustrine	4828	0.14	0.06	0.01	0.14	0.13	0.05	0.06	b.d.l.	b.d.l.	0.21	0.18	0.01	0.01	b.d.l.	b.d.l.	31.82
365.3	Lacustrine	4976	0.14	0.06	0.01	0.17	0.10	0.08	0.04	0.02	b.d.l.	0.22	0.14	0.01	0.01	b.d.l.	b.d.l.	8.93
375.3	Lacustrine	5125	0.14	0.06	0.01	0.17	0.11	0.09	0.04	0.03	b.d.l.	0.19	0.13	0.01	0.01	b.d.l.	b.d.l.	70.53
385.3	Lacustrine	5280	0.17	0.07	0.02	0.18	0.13	0.10	0.04	0.04	b.d.l.	0.14	0.09	0.01	0.01	b.d.l.	b.d.l.	80.95
394.8	Lacustrine	5435	0.16	0.07	0.01	0.17	0.12	0.10	0.04	0.03	b.d.l.	0.17	0.10	0.01	0.01	b.d.l.	b.d.l.	53.89
404.8	Lacustrine	5587	0.18	0.07	0.01	0.20	0.14	0.09	0.03	0.02	b.d.l.	0.14	0.09	0.01	0.01	b.d.l.	b.d.l.	4.48
424.8	Lacustrine	5903	0.18	0.06	0.01	0.21	0.13	0.07	0.04	0.01	b.d.l.	0.17	0.10	0.01	0.01	b.d.l.	b.d.l.	2.79
434.8	Lacustrine	6051	0.15	0.06	0.01	0.18	0.13	0.07	0.04	0.01	b.d.l.	0.20	0.13	0.01	0.01	b.d.l.	b.d.l.	68.44
454.8	Lacustrine	6322	0.26	0.08	0.01	0.26	0.19	0.10	0.05	0.02	b.d.l.	0.01	0.01	0.01	0.01	b.d.l.	b.d.l.	0.07
464.8	Lacustrine	6459	0.10	0.04	b.d.l.	0.10	0.08	0.04	0.04	b.d.l.	b.d.l.	0.27	0.22	0.06	0.00	0.03	b.d.l.	5.66
484.8	Lacustrine	6734	0.07	0.03	0.01	0.14	0.09	0.05	0.03	0.01	b.d.l.	0.32	0.23	0.01	0.01	b.d.l.	b.d.l.	6.31
494.8	Lacustrine	6869	0.16	0.06	0.01	0.17	0.11	0.08	0.03	0.02	b.d.l.	0.19	0.15	0.01	0.01	b.d.l.	b.d.l.	16.81
504.8	Lacustrine	7000	0.14	0.05	0.01	0.16	0.11	0.08	0.04	0.02	b.d.l.	0.20	0.16	0.01	0.01	b.d.l.	b.d.l.	2.59
511.2	Lacustrine	7078	0.15	0.05	0.01	0.12	0.19	0.10	0.01	0.02	b.d.l.	0.18	0.15	0.01	0.01	b.d.l.	b.d.l.	7.30
514.8	Lacustrine	7132	0.15	0.06	0.01	0.16	0.12	0.08	0.04	0.02	b.d.l.	0.19	0.14	0.01	0.01	b.d.l.	b.d.l.	28.06
523.9	Lacustrine	7253	0.14	0.05	0.01	0.15	0.12	0.08	0.04	0.03	b.d.l.	0.18	0.17	0.01	0.01	b.d.l.	b.d.l.	78.98
524.8	Lacustrine	7266	0.19	0.07	0.02	0.17	0.13	0.10	0.05	0.04	b.d.l.	0.11	0.10	0.01	0.01	b.d.l.	b.d.l.	75.36
536.6	Lacustrine	7431	0.16	0.06	0.01	0.16	0.11	0.08	0.04	0.03	b.d.l.	0.19	0.15	0.01	0.01	b.d.l.	b.d.l.	255.96
549.3	Lacustrine	7611	0.20	0.07	0.01	0.18	0.14	0.08	0.05	0.03	b.d.l.	0.13	0.10	0.01	0.01	b.d.l.	b.d.l.	12.42
558.6	Lacustrine	7697	0.17	0.06	0.01	0.17	0.13	0.07	0.05	0.02	b.d.l.	0.15	0.14	0.01	0.01	b.d.l.	b.d.l.	69.32
576.1	Lacustrine	7864	0.21	0.07	0.01	0.17	0.13	0.09	0.05	0.02	b.d.l.	0.12	0.10	0.01	0.01	b.d.l.	b.d.l.	161.28
584.6	Lacustrine	7951	0.18	0.06	0.01	0.20	0.15	0.08	0.05	0.02	b.d.l.	0.12	0.10	0.01	0.01	b.d.l.	b.d.l.	6.10
597.3	Lacustrine	8068	0.16	0.05	0.01	0.16	0.12	0.06	0.04	0.01	b.d.l.	0.19	0.17	0.01	0.01	b.d.l.	b.d.l.	9.67
607.3	Lacustrine	8167	0.14	0.05	0.01	0.30	0.03	0.07	0.04	0.01	b.d.l.	0.18	0.15	0.01	0.01	b.d.l.	b.d.l.	6.39
617.3	Lacustrine	8264	0.14	0.05	0.01	0.16	0.13	0.06	0.04	0.01	b.d.l.	0.20	0.16	0.01	0.01	b.d.l.	b.d.l.	93.38
627.3	Lacustrine	8362	0.21	0.06	0.01	0.19	0.15	0.06	0.05	0.01	b.d.l.	0.13	0.12	0.01	0.01	b.d.l.	b.d.l.	10.22
657.3	Lacustrine	8658	0.18	0.06	0.01	0.17	0.16	0.06	0.05	b.d.l.	b.d.l.	0.15	0.14	0.01	0.01	b.d.l.	b.d.l.	165.27
667.8	Lacustrine	8765	0.20	0.06	0.01	0.19	0.16	0.06	0.06	0.01	b.d.l.	0.12	0.11	0.01	0.01	b.d.l.	b.d.l.	9.26
687.8	Lacustrine	8950	0.16	0.05	0.01	0.18	0.11	0.07	0.03	0.02	b.d.l.	0.20	0.14	0.01	0.01	b.d.l.	b.d.l.	71.60
697.8	Lacustrine	9039	0.16	0.05	0.01	0.15	0.14	0.05	0.05	b.d.l.	b.d.l.	0.19	0.19	0.01	0.01	b.d.l.	b.d.l.	6.31
707.8	Lacustrine	9128	0.16	0.05	0.01	0.15	0.16	0.05	0.05	b.d.l.	b.d.l.	0.19	0.16	0.00	0.01	b.d.l.	b.d.l.	18.21
717.8	Lacustrine	9221	0.20	0.06	0.01	0.19	0.16	0.05	0.06	0.01	b.d.l.	0.12	0.12	0.01	0.01	b.d.l.	b.d.l.	139.56
723.6	Lacustrine	9275	0.20	0.06	0.01	0.19	0.18	0.05	0.06	b.d.l.	b.d.l.	0.13	0.11	0.01	0.01	b.d.l.	b.d.l.	127.69
748	Lacustrine	9477	0.21	0.06	0.01	0.18	0.17	0.05	0.06	b.d.l.	b.d.l.	0.12	0.10	0.01	0.01	b.d.l.	b.d.l.	141.02
756.7	Lacustrine	9542	0.21	0.06	0.01	0.17	0.17	0.05	0.06	b.d.l.	b.d.l.	0.14	0.11	0.01	0.01	b.d.l.	b.d.l.	17.57
757.3	Lacustrine	9549	0.16	0.05	0.01	0.15	0.16	0.05	0.05	b.d.l.	b.d.l.	0.19	0.17	b.d.l.	0.01	b.d.l.	b.d.l.	139.58
794.3	Lacustrine	9811	0.18	0.07	0.01	0.17	0.16	0.07	0.06	0.01	b.d.l.	0.14	0.12	0.01	0.01	b.d.l.	b.d.l.	233.21
844.3	Lacustrine	10309	0.19	0.07	0.01	0.16	0.16	0.06	0.07	0.01	b.d.l.	0.14	0.10	0.01	0.01	b.d.l.	b.d.l.	45.69
854.3	Lacustrine	10469	0.16	0.06	0.01	0.15	0.15	0.06	0.07	0.01	b.d.l.	0.18	0.13	0.01	0.01	b.d.l.	b.d.l.	56.47
864.3	Lacustrine	10633	0.15	0.06	0.01	0.16	0.11	0.08	0.03	0.02	b.d.l.	0.19	0.15	0.01	0.01	b.d.l.	b.d.l.	10.16
874.3	Lacustrine	10793	0.14	0.06	0.01	0.16	0.13	0.06	0.06	0.01	b.d.l.	0.20	0.15	0.01	0.01	b.d.l.	b.d.l.	46.87
884.3	Lacustrine	10953	0.14	0.06	0.01	0.15	0.13	0.06	0.05	0.01	b.d.l.	0.21	0.16	0.01	0.01	b.d.l.	b.d.l.	209.48
894.3	Lacustrine	11120	0.16	0.06	0.01	0.16	0.14	0.09	0.05	0.01	b.d.l.	0.17	0.12	0.01	0.01	b.d.l.	b.d.l.	7.81

Depth (cm blf)	Sediment type	Calibrated Age (¹⁴ C age BP)	BrGDGTs (%)															Σ brGDGTs μg/g TOC
			Ia	Ib	Ic	IIa	IIa'	IIb	IIb'	IIc	IIc'	IIIa	IIIa'	IIIb	IIIb'	IIIc	IIIc'	
904.3	Peat	11288	0.12	0.05	0.01	0.14	0.12	0.07	0.05	0.01	b.d.l.	0.23	0.18	0.01	0.01	b.d.l.	b.d.l.	26.41
944.8	Peat	12007	0.16	0.07	0.02	0.19	0.12	0.07	0.03	0.01	b.d.l.	0.19	0.13	0.01	0.01	b.d.l.	b.d.l.	48.87
954.8	Peat	12233	0.14	0.05	0.01	0.16	0.14	0.08	0.04	0.01	b.d.l.	0.22	0.14	0.01	0.01	b.d.l.	b.d.l.	44.60
984.8	Peat	12721	0.16	0.03	b.d.l.	0.16	0.13	0.06	0.02	0.01	b.d.l.	0.34	0.08	0.01	0.01	b.d.l.	b.d.l.	40.03
994.8	Peat	12951	0.13	0.02	b.d.l.	0.16	0.10	0.05	0.01	b.d.l.	b.d.l.	0.41	0.10	0.01	b.d.l.	b.d.l.	b.d.l.	4.39
995.9	Peat	12973	0.12	0.02	b.d.l.	0.14	0.09	0.05	0.01	0.01	b.d.l.	0.41	0.13	0.01	b.d.l.	b.d.l.	b.d.l.	3.81
1005.1	Glacial clay	13311	0.06	0.01	b.d.l.	0.08	0.08	0.03	0.01	0.01	0.01	0.27	0.43	0.01	0.01	b.d.l.	b.d.l.	16.18
1014.8	Glacial clay	13833	0.05	0.01	b.d.l.	0.06	0.05	0.02	0.02	b.d.l.	b.d.l.	0.40	0.33	0.02	0.02	0.01	0.01	3.26
1015.1	Glacial clay	13901	0.14	0.02	b.d.l.	0.16	0.14	0.06	0.02	0.01	b.d.l.	0.26	0.18	0.01	0.01	b.d.l.	b.d.l.	40.61
1027.6	Glacial clay	14245	0.13	0.02	b.d.l.	0.12	0.14	0.07	0.03	0.01	b.d.l.	0.24	0.21	0.01	0.01	b.d.l.	b.d.l.	31.64
1036.4	Glacial clay	14310	0.15	0.03	b.d.l.	0.10	0.14	0.05	0.03	b.d.l.	b.d.l.	0.29	0.19	0.01	0.01	b.d.l.	b.d.l.	0.33
1072.5	Glacial clay	14682	0.06	0.02	b.d.l.	0.06	0.05	0.02	0.02	0.01	b.d.l.	0.42	0.25	0.05	0.02	0.02	0.01	13.87
1088.3	Glacial clay	14844	0.07	0.02	b.d.l.	0.08	0.08	0.03	0.03	b.d.l.	b.d.l.	0.34	0.29	0.02	0.02	b.d.l.	b.d.l.	28.88
1108.3	Glacial clay	15053	0.09	0.02	b.d.l.	0.08	0.10	0.05	0.02	b.d.l.	b.d.l.	0.33	0.28	0.02	0.01	b.d.l.	b.d.l.	53.22
1118.3	Glacial clay	15157	0.10	0.03	0.01	0.10	0.10	0.05	0.03	0.01	b.d.l.	0.30	0.24	0.02	0.01	0.01	0.01	18.48
1128.3	Glacial clay	15260	0.13	0.03	0.01	0.11	0.11	0.06	0.03	0.01	b.d.l.	0.29	0.22	0.01	0.01	b.d.l.	b.d.l.	14.01
1138.8	Glacial clay	15373	0.07	0.02	0.01	0.08	0.08	0.04	0.02	0.01	b.d.l.	0.35	0.28	0.03	0.02	0.01	b.d.l.	0.07
1158.8	Glacial clay	15573	0.10	0.06	0.02	0.10	0.08	0.04	0.03	b.d.l.	b.d.l.	0.33	0.20	0.02	0.01	0.01	b.d.l.	3.37
1178.8	Glacial clay	15774	0.08	0.02	0.01	0.08	0.08	0.04	0.02	b.d.l.	b.d.l.	0.33	0.27	0.03	0.02	0.01	0.01	2.57
1188.8	Glacial clay	15876	0.09	0.02	b.d.l.	0.08	0.09	0.04	0.02	b.d.l.	b.d.l.	0.36	0.25	0.02	0.01	0.01	b.d.l.	2.62
1208.8	Glacial clay	16086	0.08	0.04	b.d.l.	0.09	0.08	0.04	0.03	b.d.l.	b.d.l.	0.32	0.22	0.05	0.02	0.02	b.d.l.	2.04
1218.8	Glacial clay	16193	0.13	0.08	b.d.l.	0.10	0.07	0.04	0.03	b.d.l.	b.d.l.	0.26	0.21	0.05	b.d.l.	0.03	b.d.l.	0.05
1289.3	Glacial clay	16908	0.15	0.06	0.02	0.13	0.13	0.08	0.05	0.01	b.d.l.	0.18	0.16	0.01	0.01	b.d.l.	b.d.l.	16.18
1309.3	Glacial clay	17000	0.13	0.03	b.d.l.	0.11	0.10	0.03	0.02	b.d.l.	b.d.l.	0.33	0.22	0.03	b.d.l.	b.d.l.	b.d.l.	3.26

Depth (cm blf)	Sediment type	Calibrated Age					pHrec	Median MAT above 0 (°C, Martinez-Sosa et al., 2021)	MAAT (°C, Bauersachs et al., 2024)
		(14C age BP)	MBT _{SME}	IR	CBT	DC			
19.3	Lacustrine	38	0.37	0.44	-0.16	0.30	8.53	10.92	10.09
29.3	Lacustrine	101	0.34	0.46	-0.13	0.28	8.60	9.74	8.26
39.3	Lacustrine	165	0.27	0.45	-0.12	0.33	8.63	7.70	7.82
59.3	Lacustrine	320	0.40	0.64	0.10	0.34	9.21	11.75	11.41
69.3	Lacustrine	462	0.21	0.22	-0.51	0.33	7.60	5.61	5.70
79.3	Lacustrine	611	0.24	0.33	-0.30	0.32	8.15	6.71	8.23
89.3	Lacustrine	763	0.35	0.44	-0.16	0.34	8.54	10.17	10.28
109.3	Lacustrine	1044	0.27	0.44	-0.15	0.30	8.56	7.62	7.20
119.8	Lacustrine	1195	0.32	0.39	-0.25	0.29	8.28	9.15	8.43
129.8	Lacustrine	1341	0.29	0.28	-0.27	0.27	8.23	8.29	7.95
149.8	Lacustrine	1625	0.37	0.37	-0.31	0.26	8.14	10.75	9.67
179.8	Lacustrine	2079	0.30	0.45	-0.13	0.30	8.60	8.59	7.55
189.8	Lacustrine	2299	0.40	0.40	-0.27	0.26	8.24	11.63	10.38
219.8	Lacustrine	2988	0.38	0.39	-0.27	0.27	8.23	11.27	10.45
229.8	Lacustrine	3198	0.35	0.38	-0.27	0.27	8.23	10.15	9.01
239.8	Lacustrine	3417	0.35	0.42	-0.22	0.27	8.38	9.99	8.63
249.8	Lacustrine	3517	0.37	0.37	-0.28	0.29	8.20	10.78	10.19
253.4	Lacustrine	3547.5	0.33	0.37	-0.29	0.29	8.19	9.51	9.00
259.8	Lacustrine	3604	0.39	0.37	-0.28	0.29	8.21	11.54	10.79
266.1	Lacustrine	3659	0.32	0.40	-0.23	0.30	8.35	9.00	8.89
278.8	Lacustrine	3767	0.38	0.37	-0.29	0.32	8.19	10.96	10.83
291.6	Lacustrine	3883	0.33	0.40	-0.23	0.32	8.35	9.57	9.52
307.2	Lacustrine	4111	0.38	0.38	-0.27	0.29	8.23	11.19	10.59
313.9	Lacustrine	4218	0.39	0.40	-0.26	0.28	8.25	11.59	10.66
345.3	Lacustrine	4681	0.34	0.40	-0.23	0.31	8.34	9.71	9.23
355.3	Lacustrine	4828	0.33	0.47	-0.10	0.29	8.69	9.61	8.09
365.3	Lacustrine	4976	0.30	0.38	-0.25	0.30	8.30	8.66	8.20
375.3	Lacustrine	5125	0.31	0.40	-0.22	0.31	8.36	8.99	8.76
385.3	Lacustrine	5280	0.36	0.41	-0.23	0.31	8.33	10.62	10.16
394.8	Lacustrine	5435	0.34	0.40	-0.24	0.31	8.33	9.95	9.53
404.8	Lacustrine	5587	0.37	0.40	-0.26	0.27	8.27	10.78	9.85
424.8	Lacustrine	5903	0.35	0.38	-0.27	0.25	8.22	10.18	8.94
434.8	Lacustrine	6051	0.32	0.40	-0.23	0.26	8.34	9.25	8.11
454.8	Lacustrine	6322	0.48	0.42	-0.29	0.24	8.19	14.43	12.38
464.8	Lacustrine	6459	0.26	0.45	-0.13	0.31	8.60	7.20	6.26
484.8	Lacustrine	6734	0.17	0.41	-0.17	0.26	8.51	4.18	4.52
494.8	Lacustrine	6869	0.33	0.42	-0.21	0.28	8.39	9.65	8.35
504.8	Lacustrine	7000	0.31	0.43	-0.18	0.28	8.48	8.86	7.86
511.2	Lacustrine	7078	0.34	0.54	-0.08	0.25	8.73	9.96	8.29
514.8	Lacustrine	7132	0.33	0.43	-0.17	0.29	8.49	9.56	8.36
523.9	Lacustrine	7253	0.32	0.46	-0.14	0.29	8.59	9.21	8.18
524.8	Lacustrine	7266	0.41	0.46	-0.18	0.31	8.48	11.92	10.47
536.6	Lacustrine	7431	0.33	0.43	-0.18	0.29	8.46	9.57	8.35
549.3	Lacustrine	7611	0.40	0.43	-0.21	0.28	8.40	11.67	9.75
558.6	Lacustrine	7697	0.36	0.45	-0.15	0.27	8.54	10.48	8.97
576.1	Lacustrine	7864	0.42	0.44	-0.23	0.28	8.34	12.44	10.05
584.6	Lacustrine	7951	0.38	0.43	-0.20	0.26	8.42	11.13	9.60
597.3	Lacustrine	8068	0.35	0.46	-0.14	0.26	8.58	10.17	8.13
607.3	Lacustrine	8167	0.27	0.28	-0.39	0.25	7.91	7.46	8.10
617.3	Lacustrine	8264	0.32	0.45	-0.14	0.27	8.57	9.16	7.91
627.3	Lacustrine	8362	0.41	0.45	-0.19	0.24	8.44	12.17	9.30
657.3	Lacustrine	8658	0.39	0.48	-0.12	0.24	8.62	11.44	9.01
667.8	Lacustrine	8765	0.43	0.47	-0.15	0.25	8.54	12.74	9.76
687.8	Lacustrine	8950	0.33	0.40	-0.24	0.26	8.32	9.40	8.14
697.8	Lacustrine	9039	0.35	0.49	-0.10	0.24	8.69	10.21	7.89
707.8	Lacustrine	9128	0.36	0.49	-0.10	0.24	8.68	10.58	8.03
717.8	Lacustrine	9221	0.43	0.47	-0.15	0.24	8.55	12.69	9.51
723.6	Lacustrine	9275	0.42	0.48	-0.15	0.22	8.55	12.33	9.19
748	Lacustrine	9477	0.45	0.48	-0.16	0.24	8.53	13.26	9.68
756.7	Lacustrine	9542	0.43	0.47	-0.16	0.23	8.51	12.75	9.27
757.3	Lacustrine	9549	0.35	0.49	-0.10	0.24	8.68	10.19	7.95
794.3	Lacustrine	9811	0.41	0.47	-0.13	0.27	8.60	12.00	9.71
844.3	Lacustrine	10309	0.42	0.46	-0.14	0.29	8.59	12.51	10.06
854.3	Lacustrine	10469	0.38	0.46	-0.12	0.29	8.64	11.10	9.06
864.3	Lacustrine	10633	0.32	0.42	-0.20	0.30	8.42	9.24	8.69
874.3	Lacustrine	10793	0.33	0.43	-0.16	0.29	8.53	9.61	8.43
884.3	Lacustrine	10953	0.33	0.45	-0.12	0.30	8.62	9.45	8.20
894.3	Lacustrine	11120	0.36	0.45	-0.15	0.30	8.55	10.43	9.09

Depth (cm blf)	Sediment type	Calibrated Age					pHrec	Median MAT above 0	MAAT
		(14C age BP)	MBT' _{SME}	IR	CBT'	DC'		(°C, Martinez-Sosa et al., 2021)	(°C, Bauersachs et al., 2024)
904.3	Peat	11288	0.30	0.45	-0.12	0.31	8.62	8.40	7.54
944.8	Peat	12007	0.35	0.40	-0.25	0.26	8.30	10.16	9.01
954.8	Peat	12233	0.30	0.43	-0.19	0.28	8.45	8.48	7.39
984.8	Peat	12721	0.24	0.30	-0.45	0.19	7.76	6.65	4.19
994.8	Peat	12951	0.20	0.26	-0.50	0.17	7.64	5.14	3.01
995.9	Peat	12973	0.20	0.29	-0.45	0.19	7.77	5.13	2.98
1005.1	Glacial clay	13311	0.16	0.60	0.13	0.22	9.30	4.08	4.52
1014.8	Glacial clay	13833	0.11	0.45	-0.08	0.26	8.75	2.26	2.38
1015.1	Glacial clay	13901	0.25	0.43	-0.21	0.17	8.38	6.86	4.80
1027.6	Glacial clay	14245	0.26	0.50	-0.08	0.23	8.73	7.22	5.41
1036.4	Glacial clay	14310	0.29	0.45	-0.18	0.20	8.49	8.18	4.89
1072.5	Glacial clay	14682	0.13	0.38	-0.19	0.25	8.44	3.03	2.48
1088.3	Glacial clay	14844	0.17	0.47	-0.07	0.26	8.78	4.27	3.82
1108.3	Glacial clay	15053	0.19	0.47	-0.09	0.25	8.72	4.86	3.82
1118.3	Glacial clay	15157	0.24	0.46	-0.11	0.26	8.66	6.41	4.89
1128.3	Glacial clay	15260	0.26	0.45	-0.15	0.25	8.57	7.38	5.34
1138.8	Glacial clay	15373	0.17	0.45	-0.08	0.25	8.73	4.37	3.51
1158.8	Glacial clay	15573	0.27	0.39	-0.20	0.31	8.42	7.68	6.46
1178.8	Glacial clay	15774	0.19	0.46	-0.08	0.25	8.73	5.04	4.02
1188.8	Glacial clay	15876	0.18	0.43	-0.16	0.23	8.53	4.65	3.55
1208.8	Glacial clay	16086	0.20	0.42	-0.14	0.30	8.57	5.39	5.27
1218.8	Glacial clay	16193	0.34	0.44	-0.19	0.33	8.45	9.93	8.95
1289.3	Glacial clay	16908	0.36	0.48	-0.09	0.32	8.71	10.49	8.93
1309.3	Glacial clay	17000	0.25	0.42	-0.22	0.20	8.37	6.98	4.62

Supp. Table S1. Fractional abundance (%) and concentration of brGDGTs. BrGDGT ratios MBT'_{SME}, IR, CBT' and DC', and derived reconstructed pH and reconstructed temperature (Trec) values.

Correlation matrix for brGDGT concentrations of Rot21-1-core						
	<i>IIIa</i>	<i>IIIa'</i>	<i>IIa</i>	<i>IIa'</i>	<i>IIb</i>	<i>IIb'</i>
<i>IIIa'</i>	0.95					
<i>IIa</i>	0.84	0.82				
<i>IIa'</i>	0.85	0.84	0.97			
<i>IIb</i>	0.86	0.84	0.96	0.94		
<i>IIb'</i>	0.81	0.81	0.93	0.96	0.90	
<i>Ia</i>	0.82	0.80	0.99	0.99	0.95	0.94

Correlation matrix for brGDGT fractional abundances of Rot21-1-core						
	<i>IIIa</i>	<i>IIIa'</i>	<i>IIa</i>	<i>IIa'</i>	<i>IIb</i>	<i>IIb'</i>
<i>IIIa'</i>	0.60					
<i>IIa</i>	-0.73	-0.77				
<i>IIa'</i>	-0.58	-0.50	0.22			
<i>IIb</i>	-0.63	-0.60	0.55	0.27		
<i>IIb'</i>	-0.59	-0.41	0.46	0.36	0.02	
<i>Ia</i>	-0.83	-0.83	0.72	0.71	0.49	0.51

Supp. Table S2. Correlation matrix for brGDGT concentrations and fractional abundances of Rot 21-1 core. Significant Pearson correlations (p -values < 0.005) are presented in bold type.

Chapter 5

Conclusion

The brGDGT-based ratio MBT'_{5ME} has been used in soil and lake systems around the world as a tool to quantify mean annual temperature changes through time. In both soils and lakes, the dependency of MBT'_{5ME} with temperature has been determined based on variation in brGDGT distribution on a large geographical scale and associated large temperature gradient. As soils and lakes generally have a different brGDGT distribution (Fig. 1), lake-specific temperature calibrations needed to be developed.

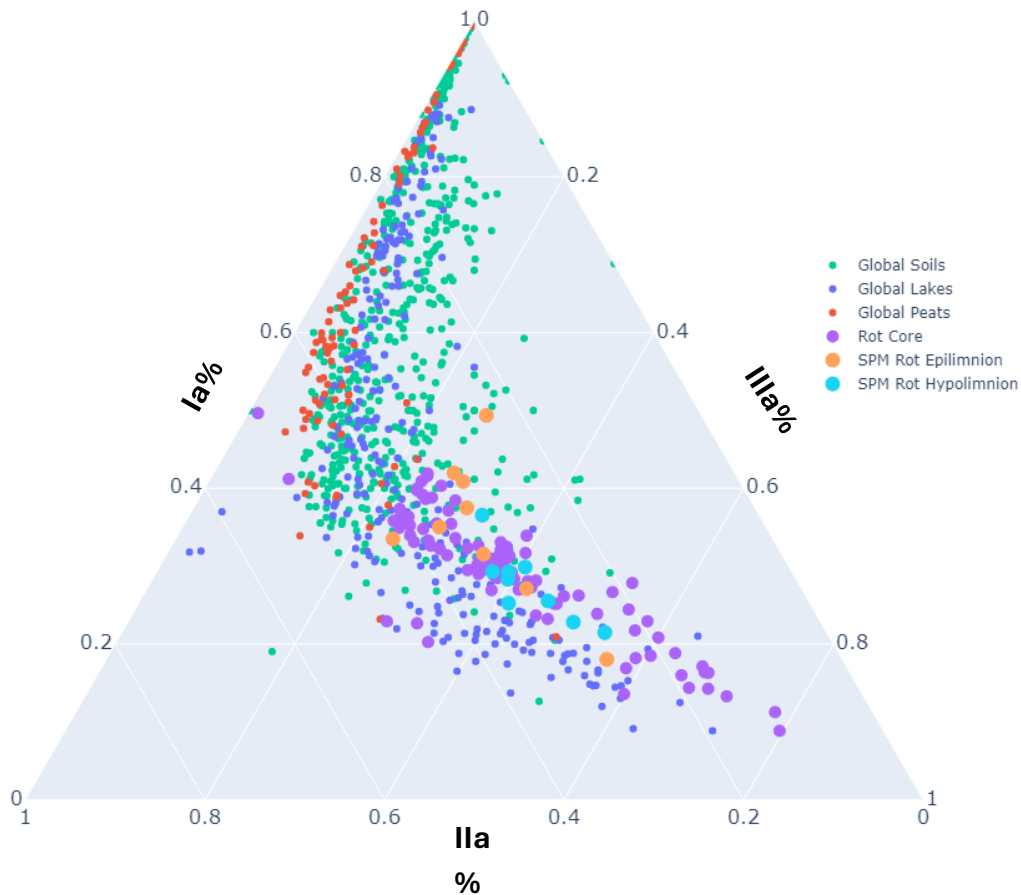


Fig. 1. Ternary plot of globally distributed soils, peats, and lakes, with samples from Chapter 3 and 4 indicated.

For the development of a temperature calibration with the MBT'_{5ME} (De Jonge et al., 2014), a dataset of 65 East-African lakes along an altitudinal mean annual air temperature (MAT) gradient was first used (Russell

at al., 2018). While this dataset allowed to develop a lake calibration with a RSME of 2.44 °C across a temperature range of 1.6 to 26.8 °C, it shows limitations when applied to lakes in different settings. For instance, Ethiopian highland lakes show an increased production of IIIa' in surface sediments (Bittner et al., 2021). Furthermore, lakes at lower latitudes show more pronounced seasonality and lake freezing during winter times, impacting the yearly range in water temperature and the decoupling of water temperatures with measured air temperature, respectively. Moreover, at higher latitudes thermal stratification during summer leads to the development of a thermally isolated, colder hypolimnion, potentially convoluting the MBT'_{SME} signal deposited into lake sediments. To address this issue, additional local (Dang et al., 2018) and global calibrations have been developed (Martinez-Sosa et al., 2021; Raberg et al., 2021). However, as these calibrations still reflect a large residual error (1.97-2.7 °C), the impact of temperature on GDGTs within a single lake system still warrants additional attention.

In addition to the MBT'_{SME}, the IR values from lake sediments on a global scale, have also been observed to respond to temperature (Martinez-Sosa et al., 2020, 2021). The substantial variation in lacustrine IR values (Fig. 2), correlates with MBT'_{SME} ($r= 0.64$, $p< 0.0001$) and reported MAT of global lakes ($r= 0.54$, $p< 0.0001$). Although not generally used as a temperature proxy, lacustrine IR can be proposed as a temperature proxy, supported by the significant correlation observed exclusively in lake settings (Fig. 2). While a weak correlation in global soils still exists between MBT'_{SME} and IR ($r^2= 0.01$, $p< 0.05$), a more robust dependency is observed only in lakes ($r^2= 0.41$).

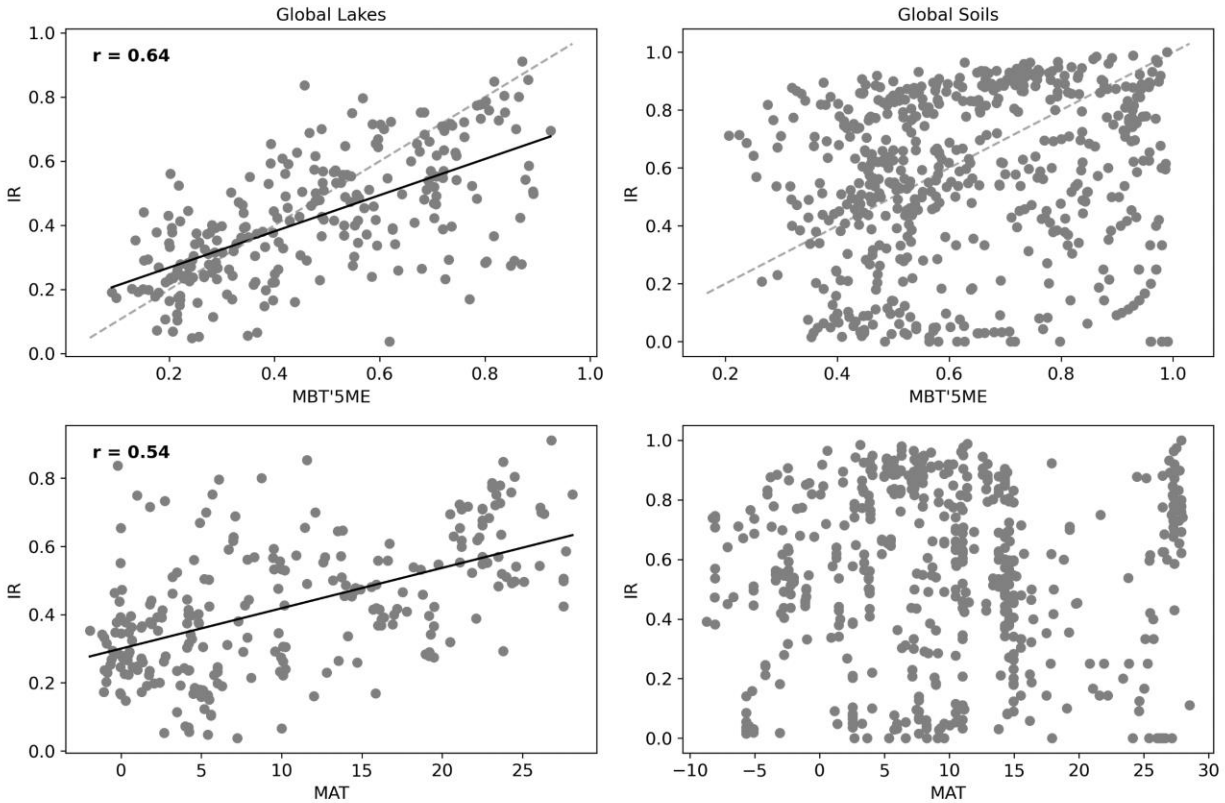


Fig. 2. The dependency between MBT'_{5ME} and IR in global lake and soil systems). Regression and 1:1 line plotted (black and dashed grey, respectively). Data credit (Crampton-Flood et al., 2020; Martinez-Sosa et al., 2021).

In order for paleoclimate records, that are formed within individual lake systems, to reflect temperature change, the current assumption is that the temperature dependencies observed on the global scale also act on single lake systems. To test this assumption both experimental and environmental studies on the drivers of brGDGTs have been performed on this scale. Initial mesocosm approaches to determine the effect of warming on the MBT'_{5ME} were pioneered by Martinez-Sosa et al. (2019, 2020), where in addition to the correlation between MBT'_{5ME} and temperature, a dependency between IR and temperature was observed as well. However, in-situ analyses of GDGTs in the lake water column performed by Van Bree et al. (2021; Lake Challa) and Zhao et al. (2021; Lake 578, Greenland) yielded different results. While MBT'_{5ME} correlated with temperature (Van Bree et al., 2020) and summer water temperatures (Zhao et al., 2021), IR did not show a response to temperature in either site.

In this study, we explored the temperature dependency of MBT'_{5ME} through three distinct approaches spanning different timescales: first, to observe the short-term response of MBT'_{5ME} to warmings and coolings, we utilized a mesocosm approach in both a lake and river system (Lake Rot and Sihl River, discussed in Chapter 2); next, we investigated the temperature response of brGDGTs within a single lake

(Lake Rot, detailed in Chapter 3) over different seasons for a year; and finally, we examined the downcore variability of brGDGTs within the context of a broader Holocene multi-proxy investigation (Chapter 4).

In Chapter 2, the temperature sensitivity of brGDGTs in different seasons, and their potential use as paleotemperature proxies were investigated. For this aim, surface water from Lake Rot and Sihl River was collected in spring, summer and autumn of 2021 and subjected to different temperature treatments, including control, warming, and cooling conditions. Because of the observed low concentrations, brGDGTs were analyzed as a combined core lipid and intact polar lipid fractions. The mesocosm setup, although informative, could not perfectly replicate natural conditions due to the presence of the so-called bottle effect, which impacted water chemistry and the bacterial community composition, also in control incubations. These factors introduced complexities and limitations that must be considered in future incubation setups.

Concerning the temperature proxy MBT'_{5ME} , a subtle increase in response to warming temperatures was observed, while its sensitivity to cold temperatures appeared muted. This suggests that MBT'_{5ME} may be more suited for capturing variations in warmer conditions rather than colder ones. Furthermore, the mesocosm experiment indicated that water chemistry variables exert an influence on other GDGT ratios, particularly the isomer ratio of brGDGTs (IR) in riverine systems. Nevertheless, despite the complexities that are associated with employing mesocosms, temperature remained the primary driver behind changes in brGDGT distribution. Thus, the continued use of MBT'_{5ME} as indicator of paleotemperature was proposed.

To further confirm the temperature sensitivity of MBT'_{5ME} , the study extended its investigation to the water column of Lake Rot, a freshwater system known for experiencing seasonal stratification (Chapter 3). This examination allowed to explore of the brGDGT response to both changes in temperature and dissolved oxygen. Building upon the insights gained from the mesocosm experiments in freshwater systems, both abiotic and biotic drivers influencing the production of core (CL), and intact polar (IPL) brGDGTs in the water column of Lake Rot were examined. Seasonal temperature fluctuations and stratification in Lake Rot led to variable brGDGT concentrations and distributions. Significant changes were observed in both bacterial community composition and brGDGT concentration during the stratified summer months when the epilimnion warmed and hypolimnion anoxia developed. BrGDGT Ia was found to respond to warmer temperatures in the stratified epilimnion of Lake Rot, while brGDGT IIIa dominated in colder and/or deeper waters. The temperature-sensitive production of CL brGDGT Ia became evident during the warm stratified summer months, supporting its role as a temperature indicator. However, the study also highlighted the influence of lake water column mixing on brGDGT distribution, with shifts in the distribution of brGDGTs in autumn caused by the upwelling of hypolimnion brGDGT distribution, rather than a significant decrease

in the brGDGT Ia. As a result, the MBT'_{5ME} showed a weak dependency with water temperature ($r= 0.59$, $p= 0.10$). The IR on the other hand, driven by a temperature dependent increase of brGDGT Ila' and IIIa' showed an excellent correlation with water temperature ($r= 0.68$, $p< 0.05$). In the hypolimnion, the production of IPL brGDGTs was limited to anoxic conditions, emphasizing the role of anoxia as a key trigger for in-situ IPL brGDGT production. Moreover, the identified specific bacterial taxa associated with the production of brGDGTs in both the epilimnion and hypolimnion, shed more light on potential brGDGT producers. The limited response of epilimnion water mesocosms of Lake Rot to cooling, along with the lack of a pronounced response to cooling temperatures observed in the mesocosms aligns with the observations in Chapter 3, emphasizing the limited sensitivity of MBT'_{5ME} to colder conditions. Furthermore, the selective increase of MBT'_{5ME} only in certain mesocosm setups strengthens the argument for the importance of bacterial community change following thermal stratification.

To determine which brGDGT signal is deposited to the sediments, two surface sediment samples, exposed to "oxic" and "seasonally anoxic" water column conditions were also analyzed. These sediments are characterized by in-situ produced brGDGTs and exhibit varying MBT'_{5ME} signals. Chapter 3 suggests that MBT'_{5ME} and IR ratio values have the potential to serve as a temperature indicator, particularly in sediments that do not receive brGDGTs produced in the thermally isolated hypolimnion. As such, more shallow sediments where a dominant signal of a stratified epilimnion is deposited are preferred. On the other hand, the observed sedimentary production of brGDGT IIIa observed in the sediment underlying an oxic water column might mask the epilimnion signature if it persists on longer timescales.

Building on the insights gained from Chapter 3, the fourth chapter of this thesis investigated a sediment core record spanning the last Glacial interstadial and Holocene. The transition from surface sediment research to sediment core investigation was driven by the hypothesis that the temperature signal primarily linked to epilimnion stratification would be best preserved in a sediment core extracted from a shallow water depth, the permanently "oxic" region of the water column. This coring location would ideally minimize the influence of the anoxic hypolimnion on brGDGT distribution, thus preserving a temperature fingerprint produced in the lake surface. The variability in sedimentary GDGTs provided valuable insights into the interdependencies among brGDGTs (Fig. 3). In Lake Rot, periods without bottom water anoxia, are characterized by correlating MBT'_{5ME} and IR, which are both proposed to be interpreted as temperature proxies. In lake sediments where brGDGTs are produced in anoxic bottom waters, an offset behavior of IR and MBT'_{5ME} values is observed. Expanding upon the temperature sensitivity in MBT'_{5ME} and IR and the previously established correlation between MBT'_{5ME} and IR in global lakes (Fig. 1), the research in Lake Rot confirms this relationship across both short (seasonal water column) and long (Holocene) timescales (Fig. 4). The implications of Chapter 4 are substantial. Notably, the variability in MBT'_{5ME} closely paralleled

changes in summer solar insolation, confirming the significant impact lake stratification and summer water temperature have on the MBT'_{5ME} . Follow-up research could focus on the potential to develop this ratio as a summer temperature proxy. In the absence of bottom water anoxia, the IR shows promise as a temperature proxy, potentially allowing to reconstruct MAT. The prospect for a coupled proxy for lake surface temperature variability is significant. As such, the potential implications of comparing MBT'_{5ME} and IR on the global scale are investigated.

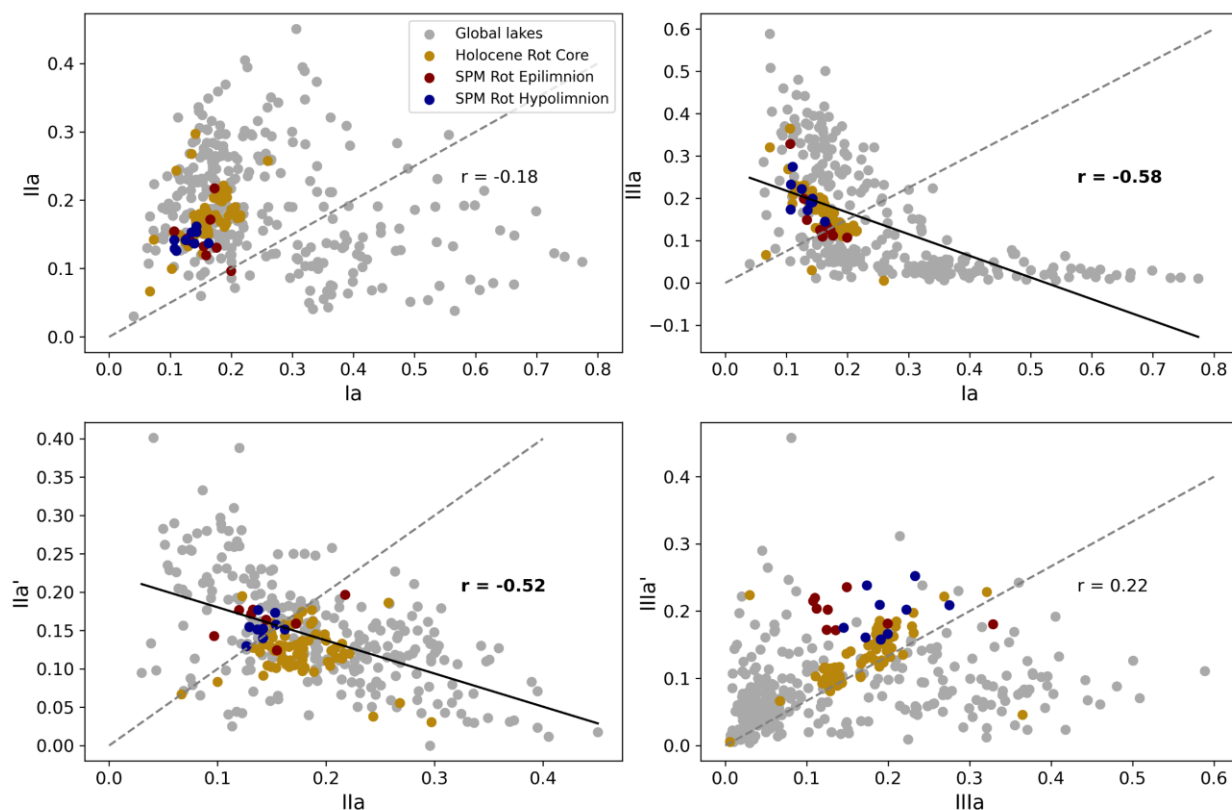


Fig. 3. The dependencies of fractional abundances of brGDGT Ia vs IIa and IIIa, and 6-methyl GDGTs IIa' and IIIa' to their 5-methyl counterparts IIa and IIIa. Regression (black) and 1:1 line (dashed-grey) plotted.

As the dependencies observed in Rotsee SPM and sediments (Fig. 3) fit with the variability present on the global scale, the impact of thermal stratification and hypolimnion anoxia can potentially be observed in globally distributed lakes. While further data analysis is required for confirmation, we can for instance consider that if the relationship between Ia and IIIa in a particular lake system falls above the 1:1 line and exhibits lower MBT'_{5ME} values (e.g., a cutoff at 0.4) in comparison to IR (e.g., 0.4-0.6), then the deposited signal may represent a hypolimnion fingerprint. Furthermore, the scattered datapoints below the 1:1 line in the global lake dataset (Fig. 2) potentially resembles a soil signal, characterized by lower IR values compared to MBT'_{5ME} values. This discrepancy may arise from an excessive production of brGDGTs Ia

concurrent to Iia (Supp. Fig. S1). As such, although soil input is determined to be limited in Lake Rot (Fig. 4), it could potentially account for the deviation in the correlation between these two indices on a global scale. By excluding such data, we can construct a more robust lacustrine-based proxy for temperature reconstruction.

Last but not least, we propose that various factors, such as brGDGTs produced in anoxic conditions, sedimentary production of brGDGTs in recent sediments, and the input of GDGTs from soils thus, influence the interdependency between MBT'_{5ME} and IR. A more comprehensive investigation of this relationship has the potential to deconvolute this complex interaction, ultimately enhancing the utility of coupled MBT'_{5ME} and IR not only as a temperature proxy, but also as a proxy for tracing the provenance of GDGTs in lake sediments.

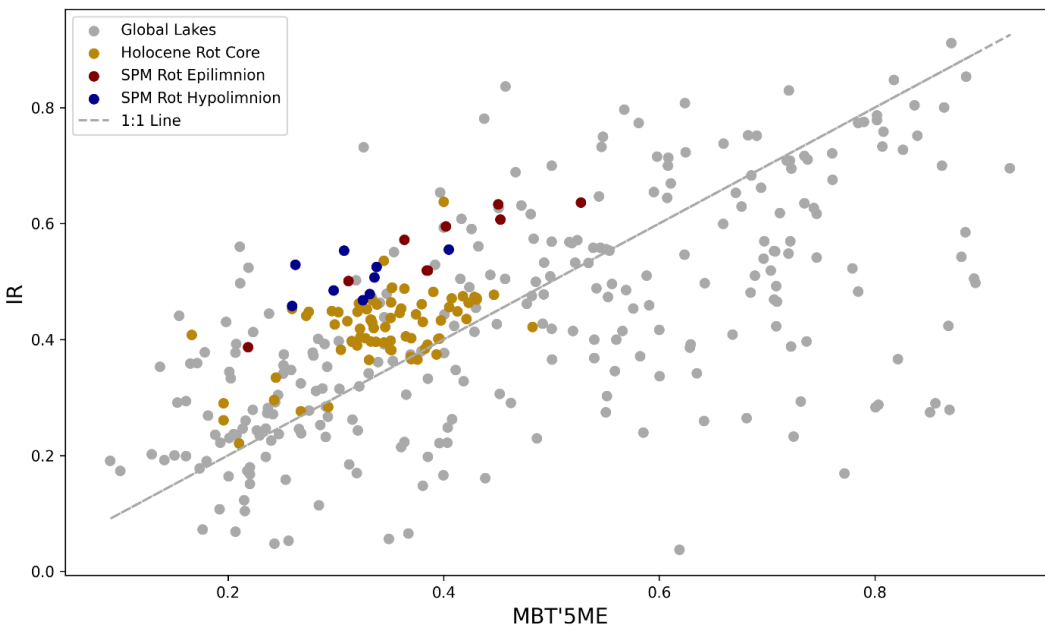
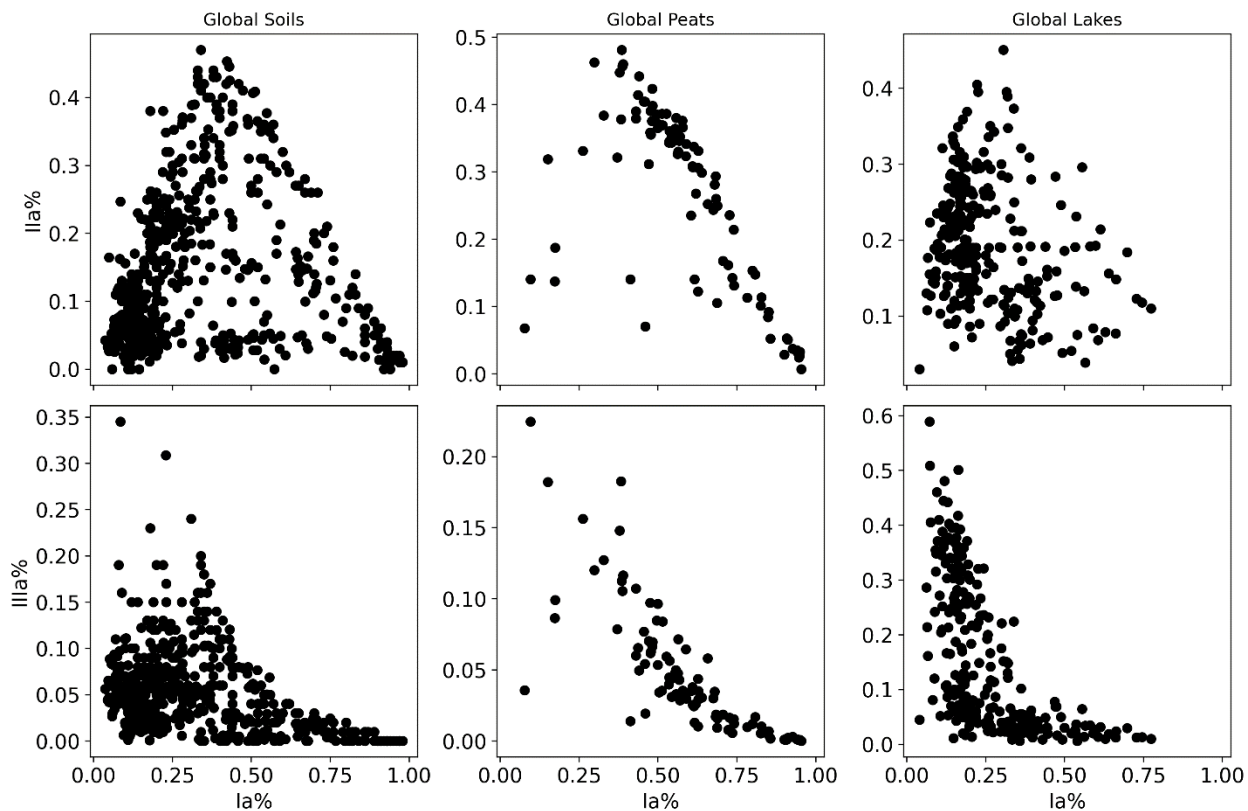


Fig. 4. Dependency between MBT'_{5ME} and IR in global lakes and Lake Rot data discussed in this thesis.

Bibliography, Chapter 5

- Bittner, L., De Jonge, C., Gil-Romera, G., Lamb, H. F., Russell, J. M. and Zech, M., 2022. A Holocene temperature (brGDGT) record from Garba Guracha, a high-altitude lake in Ethiopia. *Biogeosciences*, 19(23), pp.5357-5374.
- Dang, X., Ding, W., Yang, H., Pancost, R. D., Naafs, B. D. A., Xue, J., Lin, X., Lu, J. and Xie, S., 2018. Different temperature dependence of the bacterial brGDGT isomers in 35 Chinese lake sediments compared to that in soils. *Organic Geochemistry*, 119, pp.72-79.
- De Jonge, C., Hopmans, E. C., Zell, C. I., Kim, J. H., Schouten, S. and Sinninghe Damsté, J. S., 2014. Occurrence and abundance of 6-methyl branched glycerol dialkyl glycerol tetraethers in soils: Implications for palaeoclimate reconstruction. *Geochimica et Cosmochimica Acta*, 141, pp.97-112.
- Martinez-Sosa, P., Tierney, J. E. and Meredith, L. K., 2020. Controlled lacustrine microcosms show a brGDGT response to environmental perturbations. *Organic Geochemistry*, 145, p.104041.
- Martínez-Sosa, P., Tierney, J. E., Stefanescu, I.C., Crampton-Flood, E. D., Shuman, B. N. and Routson, C., 2021. A global Bayesian temperature calibration for lacustrine brGDGTs. *Geochimica et Cosmochimica Acta*, 305, pp.87-105.
- Raberg, J. H., Harning, D. J., Crump, S. E., de Wet, G., Blumm, A., Kopf, S., Geirsdóttir, Á., Miller, G. H. and Sepúlveda, J., 2021. Revised fractional abundances and warm-season temperatures substantially improve brGDGT calibrations in lake sediments. *Biogeosciences*, 18(12), pp.3579-3603.
- Russell, J. M., Hopmans, E. C., Loomis, S. E., Liang, J. and Sinninghe Damsté, J. S., 2018. Distributions of 5-and 6-methyl branched glycerol dialkyl glycerol tetraethers (brGDGTs) in East African lake sediment: Effects of temperature, pH, and new lacustrine paleotemperature calibrations. *Organic Geochemistry*, 117, pp.56-69.
- van Bree, L. G., Peterse, F., Baxter, A. J., De Crop, W., Van Grinsven, S., Villanueva, L., Verschuren, D. and Sinninghe Damsté, J. S., 2020. Seasonal variability and sources of in situ brGDGT production in a permanently stratified African crater lake. *Biogeosciences Discussions*, 2020, pp.1-36.
- Zhao, B., Castañeda, I.S., Bradley, R. S., Salacup, J. M., de Wet, G. A., Daniels, W. C. and Schneider, T., 2021. Development of an in situ branched GDGT calibration in Lake 578, southern Greenland. *Organic Geochemistry*, 152, p.104168.

Supplementary materials, Chapter 5



Supp. Fig. S1. Diagnostic plot (As used in De Jonge et al., 2021) depicting fractional abundance of brGDGT Ia vs Ila and IIIa in globally distributed soils, peats, and lakes. Data credit (Crampton-Flood et al., 2020; Martinez-Sosa et al., 2021).

Acknowledgment

Ladies and gentlemen, here I am, standing before you, attempting to be both heartfelt and funny, without any awkward moments (or at least trying not to make you cringe). So, fasten your seatbelts because we're about to embark on a long emotional rollercoaster with a few laughter-inducing twists and turns!

Since this might be my one and only chance to deliver a speech like this, I'll give it my all. I want to extend my heartfelt gratitude to the fantastic people who have helped me reach this academic milestone.

First and foremost, my academic fairy godmother, Cindy De Jonge. Not only did she take a chance on me, a student from a different galaxy of academic backgrounds, but she did it with the grace of a tightrope walker. Cindy, you not only supervised me but also acted as a mentor, a friend, and a source of endless inspiration. Your passion for science is so contagious that I'm convinced even our lab bacteria are excited to see you. Thanks for making my dreams come true, and for making microbiology discussions feel like comedy hour at 8 AM. So, here's to you, Cindy De Jonge, the wizard of GDGT research, the master of inspiration, and the embodiment of a "god damn magical supervisor." Thank you for being the ever-luminescent lantern in my academic universe. Your guidance has been more than supervision; it's been an enchantment, showing me the boundless possibilities of how science, and our shared love and curiosity for it, can illuminate and enrich our lives. For that, I am eternally grateful.

To Tim Eglinton, the Jedi master of academia, your sage advice has been the illuminating Force that guided me through the dark side of research. Your wisdom is the stuff of legends, and I'm forever indebted to you for helping me navigate the research realm.

A special thanks to Mark Lever, the microbiology expert extraordinaire. Your unwavering dedication to answering my emails day or night, whether you were juggling flaming bowling pins or neck-deep in oceanic hydrothermal vents sampling archaea, deserves a standing ovation. Your constructive and immensely helpful guidance has played a vital role in shaping the tiny microbiologist within me.

Now, let's not forget the unsung heroes of my thesis adventure. Marco Bolandini, you turned fieldwork into a carnival of fun, and without your help, I'd probably be lost somewhere in the wilderness, befriending squirrels, and testing if they have GDGTs. Here's to your remarkable fieldwork antics! And to Alysha, for her contagious "embrace the joy" attitude, especially during challenging times. Your 3-page long emails and your ability to infuse positivity into every situation have been a true inspiration. By observing you, I've gained invaluable insight into the kind of scientist I aspire to become - someone passionate about their work, yet a kindhearted and compassionate human being.

Julie Lattaud, my partner in research shenanigans, and all-around awesome human being. You've been my lifeline, my literal go-to encyclopedia, and the person who always knows where I left my lab notebook, which task I completed last, and answering the questions I didn't even realize I had! Thanks for being the Watson to my Sherlock in the world of science! Julie, you're not just a colleague; you're a friend who's been there to celebrate the victories and share a comforting laugh during the defeats. Your support has been the glue that held this research sip (an at time me:p) together, and I'm immensely grateful for your presence in my life.

Now, let's pivot to the real MVPs – my family! Mom, Dad, your unwavering love and support have been the solid ground beneath my academic tightrope-walking act. Without you, I might have pursued that dream of becoming a professional cake eater (not a bad gig, come to think of it). Throughout all these years, you've stood by my side, especially when I embarked on this unknown journey into the world of research. You didn't just encourage my dreams; you nurtured them. Your endless dedication to raising imaginative and curious adults is the very foundation of the person I've become today. So, Maman and Baba, this achievement is not just mine; it's a reflection of *your love*, true guidance, and endless support. I stand here today, proud of what I've accomplished, knowing that I owe so much of it to you. Thank you for being the wind beneath my wings, and the source of love that fuels my journey. I love you both more than words can express.

Mos, my coding maestro, life coach, and not just a brother but the guiding star of everything everywhere all at once, you're the secret sauce behind not only my code but also the seamless operation of... well, my life (ehem, ehem). Those late-night brainstorming sessions, ranging from tackling coding challenges to profound discussions on life's mysteries (and of course, enjoying ice-cream while doing it), have been nothing short of legendary. You've turned coding into an adventure, and my life into a well-oiled machine (well at least most of the time:p).

Your generosity and open heartedness in providing me with shelter during challenging times are cherished beyond measure. Your occasional outbursts of frustration, urging me to think of better coding solutions, may have rattled me momentarily (and made me swear to not ever ask you again for help:p), but they've ultimately pushed me to become a better scientist. Above all, you are "the" single person I look up to in life. Your unwavering dedication, intellect, and relentless pursuit of your own dreams have inspired me to aspire for excellence. You are my role model, my hero, and I couldn't be prouder to have you as my brother. Thank you for being a guiding light on this incredible journey of mine.

To my brothers, Hoss and Mohammad, the gang is complete with you in it. Thank you for always having my back and being the unwavering support that every sibling dreams of. I live life with the utmost gratitude, knowing that I have an incredible family like ours.

Last but certainly not least, my partner in crime, my laughter buddy, Jamie. Your unwavering encouragement and willingness to listen to my science rants at 2 AM have been the boost that kept my academic kite soaring high. In your own unique way, you've kept me sane the past 3 years and made me realize that life exists beyond the confines of research. Your support has been like a cup of coffee on a Monday morning – essential and uplifting. Jamie, you're the missing piece in my puzzle, so I can't thank you enough for being by my side through it all. Here's to more laughter-filled adventures in the chapters yet to come!

And to anyone who I may have unintentionally left out, I'm penning this after enduring 14-hour workdays for the past six months, so please forgive my weary mind. Know that your contributions have not gone unnoticed, and you are deeply appreciated.

Curriculum Vitae

Name	Fatemeh Ajalloeian
Date of Birth	22.09.1993
Place of Birth	Kermanshah, Iran
Nationality	Iran
02/2024-	Postdoctoral researcher, ETH Zürich <i>Biogeoscience, Institute of Geology and Biogeochemistry group, Eawag</i>
10/2019- 02/2024	Doctor of Philosophy (PhD), ETH Zürich <i>Biogeoscience, Institute of Geology</i>
Thesis	Temporal dynamics of freshwater microbial membrane lipids: Impact of environmental variables on brGDGTs across short and long timescales
Advisors	Prof. Dr. Cindy De Jonge, ETH Zürich, Switzerland Prof. Dr. Timothy Eglinton, ETH Zürich, Switzerland
09/2015- 12/2018	Master of Science in Atmospheric Sciences, University of Helsinki <i>Atmospheric Sciences, Department of Physics</i>
09/2011- 07/2015	Bachelor of Science, Shahid Beheshti University <i>Geomorphology, Department of Earth Science</i>